



Universitat Autònoma de Barcelona

# **Chemical Speciation on Urinary Lithiasis**

**Image Analysis and Separation Techniques**

**for the Study of Lithogenesis**

Francisco Blanco Lucena

Doctoral Thesis

Doctoral Studies in Chemistry

Supervisors:

Manuel Valiente Malmagro and Montserrat López-Mesas

Department of Chemistry

Faculty of Science

2014





**Universitat Autònoma de Barcelona**

Report submitted to aspire for the Doctor Degree by:

**Francisco Blanco Lucena**

Supervisors' approval:

**Prof. Manuel Valiente Malmagro**

**Dr. Montserrat López-Mesas**

Bellaterra, 22/09/2014



*the achievement of failure.*



*Por hacer posible que haya podido llegar hasta aquí,*

*A mis padres*





# UAB

Universitat Autònoma de Barcelona

The PhD thesis presented in this document has been developed thanks to public funding through:

- Pre-doctoral grant: Becas FPU (Ministerio de Educación, ES), Ref. AP2009-3245
- Becas FPU – Estancias Breves (Ministerio de Educación, ES), Refs 000011928 and EST12-00940
- MICINN (ES), Projects CTQ2009-07432, IT2009-0024 and CTM2012-30970
- ORQUE-SUDOE Project (EU), Ref. SOE3/P2/F591
- ELISA Programme (SOLEIL Synchrotron, FR), Ref. 20101061
- VALTEC 2013 (ACCIÓ, Generalitat de Catalunya), Ref. 13-1-0148

Furthermore, the author and directors of this work are especially grateful to those scientists, research centers and public institutions which have actively collaborated in the development of any part of this PhD thesis and the author's professional training (or providing the necessary funding):



Ministerio de Educación

Gobierno de España, Madrid, Spain



Professor Josef Havel

Department of Chemistry

Masaryk University, Brno, Czech Republic



Professor Giuseppe Bonifazi and Dr. Silvia Serranti

DICMA – Università di Roma – La Sapienza, Rome, Italy



Professor Orson Moe

Center of Mineral Metabolism and Clinical Research

Dallas, Texas, USA



Professor Dr. Roswitha Siener  
University Stone Center  
Universitätsklinikum Bonn, Bonn, Germany



Titular Professor Joan Serrat and Dr. Felipe Lumbreras  
Computer Vision Center, UAB, Barcelona, Spain



Dr. Fabienne Séby and Dr. Mathieu Menta  
UT2A, Pau, France



**Germans Trias i Pujol**  
Hospital

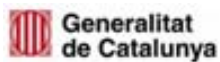
Dr. Montserrat Arzoz Fàbregas  
Servei d'Urologia, Hospital Germans Trias i Pujol  
Badalona, Spain



Dr. M. Pilar Luque Gálvez and Dr. Roberto Castañeda  
Servei d'Urologia, Hospital Clínic, Barcelona, Spain



Júlia Palma, on behalf of PRUAB  
PRUAB, UAB, Barcelona, Spain



**ACCIÓ**

Pilar Casellas, on behalf of ACCIÓ  
ACCIÓ, Generalitat de Catalunya, Barcelona, Spain



GroW Us: Ida Grad, Martin Raygoza, Lucas Roos, Nikolaos Sarafidis, Larissa Schade and Alexis Mavrommatis.  
EADA Business School, Barcelona, Spain

The laboratories at La Sapienza, UTSouthwestern, Universitätsklinikum Bonn and UT2A, along with their human team, are especially acknowledged for their kind support when hosting the author of this PhD work during different short and long term (up to 5 months) stays. They have readily collaborated in the development of this thesis but, more importantly, in the personal and professional progress of the PhD student.

The author especially appreciates the interaction, help and moments shared with the members at the Centre GTS in the UAB.

# Short-term stays

The work presented in this dissertation has been done in collaboration with other research groups, often including short-term stays in foreign institutions. The dates for the development of each stay are listed here:

- Dipartimento de Ingegneria Chimica Materiali Ambiente. Sapienza – Università di Roma, Latina, Italy.

2 Weeks stays (May 2010 and May 2011)

- University of Texas – Southwestern Medical Center, Dallas, TX, USA.

September – December 2011

- Universitätsklinikum Bonn – University Stone Center, Bonn, Germany.

February – May 2013

May 2014

- UT2A – Université de Pau et des Pays de l'Adour, Pau, France.

February – April 2013

# Contributions to Congresses and Seminars

The results presented in this Dissertation have been previously made public in the following events:

“AUSE 2013”, Barcelona (Catalunya, Spain), 3-6th September 2013. Poster contribution: “High definition and Synchrotron radiation based IR  $\mu$ -Spectroscopy approach to reveal kidney stones history”

“URINOMICS 2013”, Lisbon (Portugal), 9-11th September 2013. Oral contribution: “Comparison of kidney stone analysis by NIR-Hyperspectral Imaging technique (NIR-HSI) and the traditional Infrared Spectroscopy”

“2nd MEETING OF THE EAU SECTION OF UROLITHIASIS (EULIS)”. Copenhaguen (Denmark), 5-7th September 2013. Oral contribution: “Comparison of kidney stone analysis by NIR-Hyperspectral Imaging technique (NIR-HSI) and the traditional Infrared Spectroscopy”

“XVIII SIMPOSI SCU”, Roses (Catalunya, Spain), 23-25th November 2012. Oral contribution: “Ràpida classificació de càlculs renals mitjançant Imatge Hiperespectral (HSI) i Xarxes Neuronals Artificials”

“XXIII Reunión Nacional de los Grupos de Litiasis, Endourología, Laparoscopia y Robótica”, Valladolid (Spain), 8-9th March 2012. Oral contribution: “Rápida clasificación de cálculos renales por medio de Imagen Hiperespectral (NIR) y Redes Neuronales Artificiales”

“EUROPEAN GEOSCIENCES UNION – GENERAL ASSEMBLY 2011”, Austria Vienna Center, Vienna (Austria), 3-8th April 2011. Oral contribution: “NIR-Hyperspectral Imaging and Artificial Neural Networks for the Characterisation of Renal Calculi”

“XXème JOURNÉE GSO DE CHIMIE DU GRAND DUS-UEST ET DE CATALOGNE”, Délégation Régionale du CNRS, Montpellier (France), 26th November 2010. Oral contribution: “NIR-Hyperspectral Imaging and Artificial Neural Networks for the Characterisation of Renal Calculi”



# Contents

i. Abstract.....	xx
ii. Resum (Català).....	xxi
iii. Glossary.....	xxii
1. INTRODUCTION: WHAT LIES BEHIND “URINARY STONE DISEASE” .....	1
1.1. Description of the disease.....	3
1.1.1. Morpho-anatomical characteristics of the kidney.....	3
1.1.2. Incidence and prevalence of stone disease.....	6
1.1.3. Causes of stone formation.....	7
1.1.4. Medical manifestations and detection of stone disease.....	9
1.1.5. Urinary lithogenesis .....	11
1.1.5.1. Urinary saturation.....	11
1.1.5.2. Stone formation.....	13
1.1.6. Promoters and inhibitors of crystallization processes .....	14
1.1.6.1. Crystallization promoters.....	14
1.1.6.2. Crystallization inhibitors.....	15
1.1.7. Stone formation risk assessment.....	17
1.1.7.1. Relative Supersaturation.....	17
1.1.7.2. Activity Product Ratio .....	18
1.1.7.3. Bonn Risk Index .....	19
1.2. Classification of urinary stones .....	20
1.2.1. Calcium Oxalate .....	21
1.2.1.1. Calcium Oxalate Monohydrate.....	22
1.2.1.1.1. Cavitory Calcium Oxalate Monohydrate Stones.....	22
1.2.1.1.2. Papillary Calcium Oxalate Monohydrate Stones.....	23
1.2.1.2. Calcium Oxalate Dihydrate.....	24
1.2.1.2.1. Calcium Oxalate Dihydrate – Transformation into COM.....	25
1.2.1.3. Etiological factors.....	26
1.2.2. Calcium Phosphate.....	27
1.2.2.1. Apatite.....	27

1.2.2.2.	Brushite .....	28
1.2.2.3.	Etiological factors.....	29
1.2.3.	Infected stone disease.....	30
1.2.3.1.	Etiological factors.....	31
1.2.4.	Uric Acid.....	31
1.2.4.1.	Etiological factors.....	32
1.2.5.	Cystine .....	32
1.2.6.	Mixed stones.....	33
1.2.6.1.	Calcium Oxalate and Apatite .....	33
1.2.6.2.	Calcium Oxalate and Uric Acid.....	34
1.2.7.	Uncommon Urinary Stones .....	34
1.3.	Analysis of urinary stones .....	35
1.3.1.	Chemical Analysis.....	35
1.3.2.	IR Spectroscopy.....	35
1.3.3.	Microscopy .....	36
1.3.3.1.	Optical microscopy .....	36
1.3.3.2.	Electronic microscopy.....	37
1.3.4.	X-Ray Diffraction .....	38
1.3.5.	Methodologies overview .....	38
1.4.	Medical management of urinary stones.....	40
1.4.1.	Surgical management of urinary stones.....	40
1.4.1.1.	Extracorporeal Shock Wave Lithotripsy (ESWL or SWL) .....	41
1.4.1.2.	Percutaneous Nephrolithotomy (PCNL or PNL).....	42
1.4.1.3.	Ureterorenoscopy (URS) .....	42
1.4.2.	Metaphylaxis of urinary stones.....	43
1.4.2.1.	Diet.....	44
1.4.2.2.	Medication .....	45
1.4.2.3.	Patients compliance to metaphylaxis .....	47
1.5.	Socioeconomic impact of urinary stone disease .....	47
1.6.	Objectives.....	50
2.	IMAGE ANALYSIS: NEW OPTICS, FURTHER PERSPECTIVES.....	53
2.1.	Introduction to Image Analysis techniques .....	55



2.1.1.	Hyperspectral Imaging.....	55
2.1.2.	Data analysis techniques .....	58
2.1.2.1.	Factor Analysis.....	59
2.1.2.2.	Principal Components Analysis.....	59
2.1.2.3.	Artificial Neural Networks.....	60
2.1.2.4.	Experimental outline.....	61
2.2.	NIR-Hyperspectral Imaging: Artificial Neural Networks .....	61
2.2.1.	Experimental Section.....	62
2.2.1.1.	Samples .....	62
2.2.1.2.	Equipment .....	62
2.2.1.3.	Data selection .....	64
2.2.2.	Results and discussion.....	65
2.2.2.1.	Factor Analysis.....	67
2.2.2.2.	Principal Component Analysis .....	67
2.2.2.1.	Artificial Neural Networks.....	71
2.2.3.	Final remarks.....	73
2.3.	NIR-Hyperspectral Imaging: Pixel-to-Pixel Analysis.....	74
2.3.1.	Experimental Section.....	74
2.3.1.1.	IR Spectroscopy .....	75
2.3.1.2.	Data handling .....	75
2.3.1.2.1.	Qualitative analysis.....	75
2.3.1.2.2.	Quantitative analysis .....	76
2.3.2.	Results and discussion.....	77
2.3.2.1.	Qualitative analysis .....	77
2.3.2.2.	Quantitative analysis.....	77
2.3.2.2.1.	Performance of the HSI-NIR model .....	77
2.3.2.2.2.	Implementation of the NIR-HSI model .....	80
2.3.2.2.3.	Spatially defined analysis.....	82
2.3.3.	Final remarks.....	84
2.4.	$\mu$ -IR Spectroscopy.....	85
2.4.1.	Experimental Section.....	85
2.4.1.1.	Samples .....	85

2.4.1.2.	Spectroscopic measurements .....	86
2.4.1.2.1.	Global source IR mapping.....	86
2.4.1.2.2.	Synchrotron radiation IR mapping .....	86
2.4.1.3.	Data handling .....	87
2.4.1.3.1.	Spectral bands.....	87
2.4.2.	Results and discussion.....	87
2.4.2.1.	Calcium oxalate monohydrate .....	88
2.4.2.2.	Mixed calcium oxalate monohydrate and dihydrate.....	90
2.4.2.3.	Carbonate apatite .....	95
2.4.3.	Final remarks.....	97
3.	NANOPARTICLES IN URINE: LOOKING CLOSER TO SEE BEYOND .....	99
3.1.	Introduction to nanoparticles analysis .....	100
3.2.	Nanoparticles analysis techniques .....	102
3.2.1.	Field Flow Fractionation .....	102
3.2.2.	Multi-Angle Light Scattering Detector.....	104
3.3.	Experimental Section.....	105
3.3.1.	Samples .....	105
3.3.2.	FFF analysis .....	106
3.3.3.	Data analysis .....	106
3.3.3.1.	Box-whiskers plot .....	107
3.4.	Results and discussion .....	107
3.4.1.	Optimization of the analysis methodology.....	108
3.4.2.	Results of particle size determination.....	113
3.5.	Final remarks.....	117
4.	CRYSTALLIZATION PROMOTERS: OXALATE IN THE SPOTLIGHT.....	118
4.1.	Oxalate as crystallization promoter.....	119
4.1.1.	Analysis techniques.....	120
4.1.1.1.	Ion Chromatography.....	120
4.1.1.1.1.	IC-MS .....	121
4.1.1.2.	ICP-MS.....	121
4.2.	Determination of oxalate content in drugs and nutritional supplements.....	122
4.2.1.	Experimental Section.....	123

4.2.1.1.	Sample description .....	123
4.2.1.2.	Sample preparation .....	125
4.2.1.3.	Ion Chromatography analysis .....	125
4.2.2.	Results and discussion .....	125
4.2.2.1.	Analysis methodology .....	125
4.2.2.2.	Sample analysis .....	127
4.2.3.	Final remarks .....	129
4.3.	Determination of urinary lithiasis promoters and inhibitors in chocolate .....	129
4.3.1.	Experimental Section .....	130
4.3.1.1.	Sample description .....	130
4.3.1.2.	Sample preparation .....	130
4.3.1.3.	Ion chromatography analysis .....	130
4.3.1.4.	ICP-MS analysis .....	133
4.3.1.5.	Data analysis .....	133
4.3.1.	Results and discussion .....	135
4.3.1.1.	Methodology results .....	135
4.3.1.2.	Sample analysis .....	135
4.3.1.2.1.	General statistical parameters .....	135
4.3.1.2.2.	Principal Component Analysis .....	139
4.3.1.2.3.	Hierarchical Cluster Analysis .....	142
4.3.2.	Final remarks .....	143
4.4.	Determination of oxalate absorption using isotopic labeling .....	144
4.4.1.	Experimental Section .....	144
4.4.1.1.	Sample description .....	144
4.4.1.2.	Sample preparation .....	145
4.4.1.3.	Ion Chromatography – Mass Spectrometry analysis .....	145
4.4.1.4.	Relative Supersaturation calculations .....	146
4.4.2.	Results and discussion .....	147
4.4.2.1.	Analysis methodology .....	147
4.4.2.2.	Sample analysis .....	147
4.4.2.2.1.	Oxalate absorption .....	147
4.4.2.2.2.	Study of RSS and oxalate absorption .....	148

4.4.3. Final remarks.....	149
5. KNOWLEDGE TRANSFER: TURNING SCIENCE INTO EXPECTATIONS .....	151
5.1. Knowledge Transfer as horizon .....	153
5.1.1. Basic concepts on Knowledge Transfer .....	153
5.1.2. The University in the Knowledge Transfer context.....	154
5.1.3. Local and national environment (Spain).....	156
5.2. Patent: Method for the Characterization and Classification of Kidney Stones.....	158
5.3. myStone .....	159
5.3.1. Experimental Section.....	160
5.3.1.1. Samples .....	160
5.3.1.2. Device set-up.....	161
5.3.1.3. Classification procedure.....	162
5.3.2. Results and discussion.....	168
5.3.2.1. Classification results.....	168
5.3.2.2. Report .....	171
5.3.3. Final remarks.....	172
5.3.4. Patent .....	173
5.4. Valorization Project: VALTEC.....	173
5.5. Business Plan.....	176
5.5.1. Analysis of the idea .....	177
5.5.1.1. Company .....	177
5.5.1.2. Context.....	177
5.5.1.3. Channel .....	179
5.5.1.4. Competitors.....	180
5.5.1.5. Customers .....	180
5.5.1.6. Interviews to experts .....	181
5.5.1.7. SWOT Analysis .....	182
5.5.2. Business Strategy .....	183
5.6. Final remarks.....	184
6. CONCLUSIONS: CONDENSING THE CONCEPTS.....	187
6.1. Conclusions .....	189
6.1.1. Image analysis.....	189

6.1.2.	Nanoparticles in urine .....	190
6.1.3.	Crystallization promoters .....	190
6.1.4.	Knowledge transfer .....	191
6.2.	Insights into the future .....	191
7.	BIBLIOGRAPHY .....	193
8.	SUPPLEMENTAL MATERIAL .....	209
8.1.	Determination of urinary lithiasis promoters and inhibitors in chocolate – Data tables (Section 4.3.) .....	211
8.2.	Determination of Oxalate absorption using isotopic labeling - Data tables (Section 4.4.)...	222
8.3.	Published Article: Journal of Biomedical Optics (Section 2.2.) .....	226
8.4.	Published Article: Journal of Biophotonics (Section 2.4.) .....	<b>Error! Bookmark not defined.</b>
8.5.	Article under revision: Journal of Biomedical Optics (Section 2.3.)	<b>Error! Bookmark not defined.</b>
8.6.	Patent: NIR-HSI stone classification methodology (Section 5.2.)	<b>Error! Bookmark not defined.</b>
8.7.	Patent application: Stone analysis device (Section 5.3.) .....	<b>Error! Bookmark not defined.</b>

## i. Abstract

The formation of solid depositions along the urinary tract, also known as urinary lithiasis, is a common disease worldwide. The incidence rate is 12% of the entire population and the recurrence (suffering further stone episodes) affects 50% of the patients. The associated medical management and treatments are an important burden on healthcare systems. The challenges posed by urinary lithiasis require enhanced diagnostic and treatment options. The medical community (and the society) has a clear need of reducing incidence and recurrence rates, which should follow the path of wider knowledge in stone disease and new preventive options.

This Dissertation exposes the work developed in some areas concerning urolithiasis, which embeds image analysis, spectroscopy and separation techniques. The aim of this report is to offer answers to the above mentioned necessities using those scientific tools.

The first experimental Section in this Dissertation is devoted to the use of NIR and IR Spectroscopies to broaden the knowledge in lithogenesis and suggesting new urinary stone analysis alternatives. The precise description of the formation of a stone is a solid pillar on the definition of risk factors and influence of urinary parameters on the crystallization process and is needed for the formulation of more specific treatments. The development of a new analysis methodology, using Hyperspectral Imaging, represents a step forward in stone disease management. The process presented here offers an enhanced stone description than conventional techniques in a short analysis time and with no need of trained analysts. These highlights suggest this methodology as a solid alternative in routine clinical laboratories.

The next Section describes the use of Field Flow Fractionation for the characterization of nanoparticles in urine. Since crystallization processes start by the agglomeration of small solid particles, the interest on the development of a methodology to determine their relation to urinary lithiasis is clear. This study intends to use nanoparticles as a biomarker for stone formation risk.

The third experimental Section is focused on the importance of crystallization promoters, in particular, oxalate. This promoter is mostly integrated into the body through the diet. In this sense, this Dissertation investigates oxalate content (and other promoters/inhibitors of crystal formation) in plant extract and chocolate - common products in western diet. Oxalate absorption is also considered in this work, by using isotopic labeling and comparing the results to general risk assessment formulas.

The last Section in this Dissertation highlights the contributions of this work to knowledge transfer. It includes the intellectual protection of some of the produced knowledge and the presentation of a new medical device. This instrument is able to quickly classify urinary stones using image recognition tools, providing thus a suitable alternative for the in-site analysis of stones. The device automatically offers treatment suggestions adapted to each sample, so it offers an individualized analysis. The commercial potential of this device has been also assessed through market research.

In essence, this Dissertation can be considered as a multidisciplinary approach that provides a link between fundamental, applied and medical features of urinary lithiasis. This goal has been reached taking the improvement of patients' quality of life as permanent horizon.

## ii. Resum (Català)

La formació de concrecions sòlides al tracte urinari, malaltia que rep el nom de litiasi urinària, és un desordre molt comú arreu del món. La seva taxa d'incidència és del 12% a la població mundial, i la de recurrència (repetició d'episodis litíasis) és del 50%. Els recursos destinats al tractament de la litiasi urinària suposen un **a** important llast als pressupostos de la sanitat pública. Els reptes que fixa aquesta malaltia requereixen opcions més avançades de diagnòstic i tractament. Existeix una necessitat clara a la comunitat mèdica (i a la societat) de reduir les elevades taxes d'incidència i recurrència, que s'han de resoldre a través del coneixement i de noves opcions preventives.

Aquesta Tesi Doctoral exposa els projectes desenvolupats en diverses àrees de la litiasi urinària, que inclouen anàlisi d'imatge, espectroscòpia i tècniques de separació. L'objectiu d'aquest document és oferir respostes a les limitacions indicades emprant aquestes eines.

La primera Secció experimental està dedicada a la utilització de les espectroscòpies NIR i IR per ampliar el coneixement de la litogènesi i suggerir noves alternatives per a l'anàlisi dels càlculs urinaris. Una descripció precisa de la formació d'un càlcul renal és l'eina fonamental per a la identificació de factors de risc i la seva influència als processos de cristal·lització. Aquestes anàlisis presenten les bases de tractaments més adaptats. D'altra banda, el desenvolupament d'una nova metodologia analítica basada en Imatges Hiperespectrals representa un destacable avenç al tractament de la malaltia. Els processos descrits aquí superen les tècniques tradicionals en la qualitat de descripció de la mostra, el temps d'anàlisi, i no necessiten d'un analista format. Aquesta metodologia pot ser considerada seriosament com a alternativa als laboratoris clínics.

La següent secció mostra la caracterització de les nanopartícules presents a l'orina mitjançant *Field Flow Fractionation*. El interès en estudiar la relació entre les nanopartícules i la litiasi rau en el fet que el procés de cristal·lització s'inicia amb l'aglomeració de petites partícules en suspensió. L'objectiu final és la utilització de les nanopartícules com a biomarcador de risc litogen.

La tercera Secció experimental es centra en la rellevància dels promotors de la cristal·lització, amb especial èmfasi a l'oxalat. Aquest promotor s'acostuma a incorporar a través de la dieta. El treball presentat aquí inclou la determinació del contingut en oxalat (i altres inhibidors/promotors) en extractes de plantes i xocolata, productes comuns a dietes occidentals. Addicionalment, s'ha dut a terme un estudi enfocat a l'absorció d'oxalat, que empra el marcatge isotòpic i en contrasta els resultats amb altres fórmules de determinació de risc litogen.

En darrer lloc, aquest document detalla les principals contribucions de la Tesi a la transferència de coneixement: protecció intel·lectual i la presentació d'un dispositiu mèdic. Aquest aparell és capaç de classificar càlculs renals de forma ràpida emprant eines de reconeixement d'imatges. El dispositiu realitza automàticament suggeriments de tractament específics a cada mostra, per a una anàlisi individualitzada. El interès comercial del producte ha estat estudiat, incloent un estudi de mercat.

En resum, aquesta Tesi ofereix un enfocament multidisciplinari que pretén establir nexes entre aspectes fonamentals, aplicats i mèdics de la litiasi urinària. La millora de la qualitat de vida del pacient ha estat l'horitzó permanent que ha conduït aquesta recerca.

### iii. Glossary

ANN: Artificial Neural Networks	MA: Microscopic Analysis
A4F: Asymmetrical Flow Field Flow Fractionation	MALS: Multi Angle Light Scattering
AP: Activity Product	MIA: Multivariate Analysis
APR: Activity Product Ratio	MS: Mass Spectrometry
BRI: Bonn Risk Index	MWCO: Molecular Weight Cut-Off
BRU: Brushite	NIR: Near Infrared
CA: Chemical Analysis	NP: Nanoparticles
CaOx: Calcium Oxalate	PC: Principal Component
CaP: Calcium Phosphate	PCA: Principal Component Analysis
CAP: Carbonate Apatite	PCNL: Percutaneous Nephrolithotomy
COD: Calcium Oxalate Dihydrate	PES: Polystyrene
COM: Calcium Oxalate Monohydrate	RC: Regenerated Cellulose
CYS: Cystine	ROI: Region Of Interest
ER: Emergency Room	RSS: Relative Super Saturation
ESWL: Extracorporeal Shock Wave Lithotripsy	SEM: Scanning Electron Microscopy
FA: Factor Analysis	sFTIR: Synchrotron Radiation Fourier Transform Infrared Spectroscopy
(FI-) FFF: (Flow-) Field Flow Fractionation	STR: Struvite
HCA: Hierarchical Cluster Analysis	UA: Uric Acid
HSI: Hyperspectral Imaging	UAA: Uric Acid Anhydrous
IC-MS: Ion Chromatography- Mass Spectrometry	UAD: Uric Acid Dihydrate
ICP-MS: Inductively Coupled Plasma – Mass Spectrometry	URS: Ureterorenoscopy
IRS: Infrared Spectroscopy	UT: Urinary Tract
KT: Knowledge Transfer	XRD: X-Ray Diffraction
KUB: Kidney-Ureter-Bladder	





**INTRODUCTION:  
WHAT LIES BEHIND  
“URINARY STONE  
DISEASE”**



# General Description of Urinary stone Disease

This Section is intended to introduce the reader into the general topic of this work, namely the urinary stone formation disease. Owing to the medical nature of such topic, a general description of renal physiology, general biochemical related parameters, along with other medical issues directly related to the management of the disorder, will be outlined in this Section. This shall ease the comprehension of this work and its results to a full extent.

## 1.1. Description of the disease

The formation of urinary calculi (commonly known as kidney stones) corresponds actually to the precipitation of solid concretions at any point of the urinary tract. Generally speaking, stones are formed as a product of poorly soluble salts or compounds usually present in urine. These structures grow until they become *actual* stones. Organic depositions have also been located in urinary stones, although in a much smaller amount.

Regarding the causes of urolithiasis, it is clear that it is a very complex, multifactorial disease. Not only inherent characteristics of each individual lead to the formation of urinary stones, also environmental, lifestyle and geographic factors have been highlighted as main players in the appearance of the disease.

### 1.1.1. Morpho-anatomical characteristics of the kidney

Kidneys, those twin organs located at the middle back of human body, have the titanic mission of filtering the blood that runs the body end to end. This task prevents toxic substances and non-storable by-products of the multiple metabolic processes taking place in the organism to continue their road along blood vessels. To make things more complex, this task bears the gigantic restriction of eliminating as little water of the body as possible, since it is the base of life existence. Such is the importance of those organs that a complete renal failure leads the organism to death within less than one week<sup>1</sup>. The kidney hosts the main actors of this work, urinary stones, so this first Section will briefly describe the main renal morpho-anatomical features, along with general urinary tract considerations, for a complete comprehension of the disease.

The urinary tract (UT) is a complex system of conducts, devoted to perform the excretory function in the body. This system is commonly divided into upper UT and lower UT<sup>2</sup>. The upper UT is formed by the kidneys and ureters, while the latter accounts for bladder and urethra. Kidneys produce urine, which is evacuated through the ureters. These are low pressure conduits that allow the transit of urine only one way, directly into the lower UT. Urine is kept in the bladder, a low pressure reservoir of urine, which

allows the conscious voiding of urine by the individual. Urine is finally expelled from the organism through the urethra. These parts can be appreciated in Figure 1.1.

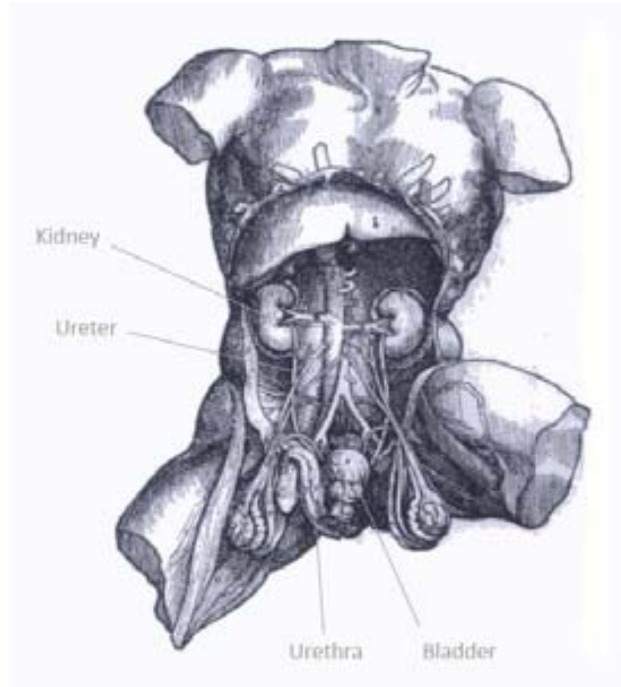


Figure 1.1 Andreas Vesalius' representation of the human urinary tract (year 1543). Most anatomic details are correct; the placement of kidney, ureters, bladder and urethra can be appreciated <sup>3</sup>.

The kidney is formed by two layers: the external cortex and the deeper medulla <sup>4</sup>. The cortex protects the internal structure (medulla), which contains renal pyramids, structures that project into the renal sinus. The pyramidal systems repeat, as renal columns and lobes. These structures conduct the formed urine into the renal calyces, which end in a funnel structure (renal pelvis), connected to the ureter. This complex system, depicted in Figure 1.2, conducts the urine from the point in which it is produced until it is drained from the kidney. The blood vessel structure in the kidney is complex, according to its filtration function.

The kidney leads the excretory function in the human body by constantly working through the nephrons, structures located partly in the cortex and partly in the renal medulla. Nephrons can be regarded as the functional units of the kidney; a kidney contains 1 to 1.5 million of these units, which actually perform the filtration task using its glomerulus part (like a ball of yarn). If the length of all the glomerulus is summed up, the amount would reach 145 km in an average adult. Nephrons filtrate up to 180 liters of fluids per day, and their efficiency is so high that, even in patients who have lost 75% of their renal function, the filtration of body fluids can be performed in a great extent <sup>5</sup>. Accounting to the huge amount of liquid filtered in the kidneys, and considering that an average adult produces 1-3 liters of urine per day, it becomes clear that their role is, besides filtration, the selective reabsorption of water and certain components.

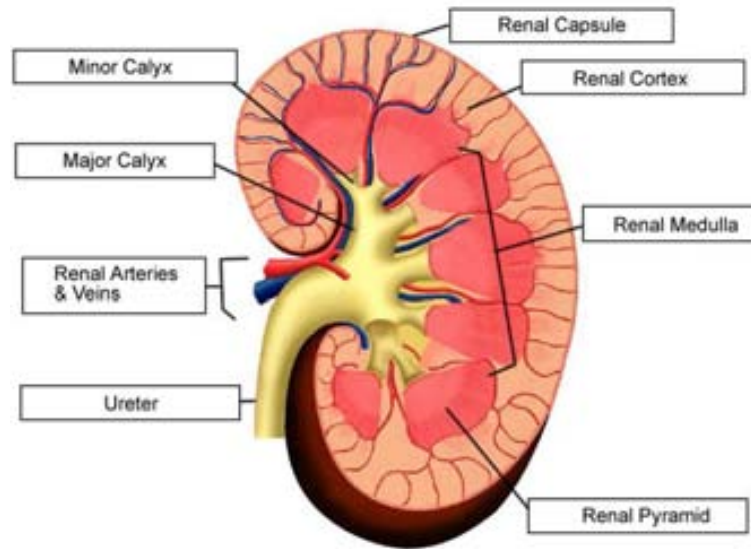


Figure 1.2 Schematic anatomy of the kidney, internal view 6.

In brief, each nephron in the kidney includes a glomerulus, a network of capillaries, and the Bowman’s capsule, which has the function of draining blood into the tubular section of the nephron 6. The Bowman’s capsule is a layer of epithelial cells, connected to the proximal tubule. This tubule drains into the loop of Henle, then into the distal tubule and finally, the last point of the circuit is the renal pelvis. Figure 1.3 shows a scheme of the nephron structure.

The first filtration step, the glomerulus, acts as a biological sieve where blood is forced through the glomerular capillaries at higher pressure than the pressure at which the blood generally travels around the body (and also into the kidney itself) because of the diameters difference of afferent and efferent arterioles. Helped by the increased pressure in the glomerular capillaries, a filtration process occurs in which some blood fluid is forced out of the glomerulus and into the capsular space of the Bowman's Capsule. Thus, it allows the passage of only some molecules found in blood. Neutral molecules smaller than 4 nm in diameter can cross this filter (so many biological polymers and proteins are kept in the blood) 7. Also highly charged molecules are prevented from crossing this barrier.

The following filtration step in the formation of urine is the proximal tubule. This section of the nephron is in charge of reabsorbing much of the filtered water (approximately 65%) and also most solutes. This part of the nephron reabsorbs most of the glucose, amino acids, vitamins, small proteins and many ions, as sodium, potassium, chloride, phosphate and bicarbonate 6, so it is energy high-consuming. According to these important functions, it can be understood how disturbing any disorder in proximal (or distal) tubules might be (i.e. the well-known renal tubular acidosis, a risk factor in the formation of some stone types, see Section 1.2. ) 8.

The loop of Henle is the next step for the solution (urine is not formed yet) to go through. This section has the goal of preparing urine for receiving more solutes; that is, to decrease the osmolality with respect to that of plasma. Only 10-15% of the filtered water is recovered here, so the concentration of

solutes is decreased by creating an osmotic gradient. Sodium and potassium ions are actively absorbed (with an energy input), while the walls in the loop of Henle are mostly impermeable to water 9.

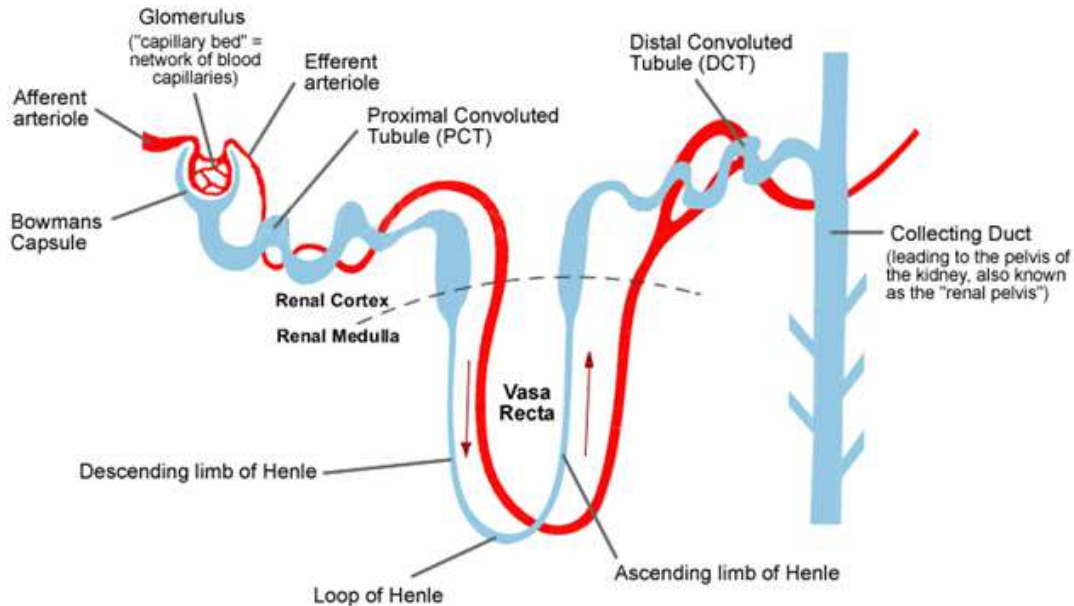


Figure 1.3 Simplified scheme of the blood supply at a nephron level.

The last step in the urine formation process takes place in the distal tubules. Again, approximately 10% of the water is reabsorbed, and the “fine tuning” of urine is performed, as a result of complex reabsorption and excretion processes, regulated by hormones 6. After this point, the urine is conducted to the renal calices and then it is drained from the kidney through the ureter.

### 1.1.2. Incidence and prevalence of stone disease

The experience of developing a urinary stone and suffering the associated inconveniences is widely known. Many reports have shown that the incidence of urolithiasis has a positive trend worldwide 10 11 12. A number of works have investigated the incidence of the disease, and the lifetime risk of developing urinary stones has been estimated at 12-15% of the population. In addition, the high recurrence rate (suffering of further stone episodes), 50% at 5 years and 70% at 10 years, should be taken into account.

Geographically, some issues should be considered. According to the direct relation that link fluid intake and body hydration and urinary stones (see Section 1.1.3. ), hot and dry climates favor the formation of stones. Indeed, the oil rich countries, especially Saudi Arabia, have been pointed out as the territories where urinary lithiasis has a highest incidence, reaching 20% of the population 13. It is worth to mention though, that reports on urinary stone incidence are available only from some countries.

**1.1.3. Causes of stone formation**

Urolithiasis depends on many different factors, comprising from individual conditions to geographical location and lifestyle. In order to help on the understanding of the disease and the correct interpretation of the results included in this work, the most important elements conditioning urinary stones formation are listed in Table 1.1 and Table 1.2. According to the complexity of those factors, a basic differentiation between factors has been done. Firstly the individual factors are listed; those inherent to the patient and that cannot be changed. In the second place, although not less important, the list includes environmental and socioeconomic factors, that can vary along the patient’s life.

Table 1.1 General factors, inherent to each individual with a demonstrated influence on urinary lithiasis<sup>i</sup>. In this table some urinary stone types are cited, whose characteristics are described in Section 1.2.

Factor	Comments
<b>Factors inherent to each individual</b>	
Age	Urinary lithiasis typically affects patients from 30 to 70 years old. Some stone types present particular risk features 14: calcium oxalate first episodes is usually experienced during the second/third decades of life (peak between 40 and 50 years); uric acid stones increase the risk of appearance in mature patients (peak at 60-70 years).
Race/Ethnicity	A careful analysis of the influence of race in the formation of urinary stones should be made, since quite often diverging races include also geographic differences. Despite this fact, some studies have been carried out in the USA, showing that Caucasians present a higher incidence of stones, while Black ethnicities suffer less (around 50%) from this disease. Asian and Hispanic stand in a middle plane 15.
Sex	As described in Section 1.1.2. , men suffer generally more often from urinary stones than women (urinary lithiasis affects 13% of men and 7% of women 10). Still, the ratio of stone episodes men:women has been decreasing for the last decades 16. The overall prevalence (part of the population affected by the disease) of urinary stones is, then, 9% in men and 4% in women 17. Epidemiologically, evidence has been shown, that different types of stones affect differently men and women. According to a local publication, the men:women stone formation ratio was for 2,8:1 calcium oxalate, 3,7:1 for uric acid, 1,4:1 for calcium phosphates and 0,7:1 for infected stone disease 18.
Genetics	Especially important for some types of urinary stones, DNA is also conditioning this disease. Cystine stones are the main known “inherited” group of urinary stones, since their formation directly depends on a genetic alteration of the metabolism of this amino acid. Besides, other disorders related to stones have been pointed out to have linkages to DNA: hypercalciuria, which affects calcium nephrolithiasis; hyperoxaluria (mainly primary hyperoxaluria), a risk factor for calcium oxalate stones and hyperuricosuria, which naturally influences uric acid stones 11.

<sup>i</sup> Although some data has been retrieved from local publications, the data can be directly extrapolated to any developed country.

The factors listed in Table 1.1 have been gathered based on epidemiological studies. Therefore, those statistics reflect general trends that have been demonstrated, but a single patient cannot act against them. Indeed, stone metaphylaxis is based on the control of other factors, i.e. those listed in Table 1.2. Although each stone type has particular prevention conditions, some general considerations suitable for all types of urinary stones can be considered.

Table 1.2 General factors, related to environmental and socioeconomic conditions that influence urinary stone formation.

Factor	Comments
<b>Environmental and socioeconomic factors</b>	
Fluid intake	Without a shadow of a doubt, the first piece of advice any physician gives to a stone patient is actually quite evident: increase the fluid intake. With the exception of some carbonated beverages and plant extracts drinks, such as tea, increasing the fluid intake is the easiest measure to sink the stone formation risk. It is generally considered that a urine volume below 1L/day is a clear risk factor; the recommended urine volume is >2L/day 19,20.
Diet	A number of studies have demonstrated that diet is a major regulatory factor of stone formation 21,22. Granted, all the promoters or inhibitors found in urine need to be first ingested by the individual, so this becomes one of the basic factors for stone formation regulation. There is a clear need to carry out more works focused on the precise role of each nutrient in the stone formation process. However, this influence is obvious, and the ingestion of some nutrients is precisely controlled by physicians: calcium, oxalate, animal protein and potentially acidic foods or drinks appear recurrently on this list.
Climatic factors	As stated, the formation and growth of urinary stones are strongly bound to the hydration degree in the body. Thus, it appears logical that certain climatic conditions can influence this disease. Certainly, it has been demonstrated that dry, hot climates facilitate the disease, with a more intense effect for temperatures higher than 27°C and humidity below 45%. Interestingly, an Italian hospital studied the seasonal influence of climate on the number of renal colic episodes attended at the Emergency Room (ER) though several years, and a cyclic response was observed (Figure 1.4.a) 23.
Socioeconomic level	Some studies have shown how the wealthiest societies suffer more from urinary stones 24. A higher income is usually linked to an increased intake of animal proteins and sugars, so urine pH and calcium/oxalate levels are altered. Figure 1.4.b clearly indicates such effect (note that, in that Figure, data stand for late 1990s).
Geographic location	Urinary lithiasis is a worldwide problem, although some specifications may be listed. The disease shares incidence and prevalence rates, as well as type of stones in USA and Europe. The countries in the Middle East seem to present an increased lithogenic risk. It must be admitted, though, that this factor is, in a great extent, mixed with socioeconomic issues and ethnicities. In the USA, where many studies focused on urinary stone formation have been conducted, even a “stone belt” has been identified, which includes the Southeastern part of the country. Remarkably, it has been suggested that climate change shall lead to an increased stone formation risk in some regions, as this stone belt (see Figure 1.4.c).



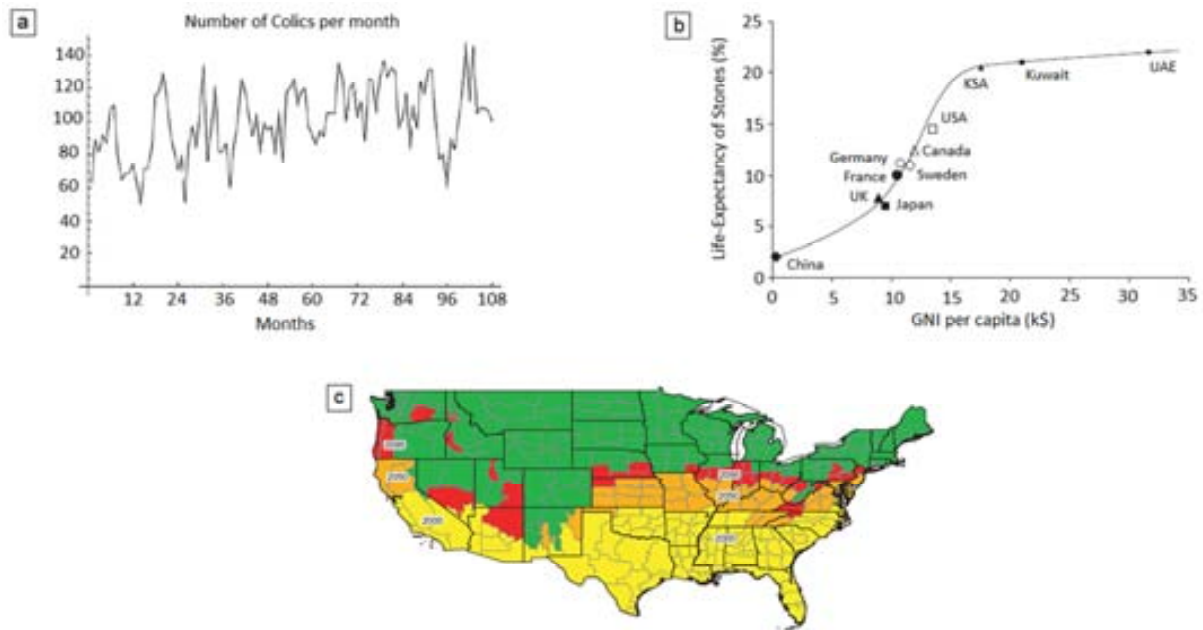


Figure 1.4 a. Number of renal colic episodes per month (Padova, Italy 23) b. Relation between life expectancy of urinary stones for men <70 years and GNI (Gross National Income) per capita, in USD, for several countries 24 c. “Urinary stone belt in the USA” yellow, orange and red stand for the predicted expansion due to climate change (and expected years: yellow 2000, orange 2060, red 2095) 10.

#### 1.1.4. Medical manifestations and detection of stone disease

The formation of a urinary stone itself should not be regarded as a diagnostic in any case. On the contrary, the stone shall be considered as an alarm going off, a signal for an underlying disease. Clinicians are supposed to solve the stone episode, but also to keep the guard up for any change in urine composition and in the patient’s general state 11. As in many diseases, several clinical manifestations can be described for urinary stone disease.

When the stone is located in the kidney it normally stays with none or little pain. Indeed, the formation of the stone usually proceeds without any ache for the patient, so the time of formation is generally unknown. This situation, described as asymptomatic lithiasis, is normal in the first stages of the disease, as well as when the stone stops its growth due to correct management. Although some stones might be expelled without pain, it is not the most common situation.

Some stones can be pushed down the ureter causing only a general, non-localized pain. These patients complain about pain in the lateral abdominal region and suffer from chronic discomfort.

However, the reality of stone disease is often different. Since stones block partially or totally the urinary tract when they migrate from the upper urinary tract to the lower, they produce a severe pain in the lumbar region. This process corresponds actually to the well-known acute renal colic 25.

Interestingly, the simple examination of a patient does not lead to the conclusion that the ongoing situation is a renal colic. Blood values are usually normal, and urine parameters tend to be within the normality intervals, only altered by the count of red or white cells, due to internal bleeding and infection.

The treatment of an acute renal colic episode is based on the administration of an adequate dose of analgesics. When a urinary stone is naturally expelled, with no surgical intervention, little can be made for accelerating the passage of the stone other than offering relief to the patient 26 (see Section 1.4.1. for detailed information).

Visits to the ER due to renal colic account for 1% of the total amount of patients treated. Although it might not seem an excessive number, it must be considered that these patients generally need a high dose of pain killers and related drugs; they suffer one of the most intense pains described 27.

Given that urine or blood analyses cannot offer a defined conclusion on whether a patient is suffering a renal colic, imaging techniques are normally the most useful tools for definitely assure the existence of a stone. Among the several approaches readily used in clinical practice, the most common will be briefly cited here 28 29 30.

Plain abdominal radiographs have been widely used, since they are accessible; cover the kidney-ureter-bladder (KUB) region and show urinary stones at any point of the urinary tract. However, only calcium lithiasis is opaque to X-Ray radiation, so 10-15% of the stones (uric acid) remain invisible to this technique (see Section 1.2. for urinary stones description).

An intravenous urography (IVU) requires the injection of iodine containing contrast solutions in the patient. IVU can clearly show which point of the KUB area is blocked, due to a stacked renal stone. This methodology is, though, more aggressive to the patient than X-Rays.

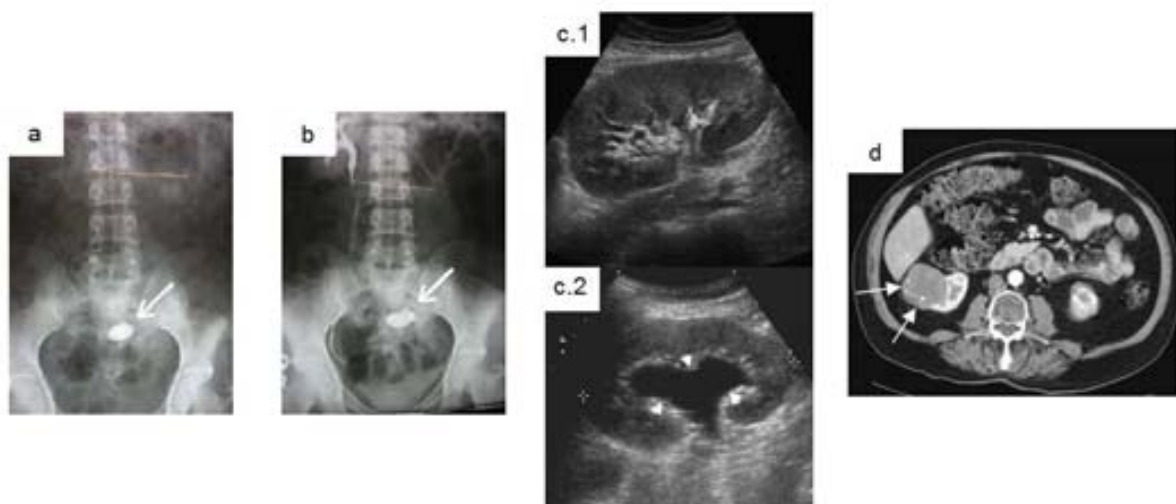


Figure 1.5 Typical images for the detection of stones. a. X-Ray image, the arrow points a bladder stone 30. b. X-Ray image after a IVU has been done (same patient as a) 30. c.1. Normal appearance of a healthy kidney. c.2. Kidney showing dilatation due to ureteral obstruction 28. d. CT scan of a patient, the white arrows show solid masses in the kidney 28.

Ultrasound (US) is often used as support diagnostic, since it requires little disturbances or exposure for the patient. The images are, of course, of a lower quality than other techniques, but they can point out local infected tissues and obstructed KUB areas.

The most effective technique is computed tomography (CT). CT allows the recording of higher quality images (see Figure 1.5) in few seconds. The whole abdominal area is pictured, so the physician can get a truly general picture of the patient state: existing stones, location of possible infection points and other issues concerning the patient’s health. As drawbacks, the administration of intravenous contrast agents and the considerable amount of radiation administered to the patient should be considered.

### 1.1.5. Urinary lithogenesis

Urine can be doubtlessly pointed out as a really complex fluid. Indeed, the formation of urinary calculi depends on a large number of chemical equilibria that take place simultaneously in urine. The term “lithogenesis” stands for the ensemble of processes that lead to the formation of calculi within the urinary tract 31.

The large number of factors involved, as well as their different nature (chemical, physical...), have led to the definition of a few stages in the urinary lithogenesis 31:

1. Urinary saturation
2. Crystal germination
3. Crystal growth
4. Crystal aggregation
5. Crystal agglomeration
6. Retention of crystallized particles
7. Growth of the stone

In this Section, only the most relevant steps for this work will be detailed. Naturally, all the steps play a role in the stone formation, but due to the focus of the present thesis, precise description of only some of them will condition the understanding of the work developed.

#### 1.1.5.1. Urinary saturation

Urine is a permanently saturated fluid, from a thermodynamic point of view 32. For the correct comprehension of the urine case, a precise definition of the term *saturation* is needed. The saturation of a solution is related to a specific compound and for ionic compounds present in an aqueous solution, as the case of urine. A saturated solution can be defined as the solution where the activity product of the given compound is higher than its solubility product,  $K_s$ . The  $K_s$  value stands for the thermodynamic

solubility constant, related to the limit amount of solute that can remain in solution before the precipitation is energetically favored.

The saturation (S) of a solution is the ionic activity product divided by the  $K_s$ . Thus, three different general states can be defined for a solution (and also urine). Saturated urine ( $S=1$ ) is stable for indefinite time; no precipitation or dissolution processes are observed. If the amount of solute increases ( $S>1$ ), precipitation will take place until saturation state is recovered. The opposite situation is described by  $S<1$  or undersaturation. This description, however, refers to the thermodynamic aspects only.

If kinetic parameters are also considered, the precipitation of components might deviate from the parameters explained above. The existence of some components in urine that might hinder the precipitation (precipitation inhibitors, some examples are listed in Section 1.1.6.2. ) causes deviations from the thermodynamic reasoning. When the concentration of a given compound is higher than its formation product ( $K_f$ ) the solution is supersaturated. This leads to nucleation and crystal growth. In the opposite scenario (concentration lower than  $K_s$ ), no solids are formed. The region between both equilibria described here is known as metastability region. Indeed, urine is usually found as a metastable solution 33. This system, defined by kinetic and thermodynamic parameters, is described in Figure 1.6.

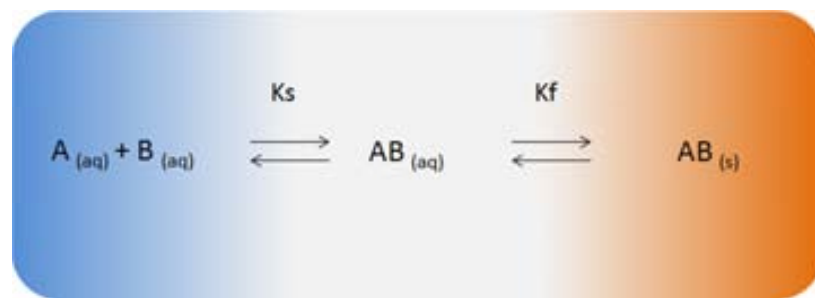


Figure 1.6 Schematic view of the three possible saturation states in urine. The two equilibria shown define the border between unsaturated, metastable and supersaturated urine. Blue: undersaturated, White: metastable, Orange: supersaturated.

The three possible saturation states of urine pictured in Figure 1.6 can also be related to certain conditions 31. The undersaturated region is only found by large liquid intake treatments; the supersaturated area, if persistent, might fit with genetic disorders. In most cases, urine is found in the metastable area, closer to any of its ends depending on fluid intake and diet characteristics.

According to their  $K_s$ , most of the ionic components usually found in urinary stones could precipitate (see values in Table 1.3). However, the conditions in urine allow most of these species to remain in solution or suspension, contained in the metastable phase. In addition, most of the stone components keep a close relation with urinary pH, so its regulation becomes a major factor when trying to avoid the formation of solid concretions in urine. For instance, according to Table 1.3, apatite would be expected to readily precipitate in urine. However, this species quickly dissolves when the acidification of the environment is effective. This observation totally fits with the implicit inclusion of pH in the thermodynamic constants of the precipitation equilibria.

Table 1.3 Relevant precipitation constants for urine components. Values expressed as  $pK_s = -\log(K_s)$ . Data tabulated at 25°C in pure water.

Component	pKs
Calcium Oxalate Monohydrate 34	8.55
Calcium Oxalate Dihydrate 34	8.31
Uric Acid Dihydrate 35	9.05
Carbonate Apatite 33	56.0
Brushite 33	6.70
Struvite 36	9.94

However, thermodynamic calculations do not explain the crystallization process on the whole. Important issues, for instance surface processes might have not been considered, although their influence on the process is remarkable. In addition, as previously stated, kinetic factors should also be considered 37.

#### 1.1.5.2. Stone formation

This Section will describe the main steps on the stone formation, explaining steps 2 to 7 listed at the introduction of Section 1.1.5.

Based on the assumption that urine is usually a saturated fluid, it can be thought that any nucleation point should serve as starting brick for the formation of the stone. In this sense, two types of nucleants can be highlighted as precursors of the crystal germination: homogeneous and heterogeneous. The former can be located in the metastable zone (see Figure 1.6), when some of the ions that will form the structure of the stone can precipitate to form a solid deposition. However, this situation case is not the most common. Urine of stone and non-stone formers is generally found in metastable region, so locating the starting point in such conditions would not fit with an important number of cases 31. On the other hand, the heterogeneous formation of crystals can take place when urine is supersaturated, state described in Figure 1.6. One of the most common situations of heterogeneous crystallization has been described as a small nidus of carbonate apatite, which serves as scaffold for the further crystal growth of calcium oxalate 38. Randall’s plaques are due to different and characteristic circumstances in which apatite acts as the seed for a calcium oxalate stone, producing an injury in the inner renal tissues. This phenomenon causes the formation of papillary stones 39 (detailed description in Section 1.2.1.1.2. ).

Once the initial step has taken place and the conditions that lead to the formation of a solid deposition keep constant, several crystals can aggregate to form a larger mass, which could be too big to leave the nephron point at which it has been formed. Indeed, crystals are aggregated in urine from non-stone formers, but the size of such crystals is usually  $<2 \mu\text{m}$ , so it can be excreted normally and its further growing is hindered 40. In any case, the nucleation step takes place continuously and the stone formation process is a consequence of the microscopic crystals aggregation to form macroscopic entities.

While the precise mechanisms describing this progression have not been well defined yet, their close relation with the lithogenesis processes was pointed out a number of decades ago 41. Crystal growth, that is, the growth of new crystals onto the surface of an existing particle (of the same chemical structure or not) is a slow process. On the other hand, it seems clearly feasible that crystals, as micrometric particles, will collide with each other while they meet in kidney cavities. Therefore, the agglomeration of already existing structures seems a feasible process for leading stone formation 42.

When the structure reaches a macroscopic dimension its normal excretion from the urinary tract turns very unlikely. This step can be stressed if the agglomeration created is found in a renal cavity with low urodynamic flow 43. In this case, the growth of the already formed stone will be favored by the existence of such cavities in the kidney, since they allow the slow crystal growth process to take place.

### 1.1.6. Promoters and inhibitors of crystallization processes

As seen in the previous section, stone formation is a complex, multistep process. In fact, because of the complex matrix represented by urine, a number of species may interact with the crystal structure and play a remarkable role in the stone formation. This Section will give details only on those species with a most significant impact on the process and thus, more relevant for the understanding of this work.

#### 1.1.6.1. Crystallization promoters

The species usually found in urine which act as crystallization promoters are, basically, the same ionic components that form the stone itself. Thus, each type of stone will be affected by a different type of promoter. In addition, other substances have also been identified as promoters.

Organic matter, often found in urine in the shape of small biological particles, can become a suitable starting point for the precipitation of some urinary components. In particular, calcium oxalate monohydrate is usually deposited on such organic seeds, so the core of the stone becomes a mixture of organic matter and calcium oxalate 44. Also some protein aggregates have been proven to act as nucleation point for the further precipitation of crystals 45.

The close relation between calcium and oxalate is described in Figure 1.7 **Error! Reference source not found.** The combined promoter effect for these ions can be appreciated here. Naturally, the increase of the concentration of calcium or oxalate ions affects the crystallization potential by increasing urine saturation respect calcium oxalate CaOx. In this Figure, the blue line represents the limit calcium concentration to consider hypercalciuria (3.8 mmol/l), while the grey line describes hyperoxaluria (0.31 mmol/l). When calcium concentration reaches hypercalciuria, an increase in oxalate concentration leads to the rise of CaOx activity product, while the  $[Ca]/[Ox]$  value decreases. This situation ends up, after a critical point, in hypercalciuria and hyperoxaluria. Thus, the risk areas correspond to the upper, lower and right regions in this Figure.

Other promoters are well described in literature 45.

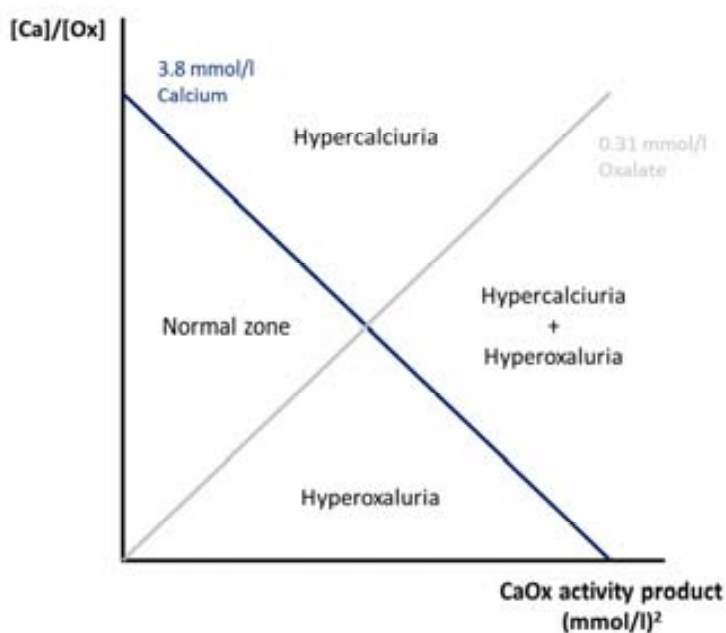


Figure 1.7 Schematic representation of the urinary saturation states in regard to calcium oxalate stones, indicating metabolic risk areas.  $[Ca]/[Ox]$ : Calcium to Oxalate concentrations ratio. The values indicated in this Figure stand for the limit of hypercalciuria and hyperoxaluria; blue line represents calcium concentration; grey line, oxalate. Adapted from Daudon, 2012 31.

#### 1.1.6.2. Crystallization inhibitors

Species proven to be effective inhibitors of urine include a high variety of substances, which embraces from inorganic cations to protein aggregates. This Section will introduce those inhibitors more widely described and also used as therapeutic agents.

The most studied crystallization inhibitor is citric acid, which chemical structure is shown in Figure 1.8. This organic acid imprints a remarkable effect on calcium stones, because the citrate ion readily chelates calcium ion, preventing it from precipitating with any other urine component. Besides, its tri-protic structure provides citrate important buffering properties. Those characteristics are emphasized by the fact that its concentration is the highest among all the crystallization inhibitors usually happening in urine, usually about 1 mM<sup>45</sup>. This component is found in a number of vegetables and fruits, this is why the consumption of citrus fruits is so recommended for combating stones. No wonder that this ion has become a recurrent treatment as an oral drug; it is not harmful and different types of stones can benefit from its action (discussed in Section 1.4.2.2. ). Low concentration of citrate is one of the main indicators of high lithiasic risk, since hypocitraturia has been described in most CaOx stone formers<sup>46</sup>.

The mechanism of action of citrate is described in the reactions shown in Equation 1.1 and Equation 1.2. Their equilibrium constants at 37°C are  $2.7 \cdot 10^4 M^{-2}$  and  $60 \cdot 10^4 M^{-1}$ , respectively<sup>47</sup>. From these values we can gather that  $Ca^{2+}$  will bind preferentially to citrate to form a very stable complex instead than forming the insoluble salt with oxalate, so the precipitation is reduced in a great extent.

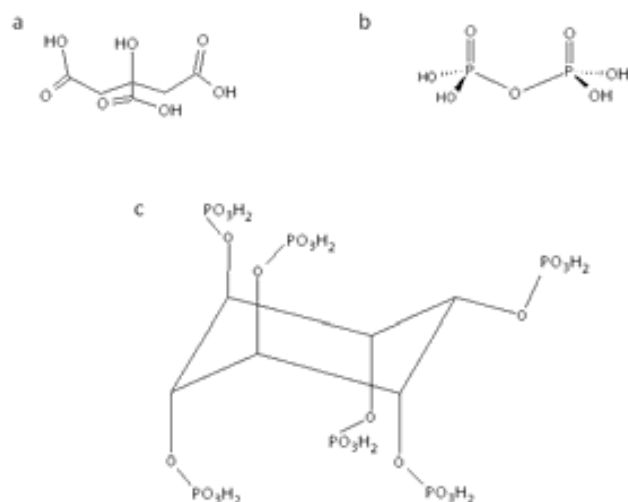
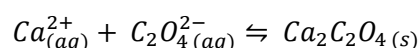
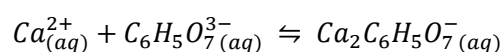


Figure 1.8 Chemical structure of some crystallization inhibitors. a. Citric acid. b. Pyrophosphoric acid. c. Phytic acid. Their most common chemical form in urine corresponds to the partially deprotonated structures, according to urine pH.

Equation 1.1 Precipitation equilibrium of calcium oxalate



Equation 1.2 Complexation equilibrium of calcium and citrate



Magnesium, widely abundant in the human body, has also been pointed out as an efficient inhibitor of stone formation. Indeed, the spike of a saturated solution in calcium oxalate with a concentration of  $\text{Mg}^{2+}$  of 2 mmol/L halves the formation of crystals. In the case of apatite stones, magnesium binds to the surface and avoids crystal growth. Despite the usefulness as inhibitor, supplementation of this nutrient for the specific treatment of stones has not been encouraged, partly because it is highly absorbed and little circulates through the blood torrent, and so, filtered in the kidneys 48 49.

Polyphosphates are powerful actors stopping stones from growing. Orthophosphate concentration in urine is high, yet it has no inhibitory effect at all. On the contrary, more complex phosphates, as pyrophosphate (PPI) and phytate (IP6), are listed among the most efficient stone formation inhibitors. PPI, which is found in urine in the range 20-40  $\mu\text{M}$ , has proven to inhibit calcium oxalate and infected stone disease calculi, and its excretion is significantly lower in stone formers 50 51. IP6 ranges in a much discrete concentration, around 1  $\mu\text{M}$ , although its inhibition capabilities (proven in urinary stones and other calcifications) are remarkable 52. Some quantification methodologies have been suggested for the identification of these urine components. However, the medical community is not totally concerned with the quantification of such analytes, in part because some of the methodologies developed are tedious or not totally accessible to hospital laboratories 53 54.

Other entities, also described as inhibitors of stone formation are listed in Table 1.4, along with the type of urinary stones whose growth they hinder.



Table 1.4 List of the main inhibitors of the crystallization of urinary stones (adapted from Daudon, 2012) 31.

Low molecular weight		Macromolecules	
Species	Target	Species	Target
<b>Cations</b>		<b>Proteins</b>	
Zn <sup>2+</sup>	CaOx	Tamm-Horsfall	CaOx
Fe <sup>3+</sup>	CaOx	Nephrocalcin	CaOx
Mg <sup>2+</sup>	CaOx	Uropontin	CaOx, Phosphates
<b>Anions</b>		Bikuin	CaOx
Citrate	CaOx, Phosphates	Fragm. 1 prothrombin	CaOx
Isocitrate	CaOx, Phosphates	Fibronectin	CaOx
Phosphocitrate	CaOx, Phosphates	Calprotectin	CaOx
Pyrophosphate	CaOx, Phosphates	Lithostatin	CaCO <sub>3</sub>
Phytate <sup>i</sup>	CaOx	<b>Glycosaminoglycans</b>	
Aspartate	CaOx	Chondroitin sulphate	CaOx
Glutamate	CaOx	Heparin sulphate	UA
Hippurate	CaOx	Keratan sulphate	CaOx
<b>Co-factors</b>		Dermatan sulphate	CaOx
pH	UA, Phosphates	Hyaluronic acid	CaOx, Phosphates
Ionic strength	All types		

<sup>i</sup>This inhibitor has been added to the information from the reference source; from Grases, 1989 55.

CaOx: Calcium Oxalate; UA: Uric Acid

### 1.1.7. Stone formation risk assessment

Urinary lithiasis is characterized by a high incidence and prevalence, which has shown a positive increase over last century (see Section 1.1.2. ) and represents a considerable portion of the budget for public health institutions (see Section 1.5. ). If this background is considered, the prevention of formation of urinary solid depositions becomes one of the main factors to control in this multifactorial process. Thus, determination of stone formation risk through the monitoring of urinary parameters has been an important goal for clinical researchers for the last decades.

Some analytical methodologies have been developed, which predict the likelihood of stone components to precipitate, either based on theoretical calculations or empirical approaches 56. This Section offers an outline on the most representative alternatives in this field.

#### 1.1.7.1. Relative Supersaturation

Urine Relative Supersaturation (RSS) is clearly different to other approaches in one facet: the estimation of stone formation risk is based on theoretical calculations. This method has naturally some drawbacks, but its advantages have let RSS become one of the most used and reference methodology for assessing stone formation risk 56.

The calculation of RSS for a urine sample is based on the determination of a series of urinary parameters and the estimation of complexation and precipitation phenomena, according to thermodynamic equilibrium constants. The value is given as the ratio of the activity product of a given component (Calcium Oxalate Mono- or Dihydrate, Apatite, Struvite...) to the  $K_s$  of the salt. For the determination of RSS values different software have been developed, as SUPERSAT 57, EQUIL 58 or JESS 59. As seen with other risk index estimations, RSS values equal to 1 mean urine saturation; values lower or greater than 1 mean under or supersaturation of urine respect that given component 57 60.

For a correct interpretation of the urine composition, a large number of components must be quantified. The list generally includes: cations ( $Mg^{2+}$ ,  $Ca^{2+}$ ,  $Na^+$ ,  $K^+$ ,  $NH_4^+$ ), anions ( $Cl^-$ ,  $SO_4^{2-}$ ,  $PO_4^{3-}$ ), organic molecules (citrate, oxalate, uric acid, creatinine), and urine pH. These twelve parameters can also be complemented by the measurement of other minor components that play an important role as inhibitors, such as glycosaminoglycans or pyrophosphate ( $P_2O_7^{4-}$ ). Other important inhibitors are listed in Section 1.1.6.2. The software used for the calculations allows a long list of other urine components to be taken into consideration 61.

The main advantage of RSS is that the stone formation risk for different types of stones is calculated simultaneously. By taking all the listed components into the calculations, a general picture of urine can be described, what makes RSS a very polyvalent methodology 62.

However, it should also be pointed out that RSS bases its results on calculations, which, in turn, rely on several assumptions, in regard to the equilibrium constants and species considered. This methodology assumes that urine behaves *ideally*, as expected from the interaction between its main components. Nevertheless, RSS undervalues the importance of inhibitors, since they are generally not quantified and, thus, not taken into the calculations. On top of this, the selection of the suitable equilibrium constants is critical; a slight change in some representative values could dramatically vary the supersaturation results. In brief, RSS is not a purely empirical model, so it has some inherent restrictions 63. Even if additional complex formation equilibria of inhibitors (that may produce masking of the related precipitation phenomena) are considered, RSS values will not be able to take into account other important phenomena taking place on the lithogenic process, e.g. superficial phenomena taking place at the micro seeds crystals that may avoid the aggregation process.

### 1.1.7.2. Activity Product Ratio

It is clear that crystallization processes in urine depend on a wide and complex number of factors. This fact poses a clear question on whether the estimation of stone formation risk can be precisely calculated only considering a simple urine analysis. Aware of these limitations, Dr Pak and co-workers developed a simple but effective method for the determination of stone formation risk based on an empirical experiment 64.

This methodology, the Activity Product Ratio (APR), was thought as an experimental approach, so it was performed using *real* urine. The fact that a real sample is used guarantees that all the components

naturally occurring in it will participate on the *in-vitro* crystallization process, including inhibitors, promoters and other agents as pH or proteins.

APR test consists on the incubation of urine with a solid seed for a given time and the determination of the activity product ratio before and after the incubation process. The seed used is usually the pure substance for which the precipitation risk is to be determined. The incubation time is typically 48 hours, since it has been demonstrated that this time frame is enough for the equilibration of the system. The APR is then calculated as the ratio between the initial and final concentration of the ions involved in the formation of the stone as shown in

Equation 1.3 for BRU stones 65. Similarly, it can be applied to other stone types 66. According to this equation, an APR value equal to 1 means that urine is saturated in this component. APR values <1 mean urine is not saturated (the solid seed is dissolved). APR values >1 mean urine is supersaturated in this compound, so the stone formation risk is high.

Equation 1.3 Calculation of APR based on the example of BRU stones (CaHPO<sub>4</sub>·2H<sub>2</sub>O). *i* and *f* represent initial and final concentrations, respectively.

$$APR = \frac{[Ca^{2+}]_i \cdot [HPO_4^{2-}]_i}{[Ca^{2+}]_f \cdot [HPO_4^{2-}]_f}$$

As deduced from the description, this method requires a long laboratory work, which has been shortened to 3 hours in a recent review of the methodology 67. Despite the improvements, urine incubations are not generally included in routine analysis.

### 1.1.7.3. Bonn Risk Index

A very interesting approach for the determination of stone formation risk; the Bonn Risk Index (BRI), was developed at the laboratories in the University of Bonn Clinic (the methodology was named after its home city). This method consists, as APR, in an empirical measurement. The time required for the analysis is much shorter, though, because the urine crystallization potential is “titrated”.

The measurement consists on the titration of a freshly collected urine sample with ammonium oxalate solution. The oxalate concentration that triggers the start of crystal formation indicates the titration end point and is determined by monitoring the formation of crystals with a laser probe (sensitivity range 0.5-250 μm). Previously to this measurement, the concentration of Ca<sup>2+</sup> is determined potentiometrically. This way, only free calcium ions are accounted for, which fits with the logical assumption that they represent the only calcium that could precipitate as calcium oxalate. After these determinations, the BRI value is calculated, as shown in Equation 1.4. As also seen for APR, the calcium oxalate crystallization risk can be defined as low or “no risk” (BRI <1 l<sup>-1</sup>) or high (BRI >1 l<sup>-1</sup>) 68.

Equation 1.4 BRI calculation. [Ca<sup>2+</sup>] is the initial free calcium concentration (mmol/l) and (Ox<sup>2-</sup>) is the added amount of oxalate (mmol) to the titration end point. The BRI units are l<sup>-1</sup>.

$$BRI = [Ca^{2+}] / (Ox^{2-})$$

It has been demonstrated, through studies including healthy controls and stone patients, that BRI can clearly distinguish both groups 69 70. BRI cannot be estimated by the only measurement of free calcium ion 71.

The main drawback of the BRI is that, due to its experimental definition, it can only be used for calcium oxalate stones. As stated in Section 1.2. , this group of stones represent the vast majority of cases, but still other type of urinary calculi cannot benefit from these measurements 56.

Despite its limitations, the BRI methodology has been commercialized by RAUMEDIC AG and a specific device was designed for this application.

Interestingly, a revision of the methodology has been recently done. It suggests the miniaturization of the BRI experimental set-up, especially the amount of urine needed 72.

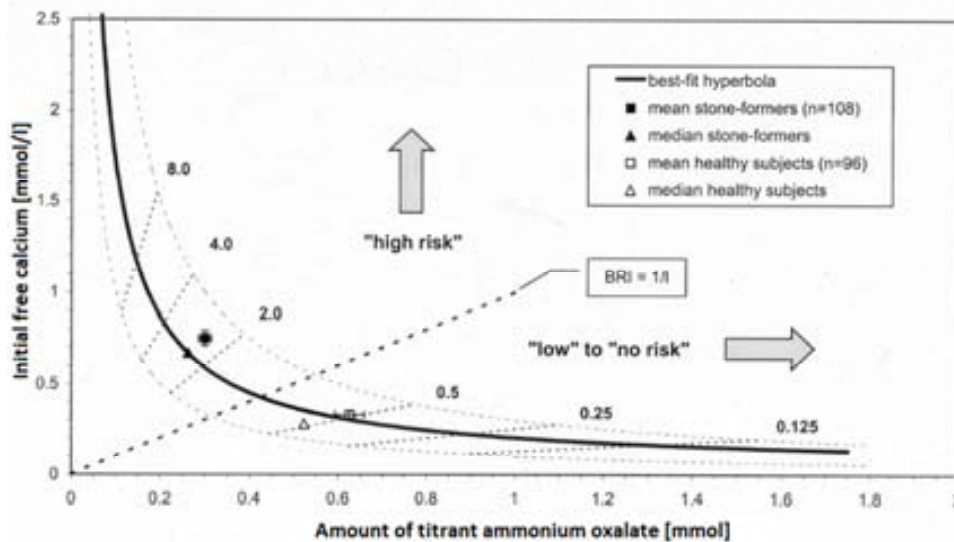


Figure 1.9 Free calcium concentration vs amount of titrant ammonium oxalate. The figure shows two areas of high and low risk, for BRI values  $>1l^{-1}$  and  $<1l^{-1}$ , respectively. Bold numbers name lines of constant BRI values. Dashed lines around the hyperbola denote 95% of data in the mentioned study. Adapted from Laube, 2004 69.

## 1.2. Classification of urinary stones

As seen in the previous Sections, urolithiasis is a complex disease that depends on a considerable list of factors and involves a large number of substances. It becomes clear, thus, that the chemical nature of stones might differ dramatically depending on the stone formation conditions. The incidence of each type of stone, according to chemical composition, is reflected in Figure 1.10.

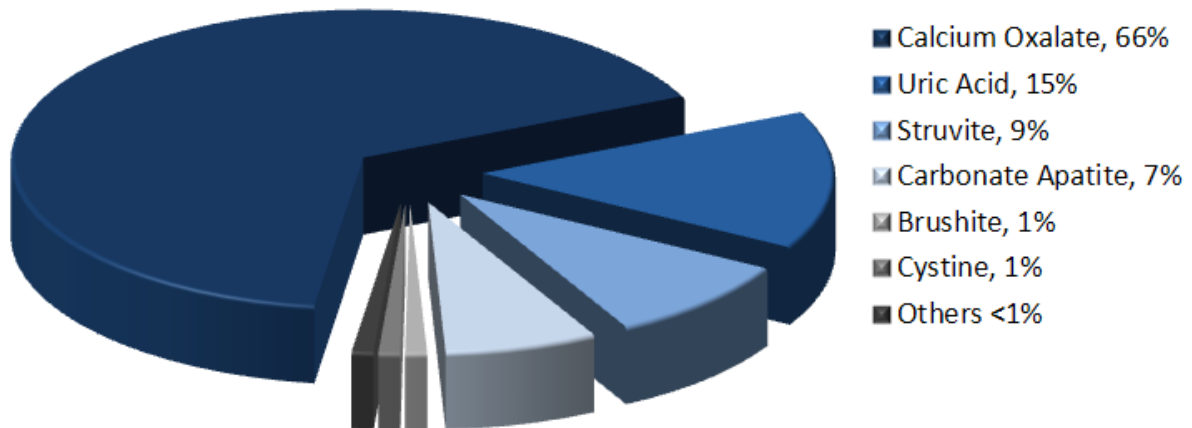


Figure 1.10 Frequency of incidence for each type of urinary stone, considering only its chemical composition 73. The values listed include the frequency of each component as a pure stone or as part of renal calculi (mixed stones). Indeed, not only the chemical composition might vary, but also the structure of the resulting stone has been pointed out as a very important feature in the stone description 44.

The proper diagnostics of the stone disease is directly linked to a precise description of the renal calculi (chemical composition and structure). In fact, the stone could be considered as a fossil that carries the patient’s medical history related to stone disease. In other words, the urine conditions and so, the metabolic disturbances the patient has gone through, leave a particular trace in the stone. The correct understanding of this trace makes possible to get a better treatment of the disease, which in turn, leads to an improvement in the patient’s quality of life.

Due to the importance of the correct description of urinary stones, this Section will introduce the main features of the most relevant types of renal calculi, along with the most important etiological factors that favour their formation.

The classification of renal calculi has been addressed by different authors. The organization of stone types described here is based on those works 44 74 75. Although other classification criteria might be considered, the one selected in this Section, based on chemical composition, seems the most suitable for the comprehension of further Sections in this work. The main chemical and physical features for each stone type will be described here, along with the most relevant etiologic factors that lead to their formation.

According to their different origin, each stone type requires a different management. A description of the main recommendations on diet and lifestyle is provided in Section 1.4.2.

### 1.2.1. Calcium Oxalate

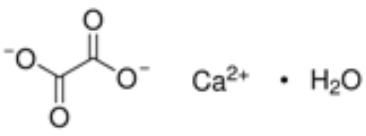
This varied group of stones is, by far, the most common in stone patients (SeeFigure 1.10). Indeed, around 60-70% of urinary stones show this composition in developed countries 76. It is important to note that, despite its chemical composition might not include any other ion, calcium oxalate (CaOx) can be found in different chemical forms. These have diverging physical properties, and more importantly,

different etiological origins. It has been determined that CaOx precipitates as the monohydrate (COM), dihydrate (COD) or trihydrate (COT) derivative. COM is the thermodynamically most stable derivative, COD is the fastest formation derivative, and COT has been rarely found in urine or urinary stones 77.

It is thus clear, that the formation of COM and COD is the result of remarkably different etiological factors, so their correct classification is needed for the correct description of the problem affecting each patient.

### 1.2.1.1. Calcium Oxalate Monohydrate

Table 1.5 Calcium Oxalate Monohydrate general characteristics 78.

Stone type	Calcium Oxalate Monohydrate
Chemical formula	$\text{Ca}_2\text{C}_2\text{O}_4 \cdot \text{H}_2\text{O}$
Molecular structure	
Mineralogical name	Whewellite
Incidence (from total) <sup>i</sup>	Cavitary 24%; Papillary 5%

<sup>i</sup>Data from own, unpublished research.

#### 1.2.1.1.1. Cavitary Calcium Oxalate Monohydrate Stones

The thermodynamically favored derivative of CaOx is often found as main component of urinary stones. Calcium Oxalate Monohydrate (COM) stones are very compact solids, which are formed by the continuous addition of crystals to the existing lattices, with little defects within the structure 79. COM stones are formed in areas where urine hydrodynamic flow is low. The core of the stone is born in these locations, usually as an agglomeration of organic matter or carbonate apatite, described as a porous, structure-lacking region. This area can vary in size depending on each case 80.

Once the nucleation point has been formed, COM crystals grow on its surface, following a columnar pattern, which is clearly recognizable by optical microscopy 33. Some clear examples of such structure are shown in Figure 1.11. COM stones tend to create a dense structure, which allows further nucleation points to stick onto the surface, so new columnar crystals grow from these *secondary* nuclei. This fact makes the external part of the stone have lobulations, recognizable even at naked eye (see Figure 1.11.c).

Despite its compact formation, COM crystals tend to accumulate organic matter between lattices 79. According to bibliography, organic matter can accumulate repeatedly on the surface during the stone formation, creating concentric accumulation every ca. 100  $\mu\text{m}$  81. While it is generally believed that the core of the stone concentrates organic matter, the composition of the described concentric rings can be

discussed. A study included in this Thesis has characterized such concentric structures as COD, as precisely described in Section 2.4.

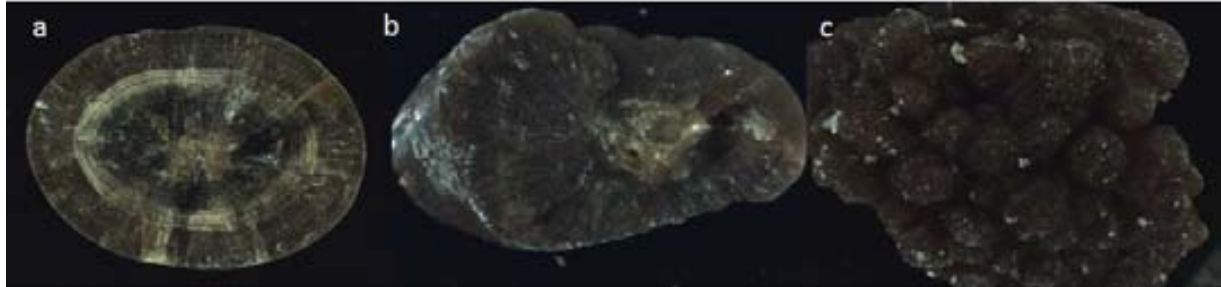


Figure 1.11 Examples of cavitory COM stones. a, b. Cut sections from COM stones. c. Surface of a COM stone, with little COD deposits. The lobulations can be clearly appreciated. Pictures from self-built database.

#### 1.2.1.1.2. Papillary Calcium Oxalate Monohydrate Stones

While the general structure of the stone is the same as cavitory COM calculi, this group of stones is characterized by a particular crystallization point, which clearly defines a unique lithogenesis process. Papillary COM calculi grow from a calcium phosphate deposition that is attached to the renal inner tissue (or renal papillae) 82. The calcium phosphate plaques on which the COM crystallizes are known as Randall’s plaques, after Dr. Randall first described them in 1940 83. These structures consist on the deposition of apatite on the loop of Henle. The existence of a solid structure stable and linked to the renal tissue favors the growth of COM crystals on it. The formation of Randall’s plaques can be related to the calcification of other tissues, as blood vessels 84. Some examples of papillary stones are pictured in Figure 1.12.

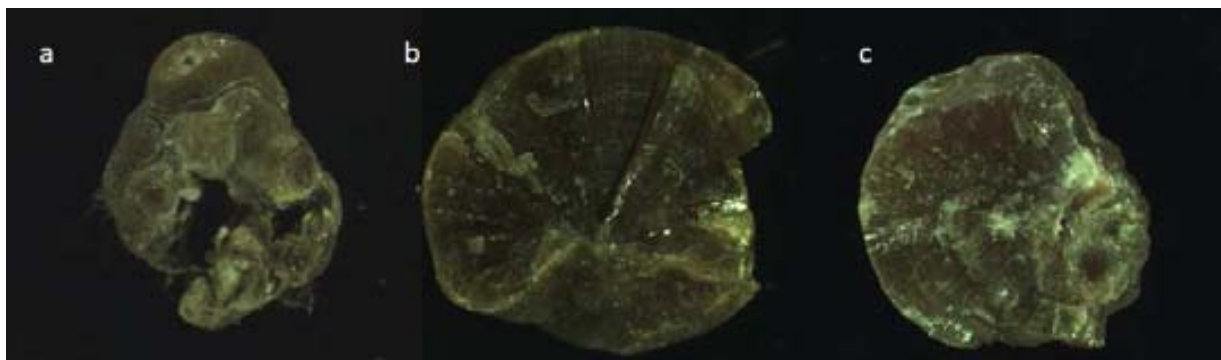


Figure 1.12 Examples of papillary COM renal calculi. a. External view. b, c. Cut stones, where the structure seen in Figure 1.13 is clearly appreciated. The stone c shows the typical Randall’s plaque as a white spot. Pictures from self-built database.

The structure of COM papillary stones can be easily recognized by stereoscopic microscopy, because this technique allows the visualization of the nucleation point (see Section 1.3.3. ). A schematic model of the typical structure is shown in Figure 1.13.a. This type of stones tends to be released from the papillae and COM crystals continue precipitating on the nucleation point. Thus, the structure of the stone is not always so clear, when it is observed by stereoscopic microscopy (see Figure 1.13.b for an example).

A model of the structure is shown in Figure 1.13.a. Papillary COM stones can also be unattached from the renal papillae. In this case, COM can continue its growing also on the Randall plaque side which was in contact with the tissue, creating a structure pictured in Figure 1.13.b. This structure makes the identification of the nucleation point somehow difficult. The core of the stone is usually formed of apatite, since it is the main component in Randall's plaques 39. However, organic matter can be found mixed with apatite very often 85.

According to some studies, the cause for the damage of the renal inner tissue might be related to intense contact to cytotoxic agents, due to professional activities or other causes. In addition, the intake of cytotoxic substances as ethylene glycol or a high dose of analgesic drugs can lead to the injury of the renal papillae at cellular level 86.

Due to the unique cause of formation of COM papillary stones, namely the injury and calcification of the inner renal papillae, it is important to characterize this group of samples. A proper treatment that avoids the formation of new stones should consider the causes of the papillae damage.

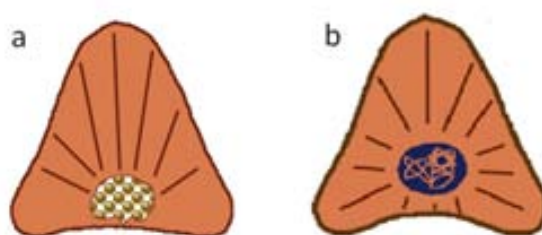
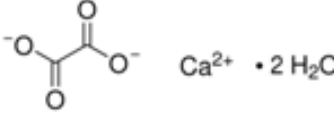


Figure 1.13 Typical structures of papillary COM stones 85. a. The Randall's plaque remains exposed. b. COM crystals grow onto the nucleation point, once the stone is unattached to the papillae.

### 1.2.1.2. Calcium Oxalate Dihydrate

Table 1.6 Calcium Oxalate Dihydrate general characteristics 78.

Stone type	Calcium Oxalate Dihydrate
Chemical formula	$\text{Ca}_2\text{C}_2\text{O}_4 \cdot 2 \text{H}_2\text{O}$
Molecular structure	
Mineralogical name	Whedellite
Incidence (from total)	Pure 8%; Transformed into COM (partially or totally) 15%

As stated, if only the kinetics of the precipitation is considered, the dihydrate derivative of CaOx is obtained. The structure of Calcium Oxalate Dihydrate (COD) is remarkably different from that seen for COM. The crystals take a characteristic, bipyramidal shape and the stone is formed when crystals attach



on to the other, creating a random arrangement. The fact that each crystal is a separate structure makes the stone more porous than COM. It is so, that even from the surface of the stone some cavities can be observed (see Figure 1.14).



Figure 1.14 a, c. External views of COD stones. b. Cut section from a COD stone. Pictures from self-built database.

#### 1.2.1.2.1. Calcium Oxalate Dihydrate – Transformation into COM

Interestingly, COD transforms into its more stable relative COM when it remains in contact with urine. This fact was described a few decades ago <sup>87</sup> and the process has been reviewed recently <sup>88</sup>. New spectroscopic data reveals that water molecules surrounding the COD solid can push the transformation. This fact has been also studied in this Thesis; high-resolution IR microspectroscopy has been used for the careful study of the structure in transformed stones (see Section 2.4. ).

This transformed product leaves a particular hint in the stone structure. Differently to pure COM and COD, the inner part of the stone presents a complete lack of structure, due to the loss of the bipyrarnidal shape of COD crystals. In addition, the presence of carbonate apatite depositions within the core of the stone (even on the surface) is often seen. Transformed stones might be created in areas of low urinary flow, so the described urine components can precipitate in these conditions <sup>33</sup>. In case of pH greater than 6, apatite is likely to create solid deposits. Figure 1.15 shows some examples where the described features can be appreciated.



Figure 1.15 a-c. Cut sections of transformed calcium oxalate stones. a. Alternate layers of COM and transformed COD are clearly seen. b, c. The core of the stone has transformed into the more stable COM, the structure, with many cavities, can be appreciated. The surface, especially in Figure b is still COD. Pictures from self-built database.

The surface of this type of calculi usually contains pyramidal COD crystals, since it is the younger part and its contact with urine has been short enough to keep COD as a pure component.

Transformed stones could even be considered as a class itself. For the reasons exposed, the existence of this stone indicates a persistent disease (probably including hypercalciuria and hyperoxaluria).

### 1.2.1.3. Etiological factors

Due to the complex mixtures found containing only calcium oxalate, often as a combination of COM, COD and/or transformed stones, the causes of the precipitation can be attributed to a number of factors, as summarized in Figure 1.16. Hypercalciuria, hyperoxaluria or lack of inhibitors stand as the main risk factors for CaOx stones 78. As generally seen for urinary stones, pH affects the formation of COM stones. Calcium oxalate generally precipitates in urines with pH values from 5.5 to 6.5 44.

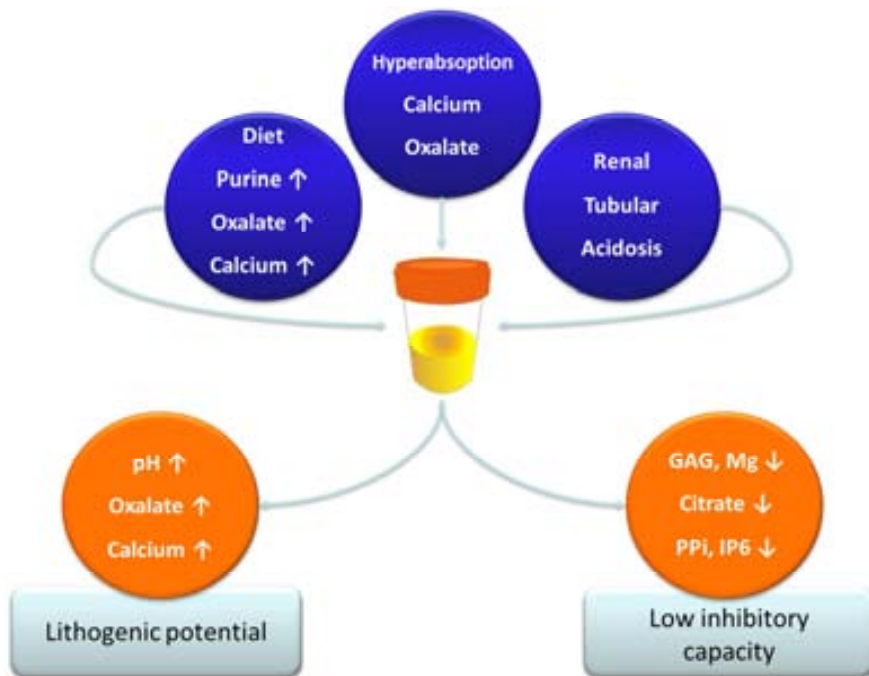


Figure 1.16 Schematic representation of the main groups of factors that pose an increased risk for CaOx crystallization. GAG: Glycosaminoglycans, PPI: Pyrophosphate, IP6: Phytate. Adapted from Hesse and Muñoz, 1994 78 89.

RTA, or Renal Tubular Acidosis, can also act as a promoter of the disease 90. Patients who suffer RTA are unable to keep urine pH at a normal - to slightly acid value, due to failure of bicarbonate absorption or impossibility to achieve a good pH gradient between blood and urine 91. A rather basic pH can be considered as an increased risk for CaOx precipitation.

Owing to the already discussed differences between COM stones (cavitary and papillary), mainly the nucleation point, some general considerations apply for the general picture of stone formation. Since COM is the thermodynamic derivative of calcium oxalate, its precipitation does not require unusually high concentrations of oxalate to occur, although hypercalciuria is usually seen in COM stone patients

92. Naturally, hypercalciuria or hyperoxaluria, either due to an excessive intestinal absorption of  $\text{Ca}^{2+}$  or oxalate ions or to other disorders, can be considered a risk factor for the formation of this group of stones, but other actors play an important role in this particular case. The driving force for COM crystallization is the existence of insufficient amounts of inhibitors. In this group, the most effective substance is citrate, which readily binds free calcium ions, thus preventing them from precipitation. However, other inhibitors such as phytic acid and pyrophosphate also have a considerable influence on COM crystallization 93 89. For a more precise description of the inhibitor mechanisms, see Section 1.1.6.2.

On the other hand, COD is normally formed at lower saturation levels, and higher calcium to oxalate ratio 94. This fact makes COD more sensitive to hyperoxaluria and, especially, hypercalciuria. It has been demonstrated in animal tests that hypercalciuria is required for the induction of COD precipitation 95. COM stone formers (which represent a higher portion of the total number of cases), are usually within normal or slightly high ranges for calcium and oxalate 96.

### 1.2.2. Calcium Phosphate

Another type of urinary stones is based on phosphate, which is one of the major ions found in urine, in terms of concentration. As a consequence, it is likely to precipitate together with calcium, due the variety of insoluble salts that this combination of species can lead to. Despite the similarity in their chemical nature, the stone structure and precipitation conditions of each type of calcium phosphate stones (CaP) differ strongly.

#### 1.2.2.1. Apatite

Table 1.7 Apatite general characteristics 78.

Stone type	Apatite
General chemical formula (apatites)	$\text{Ca}_{10-x}[(\text{PO}_4)_{6-2x}(\text{CO}_3)_{2x}](\text{OH})_2$
Specific chemical formula	Carbonate Apatite: $\text{Ca}_5(\text{PO}_4)_{2.5}(\text{CO}_3)_{0.5}(\text{OH})$
Mineralogical name	Dahllite
Incidence (from total)	7% pure, 32% as mixture

The close link existing between mammals and the ions calcium and phosphate is clear. The skeleton is basically made of hydroxylapatite, an ionic compound described by the chemical formula:  $\text{Ca}_{10}(\text{PO}_4)_6(\text{OH})_2$ . The low solubility of this species (see Section 1.1.5.1. ), though, represents a problem in urine, since the undesired formation of this solid takes place at basic pH values. The upper limit of metastability of apatite in urine remains blurry, although it has been set at the pH range from 6.5, according to Coe 97, to 6.8, as described by Bichler 98. Although the supersaturation of urine respect to

apatite can result in its precipitation, the acidification of urine effectively prevents the formation of solid concretions.

The structure of apatite in the body is still ambiguous and thus, diverging chemical formulas have been reported. In fact, apatites are a wide group of substances, found in the human body with different compositions 99. Hydroxylapatite, the most abundant apatite in biological systems, suffers structural modifications when it remains in contact with body fluids and tissues. This mineral accommodates carbonate ions within its lattices, becoming thus carbonate apatite. It is not clear yet, whether the carbonate ion actually replaces a tetrahedral phosphate ion 100.

Since the bibliography in the urinary stone field uses both terminologies (hydroxylapatite and carbonate apatite) depending on the source, this work will refer to this type of stone as carbonate apatite (CAP), in order to consider the described reaction.

CAP is usually found as the accumulation of small spheres of 5-10  $\mu\text{m}$  size, which precipitate as water-rich material 101. The dehydration process occurring afterwards defines a stone with low density and a porous internal structure 33, as seen in Figure 1.17. CAP stones show an important lack of structure, and also tend to accumulate a considerable amount of organic matter among the spheres agglomeration. Indeed, a recent study has defined CAP urinary stones as a composite together with polysaccharides and proteins 102.



Figure 1.17 a-c. Several views of internal cuts of CAP stones. The porous structure is clear in these pictures. Pictures from self-built database.

CAP stones are often found in combination with other mineralogical components. It has been estimated that 15% of all the stone samples have CAP in the core of the sample, so it acts as nucleation point 103. CAP is also frequently found as deposits on CaOx stones surface that may evolve to create a thin coating, which is then covered by further precipitation of CaOx crystals 104.

### 1.2.2.2. Brushite

Calcium hydrogenphosphate dihydrate, or brushite (BRU), represents a minor incidence in the general count of urinary stones, as seen in **Error! Not a valid bookmark self-reference.** Nevertheless, the incidence of BRU stones has increase during last decades 105.

Table 1.8 Brushite general characteristics 78.

Stone type	Brushite
Chemical name	Calcium Hydrogenphosphate
Chemical formula	$\text{CaHPO}_4 \cdot 2 \text{H}_2\text{O}$
Mineralogical name	Brushite
Incidence (from total)	1%

This stone type is closely related to CAP. They not only share part of their chemical composition (calcium and phosphate ions), but also can transform one into the other, according to *in vitro* tests performed using extreme pH environments (pH values <4 or >8) 106. While *in vitro* conditions require extreme pH (compared to the pH range in urine), the particular complexity of urine matrix (inhibitors, promoters, other components) allows milder pH values to be enough for the dissolution of CaP.

Differently to CAP, long, flat crystals, which spread radially from the stone core, can be observed in BRU calculi. These crystals can reach de surface of the stone, where they have a flat end 33. This structure leads to the formation of a very compact, hard structure, opposite to the rather soft CAP, as seen in Figure 1.18.



Figure 1.18 Internal views of BRU stones (a, c) and a fragment (b). The core structure and the organization of the crystals are clearly defined in this Figure. Pictures from self-built database.

BRU stones can also contain small amounts of CAP and organic matter, especially in the core. Figure 1.18 a and c show two examples of a cut section of a BRU stone, where it can be appreciated how the heart of the stone has a completely different structure to the rest of the sample 101.

### 1.2.2.3. Etiological factors

Both CP forms already described share some etiological factors. In both cases, the concentration of calcium and phosphate ions in urine is above the  $K_s$  value. This is needed for the stone formation process to take place 101. Recent research has shown that 80 % of CP stone formers present hypercalciuria, while this figure is only 5-10% in controls and 30-60% in general stone formers 107. The same study points at hypocitraturia as an additional risk factor (identified in 45% of the patients), fact that fits with the efficiency of citrate as inhibitor. In the particular case of CP crystals formation,

magnesium ion is believed to play a significant role as crystallization inhibitor, due to the formation of stable complexes with phosphate 101.

Besides the similarities, one main factor makes the difference between the formation of CAP or BRU, if precipitation conditions are achieved: urinary pH. Generally speaking, BRU precipitates in acidic urine. At these conditions, CAP is soluble and its precipitation is favoured at rather alkaline urine; pH>6.5 108.

### 1.2.3. Infected stone disease

Table 1.9 General characteristics for stones produced due to infected stone disease 78.

Stone type	Infected stone disease
Chemical name	Magnesium Ammonium Phosphate
Chemical formula	$MgNH_4PO_4 \cdot 6H_2O$
Mineralogical name	Struvite
Incidence (from total)	9%

This particular stone type is also a phosphate, but its precipitation takes only place when urease producing bacteria cause an infection in the urinary tract 109. In such conditions, when urinary pH is basic, the precipitation of magnesium ammonium phosphate, mineral known as struvite (STR), can occur. The growth rate for STR stones is very high; calculi can be formed within 4 to 6 weeks 110.

STR rarely precipitates alone. At basic pH CAP can also readily form crystals, so an aggregate of both substances, also including organic matter, is generally observed. Therefore, the structure is usually lacking any pattern, and consists on the accumulation of both components in this porous agglomerate, that holds pure STR crystals, which appear as shiny dots within the brownish-white background. The dark color is mainly due to the organic matter and bacteria found in the stones 98 101. Some examples for this description are shown in Figure 1.19. STR calculi can even fill all the space in the kidney (staghorn stones), due to its porosity and rapid growth.



Figure 1.19 Examples of STR urinary stones. The composition is usually mixed STR and CAP; note the similarity of texture, porosity and lack of crystallization structure between both stone types (see Figure 1.17). a, b. Internal sections, c. Surface. Pictures from self-built database.

### 1.2.3.1. Etiological factors

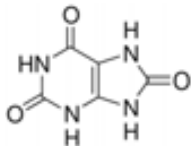
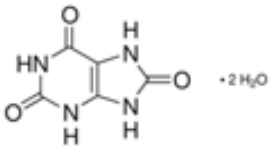
The formation of STR stones has only been seen when urea is decomposed in urine due to bacteriological metabolism. The concentration of ammonium can increase significantly, and so does pH.

According to the infectious origin of this type of stones, the incidence has reduced in the last decades. It has been reported that, in France, the percentage of STR stones sank from 20-30% in the 50s to 4% in 2005 109. This study also showed that the existence of a malformation in any part of the urinary tract was detected in 30% of STR stone patients.

Urinary pH is usually higher than 7.2 when STR stones are formed. It has been defined as the minimum pH value for this type of calculi to form 98. When urinary pH is below 7, STR calculi stop their growth and dissolve 98.

### 1.2.4. Uric Acid

Table 1.10 Uric Acid general characteristics 78.

Stone type	Uric Acid Anhydrous (UAA)	Uric Acid Dihydrate (UAD)
Chemical formula	$C_5H_4N_4O_3$	$C_5H_4N_4O_3 \cdot 2 H_2O$
Molecular structure		
Chemical name	7,9-Dihydro-1 <i>H</i> -purine-2,6,8(3 <i>H</i> )-trione (anhydrous/-2 H <sub>2</sub> O)	
Incidence (from total)	15%	

The formation of uric acid (UA) stones is especially related to a diet and lifestyle 111, as described in Section 1.2.4.1.

Uric Acid solid depositions can be classified as Uric Acid Anhydrous (UAA) or Uric Acid Dihydrate (UAD) as seen in Table 1.10. The chemical form found in stones will depend on the prevailing urine conditions at the moment of the crystal formation. The thermodynamic stability for UAA is higher than that for UAD, so the second rapidly undergoes dehydration in physiological conditions 112.

UAA stones are compact and tend to form a layer structure, as that seen with COM calculi. They show a characteristic orange color that makes them differ from any other stone type. They are usually rounded stones, with a flat surface presenting ovoidal shape. Alternatively, AUD crystals are much porous and are likely to be found either alone or in the core of UAA stones. UA stones can also include depositions of other chemical components, mostly COM, that can create thin layers visible within the stone mass. The co-precipitation of UA and COM is not commonly seen 101.

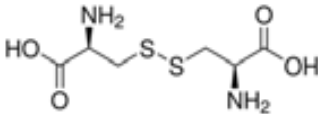
### 1.2.4.1. Etiological factors

Due to the acid-base properties of UA, the driving force for its precipitation is the pH. It has been seen that acidic urine (pH<5.5) forces the formation of crystals 113. In this stone type, the high concentration of the precipitating components (UA) is considered as a weaker risk factor than pH 11.

Diet disorders, as an excessive consumption of animal proteins, can lead to hyperuricosuria. Also related to a healthy diet, patients suffering from metabolic syndrome, which includes obesity as key factor, are more likely to develop a UA stone. As a cascade of processes, the ammonia production in the kidney is sunk, so the buffering capacity of urine is hindered. This fact forces urine pH to drop and the risk of formation of a UA stone is increased 111.

### 1.2.5. Cystine

Table 1.11 Cystine general characteristics 78.

Stone type	Cystine
Chemical formula	C <sub>6</sub> H <sub>12</sub> N <sub>2</sub> O <sub>4</sub> S <sub>2</sub>
Chemical structure	
Chemical name	(R,R)-3,3'-Dithiobis (2-aminopropionic acid)
Incidence	1%

The type of urinary stone (from those generally occurring) that can be attributed to a more specific list of causes is Cystine (CYS). The formation of such stones is a consequence of a genetic disorder, which produces cystinuria, that namely difficulties the transport of the amino acid Cysteine 114. The dimer of the amino acid is the molecule called cystine, and crystallizes as hexagonal structures, which form a very compact and pure structure. CYS stones present inclusions of other components, as CaOx 115 or organic matter 116, very seldom. The structure is usually very well defined, with oriented crystals. Some examples are provided in Figure 1.20.

Despite its low incidence, CYS stones show a higher recurrence rate than the average for urinary stones: 73% at 5 years 117.

As often seen in other types of urinary stones, CYS also show dependence on urine pH. It has been seen that the solubility of CYS increases at pH greater than 7, although these conclusions refer to *in vitro* studies. Tests performed using real urine, or on patients, have demonstrated that this relation with pH is only vaguely consistent 118.

In the case of CYS, the urinary risk factors could be reduced to a low fluid intake and the diagnosis of the genetic disorder.



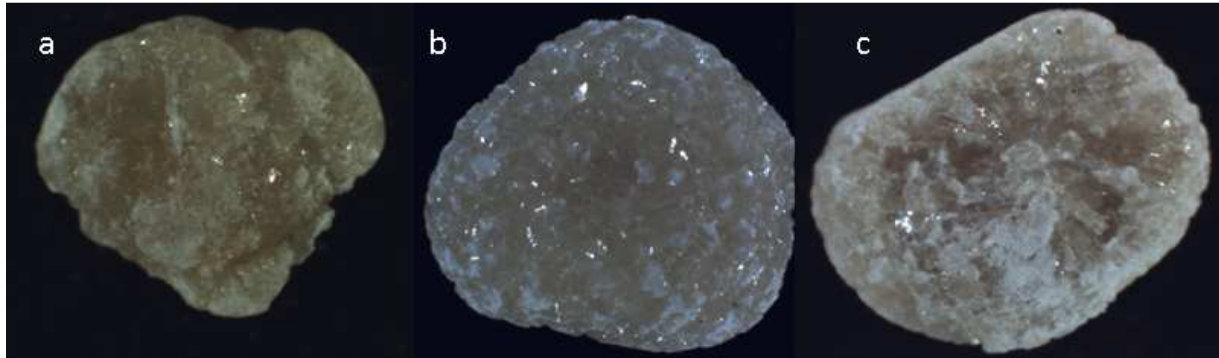


Figure 1.20 Examples of CYS stones. a, b. Surface views. c. Cut section. Pictures from self-built database.

### 1.2.6. Mixed stones

#### 1.2.6.1. Calcium Oxalate and Apatite

As described in Section 1.2.1.3. , the pH for the precipitation of CaOx lies generally between 5.5 and 6.5. Indeed, if it becomes slightly alkaline oxalate will be more likely deprotonated, so the supersaturation of urine respect CaOx is, to some extent, higher. This supersaturation value is naturally increased in case of hypercalciuria. These conditions meet an environment that also boosts the formation of CAP.

The exposed reasons support the observation that the co-precipitation of CaOx and CAP takes place very often, and so, urinary calculi with a mixed composition are found normally. The existence of CAP has been reported in 32% of the total amount of calculi; also considering stones that have just CAP heart 78 (this value includes also mixtures with STR). Another study set the total count for the combination of COD/COM with CAP, also including ternary mixtures in 19% 101. In any case, this numbers stand for a representative amount of urinary stones.

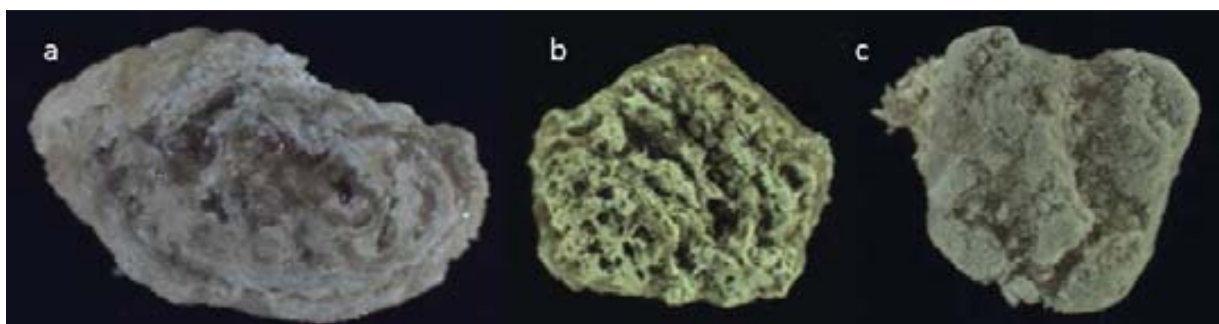


Figure 1.21 Examples of mixed CaOx-CAP stones. a, b. Cut section. c. External surface. Pictures from self-built database.

The structure of mixed calculi can be usually classified as layers or as pattern-lacking stones. As it can be deduced, stones that have been formed by adding layers of both components alternatively respond to varying urine conditions, which clearly promote either CAP or CaOx precipitation. For the reasons listed in the previous paragraph it is logical to think that urinary pH is the parameter controlling mixed stones

formation process. An example of this stone type is shown in Figure 1.21.a. However, when urinary conditions are found in a compromise range for the formation of solid concretions of both species, CAP and CaOx precipitate at the same time, creating a heterogeneous agglomeration of both components. Figure 1.21 (b and c) exemplifies this situation.

### 1.2.6.2. Calcium Oxalate and Uric Acid

UA does not always precipitate alone. Together with COM (COD is found rarely in combination with UA), they form a characteristic group of stones. Whereas other combinations of stone components lead to structures that somehow mix different species, UA-COM stones consist usually on a core-shell stone, with these two parts being independent. The composition of nucleus and shell can be either UA or COM.

This group of stones can be understood, again, due to the wide range of pH in which COM precipitates. In this case, the patient's urine is rather acid, to allow the formation of solid UA, as well. The examples pictured in Figure 1.22 can be taken as an illustration of this stone type.

This type of stones has a very low incidence, in contrast to the CaOx-CAP mixed stones. It has been reported that only 2-3% of stones present such structure and composition 101.

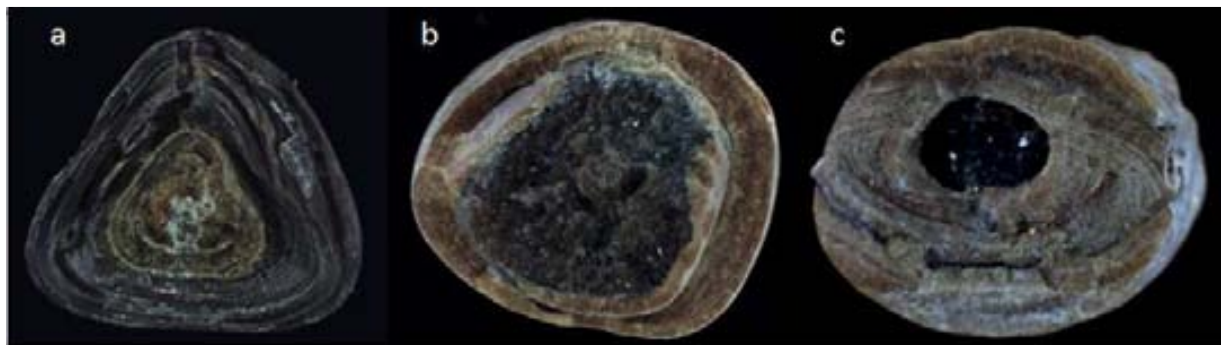


Figure 1.22 Examples of mixed COM-UA stones. a. Core UA. b,c Core COM. Pictures from self-built database.

### 1.2.7. Uncommon Urinary Stones

A precise description has been made on the main types of urinary stones, which account for more than 99% of the cases 101. In some particular conditions, though, other substances can form a urinary stone.

Ammonium Urate uroliths can be formed when an alkaline urine pH is combined with hyperuricosuria and, usually, infection in the urinary tract. These conditions can favour the formation of such stones, which are mainly seen in Asian countries, where they represent 0.7% of the cases 119.

Drug-related stones have also been detected. They include less than 1% of cases, and are divided into crystallization of poorly soluble drugs or stones resulting from a side effect from the drug intake. Some of the medicines listed here are: Indinavir (for the treatment of HIV patients), sulfonamides and some silicates 120 121.

### 1.3. Analysis of urinary stones

“I cannot forgo this opportunity to stress how undesirable it is for surgeons to seal up calculi in glass phials without investigating their chemical properties”.

Such clear statement was written by Marcet back nearly 200 years ago 122. Fortunately, the analysis of urinary stones has been the target of many scientific advances from that point. Clinical scientists have developed a number of approaches for the analysis of stones, which allow two major goals. Firstly, the characterization of the stone composition, needed for a correct metaphylaxis. Secondly, the description of the lithogenesis process, which is required for the improvement of current treatments 123.

#### 1.3.1. Chemical Analysis

The qualitative determination of the stone components using “wet chemistry” was the first methodology to be reported, and was recommended already 150 years ago 124. This analysis has been done up to date with little changes in laboratories worldwide.

Although simple to perform and with little equipment needs, Chemical Analysis (CA) shows two important drawbacks: it is tedious and the results are highly non-specific.

CA is based on the dissolution of the stone and the identification of its ionic components by means of simple reactions. The results can be verified without any specific instrument. CA can distinguish between several types of lithiasis (as phosphate from uric acid, or calcium oxalate from struvite) 125.

However, the nature of the determinations makes impossible to determine, for instance, whether a sample is made of COM or COD. As seen in Section 1.2.1. , this is fundamental to determine a proper diagnosis. Due to these limitations, actually less than 10% of clinical laboratories rely on CA for their determinations 126.

#### 1.3.2. IR Spectroscopy

Since the first use of IR Spectroscopy (IRS) for the characterization of uroliths on 1955, it has become the general routine methodology in clinical laboratories. The robustness of the measurements, together with the low cost of the analysis and wide availability, made IRS the reference technique for such examinations 101 127.

IRS provides qualitative and quantitative information (usually as percentages of each component) on the stone composition, by the interpretation of the IR spectra. The analysis of the measurements has traditionally required an expert analyst to compare the measured spectrum to reference data, from which such information can be gathered 128. Figure 1.23 plots typical spectra from COM and COD. Their different features allow the identification of pure components and mixtures, by empirical comparison between reference spectra and samples. Several molecular movements can be measured within the

common scanned region (400-4000  $\text{cm}^{-1}$ ), including: O-H, P-O, C-O and N-H stretching, C=O vibration or P-O bending. These different tensions take place at a specific energy, particular for each type of component, also distinguishing COM/COD or UAA/UAD 129.

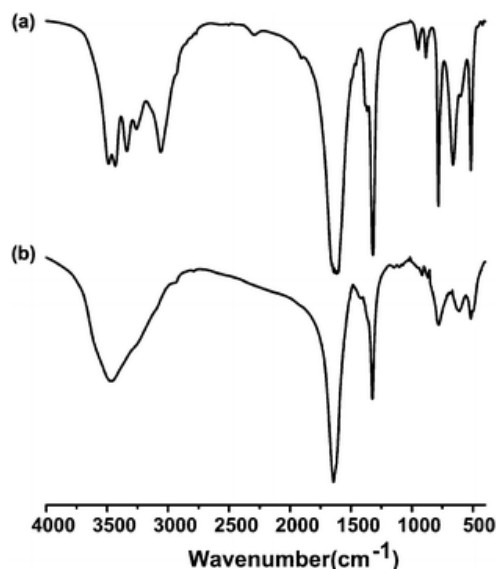


Figure 1.23 Examples of stone IR spectra. a. COM, b. COD. As it can be seen, even chemically related substances can be well distinguished. When stones are mixtures of components (which happens very often), the interpretation of the spectra becomes more difficult 130.

Urinary stones have been traditionally analyzed by grinding the stone and preparing a pellet, by dilution in KBr. During last decades, the use of ATR has extended, since it only requires a little fragment of the stone to be placed in the spectrometer, making the process more time-efficient 131.

Although the quantification of the components has usually been made relying on the analyst interpretation, some automatic quantification algorithms have been developed. These calculations are fundamentally based on the ratio of intensities for different spectral bands or on the matching with spectra libraries 132.

Advances on IRS features include the use of imaging techniques for the analysis of urinary stones 133. The use of imaging for these applications is a main pillar in this Thesis, and is conveniently addressed in Section 2.

### 1.3.3. Microscopy

#### 1.3.3.1. Optical microscopy

The optical analysis of urinary stones has been used for the description of the stone components and structure. This is the reason why this analysis is also known as morphoconstitutional analysis (MA). In this case, stereoscopic microscopes are usually the tool for depicting the composition of the stones and the interaction of the different phases, in order to describe the precise causes of the stone formation 44.

The main drawbacks of MA are both the need of a trained analyst to carefully describe the stone, and it is time consuming 74. As seen in Figure 1.24, the analyst has no analytical hint other than the careful and close visual and stereoscopic examination to the stone structure and interpretation of the observations. Up to date, this analysis cannot be done automatically, although some approaches have been suggested, as the described in Section 5.3. of this Thesis.

Besides these inconveniences, MA represents one of the best approaches to describe the lithogenesis process. Although it cannot lead to a precise quantification of the stone, unless it is combined with IRS, it allows the identification of structural features. This description has a tremendous power for the description of the disease and, thus, for the definition of the best medical treatment 134.

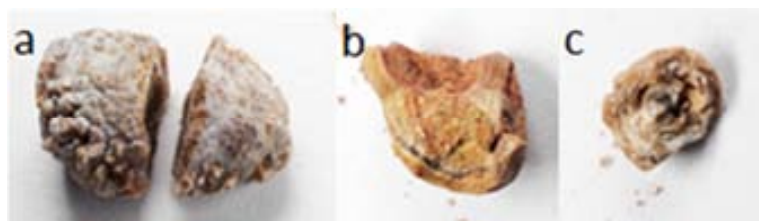


Figure 1.24 Examples of stone views recorded using stereoscopic microscopy. a. COM (surface), b. UAA (internal view), c. Mixed stone (CaOx and CAP, internal view). Pictures from self-built database.

#### 1.3.3.2. Electronic microscopy

Other techniques, generally used for the analysis of materials and surfaces, have also been considered for the study of urinary stones. Especially, Scanning Electron Microscopy (SEM) has shown interesting features for the careful analysis of these samples 44.

SEM images provide a close view of the stone structure, either surface or core. As seen in Figure 1.25, the shape of the crystals that form the sample can be clearly determined. This information yields useful hints for the study of lithogenesis processes, based on the crystal agglomeration patterns, existing cavities and interfaces between different stone components.

As stated with MA, SEM requires a trained technician to interpret the images. However, SEM microscopes are usually coupled to elemental analyzers that can perform an X-Ray scan on the surface of the sample, yielding a signal that can uniquely identify some atoms. This X-Ray analysis, known as EDS (Energy-Dispersive X-Ray Spectroscopy), stands as a useful tool for the complete identification of the composition of the stone 135.

Due to availability of the equipment, related costs and time required for the sample analysis, SEM is far from becoming a routine analysis technique, yet it has proven its suitability for advanced research in urinary stones structure. i.e. it has been used for the study of papillary calcifications (related to papillary COM calculi, described in Section 1.2.1.1.2. ) 86.

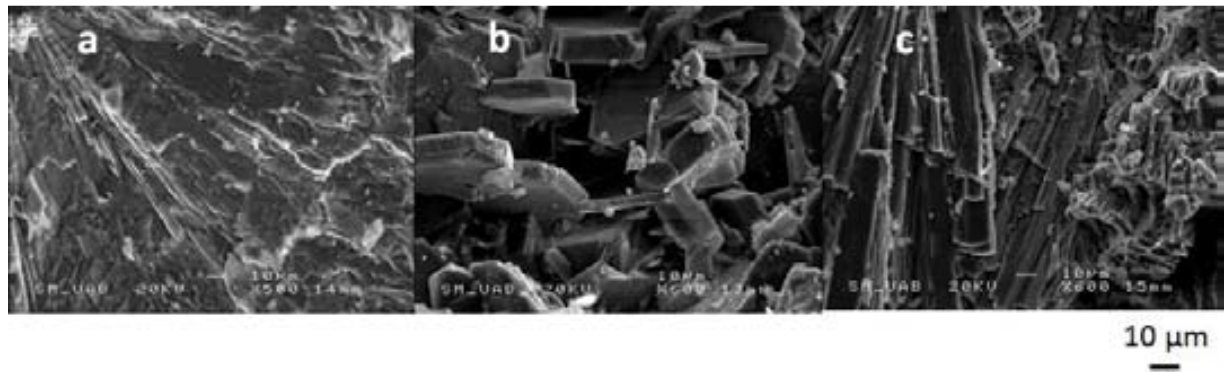


Figure 1.25 Examples of SEM images. a. COM, compact structure formed by columnar crystals, b. UAD, the dehydration of UAD into UAA creates a porous stone, c. BRU, long crystals create a solid stone with few cavities. Pictures from self-built database.

### 1.3.4. X-Ray Diffraction

X-Ray Diffraction (XRD) takes advantage of the crystallization patterns of stone components. Since each substance found in urinary stones has different lattice parameters and they have a well-defined crystalline structure, XRD stands as a useful tool for the unique characterization of the stone structure. It should also be considered, however, that the mixture of components can lead to overlapping bands that make the interpretation more complex. Stone analysis by XRD is not as simple as that described for IRS. The equipment requirements and sample preparation have allowed the latter to be set as reference 136.

The principles of XRD are based on radiation scattering by the atoms in a lattice, which occurs at different angles depending on the lattice parameters. This phenomenon follows Bragg's law. The measurement of the scattering intensity at different angles can be related to lattice parameters, and so, to stone crystal composition 137. Figure 1.26 shows the typical result for a stone analysis using XRD.

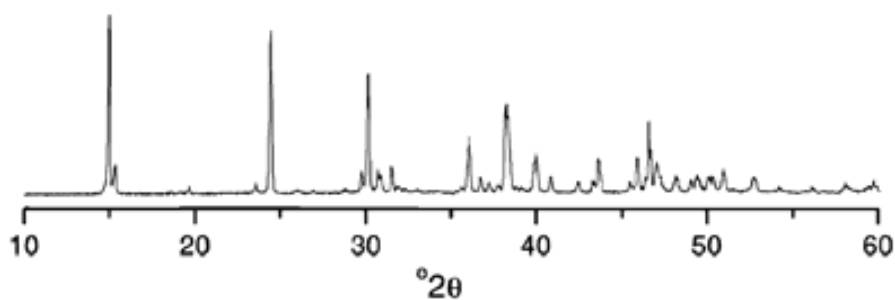


Figure 1.26 Example of diffractogram of a COM urinary stone 138.

### 1.3.5. Methodologies overview

The described techniques in this Section represent the most relevant approaches for the analysis of urinary stones taking into account the degree at which they are generally used. Each of them presents different advantages and drawbacks based on their availability, ease of use and benefit of the results. A

comparison of the basic performance features is shown in Table 1.12. From this information, it can be gathered that the relevance for the routine analysis of each methodology is really diverging.

Table 1.12 Performance overview of urinary stones classification techniques.

Feature	Chemical Analysis <sup>i</sup>	IR Spectroscopy <sup>ii</sup>	Microscopic Analysis	X-Ray Diffraction
Component identification	✓	✓	✓	✓
Chemical form identification	✗	✓	✓	✓
Component quantification	✗	✓	✓	✓
Location of components in the stone	✗	✗	✓	✗
Classification according to formation causes	✗	✓	✓✓	✓
Description of the history of the stone (description of the disorder)	✗	✗	✓	✗
Trained technician needed	✗	✓	✓	✓
Cost	€	€	€€€	€€
Analysis time	⌚	⌚⌚	⌚⌚⌚	⌚⌚

✓✓ Stands for an enhanced description of the disease, available only with this technique.

<sup>i</sup>Chemical analysis refers here to commercially available kits that do not require full knowledge in lithiasis.

<sup>ii</sup>IR Spectroscopy considers the analysis (by pellets or ATR) and spectral interpretation, not including data analysis software.

In addition to the presented methodologies, other spectroscopic alternatives have also been used for stone classification.

Some publications point out that Raman Spectroscopy is also a suitable alternative for the classification purposes. The works conducted in this field have been fundamentally focused on research; Raman Spectroscopy offers similar results to those obtained by IRS, and the medical community is already used to work with this type of data 139.

In addition, highly specific results have been achieved using synchrotron radiation. Published research works highlight the usefulness of synchrotron radiation for the precise study of the formation mechanisms of urinary stones, as well as the role of some metals in the stone structure 140 141.

This Thesis itself also poses some examples on new optical applications for the analysis and classification of urinary stones, properly described in Section 2.

Some of the described methodologies might not become part of routine analysis (especially those based on synchrotron radiation techniques), but they clearly point out that the study of lithogenesis through stone analysis is of major importance for the correct understanding and treatment of the disease.

## 1.4. Medical management of urinary stones

Renal calculi have been afflicting humans for all their history, but it was not until the very beginnings of the 20th century when Kelling performed the first laparoscopy procedure on a urinary stone patient. From that waking-up point on, several advances hit the urology operation rooms, but the suggested methods were usually based on aggressive surgical treatments. Not only stone treatment, but also stone detection techniques were presented. Urinary stones were progressively earlier detected, by means of X-Rays 142.

On the other hand, clinical scientists have devoted much effort to the study of the causes of stones, as well as the development of models to offer a proper treatment of the disease. Therefore, a number of drugs have been suggested for the care of stone patients. This is generally known as urinary stone metaphylaxis, namely, the non-surgical treatment of stones.

Urology is a notably surgical branch of medicine, so physicians pay generally little attention to the scientific description of the disease and focus their treatment on the surgical face. Therefore, a brief description of the main techniques for stone management in hospitals, as well as the general metaphylaxis treatments will be done.

### 1.4.1. Surgical management of urinary stones

In regard to the surgical approach for treating urinary stones, little discussion can be posed; the major advance in this field was developed in 1972 by Chaussey and Eisenberger in Munich. This innovation was actually an ultrasonic device that could break down the stones inside the kidney without entering the patient's body, so no (or little) bleeding was caused. The invention, which would be later known as "lithotripter", was born to give shape to the nowadays most widespread technique for the surgical management of urinary stones: Extracorporeal Shock Wave Lithotripsy, mostly referred to as ESWL 143 144.

The surgical management of urinary stones is often needed, for those cases in which the size and/or the location of the stone make its spontaneous passage unlikely. According to statistical data, some general considerations for the stone passage without using any technique described in this Section can be contemplated (see Table 1.13) 145.

As already stated, ESWL entailed a breath of fresh air for physicians already a few decades ago. The first trial with real patients took place back in 1980, using a Dornier HM1 machine 143. The commercial model Dornier HM3, commercialized shortly after, was considered nearly a revolution in the field. This machine was also known as *the bath* (see Figure 1.27), because the patient had to be introduced in a big water bath in order to be treated 146.



Table 1.13 Likelihood of spontaneous stone passage 145.

Size	Likelihood of spontaneous stone passage (%)
>6 mm	25
4-6 mm	60
<4 mm	90
Location	
Upper ureter, >6 mm	1
Upper ureter, <4 mm	81
Lower ureter, <4 mm	93

**1.4.1.1. Extracorporeal Shock Wave Lithotripsy (ESWL or SWL)**

Despite its peculiar operation way, it rapidly showed its numerous advantages compared to the traditional, more aggressive surgeries performed up to that date. ESWL is currently the technique of choice for the treatment of more than 50% of urinary stones 147.



Figure 1.27 Image of the first commercially available lithotripter, Dornier MH3. Image from Dornier website 148. Of course, lithotripters have greatly evolved in terms of simplicity (they don’t use a water bath any longer) and efficacy.

In brief, the mechanisms of stone fragmentation in ESWL rely on physical processes, whereby a stone is broken when stress, coming from a shock wave, is directly applied on it. The initial fragmentation takes place at a stone location where the force applied exceeds a given value, directly depending on the stone

type. Afterwards, the fragmentation continues due to coalescence and charge/discharge iterations of the applied pulses 149 150. A single ESWL treatment lasts around one hour, while the small fragments will need more time to be expelled, typically 30 to 50 days 151. ESWL appears to have little side effects and very few contraindications; actually, its use is non-recommended only on pregnant women due to the use of shock wave and X-Ray. As a result, the use of ESWL has been widely extended to stones between 4mm and 2 cm. Smaller calculi are naturally expelled, while those of higher dimensions require more drastic surgery 12 152.

As it can be gathered, ESWL does show advantages for the stone treatment. However, what was initially believed to be the non-invasive panacea for the treatment of stones has also some drawbacks to consider. While very useful for the treatment of already existing stones, ESWL poses no options whatsoever for the further metaphylaxis of the disease and the prevention of other stone episodes. As a matter of fact, when the patient is subjected to ESWL, the stone episode might not come to its end, due to the formation of the so called “*Steinstrasse*” (German for “Stone Street”) 153. This term refers to the little stone fragments from a broken stone that remain in the urinary tract for a long time, without being expelled. Their importance relies on the fact that they could become a seed for the formation of new stones, which would require further treatment. The overall stone-free rate three months after undergoing an ESWL session has been quantified around 60% of the patients 154.

### 1.4.1.2. Percutaneous Nephrolithotomy (PCNL or PNL)

Percutaneous Nephrolithotomy, also abbreviated as PCNL, has been usually considered as the first-line surgical treatment for big stones; that is to say, stones >20mm. Indeed, a combination of PCNL and ESWL is often used for the stone passage, because it increases the stone-free rate to 70-95%. However, PCNL is a much more invasive procedure and causes a greater morbidity on the patient 155 156. It was first used in the 1970s, but it rapidly became the technique of choice for managing big stones, even when ESWL was already available.

PCNL requires piercing the skin, since the stone is removed from the body using a tube. A previous step of ESWL is often needed. According to the nature of the technique, it generally involves general anesthesia, but is the alternative to choose when ESWL is not recommended. An evolution of PCNL, mini-PCNL, is being developed, and is likely to replace PCNL, since it needs smaller tools, so the bleeding and pain for the patient decrease notably 157.

### 1.4.1.3. Ureterorenoscopy (URS)

This technique was born two decades ago, as a less invasive approach for urinary stone removal, compared to PCNL. URS became much more useful when flexible instruments came into play 158 159. These days, URS is the second option for medium stones (stones between 10 and 20 mm), although it is gaining importance due to good performance of modern devices. The main advantages are the possibility of actually seeing the inside of the urinary tract, using a camera, and the possibility of performing the surgery accessing the stone with no skin perforation and small bleeding.

URS consists in the introduction of a flexible tube through the ureter upwards, until the position where the stone lies is reached. Modern instruments allow reaching the upper urinary tract, so most stones can be reached. In addition, stones can also be pulverized using laser instrumentation, which leads to an overall stone-free rate of 90% 160.

### 1.4.2. Metaphylaxis of urinary stones

The understanding of the mechanisms whereby stones are formed has strongly drawn the attention of scientists from many disciplines. The non-medical community has especially focused their efforts on the attack of those causes which can be regulated if a proper metaphylaxis is applied. In fact, the removal of the stone is only one step on the treatment of urinary lithiasis; special attention has to be paid on the follow-up of the patient conditions in order to decrease the high recidivism rate described for this disease. Some works have defined the bases for a proper metaphylaxis of stones 22 161, so the common points will be highlighted here.

Owing to the complexity of urine matrix and the particular situation for each patient, the physician may consider a full urine analysis for determining the most suitable treatment for the patient. As a general approach, Table 1.14 lists some of the values which can be considered as the limit for a healthy patient. Once this limit has been exceeded, medical treatment should be considered.

Table 1.14 Limit values in urine (24 hour collection) for considering the initiation of medical treatment, due to high stone formation risk 78. Values expressed as total amount in 24 hour urine samples.

Parameter	Value	Parameter	Value
pH	<5.8 or >6.8	Oxalate	>0.5 mmol, 45 mg
Density	>1.010 g·cm <sup>-3</sup>	Phosphate	>35 mmol, 1085 mg
Diuresis	<2.0 L	Magnesium	<3.0 mmol, 80 mg
Calcium	>5.0 mmol, 200 mg; >8.0 mmol, 320 mg (hypercalciuria)	Creatinine	Male: <7 or >13 mmol <0.8 or >1.5 mg Female: <13 or >18 mmol <1.5 or >2.0 mg
Uric Acid	>4.0 mmol, 672 mg	Ammonium	>50 mmol, 850 mg
Citrate	<2.5 mmol, 481 mg	Cystine	>0.8 mmol 192 mg

The parameters listed in Table 1.14 refer to a general, unspecific diagnosis of urinary lithiasis. The interpretation of a single value is not definitive, due to the multiple interactions that might take place. In addition, not only total amounts (for 24 hours) should be considered, but also concentration values (related to total volume). Indeed, the complete risk assessment is generally calculated by including main urine components, as described in Section 1.1.7.

Once the physician has a clear hint of the existence of a urinary stone, some trends can be considered for each type of stone, so the general type can be identified when the calculi remains in the kidney, as indicated in Table 1.15. **Error! Reference source not found..** The observations listed cannot provide

complete and precise information (the stone analysis is required), but they are useful for a first approach for the main groups of stones.

**Table 1.15** General parameters for a rapid identification of urinary stone type 78. The signs ↑ and ↓ refer to higher and lower, respectively, to the amounts listed in Table 1.14.

Most likely stone type	Parameters measured
Uric Acid	Urine pH <6.0 Uric acid excretion ↑ Uric acid level in blood ↑
Calcium oxalate	Urine pH normal or low (<6.5) Calcium excretion ↑ Citrate excretion ↓ Uric acid excretion ↑ Oxalate excretion ↑ Magnesium excretion ↓
Calcium phosphate	Calcium excretion ↑ Phosphate excretion ↑ Urine pH persistently >6.5 (CAP) Urine pH persistently <6.0 (BRU) Calcium level in blood ↑
Struvite	Urine pH >7 (sign of infection) Ammonium excretion ↑ Citrate excretion ↓
Cystine	Cystine excretion ↑

#### 1.4.2.1. Diet

The most difficult point to modify is, without a doubt, the diet. This involves also changes in the patient's lifestyle, and this is hard to achieve. However, some general indications have been described.

The first factor pointed out by all the studies is the attention on fluid intake. As already stated, liquids intake does directly decrease the stone formation risk, through the dilution of all the species in urine, provided the selected drink is not one with a high oxalate content, such as tea. Fortunately, this is an easy factor to control and is also accessible to the general population.

A factor with a capital importance in the stone formation process is urinary pH 20 162. The control of this parameter is, however, not so straight-forward, and requires either changes in lifestyle and diet or the intake of some specific drugs. Urine pH is strongly influenced by protein intake, being animal proteins an important cause of acidic urine. Still, the protein intake is only a factor in a more general and relevant parameter: the Net Acid Excretion (NAE). This value accounts for the "free" protons in urine and it depends on the concentrations of the major species which can release protons in urine. The NAE is calculated as displayed in Equation 1.5 22, and it can be used for the estimation of the overall stone formation risk, as well as for the diagnostics of certain kidney malfunctions 163.

Equation 1.5 Calculation of the NAE value. “Titratable H<sup>+</sup>” accounts for titrated protons from original pH value until pH 7.4. This includes free protons and other protons that could be bound to other species and be released in an acid/base reaction (titration), excluding ammonia and hydrogencarbonate. Note that this definition is specific for nephrology, but it is useful for determining the acid-base status 164.

$$NAE = \text{titratable } H^+ + [NH_4^+] - [HCO_3^-]$$

Calcium plays, of course, a relevant role in stone formation. An important part of the stones are made out of calcium salts, yet its relation to dietary calcium is delicate. Hypercalciuria is dependent not only in calcium intake, but also in oxalate consumption, since the latter acts as a regulator of the former in terms of free ion. As tricky as it may seem, a reduced calcium intake has been related with an increased lithiasic risk, due to the calcium-oxalate close relation. Low calcium intake is associated with higher oxalate absorption, and increased CaOx stone formation risk. This issue is conveniently addressed in Section 4.1. Therefore, it is recommended to stone formers to keep normal calcium intake, within the range 1000-1200 mg/day 165.

Oxalate, which is considered to have the strongest influence among calcium oxalate stones promoters, is naturally produced in the human body as a by-product of ascorbic acid metabolism 166 167. However, the levels of this metabolite in body fluids, also in urine, are not only a function of internal production, but strongly dependent on diet. Intestinal oxalate hyperabsorption (enteric hyperoxaluria), stressed by a high oxalate intake, is a key factor in this disease 168. Even when fat malabsorption arises, non-absorbed fatty acids bind to free calcium, so the availability of oxalate to be absorbed increases 169. A general advice for calcium oxalate stone formers is to reduce oxalate intake.

While stone formation promoters get usually much of the attention of clinical scientists, the effects of the crystallization inhibitors must not be overseen. This important, heterogeneous group of molecules, introduced in Section 1.1.6.2. , is usually in charge of drawing the complex line between metastability and precipitation. The part of the crystallization process that they have effect on, as well as the precise mechanism of action is clearly divergent. Any specific diet should consider the type of stone the patient suffers. In addition, it should include the most suitable of the inhibitors described in Section 1.1.6.2.

#### 1.4.2.2. Medication

The knowledge available on the influence of dietetic parameters on the development of the stone disease has allowed the formulation of some specific medications, focused on a single type of calculi, more than a general modification of urine. Details concerning particular precipitation conditions and factors affecting each composition of urinary stones have been discussed in Sections 1.1.6. and 1.4.2.1.

As deduced from **Error! Not a valid bookmark self-reference.**, the classification of the stone is a basic point to assign a correct medication to the patient. However, physicians have often accepted potassium citrate as a “one-solution-fits-all”, and have recommended it to every stone patient. Indeed, some manufacturers that commercialize this drug do announce it as the key product, which may solve all the stones at once. Not only is this statement highly imprecise, but also it leaves aside the wide research on urinary stones formation carried out.

## 1. Introduction

---

**Table 1.16** Relation of main drugs recommended for each group of stone formers, according to the etiology of their stones **22**.

Medication	Daily dose	Indications
Potassium citrate or Sodium bicarbonate	9-12 g 4,5 g	Adjustment of the pH buffering capacity at the alkaline region and Ca ion complexation (only citrate). For patients with a high uric acid production, low dietary acid tolerance or high oxalate production. Stone types: UA, CaOx
Hydrochlorothiazide	25-50 mg	Correction of hypercalciuria that cannot be corrected by dietary advice Stone types: Calcium salts
Magnesium salts	200-400 mg	Correction of hyperoxaluria. Excluded patients with renal insufficiency Stone types: CaOx
Pyridoxine	5-20 mg/kg	Correction of hyperoxaluria when it does not respond to restriction of dietary calcium and oxalate Stone types: CaOx
L-Methionine	600-1500 mg	Correction of alkaline urinary pH Stone types: Phosphates
Allopurinol	100-300 mg	Correction of hyperuricosuria when not solved by action on the diet. Patients with overweight or enzymatic disorders. Stone types: UA

Some attempts to the dissolution of the stone while it is still in the body have been made, in order to avoid surgical procedures for the patient. The main studies in this field have been done on CaOx and UA stones.

It has been reported that the dissolution of calcium oxalate stones could be possible by means of citrate. In a study performed on *in vitro* artificial solutions, the addition of a high concentration of citrate could actually dissolve existing CaOx crystals <sup>170</sup>. However, this treatment has not been applied as therapy yet. The studies have been only performed with *in vitro* solutions, which is a clearly different environment as urine. *In vivo* tests should be made to clearly confirm the power of this possible treatment. So far, the administration of citrate to patients has not lead to dissolution of any CaOx stone.

On the contrary, UA stones can be dissolved when they are still in the body <sup>78</sup>. The goal is to keep a urine pH around 7, for enough time for the stone to disappear, while sinking UA excretion through diet restrictions (as described in Section 1.2.4.1. ).

Figure 1.28 shows an estimation of the solubilization of uric acid. According to this information, the adequate treatment of uric acid stones can prevent the patient from suffering the undesired renal colic.

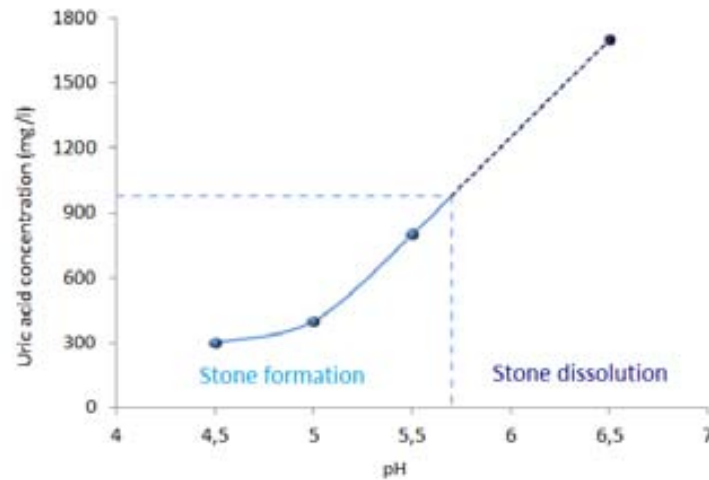


Figure 1.28 Influence of UA concentration and pH in the solubility of UA stones 78.

#### 1.4.2.3. Patients compliance to metaphylaxis

As already indicated, modifying patients' diet or, eventually, make them adhere to a long-term medication, is a challenging work. Besides, urinary stone disease has an added problem: patients tend to adhere to the recommendations and treatments as long as the memories from the last renal colic last. In other words, the most difficult issue consists actually on making the patient play by the rules for enough time not to end in another stone episode. It has been estimated that only 15-40% of urinary stone patients follow a long-term medication and lifestyle change 21 171.

In essence, the knowledge on diet, lifestyle and possible treatments has to be put closer to the patient, so that the compliance rate increases and the recidivism rate can be, in a great extent, defeated. In this sense, some interesting initiatives have already been developed, as e-tools that offer to the patients the information they need on-line 172.

Every step taken in this direction shall help fight the disease and make its tremendous socioeconomic consequences shrink. More information on this point is provided in Section 1.5.

## 1.5. Socioeconomic impact of urinary stone disease

The incidence of urinary lithiasis is far from decrease in developed countries, as already indicated. Not only stands this statement as a factor against the health and quality of life of the potential patients, but also represents a tremendous economic challenge for all the healthcare institutions. The medical community is in charge of showing their patients basic guidelines to avoid further lithiasic episodes, but

also of treating them whenever a further stone is formed. While the outcome of the former situation is pretty difficult to quantify, the costs associated to the latter are measurable 173. Despite the importance of quantifying the economic impact of the disease, only a few studies have been done in this regard.<sup>ii</sup>

Already back in the early 1990s, the budget for treating urolithiasis in the USA was around \$1.8 billion/year; by 2000 these costs had already increased up to \$2.1 billion/year 174. Since the prevalence of urinary lithiasis keeps increasing, the economic burden on the public health organizations becomes greater. More recent data (year 2012) has estimated the cost of treating urolithiasis related patients in France (approx. 65 million inhabitants) in €590 million. This amount could be reduced by €273 million if patients are conveniently treated 175. These big numbers are basically based on the costs associated to the regular treatment options available for the stone handling. Among those, the most important are, as described before, ESWL, PCNL and URS. Several works have been focused on the analysis of the cost associated to such techniques.

The values listed in Table 1.17 result from the average cost of the different approaches used for the stone treatment. Note that the German case reflects also the percentage of patients who required hospitalization. These amounts, together with the high prevalence of stone episodes, highlight the magnitude of the stone disease, in terms of clinical budget.

**Table 1.17.** Associated costs to surgical treatment of stones (amounts per patient and episode) in some countries (values calculated per single patient and lithiasic episode).

Cost (€)	Country	Year	Reference
2500	USA	2005	Saigal et. al. 174
2900	Sweden	1991	Grabe 176
3520	UK	2002	Chandhoke 177
5900	Germany	1997	Strohmaier 178

Indeed, the extent on which urinary lithiasis affects the economic aspects in the society is not only the management of the stone itself, but also the hospitalization period and temporary medical leaves. Note that only in the USA, for the period 2006-2009, more than 3.5 million patients visited the ER due to a nephritic colic episode 179, which corresponds to 278 ER visits per 100000 inhabitants. Statistically, 68-75% of the stone patients require hospitalization 178, a parameter that radically affects the general costs for a single episode treatment, as seen in Table 1.17. Getting back to the value of \$2.1 billion for treating urolithiasis in year 2000 in the USA, this cost was divided as: \$971 million for impatient care, \$607 million for attention at physician offices and \$490 million for treatment at the ER 180.

Naturally, the medical community is aware of such statistics and the implications they have on Urology services budget and waiting lists. Because of this, doctors relied on ESWL as a powerful tool for the

---

<sup>ii</sup> Note that, due to the scarce number of publications particularly focused on this topic, statistic data is extrapolated from the USA to Europe. The similarities of epidemiological data for both regions make them comparable.



management of urinary stones and the decrease of stones relapse rate. However, ESWL does not offer any treatment options for the patient to avoid further stone episodes, because it only acts when the stone has already been formed. When the technique was firstly introduced in hospitals, it was supposed to help reducing medical costs. As a German study showed, though, from its implementation to 1986 the costs associated to surgical stone management had increased as of €21 million 181. Logically, ESWL equipment has evolved in order to alleviate the side effects inherent to the technique, but still, many of them have not been overcome yet 149. It is clear, thus, that treating the stone once it has been formed is not enough to really fight this disorder.

This is the scenario where metabolic evaluation and metaphylaxis (medical treatment) have a major role in. Some studies have dug into this point, revealing and quantifying the effects of treating stones according to a metabolic study performed for each patient 182. A metabolic study of the patient, including the 24-h urine analysis as well as the study of the expelled urinary stone has been estimated to cost €250-350 per patient 183, whereas the appraisal for a personalized drug treatment lies on the range €13-130, which represents a rather modest amount of money for hospital budgets 184. These figures can only gain sense if their effect is measured according to the benefits, in terms of reduction of recidivism rates they might have. In this concert, a study has already proven that the correct application of metabolic evaluation and stone analysis, together with the supply of a personalized treatment can decrease repeating stone episodes as much as 46% 185.

Of course, the implementation of such a system is actually an investment for any health system. However, a German study faced these calculations, including the above-mentioned measures, and the output was potential annual savings for the healthcare organizations of €170 million 173. While the amount may be questionable, the direction of the best approach for the management of stones is clear.

Not to forget is the off work period each stone patient experiences because the disease. In Europe, most of hospitalized stone patients took an off work period of 14 days 174. In the USA though, where law does not favor employees in that extent, only an average of 5 days was recorded for the same patient group 186. Attending to the age in which the prevalence of urolithiasis is more common, 30 to 60 years, this point becomes definitely relevant. Whilst this aspect does not directly influence the medical costs related to urinary lithiasis, it does have an important impact in the general socioeconomic aspects of the disease.

The bibliography published so far lacks a systematic methodology for the precise calculation of the associated costs to urinary lithiasis. The number of parameters to consider for a general scheme is definitely large, and their relation is complex; each country has its own health system and it depends on many external factors. This Thesis is not especially centered on the economics related to urinary stones. Nonetheless, the numbers and information cited here help to draw a general picture of urinary stones as a socioeconomic problem. This intricate picture demands a multiple approach solution, which encompass all the roles in this big portrait, from the patient to the hospital management, including scientists from diverse fields.

## 1.6. Objectives

The previous Sections have illustrated a general picture of urinary lithiasis and many related aspects that show different relations to urinary stones. This complex, global description embraces the scientific and practical faces of the topic. Urinary lithiasis is not a solved problem; on the contrary, the incidence is increasing and the correct management of the disease demands wider knowledge and new alternatives.

The general objective of this Thesis is to bridge the existent gaps in urolithiasis knowledge, providing novel fundamental and applied solutions that support physicians in their task and lead the management of this disease towards more efficient treatments. The ultimate goal is to improve the quality of life of stone patients.

This Dissertation aims to reach the defined objective through the application of chemical speciation on the analysis of solid and liquid samples for the study of lithogenesis. This global goal has been the scientific horizon in different fields of study, each of them including some specific steps: 1. Urinary stones analysis and classification, 2. Nanoparticles in urine and 3. Study of crystallization promoters.

### 1. Urinary stones analysis and classification

- i. Use of high resolution spectroscopy for the analysis of urinary stones, to determine lithogenesis features.
- ii. Develop new analysis methodologies that overcome limitations found in the existing ones, especially in terms of dependence from the analyst.
- iii. Apply multivariate and chemometric data analysis techniques to exploit the measured data in a greater extent.
- iv. Test the developed methodologies against existing, reference techniques to prove their suitability.
- v. Design a medical device for urinary stones analysis and test it comparing to reference techniques.
- vi. Analyze the commercialization potential of the device.

### 2. Nanoparticles in urine

- i. Quantify the concentration of nanoparticles in urine.
- ii. Assess the particle size distribution and the differences found between CaOx stone patients and healthy controls.

3. Study of crystallization promoters

- i. Quantify the amount of oxalate in plant extracts used as drugs or nutritional supplements and assess their potential risk for CaOx stone patients.
- ii. Determine the concentration of some major components in chocolates and its importance to urinary lithiasis.
- iii. Use multivariate data analysis techniques for the identification of groups of samples based on their potential risk for CaOx stone patients.
- iv. Assess the relevance of oxalate absorption in the digestive tract using isotopic labelling.

In addition, transversal objectives support the scientific individual goals described above:

1. Work within multidisciplinary collaborative teams that bind different fields of expertise.
2. Apply the basis of knowledge transfer to the scientific developments accomplished. This includes giving priority to intellectual property and pushing basic into applied research.
3. Search for public funding to achieve the scientific objectives.





**IMAGE ANALYSIS:  
NEW OPTICS,  
FURTHER  
PERSPECTIVES**



## 2.1. Introduction to Image Analysis techniques

### 2.1.1. Hyperspectral Imaging

Originally designed for cartographic and satellite applications several decades ago, Hyperspectral Imaging (HSI) has arisen as a technique able to give a vast amount of information in any of the fields it has been implemented 187. Since HSI jumped from its initial purposes into the chemical analysis, an ever-increasing number of disciplines are using this technique for their own interests, being the pharmaceutical field the one which first used HSI advantages 188.

HSI is essentially the result of combining a digital camera and a spectrometer, that is, a complete spectrum is recorded for every single pixel of the image. This data is organized as a *hyperspectral cube*, a three-dimensional set of information consisting of two spatial and one spectral dimensions. This unique feature places the technique as an excellent alternative to traditional spectroscopic methods, for the study of any sample where the spatial characterization is a basic target. The definition of HSI leads to the fact that the amount of information to be handled from a single sample is large enough to require multivariate data analysis techniques for its proper and most advantageous interpretation.

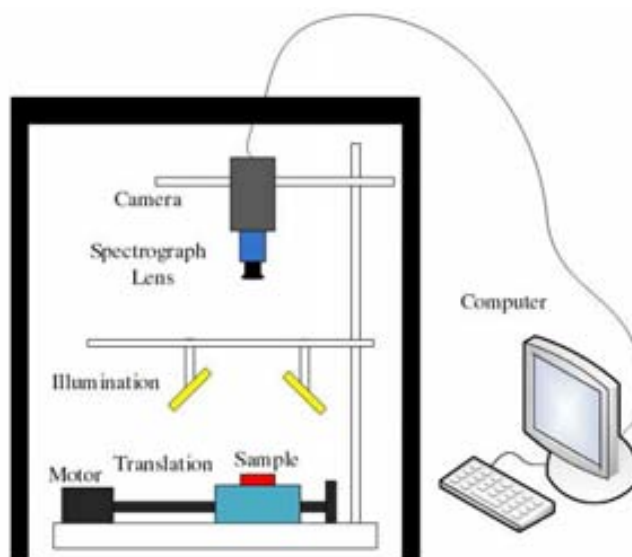


Figure 2.1 Scheme of the typical disposition of a HSI device. All the components can be adapted to specific applications. Every part but the translation motor is necessary in any HSI system 192.

Indeed, it would be hard to think of chemical analysis of hyperspectral images unless Chemometrics had taken over the interpretation of such data. It is worth to make clear that HSI is useful only for the analysis of 2D surfaces. It is possible, though, to identify different components on a surface based on

relevant spectroscopic features. Therefore, the mapping of any sample, regardless its origin, can be done 189 190 191. The variability of applications (samples, environments and type of spectroscopy) has made HSI devices to be particularly designed for each user. Figure 2.1 shows the general scheme that is shared by most HSI devices.

The analysis entity, the hyperspectral cube, is a complex array of data, which can be unfolded for its study, as pictured in Figure 2.2. According to this Figure, the whole set of data is represented by matrix  $D$  (three-dimensional), which has two spatial dimensions ( $x$  and  $y$ ), and a third, spectral dimension, including all the wavelengths measured. The matrix  $C$  (Concentrations) has two spatial dimensions and only one value of spectroscopic signal for each point. This matrix allows the representation of the signal of the whole surface for a given wavelength. The matrix  $C$  can be represented  $\lambda$  times, one for each of the  $\lambda$  wavelengths recorded. Matrix  $S^T$  contains the spectroscopic data: the signal  $n$  for each of the wavelengths measured (absorbance, transmittance, etc.). The product of both matrices allows, when the residual (error) matrix  $E$  is added, the reconstruction of the hyperspectral cube 191 193.

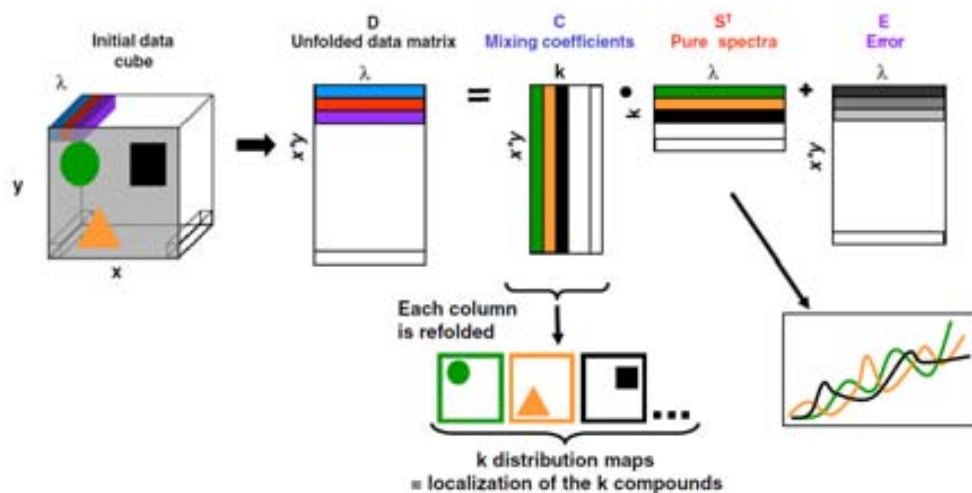


Figure 2.2 Unfolding of the hyperspectral cube into its two-dimensional components 193. This example is the previous step before multivariate quantification algorithms are used. It has been chosen as example because it clearly depicts the organization of the data.

As deduced from the configuration displayed in Figure 2.1, reflectance spectra are generally measured. Reflectance spectra are simple to measure, they do not depend on the particle size and the measurements become robust. The only requirement for recording the spectra is a flat surface, since it maximizes the signal to noise ratio, due to lower reflected signal loss 194. Some different approaches have been used for recording HSI data and creating the hyperspectral cube 191. An example of configuration is provided in Figure 2.3. The three most common configurations for recording mapping spectra are described here. The use of any of them will depend on time restrictions, resolution needed and field of application (research, industry...).

Point mapping. In this configuration, a spectrum is recorded for a single point in the sample, then the holder is moved and the next point is measured. Point mapping leads to slower measurements than



other techniques (although some Raman ultra-fast devices measure 1 point/ms). Naturally, they present a high spectral quality. This measurement configuration has been used for the measurements described in Section 2.4.

**Line mapping.** It is also known as the push-broom configuration. Similarly to the point mapping, the measurements are done by moving the sample, but in this case a whole line of pixels is recorded, so the sample moves in a single direction. It is much faster than point mapping. The works presented in Sections 2.2. and 2.3. are based on such configuration.

**Global imaging.** The last approach is the illumination of the sample for the measurement of the spectra of the whole surface at the same time. While very fast, the limit of this configuration is set by the pixel size, which might challenge the definition of the image.

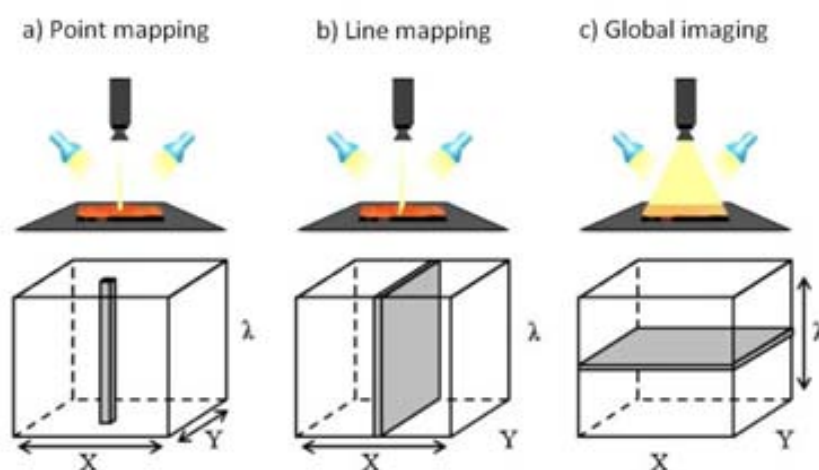


Figure 2.3 Scheme of the different types of configurations for a HSI device. In point mapping configuration, the sample is moved in x and y axes. Line mapping requires a line spectrograph and only one direction of movement for the sample. Global mapping needs no movement at all, but a pixel-array spectrograph. The arrows denote the scanned axis in each possibility (x, y: motor movement;  $\lambda$ : monochromator sweep) 195.

HSI is a versatile technique, which has been coupled to several types of spectroscopy (Raman, IR, Visible, Near Infrared, X-ray...) 188. Some important applications of HSI demand the analysis of solid surfaces with a high measurement speed. As discussed in further Sections, this work has used Near Infrared Spectroscopy (NIRS) and IRS, since they show interesting features for the analysis of urinary stones. As stated in Section 1.3.2., IRS has been widely used for this purpose. Although not that common, some other works have also tested NIRS for the determination of stone composition 196. These two sorts of vibrational spectroscopy stand as the most common ones coupled to HSI, due to the diversity of molecules that can be analyzed within the energy range they are defined by.

Other technically complex set-ups have been defined, such as the use of synchrotron radiation as the energy source 197 198. In this case, although the principles of the technique are the same, the analysis becomes more difficult. Firstly, the number of synchrotron facilities worldwide is reduced. Secondly, the sample pretreatment is much more laborious than that for conventional HSI (in this case the sample

must be polished to achieve a perfect flatness). Nevertheless, the results of this energy source are excellent, when the aim of the experiment is to improve the spatial resolution of the beam. The signal to noise ratio of synchrotron HSI microscopes is around 100 times greater than those achieved with conventional detectors 199. The benefits of using synchrotron radiation are illustrated in Figure 2.4. An application based on this coupling is described in Section 2.4.

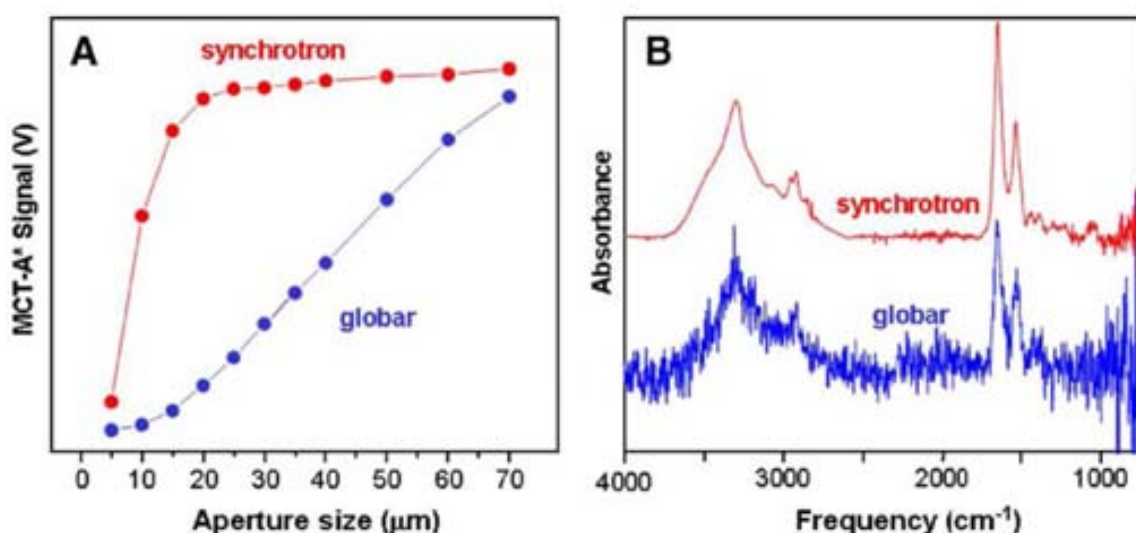


Figure 2.4 a. Beam intensity through a scan of beam apertures for globar and synchrotron radiation sources. b. The higher brilliance allows a better S/N ratio for small spot sizes 200.

Hyperspectral images were initially analyzed by means of the so called “first-order statistics”, such as grayscale or RGB color images or even histograms analysis. However, the use of some more complex, multivariate chemometric techniques is required for a total exploitation of the measurements, procedures also known as Multivariate Image Analysis (MIA) 188. MIA serves mainly for the analysis of images with multiple target compounds in every pixel.

Obviously, such a complex data treatment makes the analysis much more intricate, since the newly defined dataset does not have a simple, straightforward interpretation. Despite this added complexity in the analysis, the understanding of the nature of the samples lays in a much deeper level. This clearly remarks the convenience for the utilization of these techniques, usually linked to the use of more powerful software 201.

### 2.1.2. Data analysis techniques

The variety of MIA techniques available allows choosing the best fit for the specific goal in each analysis. Quantitative analysis of pixels demands different techniques as the classification of samples into classes. Several analysis methodologies have been used in this work, to adapt them to the required output in each case. An outline on their principles and applications is given in this Section.

### 2.1.2.1. Factor Analysis

Factor Analysis (FA) is a powerful multivariate analysis algorithm, generally used for the reduction of the variables that define a multiparametric dataset. The goal of FA is to find the “latent” variables (known as “factors”), which can describe the variance of the data, not including the error. This technique is based on variables correlation. All the real variables that show an important degree of correlation can be expressed as a single factor, thus reducing the dimensionality of the system 202 203.

FA makes possible to distinguish the number of pure components in a data matrix that includes several constituents. It can be used for screening the possibility of *a priori* identifying chemical substances, since factors potentially bear chemical meaning.

This data analysis algorithm creates a new equations matrix that can describe the dataset with the most relevant real variables. The matrix rank (number of linearly independent lines) equals the number of factors needed to reproduce the system. Each factor describes a percentage of variance in the dataset. From the highest to lowest percentage, factors are assigned a value (*eigenvalue*), which can be used for weighting the factor 204.

Some theories have been described for selecting the number of factors considered as descriptors of the model. Traditionally, only factors with an associated *eigenvalue*  $\geq 1$  have been considered. Other criteria, based on error calculations might be considered, since they adapt better for different cases 205.

### 2.1.2.2. Principal Components Analysis

One of the leading multivariate analysis techniques is Principal Component Analysis (PCA). It helps to reduce the dimensionality of the system, while keeping the most relevant information and decreasing noise. In other words, PCA is able to undercover information that might be underlying in raw multivariate data 206. PCA can be considered as a transformation of the real variables into a new coordinates system. These new coordinates are linear combinations of *real* variables (in this work, wavelengths). These units are named *Principal Components (PC)*. Each PC is, therefore, the result of different weights for each real variable. The weight of each variable is called *loading*. Each PC has the particularity of being orthogonal to the others that form the coordinates system. Logically, samples receive a new value for the new variables. This new values are called *scores*. Taking Figure 2.2 as a reference, matrix *C* would be considered as the loadings matrix; it has as many columns as the real data (as many wavelengths). The matrix  $S^T$  is the set of data that contains the values for each point and each loading; it is the scores matrix 207.

This organization of the data allows a direct identification of the most representative variables in the system. As many PCs as desired can be calculated for a system. The first PC always explains a greater part of the variance of the system than the second, and so on. Each system can usually be described by as many PCs as different groups (chemical components) form the data set. Likewise, the loading for each real variable in a PC is different, so the variable with a higher influence on a PC can be rapidly identified.

Logically, the highest loadings for the first PCs stand for the most important variables in the set. Last PCs (the number should be specifically determined for every data set) are usually noise, and provide little, if any, information.

Although FA and PCA share some characteristics, a basic difference separates them. While FA has the goal of explaining the correlation between *variables* to express those variables as fewer latent items (dimensions), PCA tends to create new variables for explaining as much variance of the *data* as possible. In other words, FA is focused on variables, while PCA takes all the data 203 208.

### 2.1.2.3. Artificial Neural Networks

Artificial Neural Networks (ANN) are considered a sophisticated and powerful computational tool that solves analytical problems by learning from real cases. It is a supervised data analysis technique. The main feature of ANN is based on its learning algorithm, which imitates the learning process in the brain. The algorithm learns from examples as an iterative process, and creates internal relations between parameters based on experience 209.

An ANN is a computational model formed from a certain number of single units, artificial neurons or nodes, connected with coefficients (weights), which constitute the neural structure. A number of structures for ANN have been described in literature. This work has used a simple structure, which allows faster calculations, based on three layers: input, hidden layer and output (see Figure 2.5). The input layer receives the information to classify; no calculation is performed at this level. The hidden layer processes the information initiated at the input. The number and weights of the connections of the hidden layer with the other items is defined during the model training. The output layer is the observable response, the classification results 210.

The optimization of the ANN has been performed in this work by minimizing the root means square error (RMS) that stands as a measure of the overall error for all the samples 211.

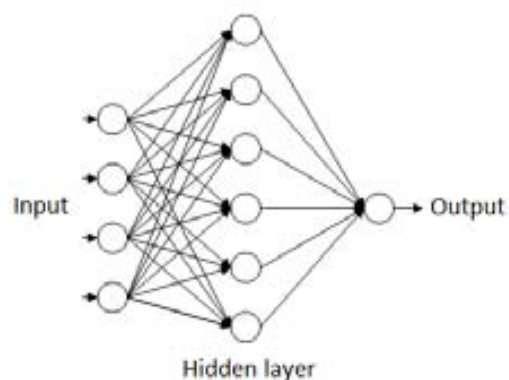


Figure 2.5 Example of ANN structure. The input corresponds to the entered data; the output is the result, as a single variable or as many separated values. The hidden layer can contain variable number of nodes, usually connected to all the other elements in the system. Various hidden layers can also be defined.

#### 2.1.2.4. Experimental outline

This Section presents two imaging works based on the same samples and technique (HSI-NIR), with the aim of offering an automatic classification of urinary stones based on their chemical composition and structure. They can be regarded as two diverging ways of analysis of the same hypercube. Not only the number of possibilities of measuring the hypercube is large; the interpretation of the data can also be done using a number of chemometric techniques. Each approach requires a given data processing, which leads to different information.

In this case, a new methodology for the classification of urinary stones was developed using a NIR Imaging Spectrometer. The results were compared to the most common stone analysis techniques: Microscopic Analysis (MA) and IR Spectroscopy (IRS). For the comparison with each of these methodologies, the most suitable data analysis procedure was selected. MA classifies the stone into groups, according to composition and distribution of components, so the hypercube was divided into regions, which yielded also a group classification (Section 2.2. ). On the contrary, IRS allows the calculation of concentration of components, so a quantification of pixels was performed in the second case, as described in Section 2.3.

In addition, a third set of measurements was done, in this case using IR microspectroscopy. The measurement of urinary stones by means of IR microspectroscopy provides a tremendously high resolution. This allows the uncover of structural properties that remain hidden when traditional IRS measurements are performed. These results, properly described in Section 2.4. , are also complemented by the use of synchrotron radiation as radiation source. The advantages of such configuration are made clear in the mentioned Section.

## 2.2. NIR-Hyperspectral Imaging: Artificial Neural Networks

The work described in this Section was performed in collaboration with the Dipartimento Ingegneria Chimica Materiali Ambiente (DICMA), from the Università di Roma (University of Rome) and located at Latina, Italy. The measurements were developed under the supervision of Professor Giuseppe Bonifazi and Professor Silvia Serranti.

The goal of this work is the development of a urinary stone analysis and classification methodology, which is comparable to MA, yet is able to overcome some of its limitations. As described in Section 1.3.3.1. , MA is an excellent alternative for precisely describing the stone structure and relating the major and minor components distribution to a specific lithogenesis process. Nonetheless, these results require a careful stone analysis, which is time consuming and, more importantly, requires a trained

technician. Naturally, the associated costs are also higher than those for IRS, fact that should be considered for the implementation of HSI in routine laboratories. This Section suggests a highly automated, novel methodology for the analysis of stones, that skips the requirement of a trained analysts posed by MA.

### **2.2.1. Experimental Section**

#### **2.2.1.1. Samples**

Urinary stone samples were collected from the Urology Services of the Hospital Universitari de Bellvitge (Barcelona, Spain). Two hundred samples were selected from a library of 1400 renal calculi. The selection criterion was to include a wide variance within each stone type, to reflect the multiple possibilities seen in real cases. In other words, several stones that belong to the same type can have different appearances (see samples images in Section 1.2. ), but the system should be able to assign the same class label to all of them.

The stones had been obtained either by surgical removal or natural expulsion. After collection, the stones were thoroughly rinsed with ethanol and water. Once clean, samples were individually stored, showing no decomposition or structural damage during periods longer than a year.

As already indicated, HSI requires a flat surface for the analysis, so all the samples were cut with a surgical knife. This step was often needed for the MA classification. Despite this theoretical limitation, the methodology could also correctly classify rounded samples. Some stones showed a heterogeneous structure. In those cases, both external and inner parts of the sample were analyzed.

#### **2.2.1.2. Equipment**

Microscopic analysis of the samples was done previously to the HSI measurements. For this purpose, a stereoscopic microscope was used to observe and describe the sample, according to the following features: color, texture, distribution and approximate amount of components, stone hardness and size. The full description of the sample included the characterization of the stone surface and core, as stated in Section 1.3.3.1.

For those samples that were difficult to uniquely classify, SEM microscopy was used. As described in Section 1.3.3.2. , X-Ray elemental analysis was done for the precise identification of the chemical nature of the sample. The equipment was a JEOL JSM-6300 Scanning Electron Microscope (Japan), coupled to an Oxford Instruments Link ISIS-200 (UK) X-Ray Dispersive Energy Spectrometer.

The results obtained from the previous methodologies were considered the reference for the latter comparison of the hyperspectral data.

The equipment used for the measurement of the hyperspectral images was located at the partner's facilities.

The HSI system was formed by the following components: optics, spectrograph, camera, translation unit, energizing source and control unit. The core of the system, the NIR spectrograph, was a ImSpector™ N17E imaging spectrograph (Specim, Finland). The spectral region scanned covered 1000 to 1700 nm. The camera consisted in a Te-cooled InGaAs photodiode array, with a spatial resolution of 15  $\mu\text{m}$  and a spectral resolution of 7 nm (a total of 121 wavelengths were measured). The spectrometer was coupled to a 50 mm lens. In this case, the measuring mode was as line scanning (example b in Figure 2.3). The image width was 320 pixels; the length depended on the number of lines used for recording the image (between 200 and 350 frames depending on the sample). The energizing source was constituted by a diffused light cylinder with aluminium internal coating, embedding five halogen lamps. This light configuration allows an intense signal, continuous in the whole spectrum, suitable for the NIR region.

The spectral camera was hosted in a laboratory platform equipped with an adjustable speed (from 0 to 50 mm/s) conveyor belt (26 cm width and 160 cm length). Samples were placed on the top of this belt, and they were pulled forward during the measurements. The hyperspectral cube was created by stacking the measured lines.

The device was fully controlled by a PC unit equipped with the Spectral Scanner™ v.2.3 acquisition/preprocessing software (DV srl, Italy). The configuration used can be seen in Figure 2.6.

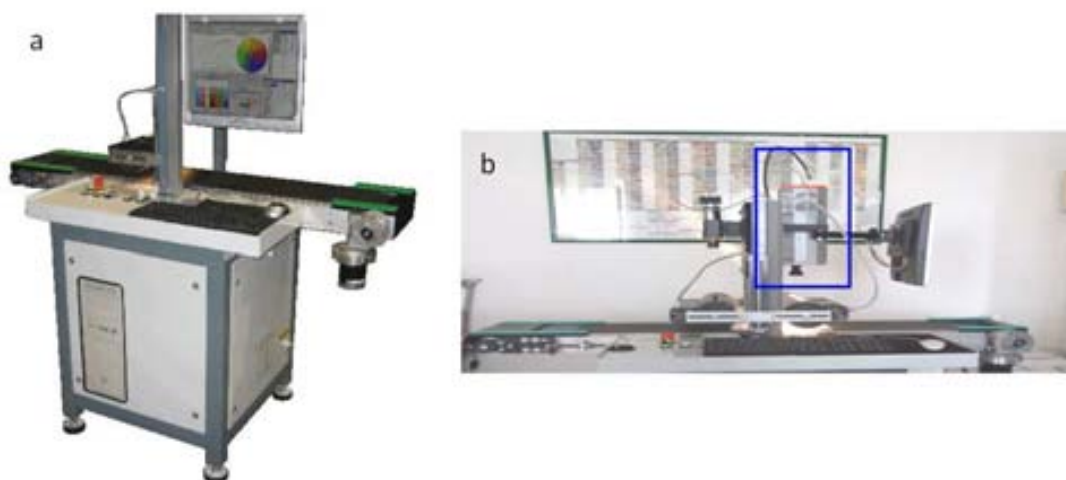


Figure 2.6 NIR-HSI architecture set-up. a. Conveyor belt and PC unit. b. Illumination and NIR spectrometer (in blue square) configuration.

It can be deduced, from the configuration of the device, that the reflectance spectra of samples were analyzed. The detector was placed over the conveyor belt, so the surface of the sample measured had to be placed upwards. Plastic holders were used for fixing the samples.

The raw signal was corrected using an absolute black and white calibration of the detector, according to Equation 2.1. In this Equation,  $R$  is the calculated reflectance value,  $r_s$  is the reflectance measured from the sample,  $r_b$  is the reflectance value for black (background noise) and  $r_w$  is the reflected signal for white (100% reflectance).

Equation 2.1 Reflectance signal correction, using black and white calibration.

$$R = \frac{r_s - r_b}{r_w - r_b}$$

When using HSI, the radiation penetration depth is defined as the depth at which the incident light is reduced by 99%. It varies, in fact, according to sample characteristics, surface attributes and investigated wavelengths (depth is lower when wavelength increases). In this study, this magnitude can be estimated in 10-20  $\mu\text{m}$ .

### 2.2.1.3. Data selection

The classification of stones into groups was done by randomly selecting some regions on the sample surface. These Regions Of Interest (ROI) were small areas of the scanned surface, so the reflectance value obtained was the average of all the pixels in the designated ROI. An example of ROI selection is shown in Figure 2.7. The distribution and size of the selected ROIs were randomly chosen, to test the independence of the methodology from the operator's experience on selecting these areas. ROI selection allows, firstly, the smoothing of the surface features, so the spectral noise is reduced. As represented in Figure 2.8, when the stone surface is scanned, data is recorded as independent pixels (grey grid). The surface of the sample might not be homogeneous considering adjacent pixels due to organic matter, which could have been trapped in the structure during the crystallization process. If a ROI is selected (black square) and the average of all the spectra is calculated, the effect of sudden composition changes on the surface fades away. Secondly, the amount of information to manage is much smaller than handling the whole hypercube. All the ROIs taken from the same stone are treated as a single sample for the following analysis steps, so the classification is based on 5 spectra (averaged) for each sample.

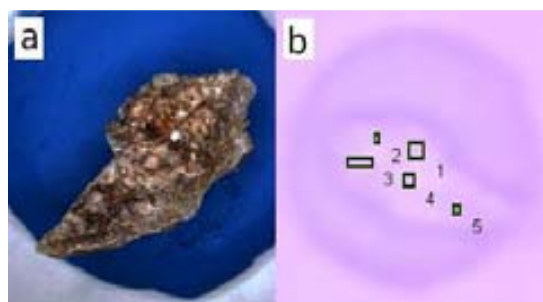


Figure 2.7 Example of ROI selection. a. Visible image of a stone. b. Reconstructed image of the same stone (from software) with a selection of ROIs.



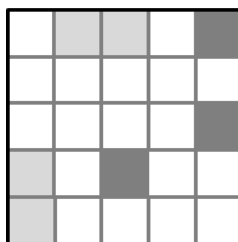


Figure 2.8 ROI selection smoothing effect. The grey grid represents the measured pixels. Different pixel color fillings symbolize different composition. A suitable ROI is indicated as a black square.

Stone types are classified according to several classes, based on their chemical composition. According to Section 1.2. , samples were sorted into several groups: uric acid (UA), brushite (BRU), calcium oxalate dihydrate (COD), calcium oxalate monohydrate (COM), cysteine (CYS), apatite (CAP) and struvite (STR). Some examples of the stones used as references or standards are shown in Figure 2.9. These seven groups formed the general classification scheme, adapted to pure components. A more complex classification was also tested, including uric acid dihydrate (UAD), layer and non-structured mixtures of CaOx and CAP (MXL and MXD respectively), and COM obtained from COD transformation (TRA). This extended classification (eleven classes) was much more adapted to the real stones, which are often found as mixtures of components.



Figure 2.9 Reference samples for the creation of the model. a. BRU b. CAP c. COD d. COM e. CYS f. STR g. UA. Each individual fragment seen in the figure corresponds to a different patient.

For each group of stones, some reference samples were first measured for creating a classification model. This model was used for the classification of all the samples and also for describing the main features of the data system, as identifying the variables with a highest weight for the description of the dataset.

### 2.2.2. Results and discussion

The NIR reflectance spectra of the reference samples were measured and used for the creation of a classification model. As it can be appreciated in Figure 2.10 (top), the spectra show some unique

features that make their identification possible. However, as often seen in NIR Spectroscopy, absorption bands in this energy range are not as sharp and intense as IRS, so the use of chemometrics data analysis techniques is needed. The intensity of the reflectance spectra is not always directly linked to the chemical composition of the component. It depends on the surface geometry, so it might carry information also from physical properties. Hence, the first derivative of the spectra is used for the calculations. Figure 2.10 (bottom) shows different trends for each compound, so their identification becomes possible. The derivative spectra were calculated after the smoothing of the curves using the Savitzky-Golay algorithm, with a 5-point window. This procedure calculates the new, smoothed curve by calculating the average from 5 consecutive spectral data points and repeats the operation by shifting the 5-point window until the complete spectrum has been recalculated 212.

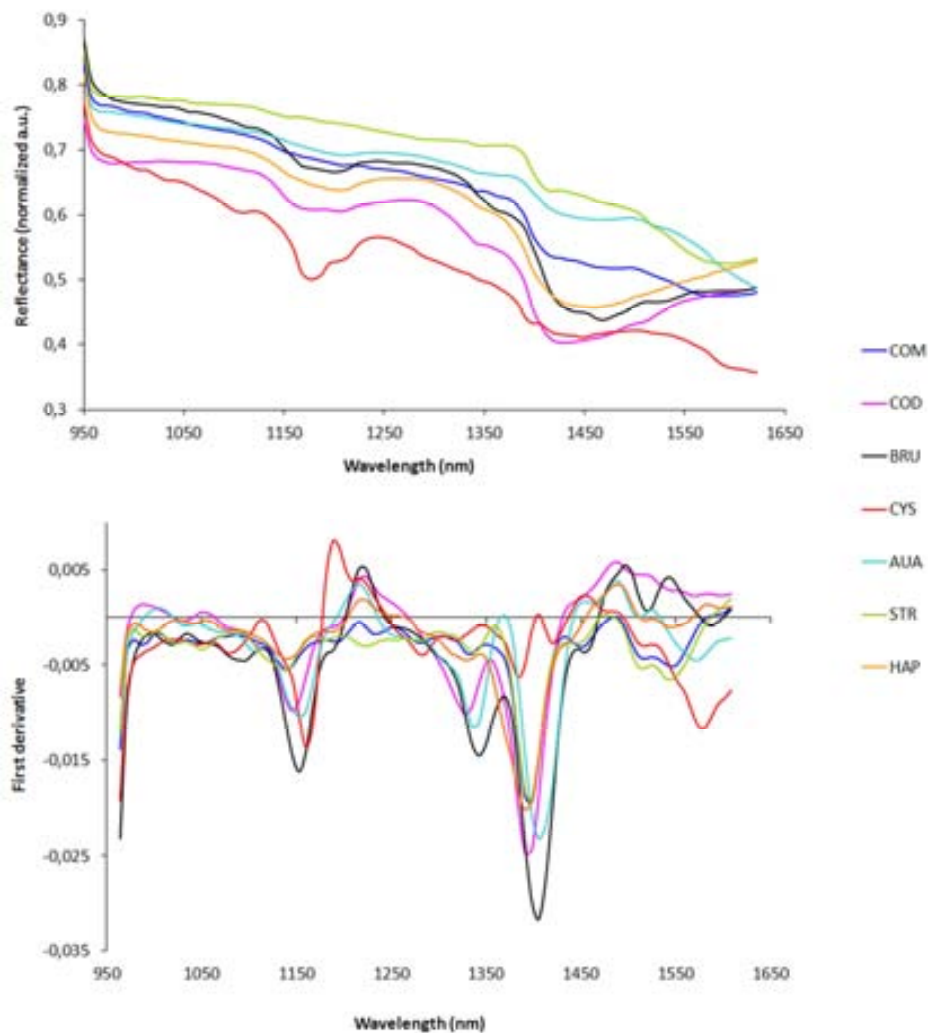


Figure 2.10 Reflectance spectra from standards. Top: Raw reflectance spectra. Bottom: First derivative of the spectra.

### 2.2.2.1. Factor Analysis

When FA is applied to ROI selected on the standards, seven factors are identified as having an *eigenvalue* greater than 1 (see Figure 2.11). According to Kaiser's rule that number of factors could point out how many different compounds can be identified in the dataset. Chemometrics techniques usually need to adapt to each specific case. In this specific case, Kaiser's rule applies, although this criterion should not be taken as a general rule. The standards include seven different chemical species, and FA has proved that they can be correctly identified through their spectra.

Taking into account these results, a PCA analysis was also used for the correct description of the samples.

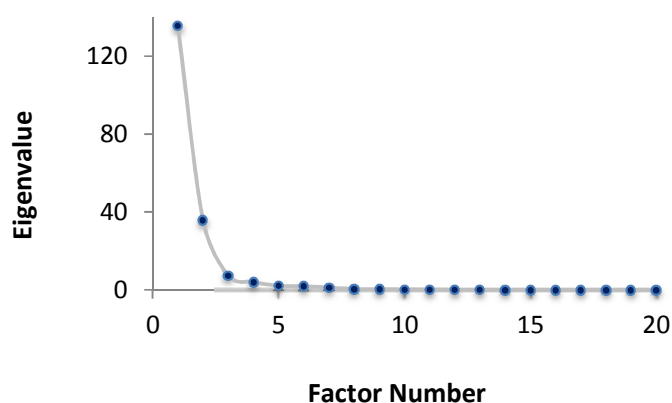


Figure 2.11 Eigenvalues associated to each factor.

### 2.2.2.2. Principal Component Analysis

PCA can be considered either the start of the data analysis (data screening) or the last step, since it allows the reduction of the dimensions of the dataset as well as sorting the samples into classes. In this work, PCA was used for the data screening and the description of the dataset. The classification of the samples was later done by ANN (described in Section 2.2.2.1. ).

Initially, PCA was performed for the classification of outliers within the reference samples set. This action, often known as "cleaning the data", should be useful to create a robust model. For this goal, seven different groups of samples, each of them including only one stone type (one chemical component), were selected. The data introduced into the PCA calculations was a selection of multiple ROIs drawn on the surface of each stone fragment. PCA analysis on an individual group can reveal if a sample has different characteristics from the rest and so, appears as a separate group of ROIs.

The elimination of any point from the original samples is a crucial step, since it decreases the variability of the system. Moreover, there is no way to be completely positive whether a sample is correctly considered as an outlier. Thus, the elimination of potential outliers has to be done carefully, so no

overfitting of the model is forced. The model is overfitted to the samples when it is too adapted to the dataset. Thus, a sample that belongs to the same group but does show slightly different characteristics can be erroneously misclassified 213.

The identification of outliers was done by plotting the Hotelling T2 ellipse of the scores plot. As already described, PCA assigns new coordinates values (scores) to the samples in a new coordinate system, whose variables are named Principal Components (PC). Thus, the representation of the samples scores for two PCs gives a two-dimensional plot, in which an outlier sample can be clearly identified as a different group. The Hotelling ellipse draws the 95% confidence region. When applied to the standards, only one sample of COM was clearly identified as an outlier (also outside the Hotelling ellipse).

Once the data from stone classes had been individually analyzed, PCA was performed on the seven groups of different components (BRU, CAP, COD, COM, CYS, STR and UA). The model was created on a large number of ROIs, taken from the reference samples fragments, and the performance was checked by means of *cross-validation-leave-one-out*. This algorithm consists on an iterative process: all the ROIs are placed in a pool and a single ROI is removed from the pool, which is now the training set. This partial model is used for the classification of the single ROI. Then, the process is repeated for each ROI in the training set until all of them have been tested 206.

The model created using the reflectance spectra explained 95% of the variance with only two PCs. On the contrary, when using the first derivative, up to 7 PCs are needed for explaining 96% of the data variance. These results are plotted in Figure 2.12. It is preferable to take the second approach, since more PCs will give a more precise description of the samples. The first derivative magnifies the slight differences existing between the spectra for different urinary stones classes. Indeed, 7 PCs is consistent with FA calculations, which also pointed out 7 factors as the more suitable number for the description of the system.

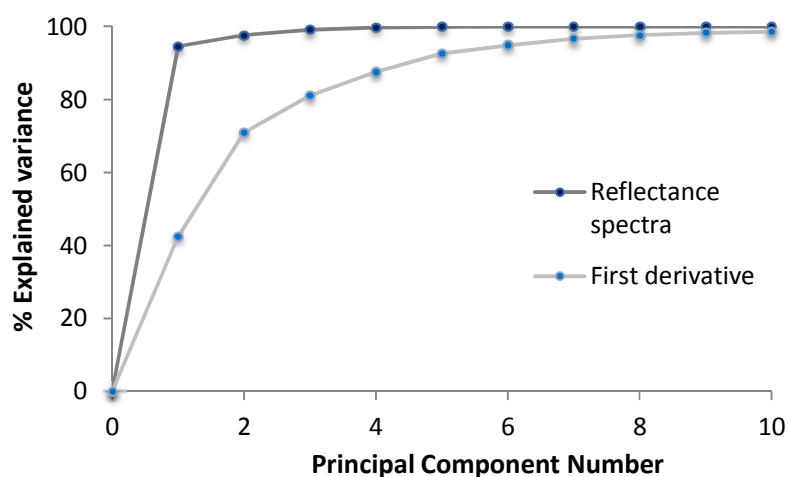


Figure 2.12 Explained variance for 10 first PCs in two models. Dark grey: raw reflectance spectra. Light grey: first derivative spectra.

One of the main claims of PCA is the reduction of the dimensionality of the dataset. Multivariate methods can certainly give a higher amount of information than univariate ones, though many variables from the measured range might not give valuable data, but spectral noise. PCA stands as an interesting data analysis technique for the variable selection, so only the data with classification power is taken for further calculations and noise is avoided in a great extent.

As described in Section 2.1.2.2. , each PC is described by a linear combination of real variables. The weighting of each real variable is defined by its loading, a value with a magnitude between 0 and 1. The loading values can be plotted, as in Figure 2.13, for the visualization of which real variables define which PC. This representation allows, firstly, the identification of which spectral regions (and so, chemical components) most influence each PC. Secondly, it also allows the localization of spectral regions of low classification power that mostly carry noise. According to this representation, some spectral regions with a high loading value for the 7 main PCs were selected for classification purposes.

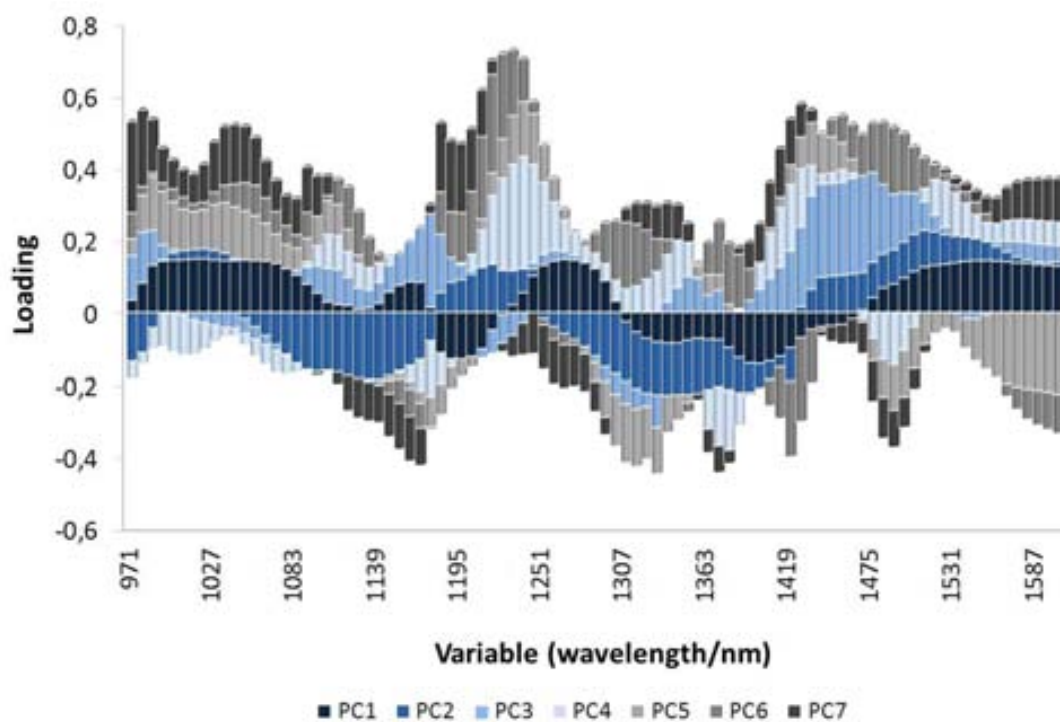


Figure 2.13 Representation of the loading values for the 7 main PCs.

When the scores values for combination of PCs for each group of samples are plotted (e.g. PC1 vs PC2, PC1 vs PC3...), it is possible to assess which chemical components are distinguished which each PC. Together with the values plotted in Figure 2.13, the wavelengths (or spectral regions) that better identify each component can be selected. Variable selection leads to the reduction of the dimensionality of the dataset and elimination of the noise, thereby increasing the model precision and simplifying calculations.

## 2. Image analysis

A general distribution of the groups of samples in the model using a two-dimensional scores plot is shown in Figure 2.14. From this graphic it can be clearly seen, for instance, that CYS stones are well defined for score values  $<0$  for PC1 and  $>0$  for PC2, while UA is mostly found at values  $<0$  for PC1 and  $>0$  for PC2. This example pictures the general use of PCA. A single PC is usually not enough to define the entire dataset, but a combination of several PCs is needed for a precise separation of the components.

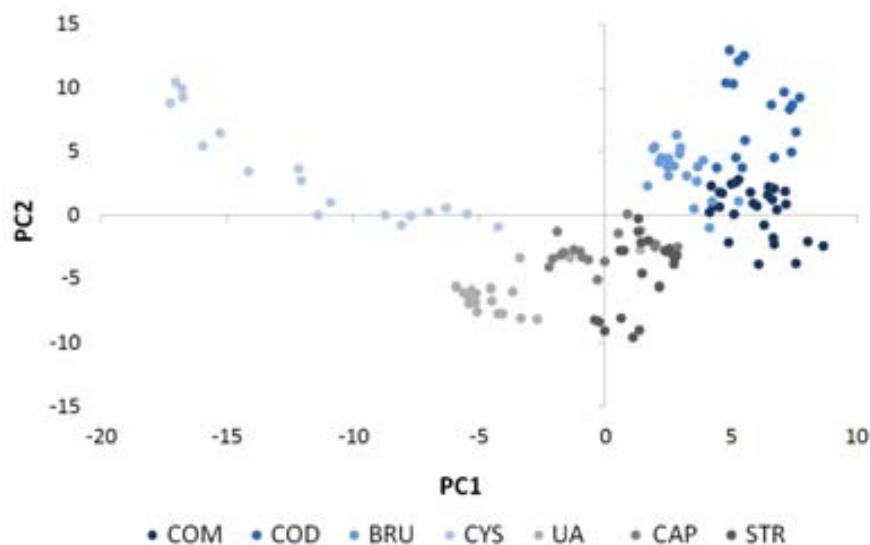


Figure 2.14 Plot of the scores values for PC1 vs PC2 for the reference set.

The careful analysis of this example shows that PC2 is well defined by positive loadings values at the regions 1200-1250 nm and 1450-1530 nm (see Figure 2.13). These regions correspond to the energy of C-H vibrations. On the other hand, the regions 970-990 nm and 1075-1175 nm, associated to Aryl-OH vibration, are described by a negative loading value. These spectral regions that strongly influence PC2 fit with the chemical structure of CYS and UA, the components it correctly identifies (see Figure 2.15).

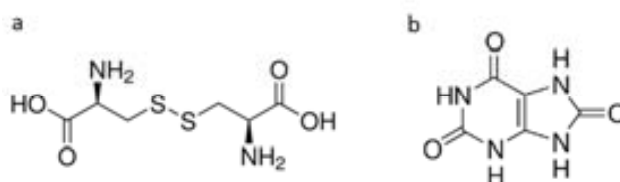


Figure 2.15 a. CYS chemical structure. It is the only component in the set that contains C-H bonds. b. UA structure, Aryl-OH groups can be seen due to the tautomeric structure.

CYS is the only compound of those analyzed here that has C-H bonds. UA is the only substance with a possible Aryl-OH vibration, due to the tautomeric form, that assures aromaticity.

When all the PCs are analyzed as shown, the spectral regions that define all the PCs can be clearly identified. COM and COD are distinguished due to the O-H vibration from water. BRU is separated from

other phosphates due to the C-H band, probably due to the high amount of organic matter these stones keep within their structure. Specific details on each energy range are listed in Table 2.1.

Table 2.1 NIR bands that define each PC and associated molecular vibrations for each reference component.

Urinary stone type	PC Characteristics	$\lambda$ with greater loading value (nm)	Associated molecular vibration
CYS	PC1<0 PC2>0	1188-1230, 1440-1542	CH, CH <sub>2</sub> , CH <sub>3</sub>
UA	PC1<0 PC2<0	971-978, 1083-1167	Aryl-OH
COD	PC3>0 PC2>0	1462-1475	H <sub>2</sub> O
COM	PC3<0 PC4>0	1223-1244	C-H
BRU	PC3<0 PC4<0		
CAP	CAP and STR are not well defined with PCA		
STR			

CAP and STR cannot be correctly defined by PCA. They appear as a single cloud of ROIs considering any combination of the seven main PCs. Although they might show some different trend, the clouds for CAP and STR are permanently overlapped, so the classification is not well achieved. Indeed, some groups do not show absorption bands in NIR (as P-O or COOH) or in the range used in this work (S-H absorbs above 1700 nm).

For accomplishing a complete identification of all the stone groups, a three-dimensional plot of several PCs combinations becomes useful. Figure 2.16 shows such plots, where the groups of ROIs for most stone types can be clearly distinguished. As stated, CAP and STR clouds appear overlapped.

#### 2.2.2.1. Artificial Neural Networks

First derivative data of the spectra were taken into calculations with ANN algorithm, due to their better behavior with PCA models. Five ROIs for each sample were selected, but not all the wavelengths were considered. Only the most important variables, in terms of loading values, were selected. Initially, from the 120 wavelengths measured, only 50 were taken for creating the ANN model. A matrix of 140 samples (the fragments for all the reference stones) and 50 wavelengths was created.

The ANN to be optimized was defined as: (input, number of nodes in the hidden layer, output). Input stands for the number of samples used to create the model, and output, for the number of types of urinary stones. The value for the output was a single variable that could take up to seven different nominal values. The scheme of the ANN structure was (140, n, 7).

The backpropagation algorithm was used for the optimization of the ANN. This procedure performs the optimization of the system by iterating connections and operations among all the input items and the nodes. The criterion is to decrease the error calculated between the input (known results) and the

output. After the optimization step, an optimal number of 4 nodes was found. The error did not decrease significantly when adding more nodes, so no more units were added, in order not to cause overfitting.

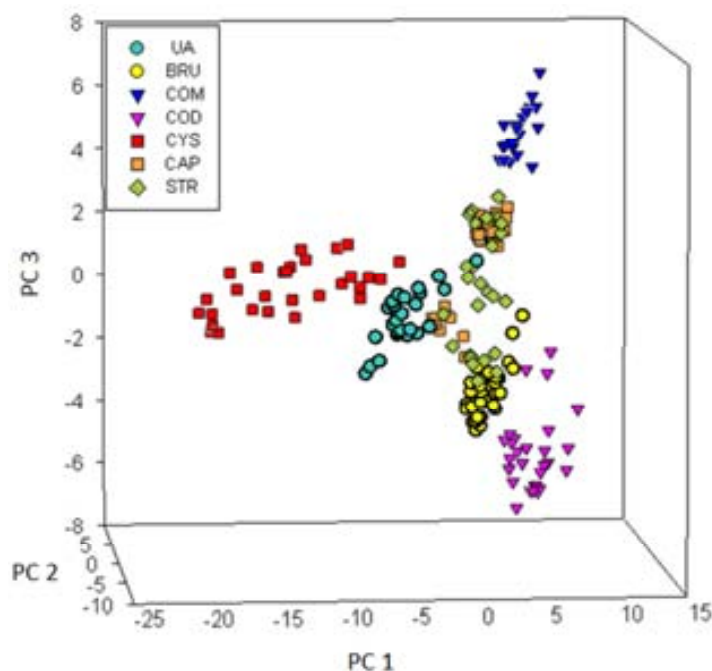


Figure 2.16 3D plot of the scores of the reference samples for PC1, PC2 and PC3.

The model was then applied to 140 samples. The efficacy was tested using cross-validation-leave-one-out. When 50 variables were used (those selected by PCA) 100% of correct classification was obtained. With only 30 wavelengths selected, taking only a few from each spectral range listed in Table 2.1, the accuracy for the classification remained at 100%. When even less variables are taken for the calculations, the percentage for right classification dropped down to 95% at most. Consequently, the final choice was the model including 30 wavelengths.

However, due to the importance of a precise classification regarding the diagnostic for the patient, the really interesting objective is the classification of 11 groups of different types of urinary stones. These groups include the seven mentioned reference samples and also their mixtures or similar chemical forms (MXD, MXL, TRA and UAD).

Thus, an optimization of a new ANN model, capable of the classification of this much more complex data was required. In this case, 215 samples were classified. For this purpose, 50 wavelengths were introduced as variables, being the structure of the optimized ANN (215, 13, 11). The rate of well-classified samples reached 94.4%. The performance of the model is summarized in Table 2.2.

The error for the last model, including all types of urinary stones, is only slightly higher than that for the simpler model. Nevertheless, the second model offers a great advantage, since it is able to deal with any



of the urinary stone types usually found. The prediction differences between the newly developed methodology and the conventional techniques involve basically calcium oxalate urinary stones.

Table 2.2 Number of samples, sorted by group, correctly classified when the ANN model is applied.

Urinary stone type	Number of samples	No. Samples correctly classified	% correct classification
COM	39	37	94.9
COD	27	24	88.9
TRA	27	23	85.2
CAP	18	18	100
STR	19	18	100
MXL	10	9	90
MXD	13	11	84.6
BRU	25	25	100
UA	17	17	100
UAD	10	10	100
CYS	10	10	100
		Total	94.4

### 2.2.3. Final remarks

This work has proven the suitability of NIR-HSI technique together with ANN data analysis for the classification of urinary stones. The results obtained are comparable to those coming from MA.

It is important to remark, however, that the methodology presented here is fast, inexpensive and independent from the analyst. The only point on which the analyst can introduce a bias on the results is the ROI selection. As described in Section 1.3, the most used techniques depend on the analyst experience, while the method presented in this work performs the interpretation of the results independently.

This Section points out NIR-HSI as a possible technique to be used in routine laboratories, according to the results shown. IRS still offers the quantification of stone components. While this interesting issue has not been addressed in this Section, it is carefully studied in the next Section.

The implementation of such methodology in clinical laboratories would only be affordable if other target samples can be analyzed. Thus, new methods should be developed to completely exploit the possibilities of HSI. In this concern, the high versatility of HSI plays a key role for the potential development of other analysis.

The work described in this Section has been published at Journal of Biomedical Optics.

Blanco, F., López-Mesas, M., Serranti, S., Bonifazi, G., Havel, J., Valiente, M. “Hyperspectral Imaging based method for fast characterization of kidney stone types”, 2012, Journal of Biomedical Optics, 17 (7), 076027. This document has been attached in Supplemental Materials (8.3. ).

The described advantages highlight its commercialization potential, so the process has been protected through a patent. A private company in the lithiasis field has actually licensed the patent, so its potential interest to be used in clinical laboratories is clear. Further details on this concern are given in Section 5.2. The register document of this patent can be consulted in Supplemental Materials (**Error! Reference source not found.**

### 2.3. NIR-Hyperspectral Imaging: Pixel-to-Pixel Analysis

This work was developed including collaborations with DICMA – Università di Roma and University Stone Centre, Universitätsklinikum Bonn.

This second work using NIR-HSI technique has important similarities with the previous Section. Indeed, the measurements and so, the dataset, are the same data. This Section represents a different way of treating the hypercube; actually exploiting to a greater extent the main feature of image analysis: spatial resolution. This work relies on a different analysis of the data for the exploration of each individual pixel. The analysis with ANN was based on ROI selection, so it had to be compared with the conventional microscopic analysis (MA), since this technique yields qualitative results. However, as described in Section 1.3.2. , IRS has become the reference methodology in the field and it does yield quantitative results. Thus, the comparison of NIR-HSI technique with the traditional IRS seems of great interest to prove its suitability to become a part of routine analysis.

NIR-HSI stands as an interesting possibility to quantify stone components while keeping information concerning their location.

#### 2.3.1. Experimental Section

The samples used in this Section are the same as in the previous, and so the traditional classification, performed using MA. Microscopy should be considered, in this work, as a support methodology used for sample selection, because it only gives qualitative information. The numerical comparison between IR and NIR-HSI was done on all the samples and standards after this selection step. Therefore, the experimental procedures associated to the previous classification of the samples (for their proper

selection, according to the defined criteria) and the NIR-HSI measurements are the same as those described in the previous Section.

#### 2.3.1.1. IR Spectroscopy

IR Spectroscopy has been used as reference methodology to test the results of NIR-HSI. The main advantages to consider IR as the standard are the robustness and wide acceptance of the technique and the calculation of a numerical value for the sample composition. The IR spectra of the prepared pellets were collected using a representative fragment of each sample, which was dried in an oven for 24 hours at 40 °C prior to the analysis. This fragment was grinded in an Agatha mortar and 0.9 mg of sample were then mixed with 0.3 g of KBr powder. A pellet was prepared by setting this mixture under 10 Tm pressure in a manual press (Perkin Elmer, MA, USA).

The IR spectra were collected using an IR Spectrometer Spectrum BX (Perkin Elmer, MA, USA). The spectral range measured ran from 450 to 4400  $\text{cm}^{-1}$  (which corresponds to a wavelength range from approximately 2200 to 22000 nm), with a spectral resolution of 4  $\text{cm}^{-1}$ .

For the determination of the composition of the samples, a comparison of the measured spectrum with those in the bibliography was done [128]. This collection of spectra considered pure compounds, combination of two species and even a combination of three components, for the common case of calcium oxalate mono and dihydrate and carbonate apatite, including different gradations for the amounts of each component in a 10% (w/w) grading.

#### 2.3.1.2. Data handling

##### 2.3.1.2.1. Qualitative analysis

The data analysis was based, in this case, in a selection of the most relevant variables by using PCA. A first approach used MATLAB software for the qualitative analysis of the surface [214]. The identification of the different compounds was done by interpretation of the colors obtained when creating reconstructed RGB images from the hyperspectral cube. When using this kind of representation, each PC is assigned a color, so the value of the score for that PC will determine the intensity of that pixel. If some PCs are combined in the same plot, the scores values for each of the PCs will determine the combination of colors for that pixel.

The qualitative analysis of urinary stones by means of HSI had already been used. Published results are nonetheless only indicative, because they rely on a description of the sample with no quantification of the components (as described in Section 2.1.) [133]. The goal of the quantitative analysis described in this Section is to offer comparable results to IRS. Since HSI allows the individual classification of pixels, a classifier has been developed for sorting into classes and quantifying the pixels in a stone. The results, calculated as percentage, should be then comparable to IRS.

### 2.3.1.2.2. Quantitative analysis

A further step in the data analysis considered the creation of a classification model, using the most suitable classifier. A classifier is any mathematical function able to assign a label “class” to a given sample, when it has been learned on a specific training set 215.

Following the criteria of the best classification rate, Quadratic Discriminant Analysis (QDA) was selected. This classifier is a classic Bayesian method, generally used on machine learning. It assumes normal distribution of the data within each class and different co-variance within classes 216. Due to the complex nature of the sample set used in this work, QDA is a good approach, since it can establish boundaries between classes based on quadratic algorithms, so it is more flexible than linear classifiers. This classification scheme showed a better performance than other also tested, including k-nearest neighbor, random forest and support vector machines.

The image analysis of the training and test sample sets was performed using SciPy and Scikit-learn, two open source Python libraries for scientific analysis 217 218. When the classification model created using the standards was applied to the samples, the structural analysis of the stone was achieved. Since the spectra were acquired using a multispectral camera, that generates a complete spectrum for each pixel, the physical structure of the stone was reconstructed, based on the result for the analysis of each pixel. This procedures lead to the creation of chemical maps of the stones, which bear the spatial resolution of the technique.

The analysis of the hypercube was performed, as explained for the ROI analysis, by reducing the dimensionality of the dataset using PCA. The advantages are also similar; the classifier has fewer parameters to work with, so the number of interactions is lower. The main features of the PCA analysis will not be outlined here, since they overlap with the previous Section.

The classification model included a variable number between 6 and 8 stone fragments of each stone type with homogeneous composition. Each stone fragment was collected from a different patient, so the model overfitting was reduced. Note that, although only a few samples were taken in the training set, and according to the characteristics of the HSI technique (i.e. acquisition of a spectrum for each pixel of the image sample), thousands of pixels were used for training purposes. The number of samples in the model was large enough to cover all the naturally occurring components in urinary stones.

The creation of the model included a test step, using the *leave-one-out* approach. The vectors of 10 principal components of every pixel of each fragment are placed in a pool. Then, each time a certain fragment has to be analyzed, that is, we want to assign a class label to each of its pixels, they are removed from the pool which now is the training set. The QDA classifier parameters are learned and the classification on the given fragment vectors, which act as testing set, is performed. This process is iterated for every fragment. In pattern classification literature this procedure is known as *leave-one-out*, although in this case it was done at a “fragment level” 206.

### 2.3.2. Results and discussion

#### 2.3.2.1. Qualitative analysis

The qualitative pixel analysis is useful for the direct observation of the distribution of pixels in a sample. To a certain extent, it represents the evolution of the microscopic analysis into an analyst independent technique.

When the qualitative pixel analysis is applied on the reference samples, the results resemble those seen in Figure 2.17. As seen in this Figure, different combinations of PC lead to diverging representations of the samples, since each one describes each component with different precision. Figure 2.17 shows different colors for each kind of urinary stones, providing a simple way to distinguish a type among the others, except for STR and CAP. Indeed, the results obtained analyzing the hyperspectral cube completely matched with those obtained by taking ROIs from the samples (when only PCA is considered).

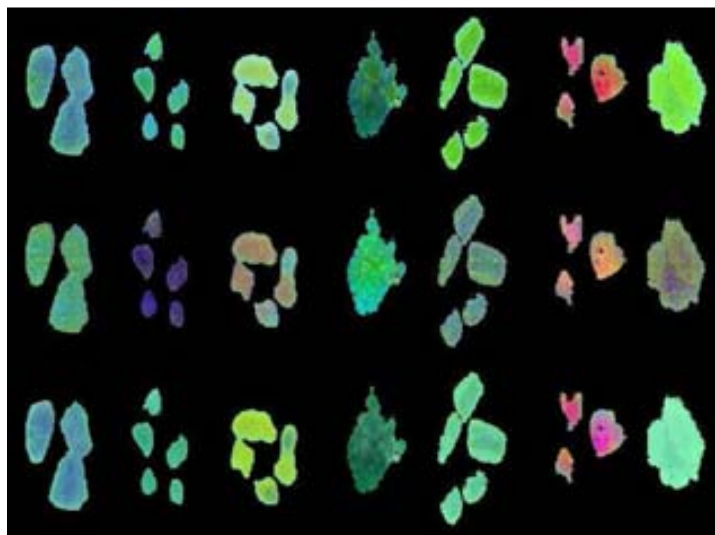


Figure 2.17 Representation of PCA results, based on the combination of 3 PCs. Top: PC1, PC2, PC3. Center: PC1, PC2, PC4. Bottom: PC1, PC3, PC4.

#### 2.3.2.2. Quantitative analysis

##### 2.3.2.2.1. Performance of the HSI-NIR model

The training set was analyzed using IR Spectroscopy (reference values) and also using NIR-HSI. In this case, only homogeneous samples were considered, since the objective of this step was to train the classifier in the recognition of stone classes using a large number of pure pixels. It was easier to isolate

pure pixels in homogeneous stones. The advantages in spatial resolution of HSI are not relevant in this step. The graphical results obtained for the HSI model performance are shown in Figure 2.18.

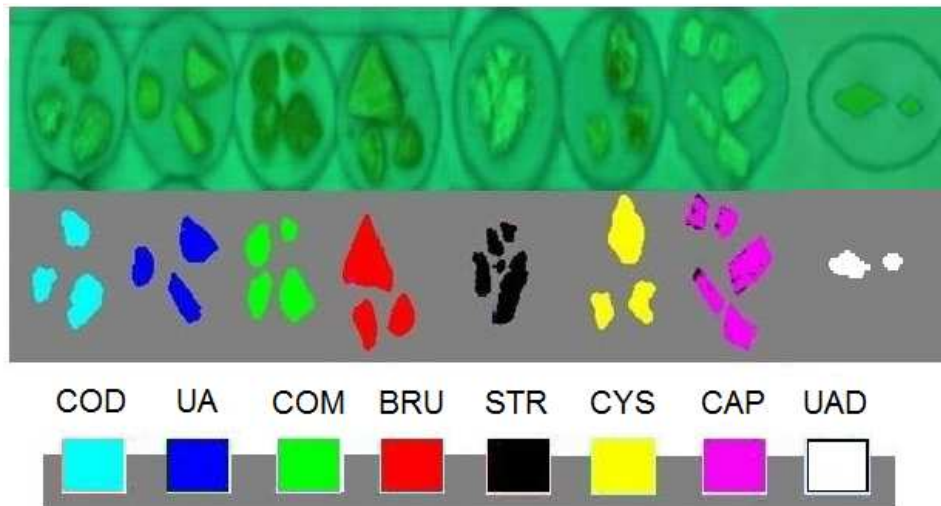


Figure 2.18 Classification results using the training set (not all the samples used for the creation of the model are shown). Upper row: Reconstructed image from original stones, generated using the acquisition software. The different fragments, each from a different patient, can be appreciated. Lower row: Results of the classification model, where each pixel is individually assigned a class and so, a different color.

The overall correct classification rate of the model was calculated to be 90.4%, in terms of correctly classified pixels, comparing to the results obtained by IRS. The specific efficacy of the model on the classification of each stone type is shown in the normalized confusion matrix (Table 2.3).

Table 2.3 Normalized confusion matrix. The efficiency of the model can be measured as percentage of correct classification for each stone class. Light blue cells highlight the diagonal, which shows that most values greater than 90%.

Type of stone	Predicted values (%)							
	BRU	COM	UAA	COD	CAP	CYS	STR	UAD
BRU	99.37	0	0.08	0.55	0	0	0	0
COM	0.04	99.75	0	0.04	0	0.17	0	0
UA	0	0	99.33	0	0.16	0.08	0	0.43
COD	0	0	0	99.77	0.17	0	0.06	0
CAP	4.83	0	0	1.26	73.33	0.07	20.51	0
CYS	0	0	0	0.03	0	99.84	0.13	0
STR	0	0	0	0	26.55	0.02	73.43	0
UAD	2.06	0	0.36	4.58	0	0.72	1.17	91.11

The diagonal of the matrix shows how, for most classes, only a residual number of pixels are confused with other classes, with the exception of CAP and STR. Indeed, CAP and STR are mostly confused with

each other (30-40% of the pixels). This lack of classification power can be attributed to the similarities in the spectra of both species. These results are similar to those obtained when only PCA is used, as described in Section 2.2.2.2.

These results can be considered as a good performance, even considering the remarkable variability of the spectra within individual groups of stones, depicted in Figure 2.19. NIR does not overlap with IR Spectral range. Despite this important difference, most of the relevant bonds in organic components can be identified in the NIR range, including: C-H, S-H, N-H, O-H or O-H linked to an aromatic ring. The sensitivity of those bonds (which are also identified in IR Spectroscopy) in the NIR range, grants a proper recognition of urinary stones mineralogical components, as discussed here.

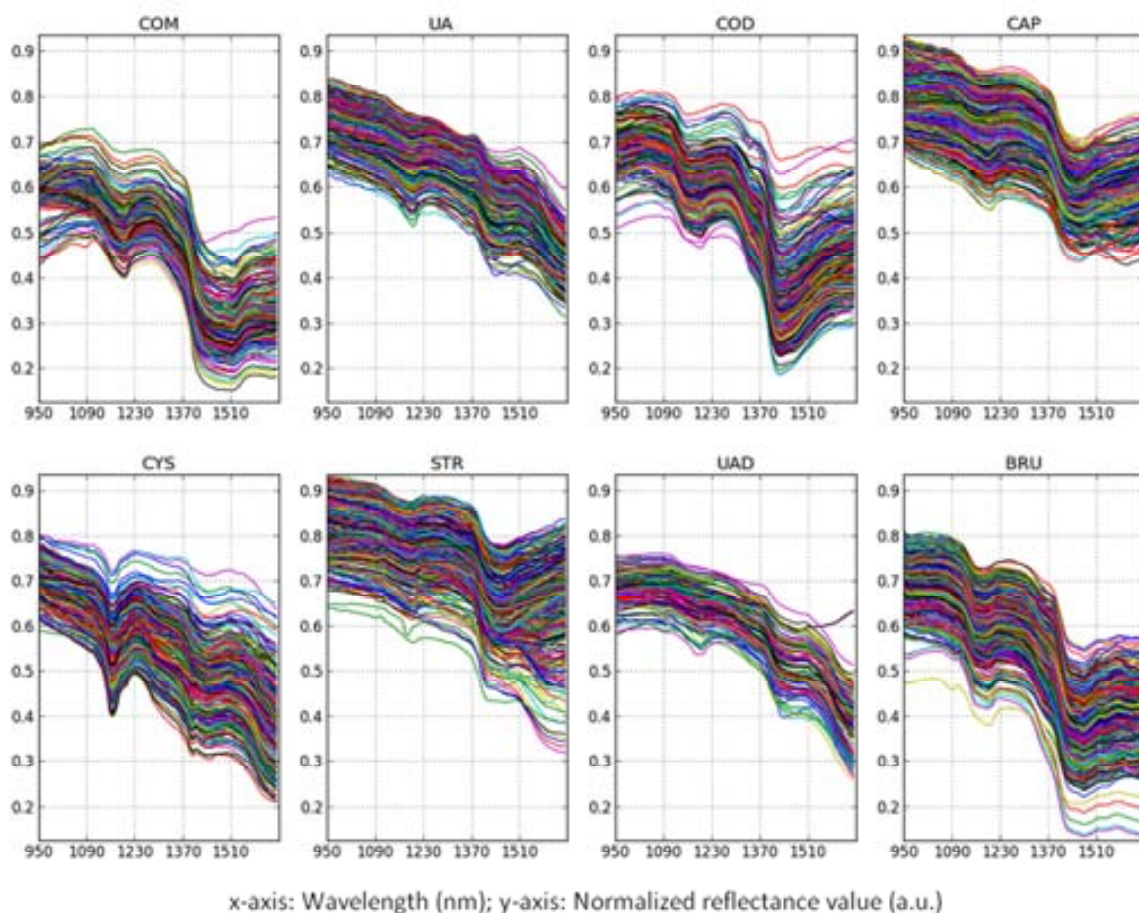


Figure 2.19 Representation of all the spectra in the training set for all the stone classes. The spectra have been normalized.

From the performance of HSI it can be deduced that thousands of pixels from each species are taken into the calculations. Although a fragment from a single patient does not contain totally independent pixels (and so, spectra), the vast number of spectra measured present an inherent variability, which benefits the creation of a more robust model. The number of pixels included in the model for each stone type is plotted in Figure 2.20. Only UAD counts with a smaller amount of pixels for the creation of the

model. It was laborious to isolate rather pure regions of UAD, since UAD rapidly transforms into UAA in contact with urine 112. The computer model, though, is able to perfectly discriminate (>99%, as seen in Table 2.3) between the two derivatives of uric acid, and also distinguish them from any other component in a great extent.

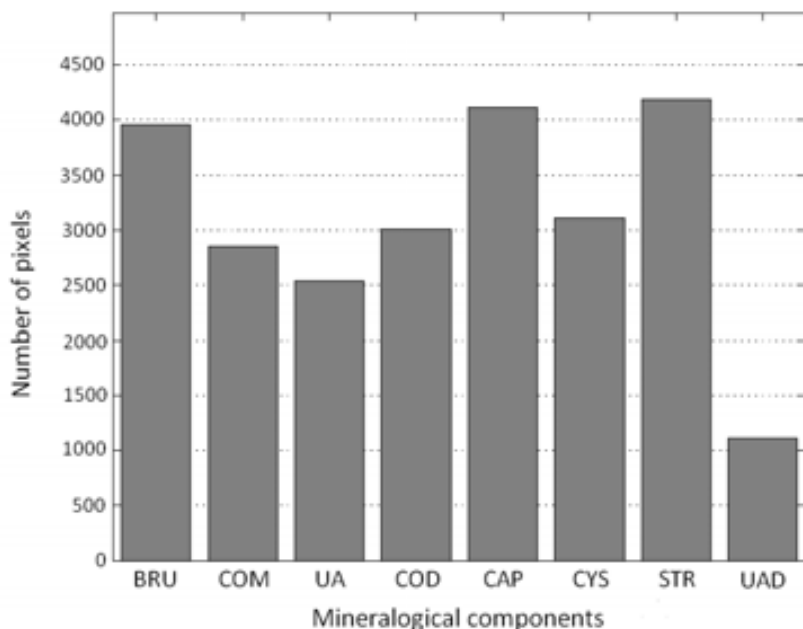


Figure 2.20 Frequencies histogram. The model is created from such pixels distribution. The total count of pixels is related not only to the number of fragments considered for each group, but also to the size of those fragments.

### 2.3.2.2.2. Implementation of the NIR-HSI model

The created model was rapidly implemented on the 200 test samples by using the described data analysis software. Two types of output were demanded from this software:

- quantification of components and calculation of composition percentage and;
- classification of each pixel into a group from the standards and a reconstructed picture of the stone.

The first item is comparable to IRS; the result is expressed as numbers that describe the stone composition. The second output is analogous to MA, because the stone structure is also described as a picture. These pictures represent the spatial resolution, that is, the possibility to perform a topological assessment of the detected species in the sample offered by this methodology: the added value that NIR-HSI offers compared to IRS.

The quantification analysis will be addressed first. Samples were analyzed using the NIR-HSI classification model and the results, expressed as percentage of each component, were compared to the composition measured by IRS. The component gradations for the mixtures in the reference IRS bibliography 128 were 10%, so an error <10% can be assigned to this classification. Thus, the results



calculated from NIR-HSI were considered to correlate with the IRS results if the composition matched, considering a  $\pm 10\%$  deviation.

A thorough analysis of the results shows the composition obtained by NIR-HSI to generally fit that from IRS (achieving 70% correlation), with some variations that require a more careful analysis. It should be taken into account that the sensitivity of minor components is higher for the NIR-HSI technique than for IRS. Minor components could cause only a small IR spectral band to grow or appear, so the spectrum would hardly be changed. IRS strongly relies on the analyst experience, so such small changes might be hard to quantify. Instead, since each pixel is analyzed individually by NIR-HSI, minor components are identified with the same precision as main constituents of the sample. Therefore, as it will be described later, NIR-HSI can give more information on lithogenesis in some cases than IRS does.

The description of the classification results and their correlation to the IRS analyses is listed as groups, based on their mineralogical composition and summarized in Table 2.4.

**Table 2.4 Overview of the classification results obtained by the NIR-HSI methodology and their correlation to IRS for each type of stone. Results correspond to a total of 200 urinary stones analyzed by both techniques.**

Type of stone	Correlation (%)
BRU	88
CAP	60
COD	78
COM	94
CYS	100
STR	64
UA	93
UAD	90
Mixed	78

Each class should be analyzed individually, because of some specific features that can make the classification error particularly increase in some cases.

Calcium oxalate. This complex group of urinary stones includes COM, COD and, frequently, a mixture of those components together with CAP. In addition, COD is not stable in contact with urine, so it slowly transforms into the thermodynamically most stable derivative COM, as introduced in Section 1.2.1. Thus, both isomers can be found in a wide range of proportions. When the model was applied to this group of samples, the classification for those containing basically COM correlated more than 90% with IRS results. For COD and mixed stones, this value stayed close to 80%. This difference could be based on terms of frequency and composition. While stones which composition is  $>90\%$  COM are very common, COD tends to be mixed with COM (often formed from COD transformation) or CAP in variable amounts

44. This fact could cause the calculated composition by NIR-HSI to lie out of the  $\pm 10\%$  error for IRS results; then a wrong correlation was considered. It should be highlighted that NIR-HSI is able to locate the different components in the stone, allowing the performance of a full textural characterization of the minerals that constitute the stone itself. Starting from these features, it is thus possible to derive useful information about stone formation and, as a consequence, to formulate a description of the position and so the moment in which each component precipitated. Hence, these mixtures of several components were described in a further dimension.

Cystine. This stone type presented the highest correlation rate, namely 100% of the samples analyzed by NIR-HSI completely agreed with IRS analysis. As stated in Section 1.2.5. , this type of stones is strictly related to a genetic disorder, so CYS precipitates in special conditions and it usually does not co-precipitate. Besides, since CYS is the only species in the studied group containing C-H bonds, its NIR spectrum shows unique features, so the identification was well achieved.

Phosphate stones. CAP and STR stones, as well as the less frequent BRU form this heterogeneous group of stones. The classification of BRU urinary stones by NIR-HSI correlated as much as 87.5% to that from IRS. Only a few pixels in several samples were confused with CAP (as seen in the model), which is also a calcium phosphate. In regard to CAP and STR, the NIR-HSI model could match around 60-65% of the pixels (see confusion matrix, Table 2.3) of the results to those obtained by IRS. Their NIR spectra are similar (see Figure 2.19) and they tend to precipitate together, so the quantification of each component in mixed stones becomes challenging. The composition obtained by NIR-HSI was not dramatically different from IRS results (most samples relied within  $\pm 20\%$  range). Nevertheless, the fraction of samples that laid outside the  $\pm 10\%$  region was higher than other stone groups.

Uric acid. This type of stones include actually two different components: uric acid (UAA) and its kinetic derivative, the dihydrate form (UAD). The analysis of both components by NIR-HSI yielded very good results, with a correlation higher than 90%. The model could distinguish with little error these two forms of uric acid, and its comparison to IRS results behaved good in a large extend.

### 2.3.2.2.3. Spatially defined analysis

As already stated, the main advantage of NIR-HSI over the conventional IRS is the spatial resolution of the analysis (i.e. topological assessment of the different mineralogical species), not available when the sample is grinded for IRS measurements. Thus, NIR-HSI offers the possibility to describe all the stages in the stone formation, and so, the urine conditions at each point of the process. This information can direct to a treatment precisely adapted to every patient. This is the advantage that the examples presented in this Section highlight.

Among the total amount of samples that were analyzed, some specific, representative examples will be accurately described in order to illustrate the performance of the developed model to remark the differential results that both techniques offer. The graphical results are shown in Figure 2.21, while the composition numerical results are listed in Table 2.5.

a. The first example shows a CaOx mixed stone, assigned a similar composition for both methodologies. This stone presents a singular structure: it is basically a COM stone, totally covered by a COD layer. Thus, the order of precipitation is important: COD (which usually precipitates due to hypercalciuria and hyperoxaluria conditions 219) precipitated exclusively at the end of the stone episode. The higher percentage of COD quantified by NIR-HSI should be noted. As appreciated in the picture, the inner and outer parts of the stone were analyzed simultaneously, so the COD surface is bigger than that for COM. HSI is a surface technique, so attention shall be paid to which part of the stone is being analyzed. Once this is clear, HSI allows the description of two steps in the stone formation, while IR can only give a general composition ratio of these two phases.

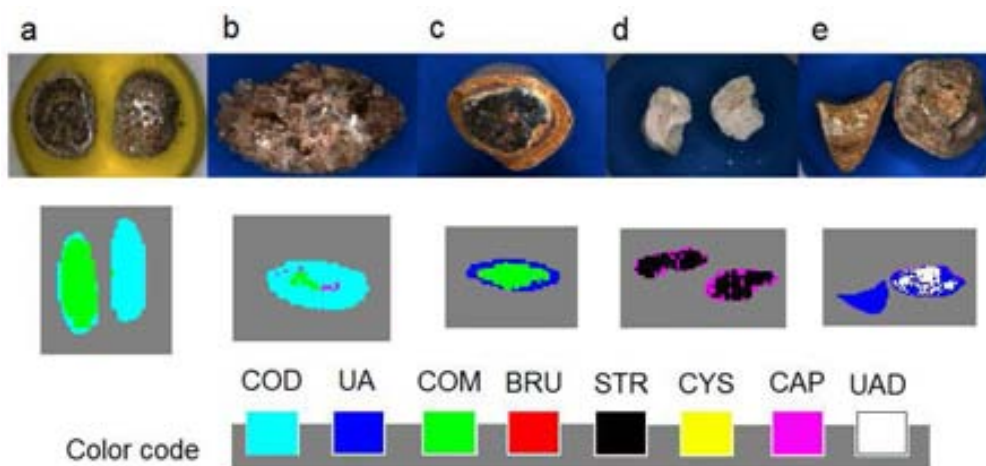


Figure 2.21 Examples of some results for stone analysis comparing NIR-HSI and IRS. First row: Color, real pictures of the samples. Second row: Reconstructed images corresponding to the samples listed in the first row; these images are the output of the imaging analysis software used. The legend (bottom) shows the correspondence between colors and components.

Table 2.5 Composition corresponding to the samples listed in Figure 2.21, for the two methodologies used. The composition values are expressed as percentage.

Sample	a	b	c	d	e
NIR-HSI	40 COM 60 COD	90 COD 5 COM 5 CAP	78 COM 22 UA	63 STR 37 CAP	55 UA 45 UAD
IRS	60 COD 40 COM	80 COD 15 COM 5 CAP	80 COM 20 UA	70 STR 30 CAP	60 UA 40 UAD

b. This stone corresponds to a very common composition: CaOx and CAP. The stone was formed as COD, and the core transformed into COM, due to the higher stability of the latter (see Section 1.2.1. ). This phenomenon can be observed here as a different color in the nucleus region. CAP did precipitate in this

stone as a few deposits within the stone structure. Both techniques could identify the same three components; the higher percentage of COM in the IR should be attributed to the difference of relative surface (NIR-HSI) and relative weight in the stone (IRS) of this component. NIR-HSI allows the location of CAP not only in the stone core, so the stone formation steps become clearer when image analysis is used.

c. This mixed stone of UA and COM yielded a very similar numerical composition when analyzed by the two methodologies suggested in this work. However, NIR-HSI allowed the location of COM in the core of the stone, so the acidic urine conditions needed for the precipitation of UA can be located in the latter stages of the stone formation. This independent analysis of core and shell requires the addition of steps to the stone analysis process by IRS (namely the measurement of two spectra), so the time for the analysis is increased.

d. This is a common mixed stone, made of CAP and STR. These stones usually lack any defined structure, and this exact situation can be appreciated in Figure 2.21. In addition, the quantification of the stone components is really similar using both techniques.

e. UAD is the kinetic derivative of UA and, as seen in the calcium oxalate case, it also transforms into the most stable UA when it remains in contact with urine (see Section 1.2.4. ). While the composition according to both techniques is basically the same, HSI also gives the distribution of components, which appears to be different in the two analyzed fragments. HSI is able to define which fragments are UAD, so the description of the sample is totally precise for this particular patient.

### 2.3.3. Final remarks

The previous section presented a new methodology that should overcome some of the main drawbacks of traditional urinary stone analysis, mainly analysis time and dependence on the analyst. However, a performance comparison with the reference technique in the field, IRS, was needed, for completely assuring the suitability of HSI for stone analysis.

The results show how HSI has a good performance on stone analysis, since it yields similar results to IRS but adding the unique distinctiveness of the appropriate location of components in the stone.

The high performance of the software enhances this methodology from the one presented in the previous Section, since no ROI selection is needed. This is a fully independent procedure that requires a very short analysis time (dozens of samples per hour can be processed), what positions NIR-HSI as an attractive update for the stone analysis in clinical laboratories.

The operational features of NIR-HSI lead to a more accurate description of the stone history, which, in turn, allows a more precise diagnosis. This is a basic issue for producing key tools for an individualized treatment.

Despite the similar results observed for NIR-HSI and IRS, it should also be considered that IRS takes the whole sample into analysis (it requires grinding the sample), while HSI is a surface technique. In some

samples, this could cause some bias in the results. This little drawback can be overcome with a basic recognition of the sample surface and core.

This work has been submitted for publication at Journal of Biomedical Optics, and was under revision at the moment this Dissertation was written.

## 2.4. $\mu$ -IR Spectroscopy

This Section also presents an HSI approach for the analysis of urinary stones. This time, however, the radiation used is IR, so the spectral features analyzed differ from those used in the previous Sections. The suitability of the radiation energy range is granted by the numerous publications that have positioned IRS as the reference technique for urinary stone analysis (see Section 1.3.2. ).

The high spatial resolution used in this work allows the fine description of the stone structure, so the amount of information achieved surpasses in a large extent the conventional IRS and even the NIR measurements presented in the previous Sections.

In this case, also synchrotron was used as radiation source, because of the advantages it shows respect conventional global sources, described in Section 2.1.1.

Differently to the NIR-HSI measurements, the work described in this Section is not intended to suggest IR Microspectroscopy ( $\mu$ -IR) as an immediate incorporation to routine laboratories, essentially due to the long time required for the analysis. On the contrary,  $\mu$ -IR is to be considered a support technique in the urinary lithiasis field, being its main core application the precise characterization of materials, with research purposes.

In fact, due to time limitations, only a few samples were studied in this work. The measurements introduced here can be regarded as indicative, although they show strong arguments that favor the use of  $\mu$ -IR for stone analysis.

### 2.4.1. Experimental Section

#### 2.4.1.1. Samples

Three samples were carefully selected from a library of renal calculi collected at the urology services in the Hospital Universitari de Bellvitge, Barcelona (Spain). These three stones include the most common components observed in urinary lithiasis: COM, COD and CAP. Despite the scarcity of sampling, the results extracted here reflect the stone classes distribution plotted in Figure 1.10. The three selected

samples included a COM sample, a mixed CaOx sample (it includes COM, COD and COD transformed into COM, as well as CAP deposits), and a CAP sample. These samples were previously classified by means of optical and electronic microscopies, as described in Section 1.3.3. This step assured the selection of representative samples.  $\mu$ -IR measurements demand flat and thin layers of samples, so radiation is not scattered. The scanned region is small, so an uneven surface could cause the loss of signal. Urinary stones were embedded in an epoxy resin and polished until they reached approximately 30  $\mu\text{m}$  thickness.

### 2.4.1.2. Spectroscopic measurements

Spectroscopic measurements were performed at the SOLEIL Synchrotron Radiation Facilities in Paris, France. The equipment used was located in the SMIS beamline. The hypercube data was created by measuring reflectance IR spectra of a given area of the sample, and perform a scan on x and y axis (point mapping). For this purpose, two microscopes were used, which differed on the energy source, global or synchrotron as described below.

#### 2.4.1.2.1. Global source IR mapping

Spectral maps from samples were measured by means of a Thermo Scientific Nicolet iN10 FT-IR Spectrometer. The spot size was set at 80 x 80  $\mu\text{m}^2$ . The surface of the sample was divided into a grid, where a spectrum was measured each 50  $\mu\text{m}$  in both axes. Note that the mapping spot size was larger than the step size, procedure known as oversampling 220 221. This process does not bring more spectral information, yet it results in images with better fidelity to the visible image. Oversampling also reduces the risk of measuring an interesting feature at the edge of a pixel, or even missing it. This ensures a better description of layers interfaces. Mapping experiments require finding a balance between number of points and spectral quality (measuring time per spectrum). While an oversampling ratio of 2 is often used, this parameter was adapted in this work, to take into account the mentioned constraints. The software processes the signal of overlapped points as an averaged value. The measured spectra covered a range from 720 to 4000  $\text{cm}^{-1}$ , with a resolution of 8  $\text{cm}^{-1}$  and storing 16 interferograms for each data point. A background using an Au layer was previously measured by storing 500 spectra, and was used to correct the mapping spectra of the samples. The measurement of the IR spectra for a whole sample required typically 8 to 10 hours, depending on the size of the analyzed surface. Due to timing reasons, the number of spectra stored for the sample was lower than that for the background.

#### 2.4.1.2.2. Synchrotron radiation IR mapping

For  $\mu$ -IR measurements based on a synchrotron energy source (abbreviated as sFTIR), a Thermo Nicolet Continuum FT-IR microscope was used. In this case, due to the higher brightness of the radiation source, a smaller spot size was used: 10 x 10  $\mu\text{m}^2$ . The step size was 6  $\mu\text{m}$ , also considering oversampling. The spectral range was the same as that for the global source, yet with a higher spectral resolution, reaching 4  $\text{cm}^{-1}$ . For the achievement of a better S/N ratio, 100 spectra were collected for each point of

measurement. Likewise, the background was collected measuring an Au layer and averaging 500 spectra. Mapping experiments become slow, since the time needed for acquiring a line of 10 pixels is roughly 30 minutes.

#### 2.4.1.3. Data handling

The software package OMNIC 8.0 (Thermo Scientific) was used for data acquisition and processing. The ratio of all spectra to the background was calculated and afterwards Kramers-Kronig correction algorithm was applied. The resulting data was then processed for the production of chemical maps, plotted as RGB color images. In this Section, RGB images have been produced not only based on the intensity of a single peak, but also using the ratio of intensities of two peaks. When plotting the ratio of intensities for various peaks, the effects of a possible uneven area in the sample, which might cause a biased signal (variations in intensity) were avoided. Indeed, the samples used in this work showed remarkable differences in the intensities of selected peaks for neighboring pixels. This can be attributed to surface imperfections, due to the porosity of the samples or to little imperfections created during the polishing process. Certainly, an analysis based on peak ratios is not quantitative, but the goal of this work was directed to a qualitative description of the samples; any quantitative result is only indicative.

##### 2.4.1.3.1. Spectral bands

The IR spectra of the studied components: COM, COD and CAP, show a number of peaks. The interpretation of the spectral results was done using only a few intense and characteristic spectral bands. These are listed in Table 2.6.

Table 2.6 Frequencies used for the identification of components.

Component	Spectral band (cm <sup>-1</sup> )	Associated vibration
COM	780	C-C/C-O single bond stretching
	1318	C-C/C-O single bond stretching
	1630	C-O double bond stretching
COD	1680	C-O double bond stretching
CAP	1060	P-O double bond stretching

#### 2.4.2. Results and discussion

This Section summarizes the details concerning the analysis of three studied samples. The description of each sample is presented individually, to emphasize the advantages of  $\mu$ -IR on each type of stone.

On the whole, the use of enhanced spatial resolution spectroscopy (considering conventional approaches for stone analysis, IRS) provides a high level of detail on the sample description. Logically, specific results direct to a much more powerful diagnosis.

### 2.4.2.1. Calcium oxalate monohydrate

This sample had been previously classified as pure COM by MA. In this analysis, concentric circumferences were appreciated within the structure of the stone, yet their nature could not be analyzed due to lack of resolution of the optical technique. Mapping spectra covering the whole area of the sample were done using the FT-IR microscope with a globar source.

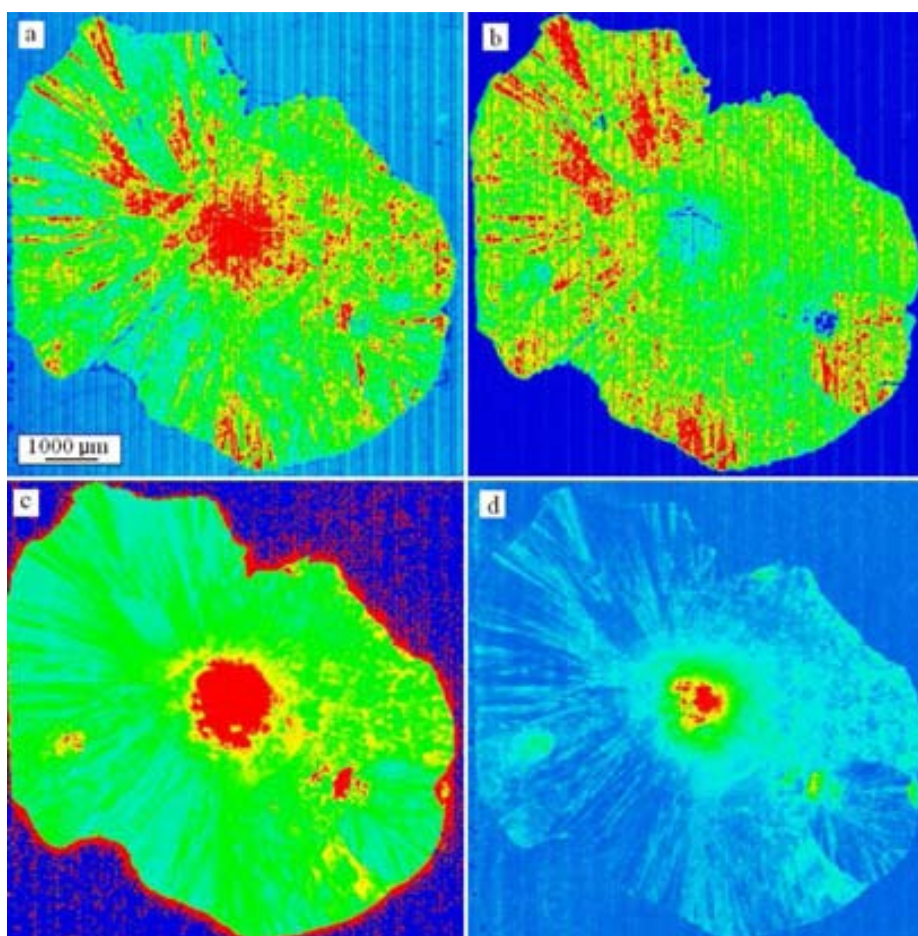


Figure 2.22 Mapping plots of the complete sample. a. Intensity of the peak at  $1630\text{ cm}^{-1}$  b. Intensity of the peak at  $1318\text{ cm}^{-1}$  c. Ratio of intensities  $1630$  to  $1318\text{ cm}^{-1}$  d. Ratio of intensities  $1630$  to  $780\text{ cm}^{-1}$ .

The chemical map for the peak at  $1630\text{ cm}^{-1}$  shows the maximum intensity at the core area of the stone (see Figure 2.22a). However, this trend is inverted when the peak at  $1318\text{ cm}^{-1}$  is taken into consideration, as pictured in Figure 2.22b. The first peak is, as known, a feature of calcium oxalate spectrum, since it corresponds to the C-O double bond stretching vibration. This spectral band is also



seen in organic matter, while the strong intensity recorded at  $1318\text{ cm}^{-1}$ , C-O and C-C single bonds stretching, is especially intense for COM. According to bibliography 44, COM urinary stones tend to grow from a core with a high content in organic matter, what corroborates the previous observation. The intensity ratio for the peak at  $1630\text{ cm}^{-1}$  to that at  $1318\text{ cm}^{-1}$  is plotted in Figure 2.22c, in order to discard any possible effect from surface defects on the signal intensity. This ratio shows a much higher intensity at the core of the stone. The intensity quickly decreases when the distance to the core of the sample increases. Therefore, only strictly the core of the stone shows this profile. Figure 2.22a evidences two other regions of the sample with a high value for the intensity of this peak.

In order to further describe those regions, the ratio of the intensity of the  $1630\text{ cm}^{-1}$  to the  $780\text{ cm}^{-1}$  was also calculated. The peak at  $780\text{ cm}^{-1}$  is a characteristic band for COM, while the other studied compounds hardly present it. According to Figure 2.22d, the core of the stone shows the highest intensity for this ratio, along with the same areas illustrated in Figure 2.22c. Since COM dominates the composition of the structure, the peak should be found overall on the analyzed surface. This peak has an intense signal, so the amide I band (C=O double bond stretching) is overlapped and not clearly identified. As shown in the referred regions of the stone, the peak around  $1630\text{ cm}^{-1}$  has a high intensity, while that at  $780\text{ cm}^{-1}$  disappears. The spectra in the core region also show a band at  $1500\text{ cm}^{-1}$ , which can be attributed to amide II (N-H bond stretching). These results support the observation that a considerable region around the core of the stone has an important amount of organic matter. These observations fit with some bibliography sources, which point out the strong dependence of the COM crystal growth on organic matter 80, and its location in the core of the stone 44.

The observation of secondary spots with these spectral features suggests the existence of new nucleation points, that promoted the precipitation of new COM crystals and they were later integrated within the structure. The absence of any characteristic CAP peak ( $1060\text{ cm}^{-1}$ ) dismisses the influence of a Randall's plaque during the development of the stone, since these structures are based on calcium phosphates (see Section 1.2.1.1.2. ).

Concerning the circular structures observed surrounding the core of the stone, the spectra in this area reveal that this component is actually not COM (Figure 2.23a). The peak with a maximum located at  $1680\text{ cm}^{-1}$  suggests that the circular COM layers are separated by a thin COD layer. It is important to note that the intensity for the COD peak shows maximum intensity at the points where the interfaces are located. Likewise, the intensity of the peak at  $1630\text{ cm}^{-1}$ , corresponding to COM, is plotted in a wider area in Figure 2.23b. In this case, the circular interfaces are recognized as a minimum. The core shows a high intensity for both wavelengths due to the high signal at this point, that masks any difference appreciated in other regions. The intensity of the spectral band at  $1630\text{ cm}^{-1}$  is stronger than that for  $1318\text{ cm}^{-1}$ , but the peak can still be distinguished from that for COD.

From these findings, it follows that the growing process of the columnar COM crystals that build up the structure of the stone was temporarily hindered due to the deposition of a thin COD layer. These changes were possibly due to punctual and regular changes in urine composition, stages characterized by a high calcium concentration, condition that especially favors the formation of the kinetic derivative

(COD). The patient has suffered these conditions regularly, fact that lead to the formation of these concentric circles, since a layer of COD covered, at that precise time, the whole urinary stone. When the conditions necessary for the formation of solid concretions of COM were achieved again, the thermodynamic derivative continued precipitating.

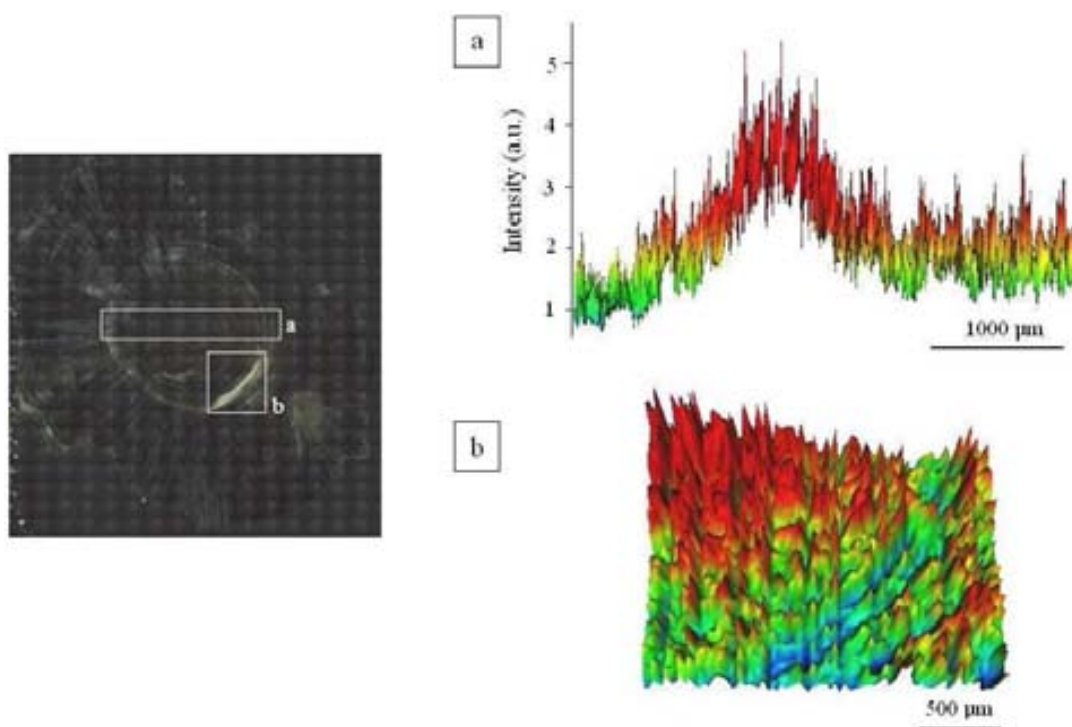


Figure 2.23 a. Map from the highlighted area, based on the intensity for the peak at  $1680\text{cm}^{-1}$ . The maximum of the COD peak overlaps with the location of the concentric circumferences. b. Chemical map from the selected sample area, the intensity for the peak at  $1630\text{cm}^{-1}$  is plotted. The circumferences appear this time as minimum intensity pixels. Note the thickness of the COD surfaces does not exceed  $100\text{ }\mu\text{m}$ . Comparable results were obtained when the intensity for the peak at  $1318\text{cm}^{-1}$  was plotted.

It was not possible to characterize the composition of these thin layers by using traditional optical microscopy.  $\mu$ -IR has shown a great advantage for the description of such small areas of the stone. Although the analysis of a single sample is not enough for the description of a general behavior of COM stones precipitation mechanisms, this finding is highly interesting, because of the high frequency in which this type of structure is found.

### 2.4.2.2. Mixed calcium oxalate monohydrate and dihydrate

The analysis of this sample using MA revealed a mixed CaOx stone. COD suffers normally a slow transformation into the most stable COM derivative due to a long-term contact with urine. Optical microscopy cannot help to define precise limits of the regions where COD or COM are most abundant, so the goal of  $\mu$ -IR mapping measurements is to precisely locate those components.

Firstly, a global source FT-IR microscope was used for the analysis of a large surface of the sample. Due to the large area of the stone and time limitations, only the half of the sample was mapped, which included the core of the stone as well as a large surface area. This region can be considered representative of the whole urinary stone.

A map based on the intensity of the signal at  $1680\text{ cm}^{-1}$ , corresponding to COD, can be seen in Figure 2.24a. As expected, the strongest signal for COD is found in the outer part of the stone, since it is the one of latest formation.

Alternatively, the intensity for the band at  $1630\text{ cm}^{-1}$  (COM) is much higher on the core of the sample. The residual signal seen on the most external part of the stone is due to the high intensity of the C-O double bond vibration. These results are plotted in Figure 2.24b.

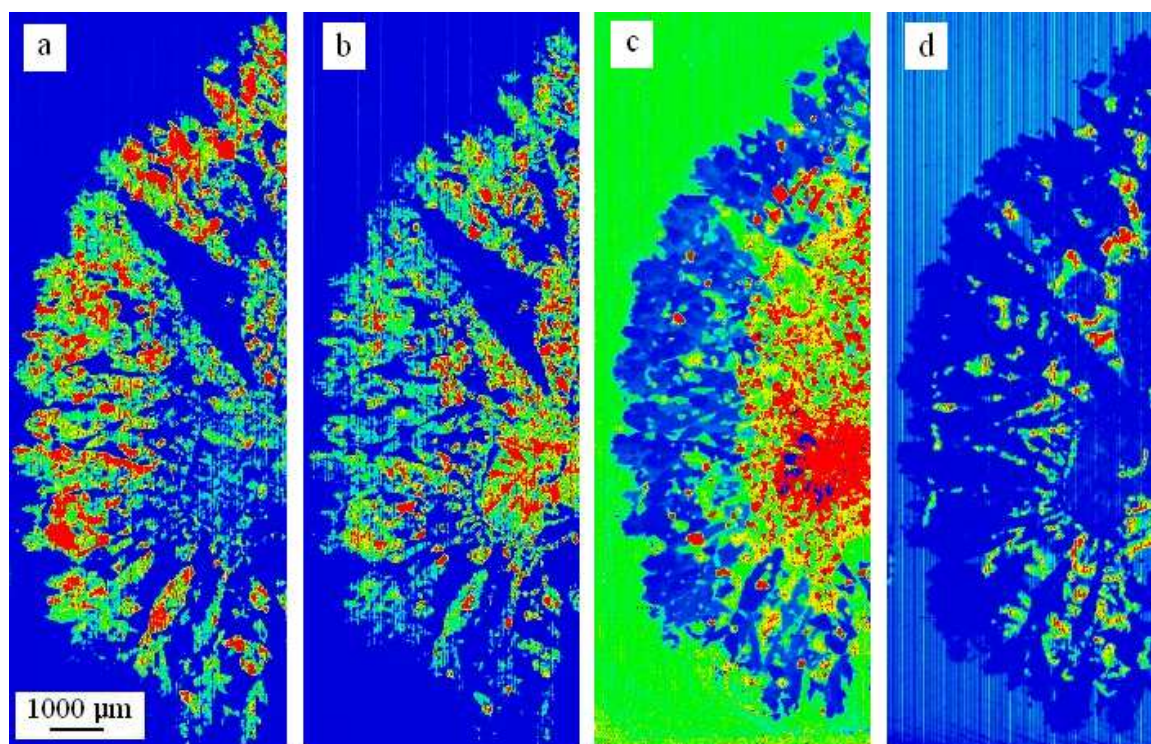


Figure 2.24 Mapping plots. a. Intensity of the peak at  $1680\text{ cm}^{-1}$  (COD) b. Intensity of the peak at  $1630\text{ cm}^{-1}$  (COM) c. Ratio of intensities of the peak at  $1630\text{ cm}^{-1}$  to  $1680\text{ cm}^{-1}$  d. Intensity of the peak at  $1060\text{ cm}^{-1}$  (CAP).

The characteristic spectral bands for the carbonyl group in COM and COD are overlapped. Their vibrational energy is close and intensity is high. The chemical map may appear to be biased because of the proximity of the bands, but the features of both spectra allow their unique recognition. This band overlapping can actually be overcome when the ratio of intensities for such peaks is used for the graphical representations.

In order to correctly define the composition for each area of the stone, a map of the sample, based on the relative intensities between the bands at  $1630\text{ cm}^{-1}$  and  $1680\text{ cm}^{-1}$ , is displayed (Figure 2.24c). The

## 2. Image analysis

areas dominated by COM appear in red, while blue represents regions rich in COD. As it can be seen, a full conversion is achieved in the core, later discussed. From the core outwards, a first radial section of medium intensity is found. This suggests that this area, due to a continuous contact with urine (because of the stone porous structure), continued its transformation to the most stable derivative. Finally, the surface of the stone comprises pure COD, in its characteristic sharp crystals. It can be concluded that the transformation has taken place progressively.

Spectral evidence can also be found for the description of the stone structure. Figure 2.25a pictures the variation of the composition throughout the stone, from the core to the surface. This figure expresses the ratio of the peaks at  $1630\text{ cm}^{-1}$  to  $1680\text{ cm}^{-1}$ , that is COM/COD. As previously, COM regions will appear as red areas. The IR spectra of the highlighted points are plotted in Figure 2.25b.

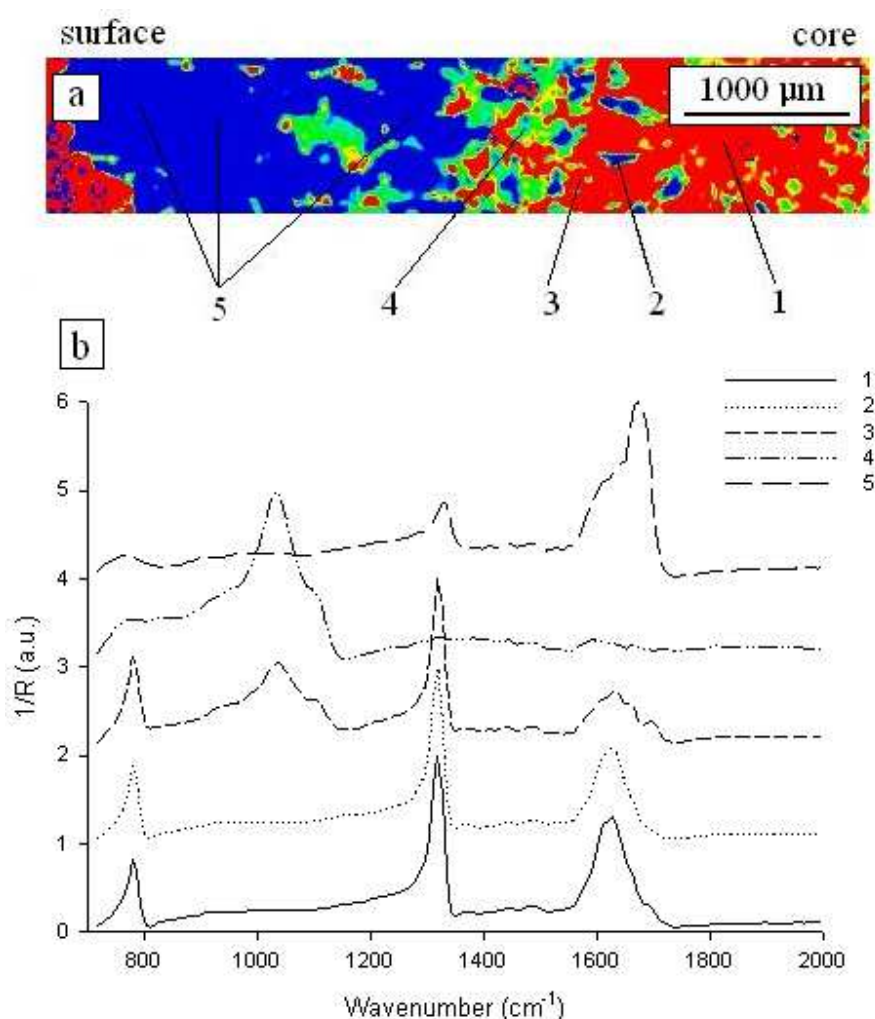


Figure 2.25 a. Map of the central area of the sample, from the core to the surface of the stone. Intensities according to the ratio  $1630\text{ cm}^{-1}$  (COM) to  $1680\text{ cm}^{-1}$  (COD) b. IR spectra corresponding to the indicated points in the mapping image.

Point 1 corresponds to the core area. The curve resembles in a great extent the spectrum for pure COM and practically no shoulder for the COD band can be appreciated, so it can be assumed that the

transformation has been virtually complete. Microscopic analysis of the sample reveals a poorly compact structure, far from that seen in directly formed COM stones, fact that supports the initial precipitation of COD.

The region immediately adjacent to the core is represented by Point 2. Although COM is still the substance that dominates this area, a shoulder can already be seen at  $1680\text{ cm}^{-1}$ , so COD was not totally transformed.

The next radial sphere surrounding the core has a different fingerprint. A spectral band at  $1060\text{ cm}^{-1}$ , that perfectly fits the absorption region for CAP, can be seen in Point 3. Indeed, CAP is the only component in some fragments of the stone located in this middle area (see Point 4). This fact suggests that, after the core area was formed, the patient experienced rather different urine conditions, probably a dramatic increase in the pH value that led to the formation of large CAP deposits.

At last, the outer area is analyzed in Point 5. This can be regarded as the youngest area of the stone, so pure COD should be expected to be found here. This curve entirely fits with this assumption.

The distribution of the components can be described not only following individual spectra, but also by the representation of chemical maps of a specific region. Figure 2.26 clearly indicates the extension covered by each type of component. COM fills the major part of the core area and also spreads towards the surface, which fits with the previous description. COD is basically located in the external region and only low intensity bands, which could be due to the overlapping peak at  $1630\text{ cm}^{-1}$ , is seen in the core area. Interestingly, CAP is found as radial depositions that spread from core to surface.

In this sample, the location of CAP deposits is of especial interest. As it can be seen in Figure 2.26 and, to a greater extent in Figure 2.24, the intensity of the band at  $1060\text{ cm}^{-1}$  defines some regions in central parts of the stone. Therefore, it could be stated that the conditions for the formation of these solid concretions did not occur either at the first steps of the stone growing nor during the final stages.

A second reasonable interpretation of these Figures could point out other details. The careful inspection of the red areas in the picture defines cavities in the structure of the stone. This fact may point out to a change in urine conditions at the later stages of the stone formation. Urine, probably at a rather basic pH, could run throughout the cavities of the stone at loose its dynamic flow in these internal paths, were CAP could have been stored as solid depositions at a later stage in the stone formation.

A further analysis of the results could locate the precipitation of CAP during the formation of the stone, due to changes in the urine composition. After the precipitation of calcium oxalate, pH and the concentration of some precipitation promoters could change, favouring the formation of CAP solid concretions.

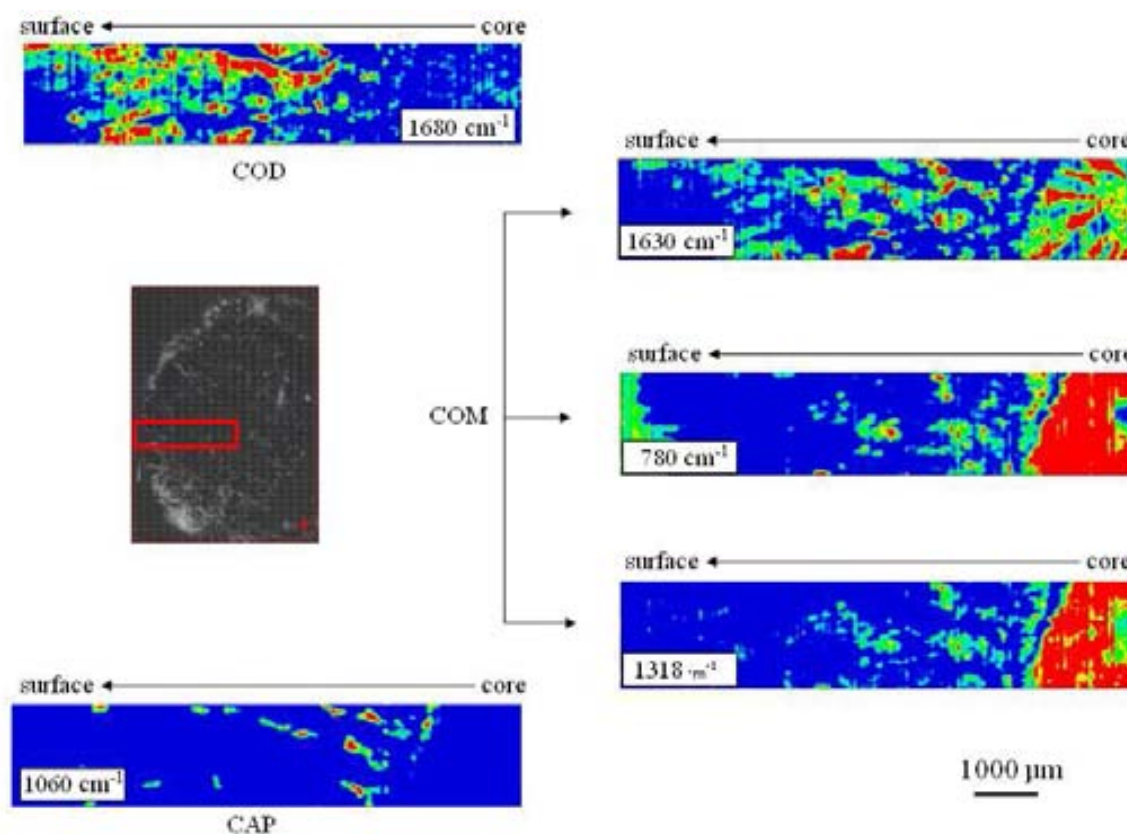


Figure 2.26 Intensity maps of a central area in the sample. The area from the core to the surface is shown. Intensities for the most representative spectral bands (COM, COD and CAP) are plotted separately.

For this sample, also a single measurement using sFTIR, which allows a higher resolution, was also performed. A single, straight line of 30 points, covering a distance of 180  $\mu\text{m}$  from the core towards the surface of the sample, was analysed (line of pixels indicated in Figure 2.27a). The spectral measurements, plotted in Figure 2.27b, show more precise information, not available when a conventional, global source is used. It appears clear that the band for COM is the one dominating the core of the stone. However, a smaller band for COD ( $1680\text{ cm}^{-1}$ ) is also seen in the core region. Thus, it can be understood that the transformation of COD into COM did not take place in a full extent, as it seemed in the previous experiments. The spectra for the outer part of the stone evidence the only existence of COD, as already seen by lower resolution  $\mu\text{-IR}$  and stereoscopic microscopy.

Likewise, Figure 2.27c supports these results, since the spectral band at  $780\text{ cm}^{-1}$ , a specific signal for COM, decreases as the position of the spectrum gets closer to the surface of the sample.

The greater resolution allowed by the coupling of a synchrotron light source to  $\mu\text{-IR}$  has led to the best description of the sample. For time reasons, the number of samples measured was small, so the results can only be considered preliminary. Nonetheless, these measurements add some hints to the results obtained by lower resolution spectroscopy. In some cases, where the resolution is a basic question, sFTIR can throw some light on the precise definition of the lithogenesis process.

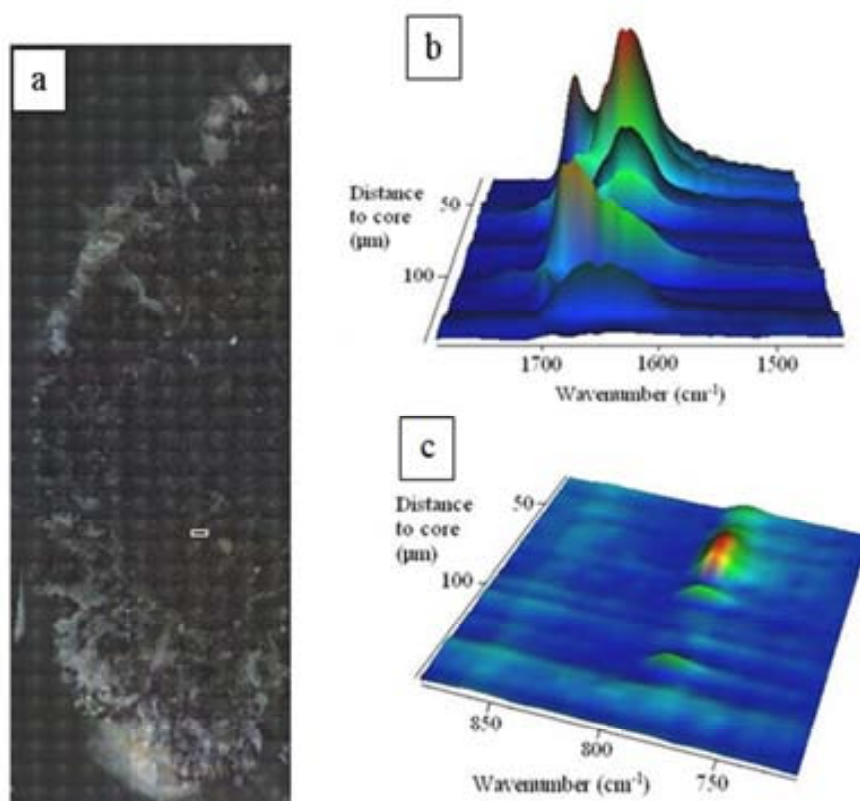


Figure 2.27 sFTIR measurements a. Localization of the measured line map in the sample surface b. Representation of the carbonyl group absorption band c. Representation of the absorption band at  $780\text{ cm}^{-1}$ , characteristic for COM.

#### 2.4.2.3. Carbonate apatite

The classification of this sample using MA yielded a pure CAP stone. As described in Section 1.2.2.1, such stones are porous, and often co-precipitate with other substances. Particularly, STR is a mineral likely to form deposits in bacteriological infection conditions, and can be mixed with CAP in variable amounts. Furthermore, due to relatively similar precipitation circumstances, calcium oxalate is also highly expected to be found within the structure of CAP samples.

Before performing this work, the CAP stone used was analyzed using SEM-EDS. This analysis did not show any magnesium peak, so the existence of struvite was discarded. The presence of CaOx deposits can be more difficult to identify. If the agglomerations are small enough, the phosphorous signal (CAP) may still appear, and the crystal structure differences between both components might be hard to appreciate using MA.

The sample was analyzed using a globar energy source. CAP stone are much softer than other stone types. As a consequence, some of the sample material could have been lost during the preparative polish procedures. This area is seen as a big blue zone in Figure 2.28. This Figure clearly shows that most

of the measured surface is CAP, since the intensity for the characteristic spectral band is maximal. Although the big blue region has a similar spectrum to the holding resin, the spectra of the small areas of low intensity for the  $1060\text{ cm}^{-1}$  band show a different pattern.

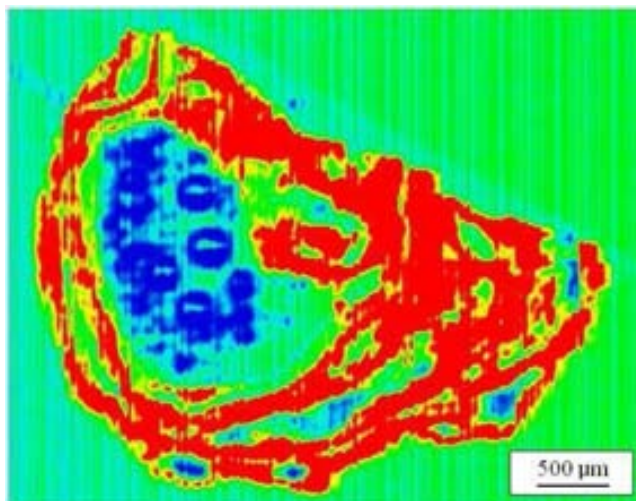


Figure 2.28 Map of the stone, intensity of the peak at  $1060\text{ cm}^{-1}$ .

Once the presence of struvite was dismissed using SEM-EDS as previously discussed, the existence of CaOx within the structure was checked. With this concern, the intensity of the CaOx spectral band at  $1680\text{ cm}^{-1}$  is plotted in Figure 2.29a. As it can be appreciated, some regions show an especially intense signal for calcium oxalate. These areas depict lines crossing the whole stone.

A more precise analysis is supported by Figure 2.29b. Point 1 in this Figure describes an outer area of the stone with a focalized region of calcium oxalate precipitation. If the spectrum from this spot is taken (Figure 2.29b), the peak position reveals the predominance of COD. In fact, the CAP spectral band is not appreciated, so no phosphates were precipitating together with calcium oxalate. In a latter step, CAP continued depositing on the surface of the stone, covering the COD deposits.

Similarly, Point 2 is representative for a long layer of CaOx deposits in the stone, which suggests that the conditions in the urine at that point lead to the precipitation of CaOx rather than CAP, for a given period of time. As seen in Figure 2.29b, the spectra from this region show a maximum absorption band at  $1630\text{ cm}^{-1}$ , so the main component can be thought to be COM. However, the existence of a shoulder at  $1680\text{ cm}^{-1}$  suggests the presence of COD. It could be understood that COD precipitated initially and then it got transformed into the thermodynamically more stable COM. According to Figure 2.29b, there is a noticeable peak for CAP, so COD precipitated along with CAP.

It is worth to say that the thickness of each of these layers is lower than  $150\text{ }\mu\text{m}$ , a similar size as the porous in the structure of mixed stones. Again, the most relevant features listed for this stone make the precise description of the structure particularly difficult, when only MA is used. The complete characterization of the stone cannot be granted even if SEM-EDS is used.



This sample, previously classified as a CAP containing stone, has been fully described by means of  $\mu$ -IR. This technique leads to the elucidation of three stages in the stone formation process.

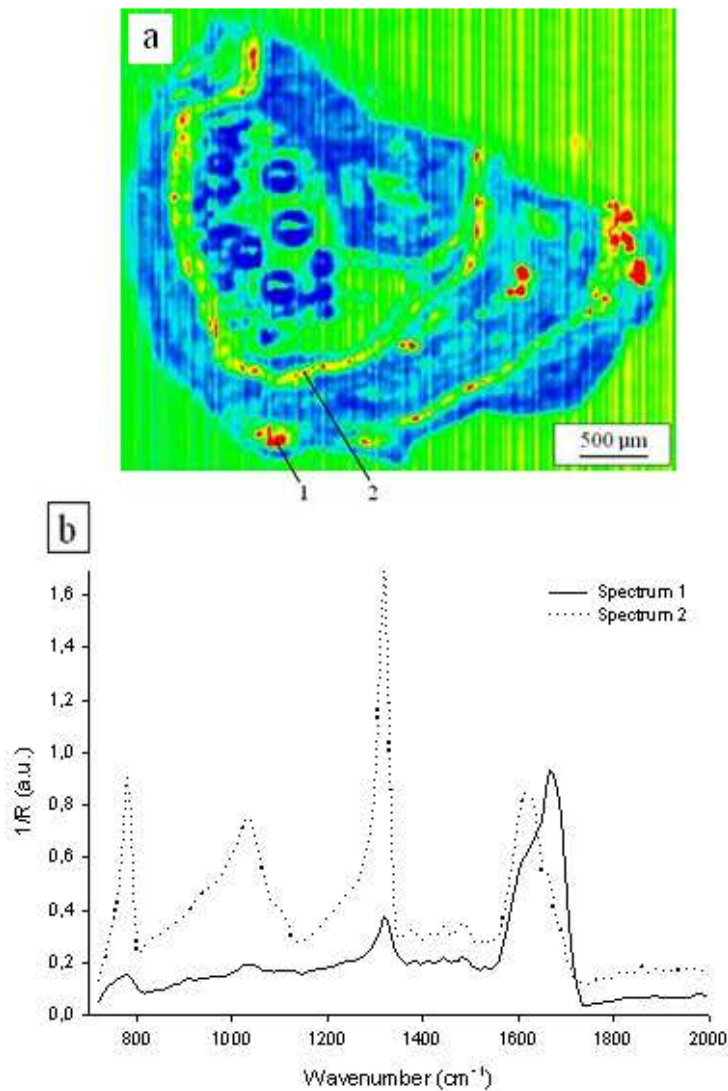


Figure 2.29 a. Map of the whole sample, based on the intensity of the spectral band at  $1680\text{ cm}^{-1}$  b. IR spectra measured at the points highlighted in Figure 7a.

### 2.4.3. Final remarks

This Section has revealed once more the importance of a good resolution power for the best description of urinary stones, getting information different to that obtained by the use of traditional techniques.

Indeed, minor components in some stones have been located, fact that helps in the definition of the stone history, that is, lithogenesis. This history is directly linked to the metabolic disturbances the

patient has gone through, so their precise description leads to the definition of the best management of the disease and selected treatment.

The formulation of precise statistically robust results is certainly hampered by the limited number of samples that could be included in the study. However, this work points out  $\mu$ -IR as an interesting approach for the study of renal calculi. It is clear that, due to the time needed for the measurements, the related costs and the equipment availability, the experiments described here, also including those using synchrotron radiation, are not likely to become a routine analysis technique for clinical laboratories. Nevertheless, the information provided by these techniques serves as a validation of the already existing methodologies. It widens the knowledge on urinary stone formation mechanisms, as the description of precipitation patterns.


This Section can be considered as the use of a more advanced approach than the available IRS for the analysis of urinary stones. It is important to highlight that the results are comparable to those usually managed by physicians.

In order to be totally attractive to clinical laboratories, the analysis should become inexpensive and fast, and new applications (i.e. spectroscopic analysis of other tissues) should be developed. This would help take profit of the most modern spectrometers, which are often used in research for the analysis of biological samples.

The work described in this Section has been published at Journal of Biophotonics.

Blanco F, Ortiz-Alías P, López-Mesas M, Valiente M. High precisión mapping of kidney stones using  $\mu$ -IR spectroscopy to determine urinary lithogenesis. Journal of Biophotonics. DOI: 10.1002/jbio.201300201.

This work has been attached in Supplemental Materials (**Error! Reference source not found.**).



**NANOPARTICLES IN  
URINE: LOOKING  
CLOSER TO SEE  
BEYOND**

#### 3.1. Introduction to nanoparticles analysis

For years, it has been a well-known fact that physical properties of substances in solution are different when particle size changes. Last decades have seen the interest of many different scientific fields on nanoparticles dramatically rise. The number of applications recently developed exceeds the barriers of any scientific discipline, and links the use and/or study of nanoparticles (NPs) to environment and food research/monitoring, chemical synthesis, biochemistry and medicine 222 223.

In order to conveniently address this topic the size criteria should be discussed. Synthetic and natural NPs are considered so when at least one dimension is found in the size range 1-100 nm 224. According to IUPAC, natural colloids of organic or inorganic origin are considered into this group even broadening this size range: 1-1000 nm 225. NPs often show aggregation properties that can cause the identification of colloids that actually exceed the theoretical upper limit of NPs. This is the case of this work, so the results discussed here should consider this particular issue.

Naturally occurring NPs present a remarkable heterogeneity in the radius of morphology, physical characteristics and chemical reactivity. Hence, analysis of NPs in natural media should consider a proper characterization of their size and nature. The role of these colloids in the environment and biological systems influences biogeochemical cycles of the elements, due to the different degree of interaction with living organisms and other particles 226.

As already described in this work, urine is a complex matrix, which contains organic and inorganic components, as well as biological macromolecules. It appears clear that natural NPs could strongly influence physical and chemical processes in urine. Some studies have addressed the influence of NPs of different nature in urine processes. For instance, proteins are known to aggregate and form structures in the size range of NPs. It has been demonstrated that the urinary proteome can be described via the characterization of the NPs content in this matrix 227.

Indeed, the interaction between nanoparticles could play a role in the lithogenesis, process on which this work is focused on. Some works have already tried to describe the influence that nanocrystallites in urine could have in the formation of urinary stones. The assumption of NPs as the precursor for urinary stones appears logical. As described in Section 1.1.5. , urine is supersaturated respect some components, fact that could make them aggregate to form nuclei (usually <10 nm). These crystals are retained within the urinary tract or get fixed to a part of it and form a urinary stone (generally 0.1 to several cm) 228.

The observation of urinary crystallites has been done for many decades. Nonetheless, the technique of choice was typically optical microscopy, so the observation of crystals was limited to the micrometers range. In addition, the observation of such images could be influenced by metabolic processes and

include organic debris 229. An example of the typical images observed with this type of microscopy is shown in Figure 3.1.

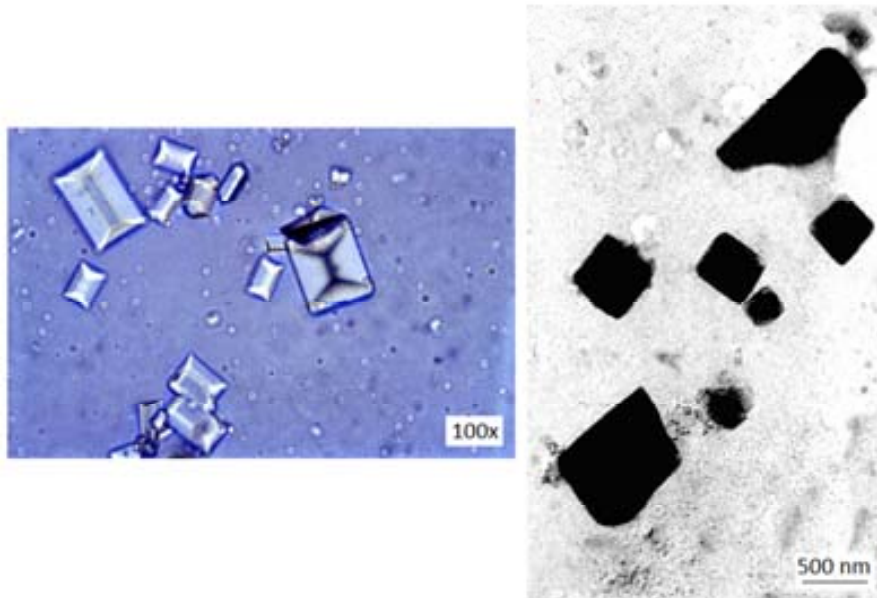


Figure 3.1 Images of urinary crystallites. Left: Optical microscope view of STR crystals. Right: CaOx crystals observed at Transmission Electron Microscope 230.

Aware of these limitations, crystallite formation in urine has been studied with more advanced techniques, which reflect the importance of those processes 231. The main advantage this observation shows is that the characterization of urine crystallites can be used as a prediction of the risk of a given patient to suffer from urinary stones. As discussed in Section 1.1.7. , some stone formation risk markers have been described, yet the results might depend on the variables measured. The characterization of urinary crystallites is purely empirical, so it takes into account promoters, inhibitors and any other trigger that may force urinary components to precipitate.

Previous studies have been focused on the characterization of morphology, particle size, aggregation and Z-potential of urinary particles.

The particle morphology, size and aggregation have generally been determined using Transmission Electron Microscopy (TEM). This technique allows the analysis of images with nanometers resolution. The determination of crystals aggregates is also achieved by direct observation of the structures 230 232. The limitations of this methodology are given by the selection of a representative aliquot of the sample, the need to take several aliquots for each sample for a statistical approach and the need of a trained technician for a rather tedious analysis. Figure 3.1 shows an example of the images usually acquired using TEM.

As mentioned, Z-potential has also been monitored for urinary crystallites in stone formers and healthy controls. This magnitude depends on the surface negative charges of the crystals, so a greater absolute value for Z-potential correlates with a higher density of surface charges. A higher density of negative

charges implies more repulsion between crystals, so the stone formation risk is sunk. This parameter has been detected to be lower (more charges) in healthy controls than in stone formers. Z-potential measurements have been done on CaOx and UA stone patients 230 233.

The methodologies listed are either tedious or not generally available. This makes the determination of the stone formation risk via nanoparticles characterization difficult to integrate into routine laboratories. Hence, the goal of the work described in this Section is to suggest a new methodology for the quantification and characterization of nanoparticles in urine, for its use as urinary stone formation risk biomarker. For this purpose, one of the leading techniques for the analysis of NPs is used: Field Flow Fractionation (FFF).

The experimental work presented in this Section was performed at UT2A, Université de Pau et des Pays de l'Adour, Pau, France.

## 3.2. Nanoparticles analysis techniques

### 3.2.1. Field Flow Fractionation

NPs have traditionally been analyzed using a variety of techniques: sieving and ultra-filtration, sedimentation and centrifugation, size exclusion chromatography and capillary electrophoresis. It was not until the 1980s when FFF became commercially available. FFF resulted one of the most capable techniques, due to improvements in separation range, selectivity and resolution 222.

FFF bases the NPs separation capacity on the interaction between them and a field, produced by some kind of auxiliary flow. Although FFF represents a family of separation techniques, only Flow-Field Flow Fractionation (FI-FFF) will be introduced here, since it is the technique selected for the experimental section. In FI-FFF, the separation force relies on a perpendicular flow applied simultaneously along the separation channel (cross flow). The inlet flow takes a parabolic form that drives the NPs in the sample throughout the channel, while the cross flow interacts with these particles. Smaller particles will interact less with this force and will elute first; bigger particles will be more retained in the channel. The separation principles are thus based on classical, physical chemistry laws: Brownian motion, translational diffusion, laminar flow and frictional forces 234. NPs are kept in the channel due to the existence of a membrane of variable composition and porous size (also known as accumulation wall) on the channel bottom. The chemical nature of this membrane plays also a role in NPs interaction and retention. Figure 3.2 represents the disposition of the basic items in FI-FFF.

Some particularities can also be pointed out in regard to the channel configuration. A popular approach in FI-FFF consists on the use of an asymmetrical channel, variation known as As-FI-FFF (A4F). This variation represented the resolution of some technical problems, related to the stability of a

homogeneous cross flow along the channel 235. In addition, the peak resolution and fractionation speed increase when asymmetrical channels are used. A schematic view of the channel form can be seen in Figure 3.3. The trapezoidal shape of the channel is produced by a plastic part with such a hole and a given thickness, both relevant in the fractionation efficiency.

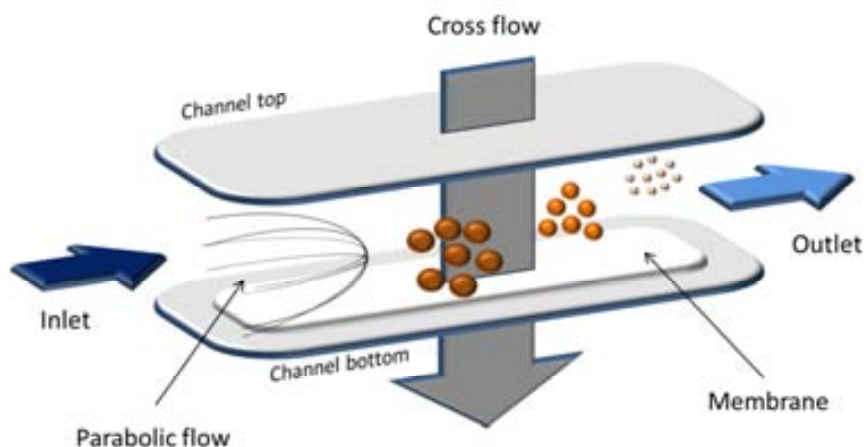


Figure 3.2 Basic items that play a role in NPs separation.

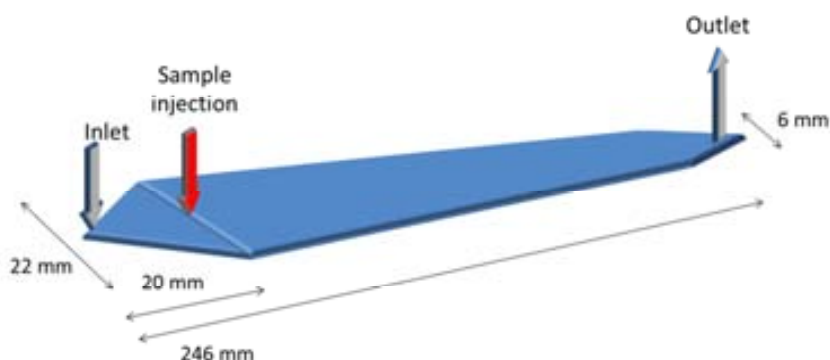


Figure 3.3 Schematic view of the separation channel. Note that the inlet and outlet ports (for the carrier solution) are located at both ends of the channel. The sample enters the channel 20 mm downstream from the carrier injection port (red arrow). All the size indications refer to the unit used in this work.

According to the previous statements, the retention time should conduct to the determination of the particle size. This theory should be analyzed carefully, since some deviations can arise from the calibration method. The calibration is usually performed using commercially available standards, which are generally polystyrene spheres. Due to the different behavior of spherical NPs, they might not be regarded as good indicators of the particle size when compared to heterogeneous urine NPs 236. In this work, particle size has been calculated using an on-line detector, later described.

The sample introduction differs from the mode used in chromatography. In A4F the sample is introduced downstream from the carrier flow inlet. During the injection, the sample is subjected to a focusing step. During this period of time (typically a few minutes) both inlet and outlet ports let carrier

solution *into* the channel and the exceeding solution leaves the channel through the membrane (channel bottom). This process assures that all the NPs are located at the same point within the channel in a Gaussian distribution around the focusing point 237. After this step, the separation conditions start, so the carrier flow crosses the channel from inlet to outlet, while the cross flow leaves the channel through the membrane.

A4F does present some advantages against other separation techniques, as the absence of a higher molecular weight limit, but one of the most relevant is the possibility to couple a large number of in-line detectors, that complement the information obtained for the characterization of NPs. Due to its applicability to this work, the specific characteristics of the Multi-Angle Light Scattering detector (MALS) will be described.

#### 3.2.2. Multi-Angle Light Scattering Detector

This type of detector measures the light scattered by NPs in a liquid medium. Light scattering shows some important advantages when it is combined with A4F. It can give information on particle size over a wide range (1 – 50.000 nm) with no need of running a calibration curve and its short measurement time allows an on-line use. For these reasons, the hyphenation A4F-MALS has been widely used 226.

NPs are in constant random motion when they are in a liquid medium. Theoretically, a particle irradiated with light produces a scattering pattern based on light and dark bands that decrease for higher radial positions. Since the scattered radiation intensity ( $R_{\theta}$ ) depends on the scattering angle, MALS detectors are equipped with a series of individual detectors that simultaneously measure the emitted signal 238. The intensity of scattered radiation depends on the mass/size of the NPs in the sample, being bigger NPs the ones that scatter light more efficiently 239.

The theoretic principle of light scattering, according to Zimm, follows Equation 3.1. Although there are other approaches for the estimation of the NPs size and molar mass, Zimm does not assume spherical particles. This is especially useful in our case, because the particle shape in urine samples will probably be irregular, and assuming any shape restriction would entail the introduction of bias in the calculations 240.

Equation 3.1 Zimm Equation

$$\frac{R_{\theta}}{K^*c} = MP(\theta) - 2A_2cM^2P^2(\theta)$$

In Equation 3.1,  $R_{\theta}$  is the scattered radiation intensity,  $K^*$  is an optical constant depending on the fluid,  $c$  is the mass concentration of the NPs,  $M$  is the molar mass,  $P(\theta)$  is a theoretically derived factor that depends on the scattering angle and  $A_2$  is the second virial coefficient, which includes the interaction between particles.



According to these observations, if Equation 3.1 is solved, the molecular weight and radius of the NPs analyzed can be calculated by measuring the scattered light, if the fluid characteristics (i.e. water) are known.

The solution of the Zimm Equation is done by fitting  $\frac{1}{R_\theta}$  vs  $\sin^2(\theta/2)$ . Since MALS detectors have individual detectors at different angles from the incidence point, a regression response curve can be calculated. The y-axis intersection will lead to the calculation of the molar mass 241.

The NPs radius can be then calculated, since it is proportional to  $\lambda$  (incident wavelength) and M (molar mass). Equation 3.2 shows the dependence of  $r^2$  (square radius, from which  $r$ , the radius, is calculated).  $m_0$  can be calculated using the derivative of the fitted curve at each point. The calculated value is the hydrodynamic radius.

Equation 3.2 Calculation of the particle size, as a function of the second power of the radius.

$$\langle r^2 \rangle \propto \frac{3m_0\lambda^2 M}{16\pi^2}$$

### 3.3. Experimental Section

#### 3.3.1. Samples

Urine samples were collected from healthy controls and stone patients. Healthy participants were recruited from Barcelona area, while patients came from Hospital Trias i Pujol (Badalona) and Hospital Clínic (Barcelona). The selection and exclusion criteria for the recruitment of the volunteers are detailed in Table 3.1.

Note that the inclusion criteria for the stone formers cite only calcium urolithiasis as possible stones to consider. As described in Section 1.2., CaOx and CaP stand for more than 75% of the total amount of cases, so the results achieved represent the majority of cases. The time limit of 6 months after the lithiasic episode should limit the variation in urine conditions after the stone is passed. All the patients recruited had already experienced at least one stone episode previously, to assure urine conditions were more likely to belong to the stone formers group.

24 hour urine samples were used. The whole volume was collected in the same bottle, mixed and then homogenized aliquots of 100 ml were frozen and stored at -20°C until the analysis was performed.

The sample treatment for the FFF analysis included filtration of the samples with a 0.45  $\mu\text{m}$  filter to eliminate debris and prevent largest particles to be injected into the FFF channel. Once filtered, the

### 3. Nanoparticles in urine

---

samples were left in an ultrasonic bath for 15 minutes, to minimize particle aggregation, and then analyzed immediately.

Table 3.1 Inclusion and exclusion criteria used for the selection of the volunteers for urine collection.

Stone patients	Healthy controls
<b>Inclusion criteria</b> <ol style="list-style-type: none"><li>1. Recurrent urinary stone patients (CaOx and CaP)</li><li>2. Patients recruited during 6 months following to the lithiasic episode</li></ol>	<b>Inclusion criteria</b> <ol style="list-style-type: none"><li>1. Healthy individuals, with no previous history of urolithiasis</li></ol>
<b>Exclusion criteria</b> <ol style="list-style-type: none"><li>1. Underage (&lt;18 years old)</li><li>2. Women in pregnancy</li><li>3. Serious illness (oncologic process...)</li><li>4. Osteoporosis or on-going related treatments</li><li>5. Morbid obesity</li><li>6. Associated urinary pathology (benign prostatic hyperplasia...)</li><li>7. Potentially lithogenic drug treatment</li><li>8. Last urinary stone expelled not analyzed</li></ol>	<ol style="list-style-type: none"><li>8. Urinary lithiasis, with or without symptoms</li></ol>

#### 3.3.2. FFF analysis

The equipment used was served by a HPLC quaternary pump G1311A from Agilent Technologies (Santa Clara, CA, USA) and an autosampler G1329A from Agilent Technologies, equipped with a 900 µl variable injection syringe. The separation was performed using an A4F separation channel (Wyatt Technologies Europe, Dernbach, Germany) and controlled by an Eclipse Separation System (Wyatt). The channel had a trapezoidal shape, with the injection point located at 20 mm of the wide end (see Figure 3.3).

Particle size measurements were performed using an on-line MALS detector, equipped with 18 individual observation angles (Wyatt Dawn Helios II, Wyatt Technologies). The data collection interval was 2 Hz.

#### 3.3.3. Data analysis

The fractograms (intensity vs time plot, similar to a chromatogram in chromatography) were analyzed using ASTRA v.6.0.2 (Wyatt Technologies) software, which allowed the measurement of particle size and particle size distribution for each sample. The MALS signal was treated according to Zimm approach. The fitting of the data was done using a first order approach, and the calculations were done for each data point, so for each slice of the fractogram. Thus, each point was represented by an adjusted curve that allowed the calculation of the radius (see Section 3.2.2. for the description of the theoretical basis). It was possible, thus, to record the intensity and particle size at each elution time and calculate the cumulative particle size: the particle size distribution.

### 3.3.3.1. Box-whiskers plot

Due to the interest in this precise case, a particular type of graphical representations will be introduced here.

Box-whiskers plots are a clear representation of the distribution in a population, since they also consider the variability within the data in each class. Figure 3.4 shows the basic points in such plot, which are: minimum and maximum in the series, and the 25, 50 and 75% marks of the data available. The plots shown were calculated as the histogram in Figure 3.15, so each size fraction was represented by a box. Note that, for a better data analysis, the outliers points were subtracted from the calculations. A data point was considered an outlier if the distance to the Q3 point (see Figure 3.4) was higher than 1.5 times the IQD (Inter Quartile Distance,  $Q3 - Q1$  distance), as widely accepted 242.

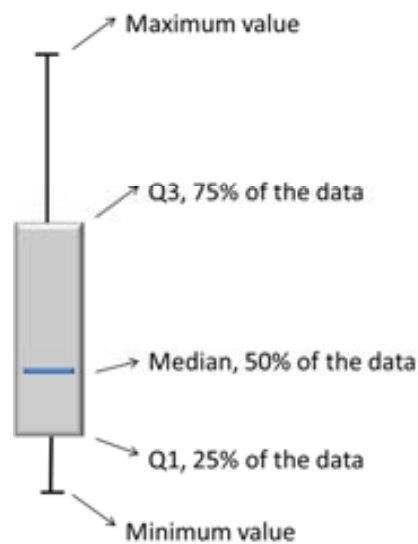


Figure 3.4 Basic points in a box-whiskers plot. This representation helps understanding the data distribution in a population and the variability of the data at the same time. Quartiles 1 and 3 (Q1 and Q3) represent the central part of the data, used for the determination of outliers.

## 3.4. Results and discussion

This Section includes not only the results on particle size determination, but also the preparation and test of the analysis method, since it had to be specifically developed for this case.

#### 3.4.1. Optimization of the analysis methodology

According to the particularities of the technique, a number of tests were run to choose among several parameters and configuration possibilities. The goal of this optimization was the fractionation of the NPs content in urine. Ideally, if the NPs population in urine included variable concentrations of different sizes, the fractogram would show well resolved peaks with different intensities. Totally resolved peaks would be characterized by a single NP size, so the radius measured at each of them would be constant along the peak (except for the start and end of the peak, when a low signal might do the measured radius slightly differ). These results are usually achieved when the system is polydisperse (some populations of NPs of different size can be found), and the particle size distribution is not continuous. Although this condition might not be achieved, due to the heterogeneity of nanoparticles in natural matrices, it is will be regarded as the reference for the final step of the optimization. The described situation is shown in Figure 3.5.

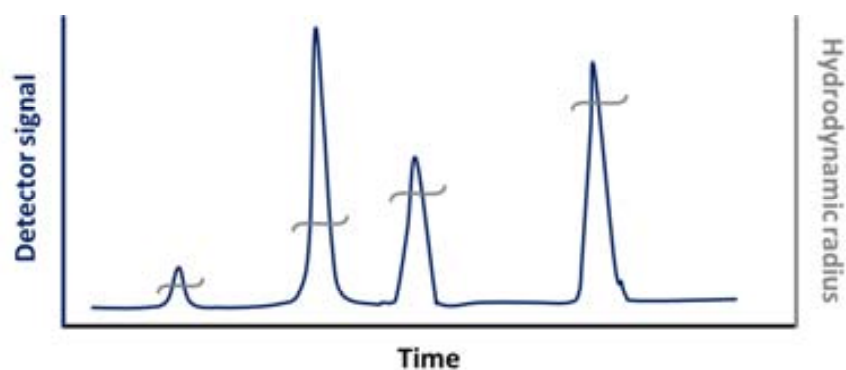


Figure 3.5 Ideally, in a polydisperse system, the fractionation should achieve the separation of several NPs populations. The quality of the separation can be measured, in addition to the peak resolution, by checking the stability of the hydrodynamic radius within the peak. Blue line and axis represent the detector signal; grey ones, the hydrodynamic radius.

The optimization of the methodology was done using a spot of urine sample. More than 100 ml of this sample were collected, so it could be kept during the optimization process.

With this aim, the parameters that were optimized included: Carrier and cross flows, nature of carrier solution, nature of the membrane and channel spacer (namely the thickness of the separation channel). Some fractograms will be shown, in order to graphically describe the criteria used for the conditions selection. Note that the parameters used for the determination of a correct fractionation are the fractograms (signal vs time) or the determination of the hydrodynamic radius. Both can be considered as good indicators of the fractionation efficiency 243.

This Section will only emphasize some representative optimized parameters. Besides the variables here discussed, the sample preparation (filtration/centrifugation), amount of sample injected and carrier flow were also studied. The best results were seen for filtered samples (using a 0.45  $\mu\text{m}$  filter), 200  $\mu\text{l}$  urine injected and 1 ml/min for the carrier flow.

For a carrier flow of 1 ml/min, which is a generally used value, the influence of varying the cross flow was checked. The important effect of changing the cross flow within 0-2 ml/min range is seen in Figure 3.6. Low particle interaction when no cross flow is used leads to a poor fractionation. On the other side, when high cross flow values are used, the NPs are so retained that they hardly leave the channel during the separation. It is only after the separation time, during the cleaning step, that they elute the channel (large peaks at the end of 1 and 2 ml/min curves). Thus, in these fractionation conditions, the system will be kept at cross flow values lower than 1 ml/min.

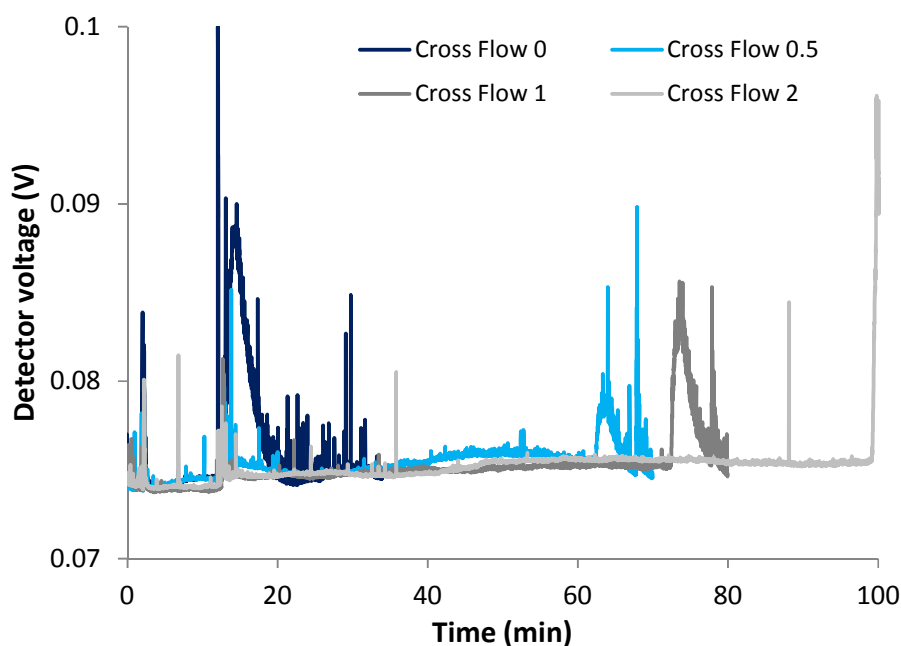


Figure 3.6 Fractograms of the test sample, using a range of cross flow values and keeping the carrier flow at 1 ml/min.

The nature of the mobile phase was also tested, since it is crucial for the efficiency of FFF separation. Different compositions in the carrier solution cause variations in particle stability and interactions with the membrane. Water can be enough for the fractionation of particles depending on the matrix, although the results are often improved when a surfactant is used. These molecules influence electrostatic interactions and stabilization, due to the steric effects derived from surfactant organic chains 243. The results from the separation using surfactant were not satisfactory (in our case ionic and non-ionic components were selected). The list of surfactants tested included Tween 80, Tween 20 and SDS (sodium dodecyl sulfate) 0.05% w/w, highly used in FFF. From these, the results for Tween 80 (see chemical structure in Figure 3.7) are used as an example. As seen in Figure 3.8b, the calculated radii result noisy and somehow illogical. Apparently, bigger NPs elute first from the channel, which is contradictory with FFF theory. These unexpected results could be attributed to the interaction between NPs surrounded by surfactant and the membrane, which could make the fractionation process less efficient. Instead, when sodium azide is added to the solution, the radius obtained is much nicer. Besides the extremes of the peak, where the low signal (due to low amount of particles) can cause noise and imprecise calculations, the radius is stable and follows the theoretical trend (see Figure 3.8a).

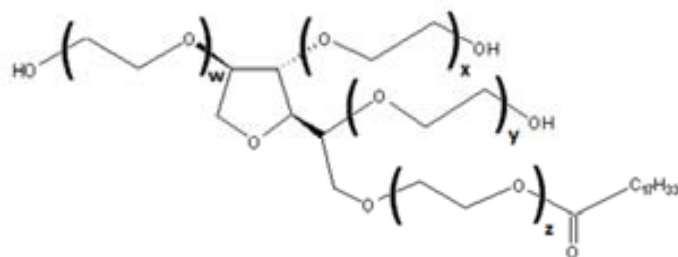


Figure 3.7 Structure of Tween 80 (also polysorbate 80). Polysorbates are a family of compounds; for 80,  $w+x+y+z$  equals 20.

Consequently, the carrier solution chosen is  $\text{NaN}_3$  0.05% adjusted at pH 6. A lower pH could dissolve CAP NPs, as described in Section 1.2.2.1. On the contrary, higher pH values could force the precipitation of  $\text{CaOx}$ . Although the pH of the carrier solution was not adjusted to each urine sample, it was kept in a compromise area, thus balancing the complex equilibria existing in urine. According to bibliography,  $\text{NaN}_3$  also contributes to stabilize the ionic strength of the solution and prevents bacteriological growth in the channel, useful when working with biological samples 244.

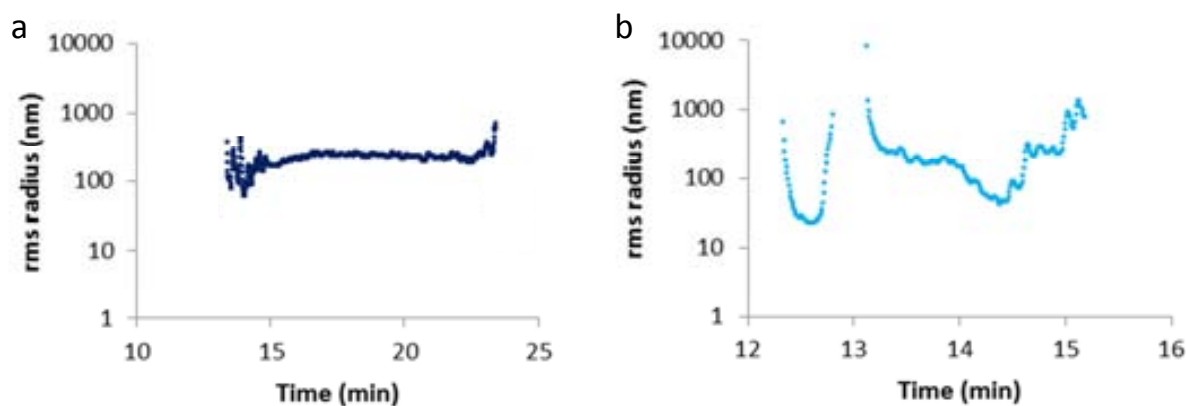


Figure 3.8 Results using different carrier natures. a.  $\text{NaN}_3$  0.05% w/w at pH 6. b. Tween 80 0.05% w/w.

As stated in the introduction of the FFF technique, the accumulation wall, physically defined by a polymeric membrane, is a key point in the optimization of a separation method. It strongly interacts with NPs, therefore influencing the fractionation speed and efficiency. Two of the most common membrane types were compared: regenerated cellulose (hydrophilic) and polystyrene (hydrophobic). In both cases, the molecular weight cut off (MWCO) was 10 kDa, the lowest available, so smaller NPs were not removed from the channel during the focusing time. MWCO is defined as the molecular weight at which >90% of the NPs are retained in the channel 245. The fibrous nature of the membranes can cause the MWCO to slightly vary within a range and also increase the interaction NPs – membrane. As seen in Figure 3.9, the cellulose membrane caused a much noisier signal, due to a higher interaction with the NPs. The PES unit was selected to improve peak resolution and allow better calculations of radius. This different behavior can be attributed to: 1) diverse degree of heterogeneity on the membrane surface that may make NPs interact more with it and 2) cellulose membranes have a highly negatively charged

surface, fact that can retain more the particles, thus leading to a poorer separation efficiency and an increase in the signal noise (the effects observed in Figure 3.9).

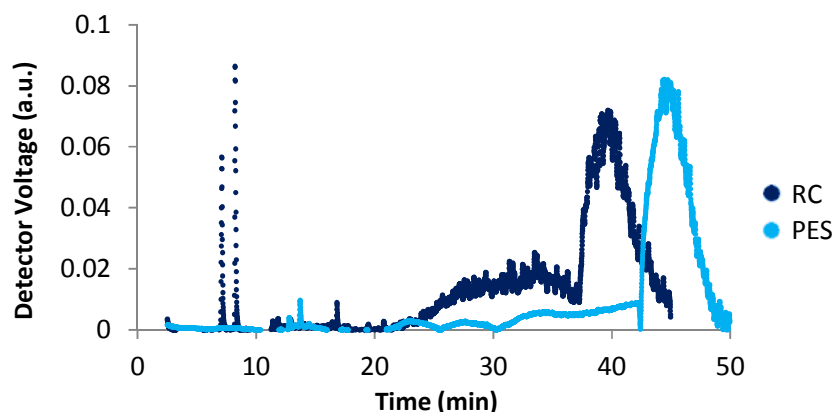


Figure 3.9 Comparative fractograms of a urine sample analyzed using Regenerated Cellulose (RC) or Polystyrene (PES) 10 kDa membranes as accumulation wall.

The next parameter optimized was the channel thickness, regulated through the spacer. The initial 350  $\mu\text{m}$  thick spacer was changed for a 250  $\mu\text{m}$  one. A thinner channel should reduce band broadening, due to the increase in the carrier flow and the establishment of more efficient equilibria within the channel volume. This fact is analogue as increasing the number of plates in a chromatographic column 246. The results obtained by using a different spacer are shown in Figure 3.10. As expected, the separation performance increases and a better separation of NPs sizes can be obtained. The results do not show different peaks with a unique size, but a continuous size distribution starting around 10-20nm.

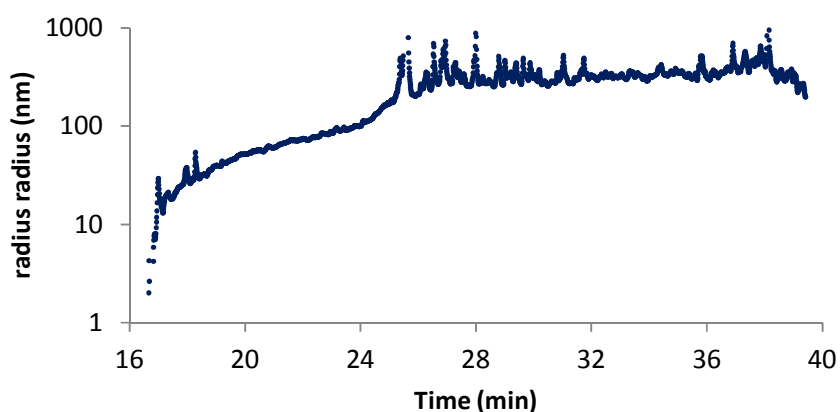


Figure 3.10 Radius measured when a 250  $\mu\text{m}$  channel thickness is set. The size distribution is logical and spreads from 10-250nm. The noise in the last part of the curve is due to the low amount of particles (and so low signal) at the end of the peak.

Finally, the reproducibility of the separation conditions selected was checked by injecting 10 times aliquots of the same sample. The fractograms and size distribution profiles were considered basic criteria for the reproducibility, so they were carefully analyzed. As seen in Figure 3.11, the fractograms

for all the analyzed aliquots are overlapped, which indicates a similar behavior of the sample in the channel. The average hydrodynamic radius calculated was  $63 \pm 6$  nm, which relies within 10% error.

As previously indicated, the total fractionation of the NPs of the sample, to obtain separate peaks of individual size, was not possible. Instead, the results resembled a partial fractionation of different sizes of NPs that eluted as a single, wide peak. The particle size distribution could still be calculated, according to the increasing radius calculated along the peak. This relation between peak shape and particle size can be clearly appreciated in Figure 3.12.

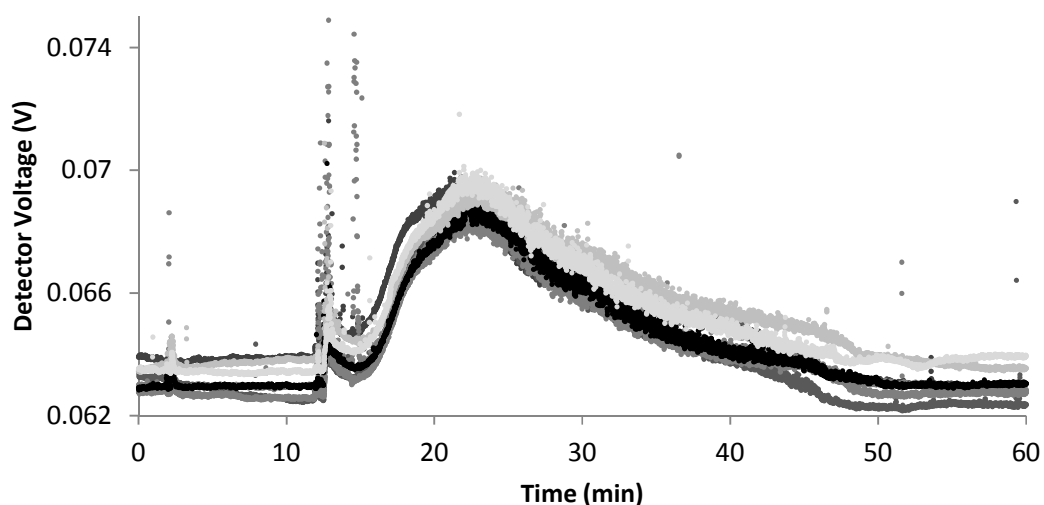


Figure 3.11 Fractograms of the 10 analyzed aliquots. Each tone (from light grey to black) represents the measurement of a different aliquot.

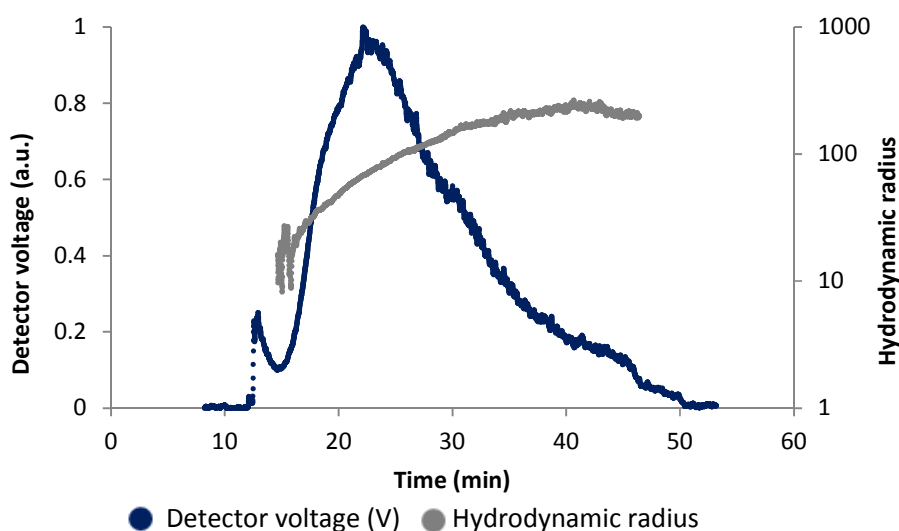


Figure 3.12 Representation of the signal (detector voltage) and the hydrodynamic radius vs time. Note the logarithmic scale for the hydrodynamic radius axis.



To sum up, the general conditions selected for the fractionation of NPs in the samples were: 1 ml/min carrier flow, 0.5 ml/min cross flow, carrier phase  $\text{NaN}_3$  0.05% w/w adjusted at pH 6, PES, 10 kDa MWCO membrane and 250  $\mu\text{m}$  spacer.

### 3.4.2. Results of particle size determination

Once the fractionation methodology had been defined, the analysis of the collected samples was performed according to the selected parameters. The samples have been sorted into two groups: healthy controls and stone patients (cases), according to the criteria described in Section 3.3.1.

Due to the limitations of FFF technique for the NPs size determination in urine, namely the existence of a continuous size distribution that makes not possible to obtain and individually quantify NPs populations, the comparison of the data includes the calculation of mean values for selected magnitudes.

Firstly, the mean radius is compared. This parameter refers to the mean radius calculated for each sample, not considering the particle size distribution. As seen in Figure 3.13, the average value is very similar in both cases, and the standard deviation is so high, that it makes both groups identical for this parameter.

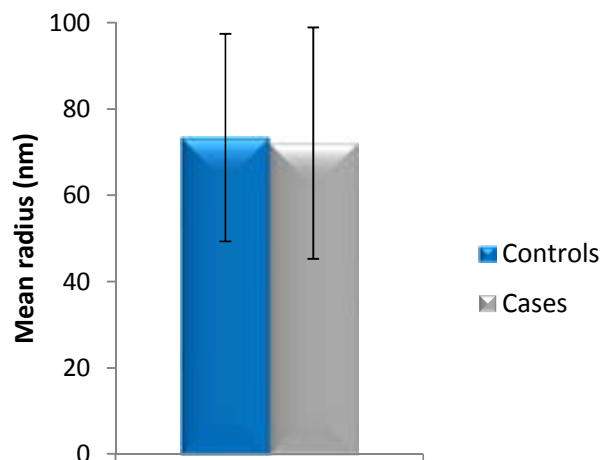


Figure 3.13 Mean NP radius for controls and cases.

Since the comparison of the mean radius does not bring any difference between controls and cases, the mean minimum and maximum sizes are also compared. Assuming particle size distributions are different, the mean hydrodynamic radius might not be a good parameter to reflect differences in such distribution. The average minimum and maximum radius can give a better idea on the size distribution. Again, the results define two similar groups (see Figure 3.14). The values are close within both groups and the variation within each class is so large that they include each other. Interestingly the standard deviation is especially high for the cases group.

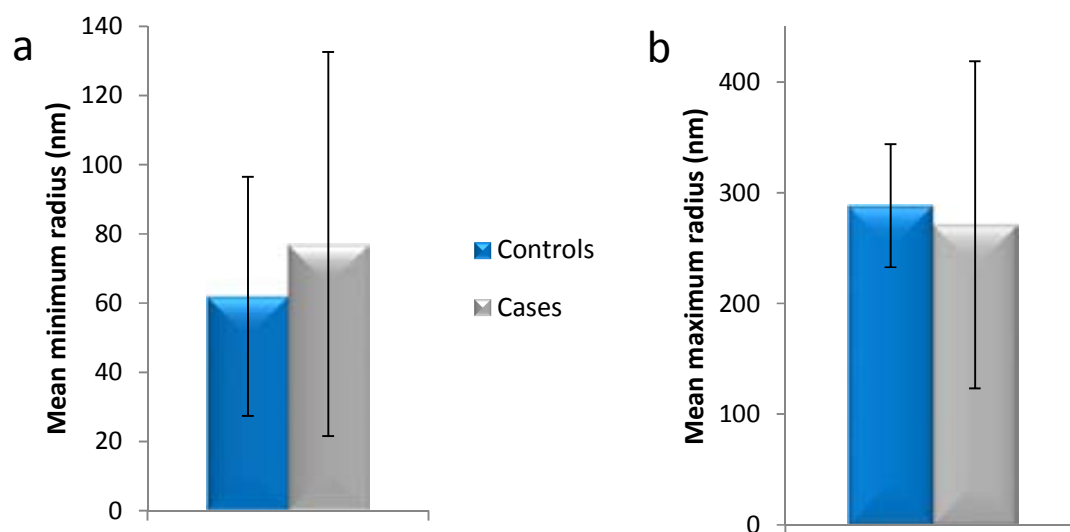


Figure 3.14 Representation of the average minimum (a) and maximum (b) hydrodynamic radius for the two study groups.

The comparison of the mean values is also confirmed by the absence of statistical differences between these values (see Table 3.2). The statistical test run was the comparison of two means using a one-tail t-test; the alternative hypothesis was that the cases mean could be greater or smaller than the controls.

Table 3.2 Statistical analysis of the NP mean particle size measurements.

Parameter	Controls	Cases	$p^i$
Mean radius	73 ± 24	72 ± 27	0.42
Mean minimum radius	61 ± 34	77 ± 55	0.11
Mean maximum radius	288 ± 146	271 ± 147	0.33

<sup>i</sup> p values bigger than 0.05 indicate not significant statistical differences between means.

These results do not fit exactly with some reported particle size studies on urinary stone patients. Duan and colleagues 230 reported a medium diameter (note that radius have been calculated in our work) of  $310 \pm 160$  nm for controls and  $524 \pm 320$  nm for CaOx stone patients. Indeed, after a treatment with potassium citrate, the particle size in stone formers was reduced to  $354 \pm 173$  nm (for the properties of citrate as stone inhibitor, refer to Section 1.1.6.2. ). In that study the difference was reported to be statistically significant. The basic similarity with the results expressed in this Section is the high variability within groups, especially in stone patients. Differently to the work presented in this Section, the work cited used TEM (Transmission Electron Microscopy) as the technique for the determination of the particle size. TEM presents some limitations to avoid particle aggregation and provide representative aliquots from the sample. Even considering the filtration step ( $0.45 \mu\text{m}$ ) previous to the analysis used in this Section, the average particle size is distant to that published.

Comparing the mean particle size has not lead to a clear difference between both study groups. Indeed, the values discussed do not represent the size distribution of the NPs in urine. As shown in the histogram represented in Figure 3.15, the size distribution in both groups could be different, although

the mean value does not reflect this. This Figure shows similar particle distributions for both groups, with some remarkable differences. While the percentage of particles with a radius >200 nm for controls is low, and the probability of finding radius greater than 300 nm is very low for this group, the cases show a different profile in this part of the representation. Cases show a higher percentage of particles with a radius above 300 nm. If the filtering step (0.45  $\mu\text{m}$  filters) is considered, the calculation of such high radius that describe NPs of 600-800 nm diameter, indicates a high aggregation potential of the NPs in patients. For a clearer analysis of the size distribution, box-whiskers plots are also shown.

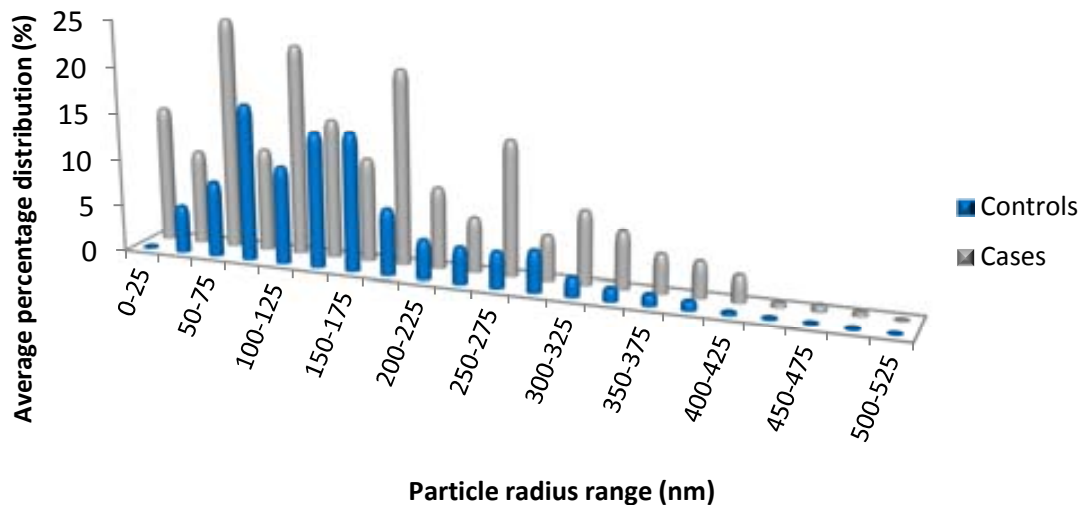


Figure 3.15 NPs size distribution for both groups. The percentages shown have been calculated by calculating the percentage (from the total value in each sample) of NPs found in each size fraction of 25 nm. This Figure represents, for each size fraction, the average percentage of NPs for each group.

The distribution analysis of the data using box-whiskers plots is shown in Figure 3.16. Because of the high variability of the data within each size fraction, the maximum value (not considering outliers) is in many cases distant from the box. Indeed, the first quartile (lower end of the box) is zero in many size fractions; for the cases group this value is found in all the fractions. This detail makes clear that the size dispersion is much wider in patients than controls.

While these results show some particularities for cases and controls, they are not enough to correctly discriminate between both groups. Although the sample selection criteria were intended to reduce any bias within the data, it could have induced some trends. Note that urine from patients was collected during the following 6 months to the stone episode. During this period of time, the patients were probably treated with some drugs (e.g. potassium citrate) and this could have made the particle size of their urine decrease. In addition, since the stone episode was recent, they might have kept adhered to a high liquid intake, fact that would have made concentration and aggregation of particles lower. Still, a slightly higher degree of particle aggregation has been observed.

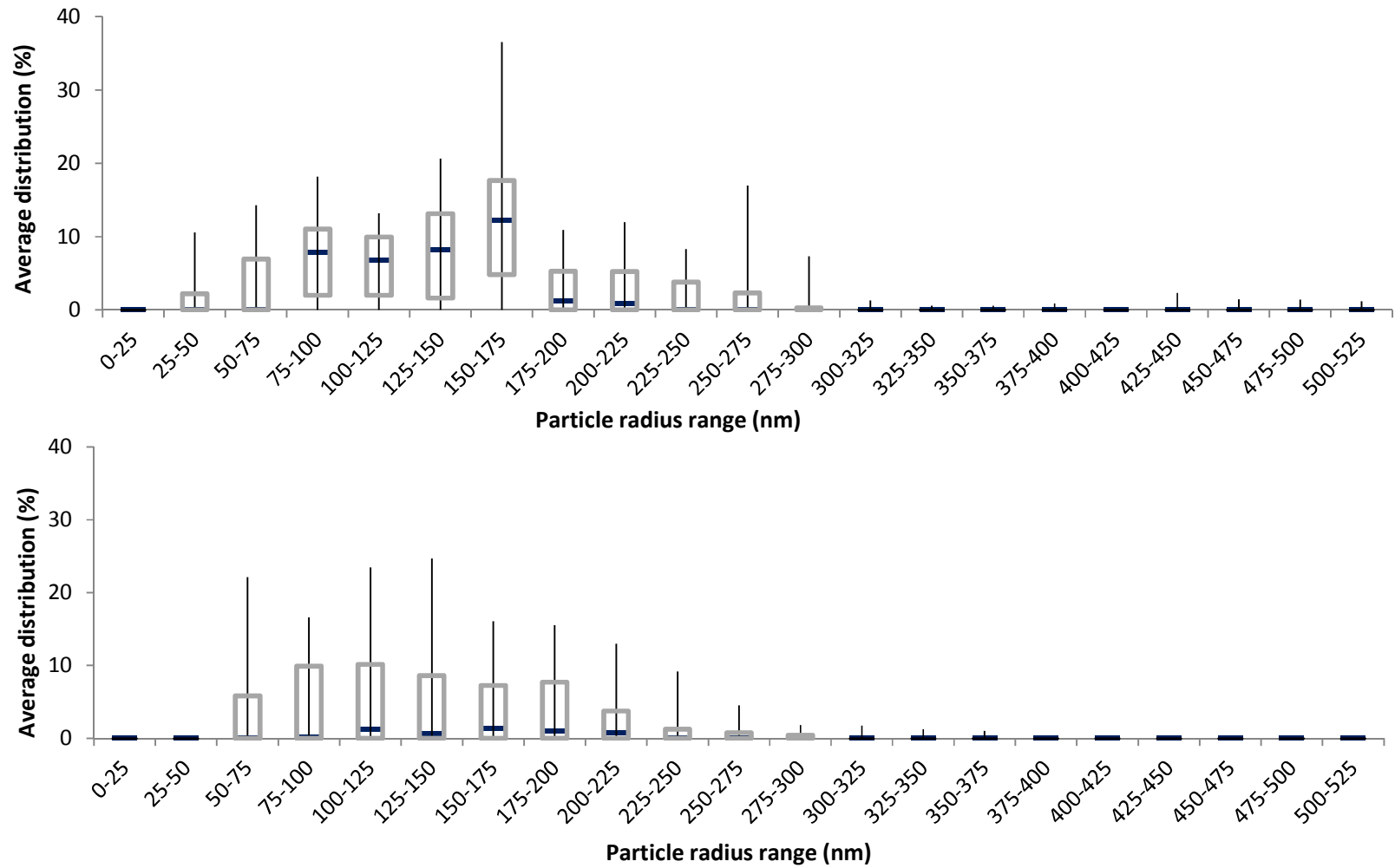


Figure 3.16 Box-whiskers plots of the NPs size distribution for controls (top) and cases (bottom).

### 3.5. Final remarks

The idea of a fast NPs size analysis using FFF for the immediate indication of the stone formation risk is attractive. This Section has tried to address this point from the creation of a suitable fractionation methodology to the test of it with real samples.

The first step has been achieved. Assuming a continuous size distribution, typically found in natural NPs, the developed FFF method has allowed the analysis of the size distribution of NPs in urine samples. It represents the first attempt to achieve this goal using FFF. As stated, other approaches have been reported, basically focused in the use of electronic microscopy. However, this work intended to define a methodology which does not rely on a tedious analysis performed by a trained person, but on an automatic analysis that could be offered to routine clinical laboratories.

The achievement of the method details definition has not granted the determination of significantly different particle size or particle size distributions for healthy controls and stone patients. As discussed, some previously reported results point out to a difference in average NP diameter (also with a remarkable variability within groups), but these differences have not been appreciated in our case.

In order to contrast this data, new sampling could be carried out, including patients with a very recent stone episode, patients who do not adhere to any stone treatment, or even a follow-up study on some stone patients. This would be more challenging, but the characterization of NPs at all the steps of the stone treatment could through some light on the process, and help use the NPs size determination as lithogenic risk biomarker.

A different approach would include the use of elemental analysis to perform chemical speciation on NPs. Thanks to the easily coupling of ICP-MS to FFF, the analysis of NPs could be complemented with a description of which is the concentration of e.g. calcium-containing NPs in each size fraction. This elemental characterization would represent an additional dimension to the description of these samples, that might yield better results for its use as lithogenic risk biomarker.

# 4

**CRYSTALLIZATION  
PROMOTERS:  
OXALATE IN THE  
SPOTLIGHT**

## 4.1. Oxalate as crystallization promoter

The complex interaction between those urine components that directly affect the formation of urinary stones has been described in Section 1.1.6. In brief, the existence of two diverging groups is clear: some molecules promote crystal formation while others reduce the precipitation speed instead. The identification of which component is playing in each of those sides has been a key factor in urinary stone management for a long time 247. As made clear throughout Section 1. , one of the goals of physicians is to reduce the incidence of urinary stones, and also the recurrence of this disease. This objective should be achieved by the careful study of the influence of promoters and inhibitors on lithogenesis.

The close link between stone formation risk factors and patients' diet and lifestyle is a basic issue when addressing stone formation risk 248 249. The general advice for the prevention of urinary stones of increasing the amount of ingested liquid should be given hand in hand with specific diet recommendations or even restrictions. This would require an individualized treatment of the patient, but would also lead to the best results.

The medical community and the stone patients are generally aware of possible beneficial and harmful effects of the diet. This concern has been reflected in many studies, conducted in order to determine the content of promoters or inhibitors in many food varieties 250. Consequently, some foods have been traditionally pointed as adequate or not for avoiding (certain types) of stones.

The studies conducted in this Section have been focused on CaOx lithiasis, due to its higher incidence and the morphology and composition variety seen within this class (discussed in Section 1.2. ). CaOx lithiasis is closely linked to the concentration of  $\text{Ca}^{2+}$  and oxalate as main promoters. Likewise, inhibitors as phytic acid, pyrophosphate or glycosaminoglycans strongly affect the crystallization of CaOx, as reported in bibliography 89. This complex combination of factors makes the study of the causes of formation and interaction between these molecules particularly interesting.

Oxalate has been often considered as bearing the strongest influence on CaOx precipitation among all the promoters, when its concentration in urine is high (condition known as hyperoxaluria, often corresponding to >45 mg/day excreted in urine) 166 167. Several causes for increased urinary oxalate levels in urine have been described.

Oxalate ion is produced in the human body as a by-product of ascorbic and glyoxalic acids metabolism. Primary hyperoxaluria is related to the overproduction and accumulation of oxalate, what might cause stone formation and renal damage. This is not the most common cause of hyperoxaluria 251.

Diet is an important source of oxalate. Some ranges have been indicated as the normal level of total oxalate absorbed from diet: from 10-20% to 40-53%. While very diverging, the amounts are

representative. It has also been reported that the consumption of a low oxalate content diet directly causes the excreted oxalate concentration to sink 252. Secondary hyperoxaluria is linked to these exogenous sources of oxalate, since it has been defined as the increased intake and/or intestinal hyperabsorption of oxalate. An increased oxalate load through the diet might cause the amount of oxalate absorbed in the colon to rise. Oxalate can also be absorbed in a degree higher as desired depending on complementary nutrients intake. For instance, bile acid malabsorption increases the permeability of the colon. Likewise, fatty acid malabsorption is also related to hyperoxaluria: free fatty acids bind to free intraluminal  $\text{Ca}^{2+}$ , thus preventing it from binding to oxalate. This causes a higher intraluminal oxalate availability and so increased absorption 168 169. This effect is emphasized when calcium intake is restricted. Diets poor in calcium were thought to be suitable for CaOx stone formers treatment, although it has been demonstrated that this effect was actually the opposite 167.

The presence of the bacteria *Oxalobacter formigenes* has also been identified as an additional cause for hyperoxaluria. These bacteria selectively use oxalate as their carbon supply and are naturally found in the digestive tract. The lack of *O. formigenes*, e.g. due to antibiotics administration, might force oxalate absorption levels to rise 253.

Due to the relevance of secondary hyperoxaluria, some works mainly focused on this promoter are presented in this Section. The studies presented here investigate the oxalate (and other promoters and inhibitors) content of some foods, nutrition complements and drugs, since they could greatly influence the oxalate load of the consumer. The control of the ingested oxalate is a key point in the treatment of stone patients. It has been seen that 3-12% of the dietary oxalate intake is absorbed in the digestive tract. This amount is greater in calcium oxalate stone formers than in healthy controls 254 255.

Other promoters and inhibitors have also been studied, as phosphate or metals: Na, Ca, K and Mg. They will be introduced in Section 4.3.

The analysis of the mentioned components has been done using two of the most suitable techniques for the analysis of organic ions and metals. Oxalate was analyzed by Ion Chromatography and all the metals and phosphate, using ICP-MS. The basic principles will be described here for a proper comprehension of the numerical results.

### 4.1.1. Analysis techniques

#### 4.1.1.1. Ion Chromatography

Chromatography is the most used analysis technique based on the separation of analytes. In our case, a specific type applied to liquids (ion chromatography) was used. The versatility of this technique relies on the variety of columns that can be fitted. The equipment used in this work used an anionic column, so anions were retained and gradually eluted for their detection. These columns are typically filled with small spherical particles of organic chains functionalized with acid or basic groups 256.



Ion chromatography allows the introduction in the separation column of a liquid sample, which is pushed by the carrier solution. The carrier solution regulates the degree in which different species are pushed downstream the column. The composition of this solution is a key point for the achievement of a good separation performance. It sets the environment that surrounds the components in the column, so the equilibria that take place in the system strongly depend on it. For the separation of anions, the basic parameter to change is solvent pH.

The components in the sample are separated (optimally) in the column according to different retention times. As a general rule, a good resolution is achieved when the baseline is reached between two peaks, so their signal is totally independent. This is the basic parameter to account for in a method development.

Once the species elute from the column, they run through the detector. A conductivity detector is generally fitted in these instruments. The detector measures the difference of conductivity between the eluent from the column (which carries the analytes) and the carrier alone. Conductivity detectors are normally coupled to an upstream ion suppressor. This is a small column that converts the ions in the mobile phase into molecular species with little ionization, while the analyte remains ionized.

This technique is simple, robust and provides a good sensitivity to work with anions at relatively low concentration levels (ppm).

#### 4.1.1.1.1. IC-MS

The work presented in Section 4.4. includes the analysis of isotopic labeled molecules. When a molecule is signaled with some isotope that makes the composition different to the natural abundance, a mass spectrometer is required for its analysis, since chemical properties remain unchanged.

The eluent of the column is divided into two parts, so only a small part of the total amount of liquid is driven into the MS. In this case, the ionization type is ESI (Electrospray Ionization). High voltage is applied to the sample, so the liquid becomes an aerosol (nebulization) and is also ionized. ESI is known as a soft ionization technique, because little fragmentation of the molecules is done (it occurs at low-moderate energy, 30-40 kV). In these conditions, a *pseudo*-molecular ion is usually created. Organic acids tend to form  $[M-H]^+$  ions, so the target molecule can be recognized easily 256.

The coupling of IC-MS allows not only the quantification of molecules signaled with specific isotopes, but also the improvement of LOD down to ppb-ppt scale. It can also be applied to different molecules that have the same retention time, so appear as a single peak when only using conductivity detectors.

#### 4.1.1.2. ICP-MS

Inductively Coupled Plasma is one of the most used multielemental analysis techniques. When linked to Mass Spectroscopy, the advantages of measuring many elements simultaneously are complemented by

extremely high sensitivity that reaches ppt levels for some elements. The basis of ICP-MS is the atomization and ionization of the sample to determine the mass/charge ratio ( $m/z$ ) 256.

Samples are generally liquid, so a nebulization process using a carrier gas is needed (Ref). The carrier gas is usually Ar, due to its low reactivity. The nebulization process is so efficient, that only 1-2% of the sample finally continues its path forward. After the nebulization process, the aerosol is guided through the torch. The torch holds the plasma, a highly ionized and electrically conductor gas mixture, which is kept at  $10^5\text{K}$  and facilitates the cleavage of chemical bonds and creation of ions.

This ion cloud is conducted through a lenses system into a high vacuum area where the detector is located. Atoms with a high ionization potential (non-metals) yield a low signal, since the ionization process is less efficient and neutral molecules are removed from the torrent in the lenses step. A quadrupole system sorts the ion cloud according to individual  $m/z$  ratios, so each mass can be analyzed individually. Each separated  $m/z$  group (ideally a single ion) goes into the detector, an electron multiplier that amplifies the signal. This process takes a few ms, typically 10-50 ms for each  $m/z$  ratio 257.

As any other analytical technique, ICP-MS is affected by the existence of interferences. Two types of interferences are mainly described: spectral and matrix interferences. Spectral interferences are caused by ionic species that have the same  $m/z$  ratio as the analyte. These interferences are either monoatomic ions (as  $^{40}\text{Ar}^+$  and  $^{40}\text{Ca}^+$ ), or polyatomic ions produced in the plasma (e.g.  $^{40}\text{Ar}^{16}\text{O}^+$  and  $^{56}\text{Fe}^+$ ). The second type of interferences is due to the own sample matrix, which can affect the signal by altering the ionization processes occurring in the plasma.

Spectral interferences can be minimized by using CCT (Collision Cell Technology), which requires the use of an auxiliary gas in the lenses. This gas, generally He, causes polyatomic ions to leave the channel, since they are bigger and will collide more often with it. However, this also produces some analyte ions to leave, so the sensitivity decreases. A compromise solution is then required.

On the other hand, matrix interferences are often solved by diluting the sample and so, the ion content in the ionized liquid. In most cases the use of internal standards can help measuring and controlling this possible signal bias.

## 4.2. Determination of oxalate content in drugs and nutritional supplements

According to the described dependence of the urine oxalate levels on the oxalate intake, some studies have addressed the content of oxalate in plants and vegetables. Several roles have been described for oxalate in plants 258. CaOx crystals act as a calcium reservoir in plants; it has been seen how, during periods when calcium is scarce, the amount of these crystals dramatically increases in many plant

species. The low solubility of many metal-oxalate salts is used by some species for the detoxification of toxic metals, since they can be kept as crystals and accumulated in leaves. Some plants use CaOx crystals as a protection against predators, due to dermal irritation.

Most vegetables and fruits regularly consumed in Western diets have low-medium oxalate content 259. This oxalate intake has been estimated in 50-350 mg/day, value that advises a controlled intake of these vegetables for CaOx stone patients 168. Owing to the relevance of oxalate amounts in vegetables, many foods have been examined to determine their oxalate content (see Table 4.1, for some examples).

Table 4.1 Examples of oxalate content in vegetables already found in literature.

Food	Oxalate content
Green tea infusions 260	95-139.5 (mg/l)
Spinachs 261	760 – 1580 mg/100g
Bread 262	16.5 – 111.5 mg/100g
Pasta 263	10.2 – 91.8 mg/100g

The previous examples make clear that the ingestion of some foods represent a considerable oxalate ingestion if their consumption is regular. However, not only the total amount of oxalate should be considered; the quantification of the soluble fraction is also necessary. As described in Section 4.1. , the insolubility of CaOx plays an important role in the digestive tract. While oxalate ion is readily absorbed, the bioavailability of the solid CaOx is much lower. Although this behavior of calcium and oxalate is known, the estimation of the amount of oxalate lost as solid depositions in gastric fluids is complex. Still, the calculation of the soluble to total oxalate ratio is a rather good approach to guess its bioavailability. This aspect is solved by analyzing the oxalate content soluble in water (or bioavailable) and the oxalate soluble in acidic environment (total content) 167 259.

The intake of dietary supplements has been promoted in the last decades, due to the benefits they can exert on the organism. One of the most common, tea leaves extract, has been attributed properties related to: antioxidant effect, anti-mutagenic effect and capacity to sink blood cholesterol 264. Because of the popularity of nutritional supplements, and given the remarks listed in the previous paragraphs, it is worth to examine if the intake of such plant extract might be harmful for CaOx stone patients.

#### 4.2.1. Experimental Section

##### 4.2.1.1. Sample description

The selection of 18 commercially available drugs and nutritional supplements containing plant extracts were chosen, in order to cover a wide range of plant families. The samples were purchased in Germany. They are generally used as nutrition supplementation or for fighting general physical discomfort related to cold and flu, so their use is remarkably widespread. Although all the samples are plant extracts, the collection included different intake formats (capsules, liquids...), as described in Table 4.2.

#### 4. Crystallization promoters

Table 4.2 Description of the samples. The commercial names and distributors correspond to the German market, from which the samples were purchased.

Plant (Commercial name)	Distributor	Plant Family and Species Supplement components	Plant part	Intake format
Green tea (Praevent-loges)	Dr. Loges GmbH	<i>Camellia sinensis</i> Green tee extract (59% w/w), Acerola powder (12% w/w)	Leaves	Capsule
Chamomile (Eukamillat)	Dr. Rentschler Arzneimittel GmbH	<i>Matricaria chamolilla</i> Chamomile flowers essential oil (liquid)	Flower	Liquid
Echinacea (Vita Echinacea solution)	Bergwalder	<i>Echinacea purpurea</i> Echinacea flowers pressed extract in ethanol (liquid)	Flower	Liquid
Black cohosh		<i>Cimicifuga racemosa</i>	Root	Tablet
Vitex (Monchspeer)	Ratiopharm GmbH	<i>Vitex agnus-castus</i> Dry extract (7-13:1) from plant fruits in ethanol	Fruit	Tablet
Hypericum (Johanniskraut)	Ratiopharm GmbH	<i>Hypericum anagalloides</i> Dry extract (3.5-6.0:1) from leaves, ethanol	Leaves	Capsule
Valerians (Baldrian-Dispert)	Chelapharm Arzneimittel GmbH	<i>Valeriana officinalis</i> Dry extract (3-6:1) from valerians root in ethanol	Root	Tablet
Thyme (Bronchicum)	Cassella-med GmbH	<i>Thymus vulgaris</i> Liquid extract from thyme (2-2.5:1) and primula roots (5:1)	Leaves, roots	Liquid
Camphor, Hawthorn (Korodin)	Robugen GmbH	<i>Cinnamomum camphora</i> , <i>Crataegus monogyna</i> Liquid extract from Hawthorn fruits (1.3-1.5:1) and camphor (2.5% w/w)	Leaves, Fruit	Liquid
Birch, Orthosiphon, Goldenrod (Harntee 400 TAD N)	TAD GmbH	<i>Betula pubescens</i> , <i>Orthosiphon stamineus</i> , <i>Solidago virgaurea</i> Birch extract (4.3-7.7:1), orthosiphon (4.5-70.1:1) and goldenrod extract (5.0-7.1:1)	Leaves	Solid, granulate
Ginkgo (Ginkobil)	Ratiopharm GmbH	<i>Ginkgo biloba</i> Extract from ginkgo leaves (35- 67:1) in acetone	Leaves	Tablet
Activated carbon (Kohle-Compretten)	Merck	Medical carbon	-	Tablet
Hawthorn (Crataegutt novo)	Schwabe	<i>Crataegus monogyna</i> Hawthorn extract (4-6.6:1) in ethanol	Leaves, Flower	Tablet
Common vervain, Gentian, Sorrel, Elder, Cowslip (Sinupret forte)	Bionorica	<i>Verbena officinalis</i> (23%), <i>Gentiana verna</i> (8%), <i>Rumex acetosa</i> (23%), <i>Sambucus</i> (23%), <i>Primula veris</i> (23%)	Leaves, Root, Flower	Tablet
Ivy-leaved Speedwell (Prospan)	Engelhard	<i>Veronica hederifolia</i> Leaves extract (5-7.5:1) in ethanol 30%	Leaves	Liquid
Uzara (Uzara)	Hemopharm	<i>Xysmalobium undulatum</i> Extract from root (4.5-6.2:1) in methanol 60%	Root	Liquid
Iceland moss (Isla moos)	Engelhard	<i>Cetraria islandica</i> Extract from leaves (0.4-0.8:1)	Leaves	Capsules

#### 4.2.1.2. Sample preparation

Two different conditions were used for the sample preparation, in order to determine the soluble to total oxalate ratio. The soluble oxalate fraction was obtained using Milli Q water (18.3 M $\Omega$  filtered), whereas 2 M HCl (Merck, Darmstadt, Germany) was used for the total oxalate content. The acid treatment was selected to imitate the conditions that samples would suffer in the stomach. In both cases, one sample unit (capsule or tablet) was weighted and dissolved in 4 ml of water or HCl and stirred for 15 minutes at room temperature using a magnetic stirrer. The resulting solutions were filtered at gravity and, immediately afterwards, the samples were placed in the analyzer. For those samples in a capsule format, only the inner content was used for the analyses, since the composition of the capsule did not contain oxalate or any precursor, according to the manufacturers' information.

#### 4.2.1.3. Ion Chromatography analysis

In the present work, the equipment used was a Dionex ICS2100 (Dionex, CA, USA), served by a Thermo Fisher Dionex AS-AP auto sampler. After a 1:50 to 1:200 dilution, adapted to each sample, in 0.3 M H<sub>3</sub>BO<sub>3</sub> (Sigma Aldrich, Steinheim, Germany), the sample was injected through a 25  $\mu$ l loop into the separation system. This part of the equipment consisted on a pre-column Dionex Ion Pac AC11 (2 x 50 mm), followed by an anionic separation column Dionex IonPac AS11 (2 x 50 mm), operated at 35 °C. the detector used was an ion suppressor, Dionex ASRS-300. The software Chromeleon (Dionex) allowed the experiment performance and data recording.

These conditions were adapted from the existing bibliography 265 266. The mobile phase used was KOH (flow 1.5 ml/min) with a concentration gradient as follows: 0.2 mM during 6 minutes; then, KOH concentration increased up to 5 mM at 0.8 mM/min (total run 12 min). After 12 minutes, the separation gradient was followed by a cleaning sequence (5 minutes running 100 mM KOH) and a stabilization time of 5 minutes.

A six-point calibration curve was measured; covering oxalate concentrations in the range 0-10  $\mu$ M. the set of standards was prepared from a concentrated 2 mM sodium oxalate solution (Sigma Aldrich, Steinheim, Germany). All samples, including both oxalate extraction methodologies, were analyzed in duplicate.

### 4.2.2. Results and discussion

#### 4.2.2.1. Analysis methodology

The methodology yielded good results in terms of component separation and, especially, oxalate quantification.

A standard solution containing possible interferences, which might induce overlapping peaks, was also measured. Sulfate and phosphate ions, usually occurring in natural samples, were added to a standard

solution as a test. As observed in Figure 4.1, the resolution of the oxalate peak was satisfactory, and the baseline, nicely reached after the sulfate peak.

QA/QC was performed by checks on the samples. A standard was checked each 10 samples and a spiked sample was added every 4 analyses. Spikes were done on the samples before and after the dissolution with water and HCl. The absence of oxalate contamination was checked by measuring a blank sample after the last calibration point and after each run. The values for the calibration curve are shown in Table 4.3. LOD and LOQ were calculated as the concentration associated to the blank signal plus its standard deviation multiplied by 3 and 10, respectively. The methodology reproducibility (calculated as RSD, Relative Standard Deviation) was measured by repeatedly running the same sample in the same and different batches.

As seen in Table 4.3, the parameters concerning the suitability of the chromatographic method for the analysis of the plant extract samples laid within acceptable quality and reproducibility limits.

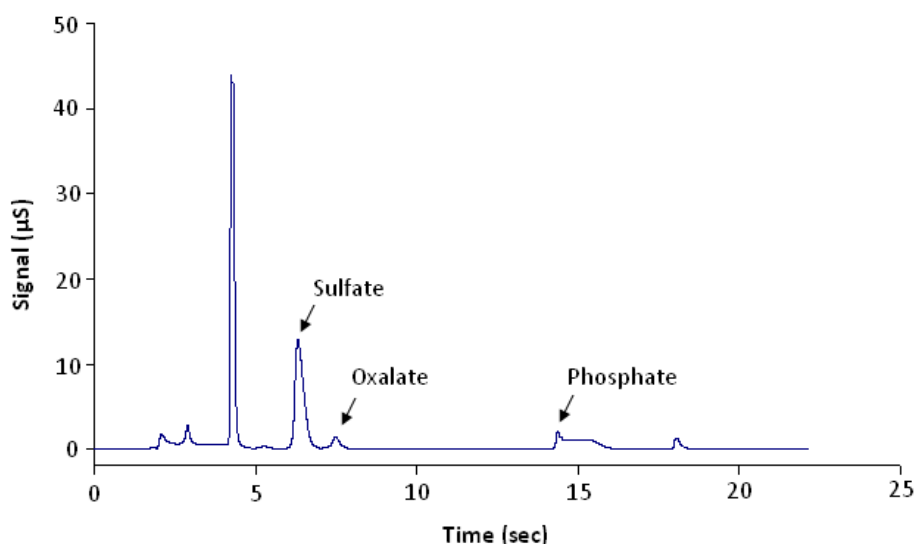


Figure 4.1 Example of a chromatogram for a standard solution containing 10  $\mu\text{M}$  oxalate. This standard was spiked with 20  $\mu\text{M}$  of potential interferences: sulfate and phosphate.

Table 4.3 Calibration results and quality control checks.

Calibration curve: $y = 5.56 (\pm 0.04) \cdot [\text{oxalate concentration}] - 1.40 (\pm 0.03)$ (Values expressed as $\cdot 10^2$ , sensitivity units: $\mu\text{S}/\mu\text{M}$ )			
LOD	0.26 $\mu\text{M}$	Sample spike recovery	within $\pm 10\%$
LOQ	0.28 $\mu\text{M}$	Reproducibility intra-batch (RSD)	< 5%
$r^2$	0.998	Reproducibility inter-batch (RSD)	< 5%

#### 4.2.2.2. Sample analysis

According to the different plant species the samples belong to, their oxalate content lies within a wide range (from 0.04 to 2.2 mg/g extract). The results are listed in Table 4.4. When describing the samples, “unit” refers to an intake unit; capsule or tablet.

As expected, green tea extract has a remarkably high oxalate concentration, as the plant itself does, as reported in several publications 260 267. Soluble and insoluble oxalate contents were compared: 1.8 and 1.9 mg/g extract. Most of the oxalate might be, thus, easily absorbed, so the intake of such complements could have negative effects for patients with risk profile.

Table 4.4 Oxalate concentrations in the analyzed samples (solid).

Plant	Oxalate concentration mg/g extract				Unit weight (g/unit)		Oxalate amount per unit (mg/unit)			
	Total	±SD	Soluble	±SD	Value	±SD	Total	±SD	Soluble	±SD
Green tea	1.9	0.1	1.8	0.1	0.47	0.01	0.91	0.06	0.86	0.05
Black cohosh	0.04	0.01	0.03	0.01	0.28	0.01	0.011	0.003	0.007	0.002
Vitex	0.030	0.001	0.024	0.001	0.26	0.01	0.0078	0.0001	0.0062	0.0002
Hypericum	0.37	0.01	0.17	0.03	0.55	0.01	0.20	0.01	0.09	0.01
Valerians	0.51	0.01	0.47	0.03	0.14	0.01	0.074	0.002	0.068	0.006
Birch, Orthosiphon, Goldenrod	0.18	0.01	0.17	0.01	1.0	0.1	0.18	0.01	0.17	0.01
Ginkgo	0.086	0.003	0.058	0.004	0.27	0.01	0.023	0.001	0.015	0.001
Activated carbon	<LOD		<LOD		0.42	0.01	N/A		N/A	
Hawthorn	0.27	0.01	0.25	0.01	0.43	0.04	0.12	0.01	0.10	0.01
Common vervain, Gentian, Sorrel, Elder, Cowslip	2.2	0.2	0.22	0.03	0.51	0.02	1.1	0.1	0.11	0.02
Iceland moss	0.41	0.01	0.02	0.01	0.99	0.02	0.41	0.02	0.019	0.001

<LOD: Concentration below the LOD.

N/A: not applicable

Interestingly, from the plant extract listed in Table 4.4, the one which showed the highest oxalate content was that containing the most complex mixture of plants. Indeed, the amount of oxalate in this case was even higher than that for tea. Some components listed in this mixture have been reported to have high oxalate content or even pointed out as potentially harmful for kidney function 259 268. These results advise stone patients to carefully consider the intake of such plant extract.

On the other side, some of the analyzed extracts showed little amounts of oxalate. In fact, black cohosh, vitex and ginkgo had oxalate concentration below 0.1 mg/g extract. For the activated carbon, this value was even below the LOD, fact that fits to its nature, based on elemental carbon.

#### 4. Crystallization promoters

In regard to the extracts in liquid format, the oxalate content range was not as wide as for the solids (see results in Table 4.5). Nevertheless, three groups could be defined: the concentration for ivy-leaved speedwell and uzara extracts was around 5 mg/l; Echinacea laid over 70 mg/l; the rest ranged from 10.4 to 23 mg/l.

Table 4.5 Oxalate concentrations in the analyzed samples (liquid).

Plant	Oxalate concentration mg/g extract	
	Total	±SD
Chamomile	12.9	0.5
Echinacea	73	3
Thyme	23	1
Camphor, Hawthorn	10.4	0.1
Ivy-leaved Speedwell	5.52	0.04
Uzara	5.17	0.08

Table 4.6 Oxalate daily intake, according to recommended dose. In liquid samples, the whole oxalate fraction was assumed to be in soluble form or as very small particles in suspension, but not as crystals.

Plant	Daily dose		Total oxalate intake/day		Soluble oxalate intake/day (solid samples)			
	Unit	ml/g	mg	±SD	mg	±SD	% Soluble	±SD
Green tea	2		1.8	0.1	1.7	0.1	94.7	0.1
Black cohosh	2		0.023	0.006	0.015	0.004	65.9	0.4
Vitex	1		0.0078	0.0001	0.0062	0.0002	80.1	0.0
Hypericum	2		0.41	0.01	0.18	0.03	44.9	0.1
Valerians	9		0.67	0.02	0.61	0.06	91.5	0.1
Birch, Orthosiphon, Goldenrod		16 g	2.92	0.04	2.7	0.1	93.2	0.0
Ginkgo	6		0.14	0.01	0.093	0.008	67.0	0.1
Activated carbon	16		N/A		N/A		N/A	
Hawthorn	2		0.23	0.02	0.21	0.02	90.7	0.2
Common vervain, Gentian, Sorrel, Elder, Cowslip	3		3.3	0.4	0.33	0.06	9.90	0.03
Iceland moss	2		0.81	0.04	0.038	0.001	4.68	0.00
Chamomile		6 ml	0.077	0.003				
Echinacea		3 ml	0.22	0.01				
Thyme		7.5 ml	0.18	0.01				
Camphor, Hawthorn		1.5 ml	0.016	0.000				
Ivy-leaved Speedwell		15 ml	0.083	0.001				
Uzara		30 ml	0.15	0.00				

N/A: not applicable



Based on the concentration values, the daily oxalate intake, according to the manufacturer recommended dose, was also calculated (see Table 4.6). In this sense, only in three of the analyzed plant extracts (green tea and the mixtures birch-orthosiphon-goldenrod and common vervain-gentian-sorrel-elder-cowslip) resulted on a total daily amount close or greater than 2 mg. The oxalate content determined in the rest of the samples was rather low.

As previously stated, the quantification of the soluble fraction is also necessary for a correct understanding of the oxalate absorption in the digestive tract. Table 4.6 lists these values, which range from more than 65% to 95% in green tea. A few exceptions were found, namely Iceland moss extract and the mixture containing common vervain-gentian-sorrel-elder-cowslip, for which really small oxalate contents were determined.

#### 4.2.3. Final remarks

The oxalate concentration of the plant extracts analyzed in this work shows a high variability. The influence of such amount on the total oxalate intake should be considered. Although strongly influenced by the type of diet, a general value for the oxalate intake ranges from 50 to 350 mg/day, not including diets that incorporate a high portion of oxalate-rich vegetables. Those plant extracts with the highest oxalate content (green tea and the mixture of common vervain, gentian, sorrel, elder and cowslip) might represent a relevant fraction of the total amount of oxalate. In the most dramatic case, for those diets with low oxalate content, the intake of these supplementations would account for 8% of the total oxalate.

These results should be carefully considered, especially in those cases in which the patient is strongly affected by increased oxalate intakes.

When the results obtained are carefully examined, it can be gathered that the normal consumption of the mentioned nutrition supplements could account for an 8% of the total oxalate intake in the worst case. Therefore, the intake of some of the plant extracts analyzed in this work should be considered, especially for those patients who develop calcium oxalate stones.

### 4.3. Determination of urinary lithiasis promoters and inhibitors in chocolate

One of the most beloved foods is chocolate. This food, which is a highly processed product made from cocoa beans, has also been pointed out as a healthy food, due to the considerable levels of antioxidant that it contains 269. Nonetheless, chocolate intake has often been questioned, basically due to its high

caloric content (>3000 kcal/kg) 270, which can become a problem in over-weighted societies, as the Western one.

Not only the caloric content of chocolate, but also its oxalate content (derived from cocoa beans) has often been addressed. Some studies have indicated high content of oxalate in chocolates, which has been described to surpass 600 mg oxalate/100 g chocolate 271. This value might represent an increased risk for those CaOx stone patients who suffer oxalate hyperabsorption.

This Section intends to throw some light into the description of the stone formation risk associated to chocolate intake. In this concern, not only the oxalate content of the chocolate samples was analyzed, but also the content of some other promoters and inhibitors has been quantified. The collection of samples chosen includes a wide variety of chocolates, with different cocoa content and also including mixtures with other products, such as nuts, milk or caramel. This selection should provide a general overview of chocolate containing products as potential harmful foods for CaOx stone patients.

This goal will be addressed by determining the concentration of some important nutrients in chocolate. Special attention will be given to oxalate and calcium content, due to its direct relation to the mentioned group of urinary stones.

### **4.3.1. Experimental Section**

#### **4.3.1.1. Sample description**

The collection of samples included 94 different commercially available chocolate products and also pure cocoa beans; a total of 95 samples were studied. All the samples were purchased in Germany. In order to correctly reflect chocolate intake in Western society, different cocoa contents and combination of ingredients were selected. The samples included in the study are listed in Table 4.7.

#### **4.3.1.2. Sample preparation**

The sample preparation was done according to the description in Section 4.2.1.2. As described in that section, two different preparation procedures were followed, in order to quantify only soluble or total components in chocolates (water and hydrochloric acid were used). The chromatographic analysis was performed immediately after the sample preparation. The samples were then kept frozen until the elemental analysis on ICP-MS was done.

#### **4.3.1.3. Ion chromatography analysis**

The system, analysis conditions and sample dilution used in this step are the same as those described in Section 4.2.1.3.

Table 4.7 Description of the samples. The commercial names correspond to the German market. The cocoa content was the indicated by product labelling.

Type of chocolate	Commercial brand	Cocoa content (%)
Nougat	Ritter Sport	20
Joghurt	Ritter Sport	15
White	Ritter Sport	27
Milk and cereal	Ritter Sport	25
Hazelnut	Ritter Sport	20
Cookies	Ritter Sport	9
Milk chocolate	Ritter Sport	30
Cereals	Ritter Sport	15
Marzipan	Ritter Sport	25
Coconut	Ritter Sport	20
Himbeer-Cranberry Joghurt	Ritter Sport	17
Cookies and nuts	Ritter Sport	15
Alps milk chocolate	Ritter Sport	30
Erdbeer Joghurt	Ritter Sport	15
Dark Mousse	Merci	48
Cafe-Crème	Merci	33
Milk Praline	Merci	32
Hazelnut	Merci	32
Dark Cream	Merci	45
Marzipan	Merci	48
Almonds	Merci	32
Milk chocolate	Merci	32
Dark chocolate	Moser Roth	85
Dark chocolate	Moser Roth	70
Edel Vollmilch	Moser Roth	32
Bitter	Moser Roth	85
Milk chocolate	Moser Roth	32
Dark bitter	Herren Schokolade	60
Milk chocolate with almonds	Choceur	33
White	Choceur	28

Type of chocolate	Commercial brand	Cocoa content (%)
Bitter	Choceur	45
Milk chocolate	Choceur	33
Delicate bitter	Choceur	50
Marzipan	Choceur	25
Creamy milk chocolate	Choceur	33
Milk and nuts	Choceur	30
Hazelnuts	Choceur	33
Milk chocolate	Choceur	16
Alps milk chocolate	Choceur	30
Coconut	Choceur	27
Grapes nuts	Choceur	32
Marzipan	Mirabell Mozartkugeln	13.4
Cocoa beans	-	100
Milk Choc. w/ Honey and almond nougat	Toblerone	28
Milk chocolate	Kinder Ferrero	20
Milk chocolate	Schogetten	30
Bitter	Schogetten	65
White	Schogetten	25
Milk chocolate	Milka	30
White	Milka	27
Delicate bitter	Milka	45
Milk chocolate	Gut & Günstig	30
Milk and hazelnuts	Gut & Günstig	30
Cocoa powder	Bensdorp	100
Nougat Cream	Noccionlino	7
Shortbread Cookies (Hawaii)	Candies Big Island	20
Caramel	Storck	12
Bitter	Dr. Oetker	39
Milk chocolate w/ wallnuts	Nussknacker	32

Table 4.7. Continuation from previous page.

Type of chocolate	Commercial brand	Cocoa content (%)
Caramel dark	Confiserie Premium Trüffel	50
Cherry dark	Confiserie Premium Trüffel	50
Orange dark	Confiserie Premium Trüffel	50
Cream hazelnut	Confiserie Premium Trüffel	50
Pistachio dark	Confiserie Premium Trüffel	50
Lemon dark	Confiserie Premium Trüffel	50
Latte Macchiato	Confiserie Premium Trüffel	50
Vanille dark	Confiserie Premium Trüffel	50
Caramel	Crispy bits	30
Milk chocolate	Lindt Excellence	30
Milk chocolate	Ja	30
Caramel	Mars	25
Milk caramel	Bounty	25
Caramel	Bounty	25
Caramel	Milky Way	25
Milk	Dove	25
Milk caramel	Dove caramel	25

Type of chocolate	Commercial brand	Cocoa content (%)
Milk	Malteser	25
Schoka-Kola	Schoka-Kola	30
Caramel	Snickers	25
Caramel cookie	Twix	25
Hazelnut cream	Ferrero	7
Coconut	Ferrero	15
Hazelnut	Ferrero	20
Nuts	Ferrero	15
White	Ferrero	25
Joghurt	Ferrero	17
Hanuta	Ferrero	15
Mint chocolate	After Eight	70
Milk chocolate	Ferrero Kinder	15
Erdnuss	M&M	15
Peanuts	Mr. Tom	30
Chocolate powder	Dr. Oetker	15

#### 4.3.1.4. ICP-MS analysis

ICP measurements were performed using a Thermo Fisher Scientific XSeries 2 ICP-MS. A conical quartz nebulizer (Ar flow 0.8 l/min) was used. The radiofrequency generator power, used to keep the plasma, was 1400W. The torch included a 1 mm injector. Before acquiring the sample signal, the stabilization time was set at 50 sec, and a cleaning step of 90 sec was set after each sample. The mass spectrometer analyzer was configured to perform each measurement three times and the measuring time at each mass was 30 ms (50 ms for Ca, due to its low sensitivity). This yielded an analysis time of 25 seconds/sample.

Due to the measurement of ions with potential mass interferences from other polyatomic ions, CCT (Collision Cell Technology) was used. An auxiliary He flow (4.5 ml/min) was injected in the hexapole (See Section 4.1.1.2. ).

The only sample preparation required was a 1:1000 dilution of the sample using 2% HNO<sub>3</sub> (JT Baker, Center Valley, PA, USA). The same solvent was used for the external calibration curve (1-500 ppb) and for cleaning between samples. Each sample was diluted up to 10 ml, and then 50 µl of a solution containing 1 ppm Sc were added. Sc, at a final concentration of 5 ppb, was used as internal standard. The most suitable isotopes were selected, in order to minimize interferences and optimize the signal, as listed in Table 4.8. The list of interferences described shows some cases that could represent a problem for the measurements. However, the use of CCT allowed to satisfactorily minimizing those, as checked using quality control samples.

Table 4.8 Isotopes determined in the ICP-MS analysis.

Isotope	Abundance (%)	Main interferences
<sup>23</sup> Na	100	<sup>14</sup> N+ <sup>9</sup> Be, <sup>16</sup> O+ <sup>7</sup> Li
<sup>24</sup> Mg	78.6	<sup>12</sup> C+ <sup>12</sup> C, <sup>1</sup> H+ <sup>23</sup> Na
<sup>31</sup> P	100	<sup>17</sup> OH+ <sup>14</sup> N, <sup>16</sup> O+ <sup>15</sup> N
<sup>39</sup> K	93.08	<sup>16</sup> O+ <sup>23</sup> Na, <sup>12</sup> C+ <sup>27</sup> Al
<sup>44</sup> Ca	2.13	<sup>17</sup> OH+ <sup>27</sup> Al, <sup>40</sup> Ar+ <sup>4</sup> He
<sup>45</sup> Sc	100	<sup>14</sup> N+ <sup>31</sup> P, <sup>17</sup> OH+ <sup>28</sup> Si

The list of interferences has been obtained from PlasmaLab software, Thermo Fisher Scientific.

The analysis of P at ICP-MS can be extrapolated as phosphate content. Phosphorous molecules other than PO<sub>4</sub><sup>3-</sup> are found in chocolate in a much lower concentration. Since mass 31 (phosphorous) was measured, the analyte P will be cited in this Section, referred to PO<sub>4</sub><sup>3-</sup>.

#### 4.3.1.5. Data analysis

The analyte determination in chocolate samples included 6 different components. This leads to a complex dataset, since each analyte might show a different trend, besides the large number of interactions that could link some of them. For this reason, some multivariate data analysis techniques

have been used in this Section. Data analysis has been performed using The Unscrambler X software (CAMO, USA).

Principal Component Analysis (PCA) was used for the analysis of this dataset. In brief, PCA allows the reduction of the dimensionality of the dataset, by creating a new variables system, based on the description of the data variance. The new variables (loadings) are a combination of real variables, combining different weights. The coordinates that describe each sample in the new variables set are called scores. For more details on PCA theory, refer to Section 2.1.2.2. In this Section, PCA was performed by mean-centering the data, so the mean for each parameter was subtracted from each value. This step allows not considering the magnitude, if different parameters are compared. The PCA model was validated using cross-validation, establishing 20 segments (or independent sample groups) within the dataset.

Hierarchical Cluster Analysis (HCA) 206 was also used for the unsupervised classification of the samples. HCA is able to group the samples into groups (clusters) according to underlying interactions between variables. The real classes or groups are not an input in the data analysis. Clusters are defined according to “distance” criteria. Indeed, the method used for calculating the distance is a key point in HCA, since it conditions the shape of the classes’ distribution, generally plotted as a dendrogram (see Figure 4.2 for an example). Many approaches have been defined for the cluster-to-cluster distance calculations as well as for building the cluster. Here, the ones selected for the analysis of the data presented in this Section will be described. The selection criterion was based on the most coherent group clustering, according to the samples nature.

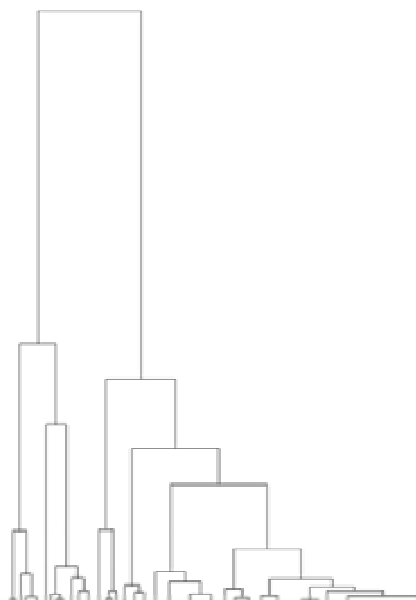


Figure 4.2 Example of a dendrogram. Samples are sorted in pairs according to minimum distance. The distance is represented in the vertical axis. Each pair is linked to the closest one to create a new group, and this procedure is repeated until the whole dendrogram has been defined.

Complete linkage clustering was chosen for the construction of the dendrogram. This algorithm, also known as farthest neighbor method, sorts the samples into pairs according to maximal object-to-object distance. The distance between two clusters is calculated as the distance between the two furthest objects within the groups. This process is iterated to create a net (dendrogram) as shown in Figure 4.2.

The distance itself was calculated by a correlation algorithm. The distance between two objects is assigned a value between -1 and +1, according to the dependence of those. The absolute value of the correlation gives meaning to positive or negative correlations.

### 4.3.1. Results and discussion

#### 4.3.1.1. Methodology results

Ion chromatography analyses yielded similar results as described in Section 4.2.2.1. , referred to separation efficiency, reproducibility and quality control. ICP-MS analyses also behaved in an appropriate way, and were subjected to similar quality controls as ion chromatography (duplicated sample measurements, quantitative spikes and correlation of the calibration curves). Ion Chromatography results and quality control criteria have been cited in Section 4.2.2.1. , and also apply in this case. Only the LOD and LOQ values for ICP-MS analyses will be described here (Table 4.9).

Table 4.9 ICP-MS analyses quality parameters.

Parameter	Na	Mg	P	K	Ca
Calibration slope (counts/ppb)	165.6	70.5	0.5	113.5	4.2
Correlation ( $r^2$ )	0.99993	0.99998	0.99976	0.99994	0.99688
LOD (ppb)	5.5	2.6	32.3	5.8	77.0
LOQ (ppb)	7.2	4.4	124.7	7.0	182.5

#### 4.3.1.2. Sample analysis

##### 4.3.1.2.1. General statistical parameters

It was the goal of this study to offer a general view of lithogenic risk associated to different chocolate types. This led to the collection of a large number of samples, so the data associated was also abundant. Since a precise data analysis (sample by sample) will not offer a clear trend within groups, the specific results have been omitted in this Section. They can be consulted at Supplemental Materials (8.1. ). The results shown there include oxalate, sodium, potassium, magnesium, phosphorous and calcium concentrations. They have been organized in two tables (Tables 8.1 and 8.2), that collect the results for total components (homogenized in HCl) and soluble ones (homogenized with H<sub>2</sub>O) separately.

Instead of discussing those specific data, a general description of the data set has been done in this Section. Statistical parameters that describe the general trends in the dataset are listed in Table 4.10. As appreciated in from the values in this Table, oxalate content has a wide variation range. In the worst case the intake of oxalate would be higher than 600 mg/100 g chocolate. This is a considerable amount for CaOx stone formers, since it nearly doubles the highest range of estimated daily oxalate (350 mg). In addition, the bioavailability of oxalate (soluble oxalate) is also high, with its maximum reaching 571 mg/100 g chocolate in the analyzed sample collection. However, the variation range is also remarkably high, so samples are very different in regard to oxalate content. Indeed, the range for all the analyzed components is wide. This could be expected from the different composition of the sample set. As described in Table 4.7, the samples include dark chocolate, which is supposed to have high oxalate content, but also milk chocolate and some products with caramel and yoghurt. The soluble content fraction depends on which component is analyzed. An important fraction of Na and K, 75-80%, is soluble, and this value remains at 60 % for P. The rest of components are more sensitive to the treatment environment. This is especially interesting for calcium and oxalate, due to their close relation in the digestive tract and the link between oxalate bioavailability and its hyperabsorption (see Section 4.1. ).

Table 4.10 General statistical parameters that describe the total and soluble content of the analyzed components.

	Total (mg/100 g chocolate)					
	Oxalate	Na	Mg	K	P	Ca
Mean	72.1	20.3	17.9	106.2	93.5	37.5
Maximum	619.3	71.3	57.3	384.1	150.0	80.3
Minimum	2.6	<LOD	<LOD	2.2	1.6	0.5
Range	616.7	71.3	57.3	381.9	148.4	79.8
Standard deviation	89.8	13.4	11.9	44.5	27.8	16.6
	Soluble (mg/100 g chocolate)					
	Oxalate	Na	Mg	K	P	Ca
Mean	28.7	17.0	7.5	80.2	56.2	13.2
Maximum	571.3	59.5	32.2	208.0	129.9	38.9
Minimum	1.1	<LOD	<LOD	2.0	2.5	<LOD
Range	570.2	59.5	32.2	206.0	127.4	38.9
Standard deviation	69.8	11.3	5.8	27.2	19.3	9.2

<LOD: Below Limit Of Detection. LOD is equivalent, in mg/100 g chocolate, to: Na: 0.55, Mg: 0.26, Ca: 7.7.

Cocoa beans have also been included within the sample set. The oxalate content in those was 378 mg/100 g product and was. Indeed, the highest value within the whole set was attributed to cocoa powder (according to the manufacturer, 99.8% pure), which had 619 mg/100 g product. Different origins also condition the amount of oxalate in cocoa beans 272.

In order to better describe the structure of the sample set, box-whiskers plots have also been plotted for total and soluble content of the analyzed components. The results are shown in Figure 4.3. For further indications on theory and interpretation of box-whiskers plots, refer to Section 3.3.3.1. Besides some



particular values, that make the upper quartile more distant to the Q1-Q3 box, it can be clearly appreciated that soluble oxalate lies in a much narrower region (lower variability). The absolute value (mg/100 g chocolate) is also lower for soluble oxalate. Emphasis should be made on the similar behavior of calcium. This suggests the existence of some relation between both components.

Figure 4.4 specifically shows the correlation between oxalate and calcium results. The fraction (%) of insoluble oxalate vs insoluble calcium in chocolate samples has been represented. Despite the low correlation value ( $r^2$ ) achieved (0.05), which does not indicate a close relation, some interesting features are made clear in this representation. In this plot, most of the samples form a dense cloud in the high percentage of insoluble oxalate and calcium area, observation that fits with the results in Figure 4.3.

Two other particular regions can be defined. Some samples can be classified as having low insoluble oxalate content (<50%), yet a high portion of calcium is insoluble. This group of samples also happens to be characterized by low total calcium content and medium to high oxalate concentrations. Most of these samples are indeed dark chocolates (>60% cocoa content). This could be a result of oxalate binding nearly all free calcium, so much oxalate remains soluble. This fact locates dark chocolate samples as potentially risky for CaOx stone patients. A second region in Figure 4.4 presents low insoluble calcium fractions together with high insoluble oxalate fractions. Chocolate types in this region have medium to high oxalate content (>Q3 in Figure 4.3) and low total calcium (<Q1 in Figure 4.3). These samples are mostly those containing ingredients different to chocolate in important amounts: caramel, yoghurt and nuts.

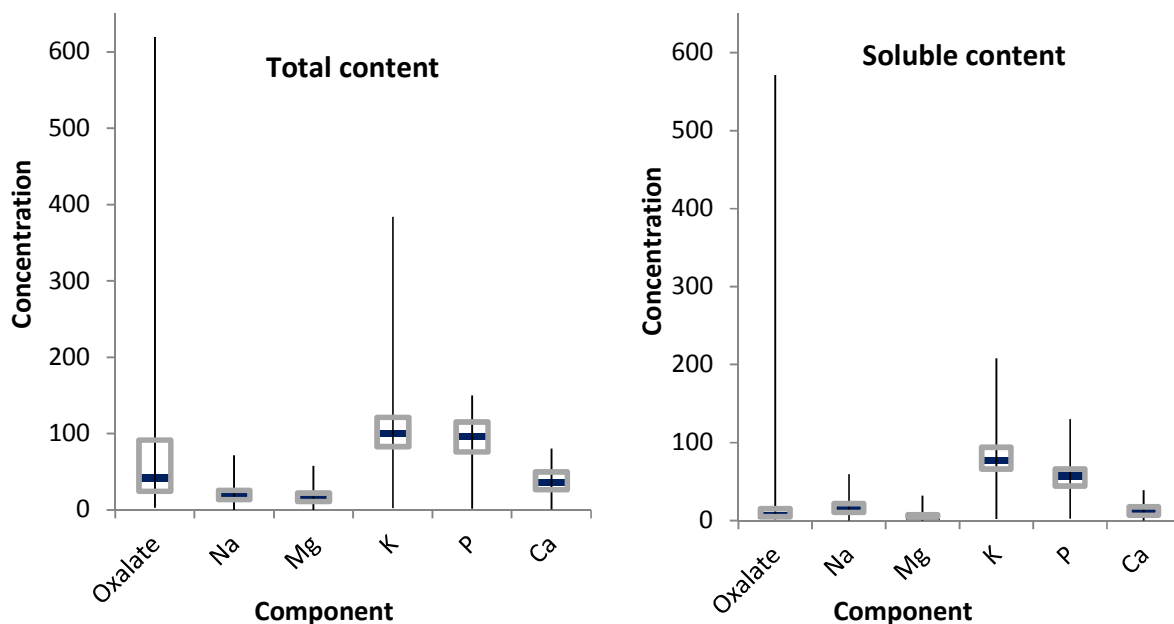


Figure 4.3 Box-whiskers plots for total and soluble content of each component.

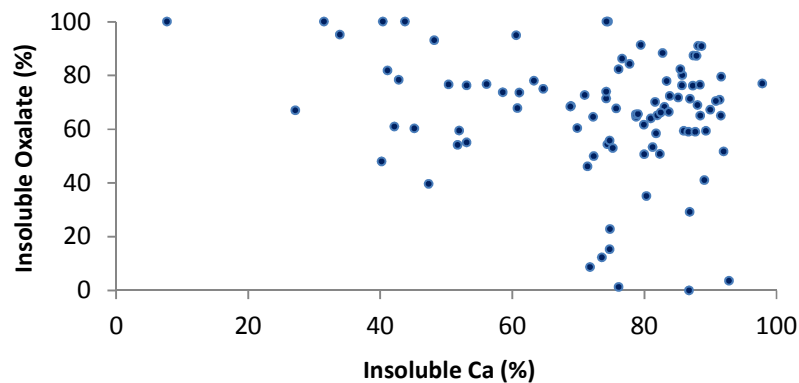


Figure 4.4 Insoluble oxalate vs insoluble calcium (calculated by subtracting soluble to total amounts).

As previously indicated, cocoa beans are oxalate-rich. Thus, it would be expected to measure a high oxalate content in those chocolates containing a higher cocoa fraction. The correlation calculations between both magnitudes are shown in Figure 4.5. R2 values are close to 0.45; although it denotes a weak correlation between both variables, the general trend is clear. A higher correlation could be expected for oxalate and cocoa, however the chocolate samples in the analysis set included a number of different components other than chocolate, so the deviation of linearity of the clouds in Figure 4.5 can be attributed to this.

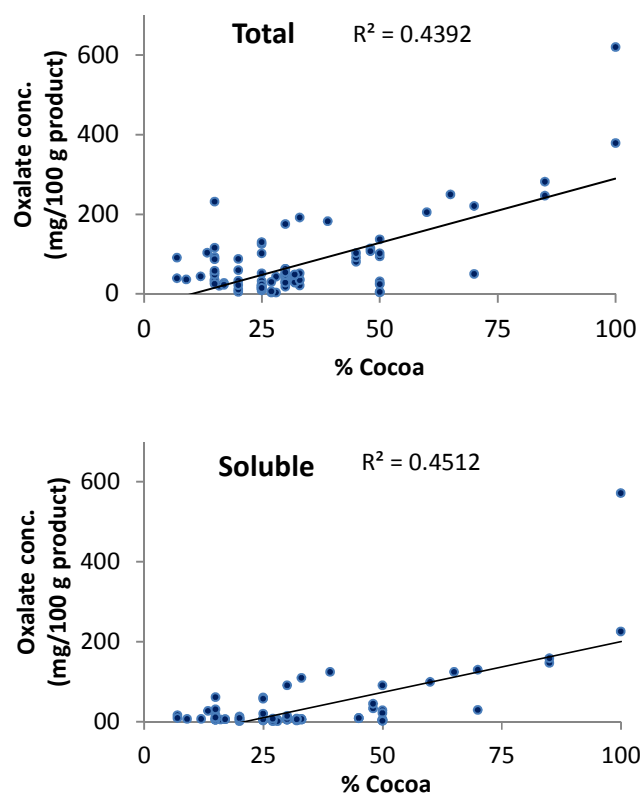


Figure 4.5 Correlation between oxalate concentration (total, top; soluble, bottom) and % cocoa in chocolate samples.

Oxalate was the variable that showed a higher correlation with cocoa content (%) in samples. The rest of components determined (Na, K, Mg, Ca and P) showed weaker or even lack of correlation with cocoa content.

#### 4.3.1.2.2. Principal Component Analysis

The analysis of the value, variability and dispersion of the data for each variable can give a general idea on the characterization of the sample set. However, the interaction between different variables becomes very complex when the trends and variance are independent one from the other, as seen in this dataset. Indeed, the previous Section has not clearly indicated which groups are found underneath the data matrix. The data analysis was done on values considering soluble and total components separately, and also including and taking out from calculations cocoa content. Thus, four different sets of values were used for the calculations.

Firstly, the variance explained by each Principal Component (PC) was calculated. The similarity of the sample sets in regard to interactions between variables was checked by analyzing the variance explained by each PC. Despite the slight differences of the data collections, if the datasets are explained using a similar number of PCs and these PCs depend mostly on the same real variables, the interaction between them can be considered similar.

Indeed, these are the results seen in Figure 4.6. This plot shows the average value of the explained variance for each PC, considering the four groups of samples listed. The reduced standard deviation clearly points out that the number of PCs needed for the description of the system is the same in all four groups. This fact suggests that the variables with a higher classification power are the same in all the sample sets. However, those PCs can be influenced by different real variables (indeed only two groups include “cocoa content”). The study of the influence of each variable on every PC (loadings determination) should throw some light onto this relation.

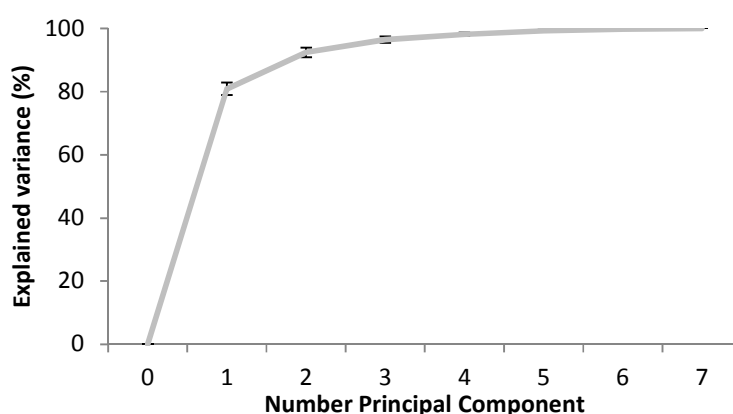


Figure 4.6 Average ( $\pm$ SD indicated by the error bars) of the explained variance by each PC for the four sample groups investigated. SD values are low, especially for PCs 4 to 7.

#### 4. Crystallization promoters

The loadings values, which help understanding the description power of each real variable, are shown in Figure 4.7 (see Section 2.1.2.2. for more precise indications on loadings). The data in this Figure corresponds to the soluble values of each measured parameter.

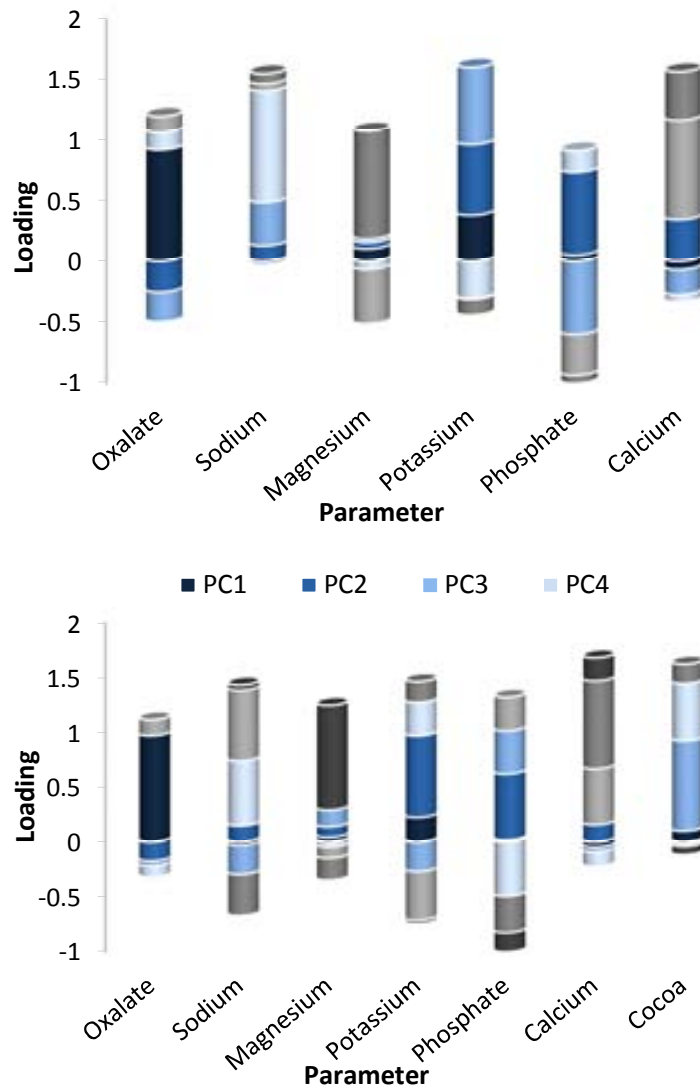


Figure 4.7 Loadings values for each PC. Data correspond to the soluble amount of each component. The plot at the top shows loadings distribution when cocoa is not included as a variable in the dataset; the bottom plot includes this seventh variable. Note that the number of PCs is equal to the number of variables in each case (PC 7 only applies to the bottom plot).

Soluble values were chosen for this analysis, since they represent the bioavailable portion of every parameter and so, is more representative for its real effect. The data associated to the total amount does not present remarkable differences with that shown here. As clearly seen in Figure 4.7, PC1 depends, on a great extent, on oxalate concentration. Interestingly, PC1 describes most of the variance within the data set (see Figure 4.6). According to PCA theory, PCs are calculated to describe the dataset starting from the direction in which the variance is bigger. This observation fits with the results seen in

Figure 4.3, since oxalate (followed by potassium) is the component that shows a greatest variance among the analyzed ones.

Despite the link between oxalate and calcium concentrations seen in Figure 4.4, PC1 does not directly relate those ions. Calcium mostly influences PC5 and PC6, which describe little variance in the dataset.

Cocoa bears also some classification power, but clearly behind oxalate. When this variable is introduced into the dataset, PC3 and PC4 are basically affected. Thus, cocoa content does not seem a good indicator of potential lithogenic risk of chocolates.

These observations lead to the conclusion that chocolates are basically differentiated by their oxalate content. Since the relationship between oxalate hyperabsorption in diet and oxalate intake has been described, some chocolates could be quickly assigned a label of “increased lithogenic risk”.

In order to identify which chocolates might represent an increased risk due to their composition, the scores representation for PC1 vs PC2 was done. This plot should position the samples according to their widest variability, since the two first PCs explain 91% of the dataset variance. This representation is shown in Figure 4.8. Basically, two groups can be appreciated: positive and negative score values for PC1. If we focus on the PC1>0 group, it includes dark chocolate samples.

The characteristics of this group of samples are different from the average values of the whole collection. As an example, average soluble oxalate, calcium and cocoa content have been calculated and compared to the values from the whole collection (see Table 4.11). According to this Table, those values are significantly different for the selected group of samples. As described before, dark chocolates have higher soluble oxalate and lower soluble calcium, which increases the likelihood of oxalate being absorbed in the digestive tract.

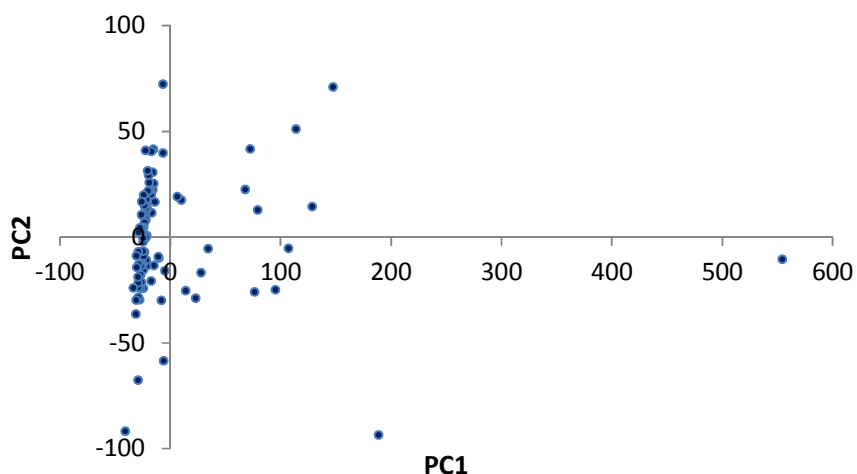


Figure 4.8 PC1 vs PC2 plot of all chocolate samples.

**Table 4.11 Average comparison of soluble components, using a t-test (95% confidence). p values <0.05 denote significantly different populations.**

Parameter	Group PC1>0		Group PC1<0		p value
	Average	SD	Average	SD	
Oxalate	116	122	28	69	<0.05
Calcium	5	15	13	83	<0.05
Cocoa	54	24	32	18	<0.05

#### 4.3.1.2.3. Hierarchical Cluster Analysis

PCA analysis allowed the identification of a group of samples presenting a higher risk for CaOx stone patients. It would be still useful to define some groups also at other levels, to establish some criterion on the chocolate intake by stone formers.

For this reason, Hierarchical Cluster Analysis (HCA) was done over the results. Here, the results of the HCA classification including cocoa content will be shown. Figure 4.9 defines some groups within the sample collection, which share some significant characteristics. These results have been calculated using soluble amounts, but total content yielded comparable results, with little difference in group composition.

HCA reinforces the results seen using PCA. Again, dark chocolate samples form a single group (Group A in the Figure), defined by the magnitudes described in point 1 in the Figure. Oxalate content is higher than 30 mg/100g chocolate, while calcium is lower than 10 mg/100g chocolate. These values show a higher lithogenic risk for this sample group. Magnesium acts as an inhibitor in stone formation (see 1.1.6.2. ), and the concentration values for this metal in this group have also been identified as high among the sample collection (>15mg magnesium/100g chocolate). This fact could help on the prevention of stone formation, although the high soluble oxalate content represents for sure a high amount of this component in urine. The inhibitory potential of urine (not only magnesium) should compensate for the oxalate load.

Also with a high cocoa content, but lower oxalate values, chocolates containing caramel are identified as group B in the Figure. They represent a lower lithogenic risk, followed by group C that corresponds to nut-containing chocolates. As expected, group D, that of lower lithogenic risk, is the largest, including white and milk chocolates. Oxalate content is <10mg/100g chocolate and calcium has been quantified above 10mg/100g sample.

The description of these groups has been done qualitatively. A table that lists all the samples and their assigned class is included in Supplemental Materials (8.1. ), Table 8.3.

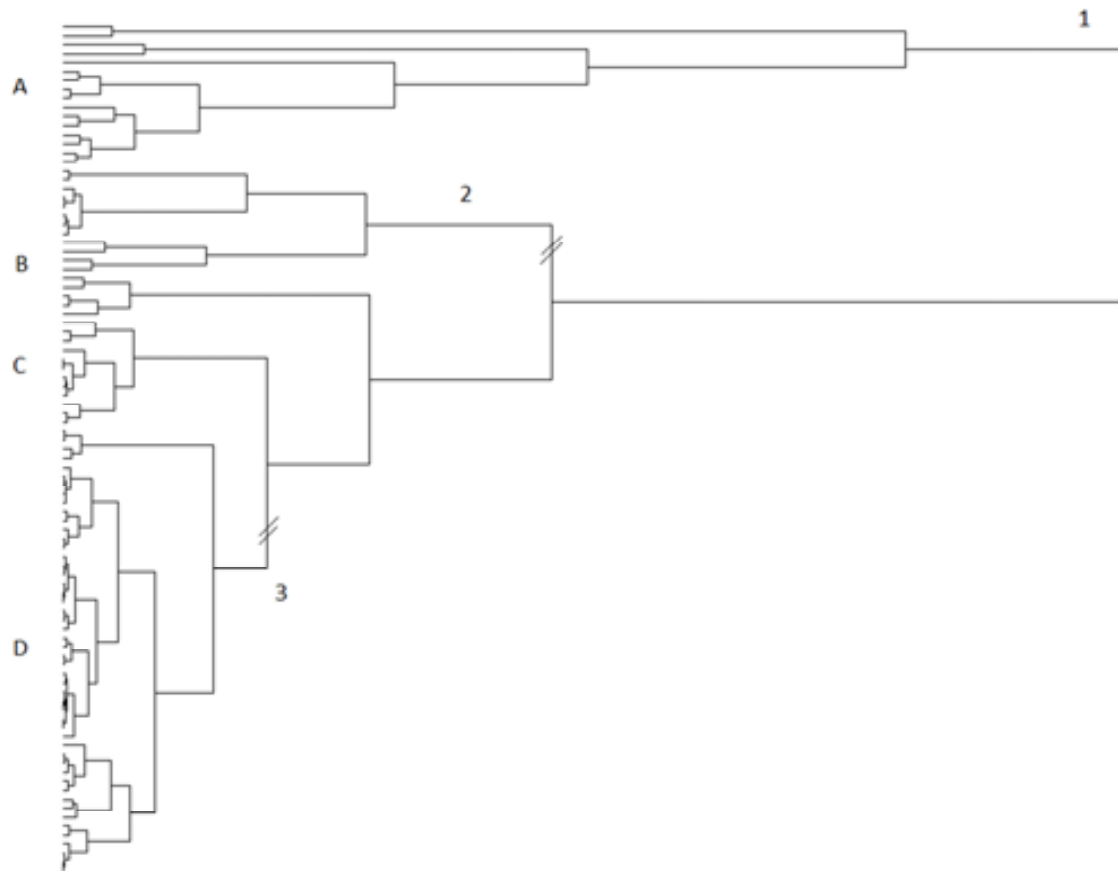


Figure 4.9 Dendrogram resulting from applying HCA to soluble data. The distance between samples is proportional to horizontal distance in this representation. A: Dark chocolates, B: Caramel chocolates, C: Nut chocolates, D: Milk/White chocolates. 1: <10mg calcium/100g choc., >30mg oxalate/100g choc., >15 mg magnesium/100g chocolate, >50% cocoa; 2: >50% cocoa; 3: <10mg oxalate/100g choc., >10mg calcium/100g choc.

#### 4.3.2. Final remarks

The wide consumption of chocolate requires an adequate comprehension of its risks for stone patients, due to the well-known high oxalate content of cocoa beans. This Section has assessed this risk, providing a general classification of diverse chocolate types and so, an answer to the question whether stone patients should avoid eating chocolate.

The wide variability within data, derived from a large variation in composition, does not indicate itself the lithogenic risk. However, it has been assessed by multivariate analysis techniques. Oxalate has been identified as the most important factor to discriminate between different chocolate sorts. A clear correlation between oxalate and cocoa content was expected, but this was only weak.

Not only cocoa content, but also the whole chocolate composition should be considered, because it can affect the total (and soluble) oxalate content. This composition has also an important effect on other components (mainly calcium), that can prevent oxalate from being highly bioavailable.

This work indicates the clear advice of avoiding those chocolates in groups A and D (dark and caramel chocolates) for CaOx stone formers. Due to the low amount of stone formation promoters found in white and milk chocolate, its intake should not imply an increased risk for those patients.

### **4.4. Determination of oxalate absorption using isotopic labeling**

As described in Section 4.1. diet is an important source for oxalate. It has been estimated that 10-20% of the oxalate content excreted in has this origin 252. Oxalate is a component often used in many vegetal species in remarkable concentrations, so keeping intake oxalate levels below 50mg/day becomes difficult in general diets.

Due to the importance of oxalate as a promoter, major concerns affect its intake and absorption. The statement that oxalate absorption is closely related to other components has been introduced in Section 4.1. Calcium is especially important in this concern, although other nutrients might also affect indirectly.

Some studies have addressed the effect of diet on the oxalate excretion. This study is not based on calculations of the total oxalate intake based on tabulated values for foods. Although this can yield precise results, this work relies on isotopic labelling for this determination. In our case, oxalate has been tracked using  $^{13}\text{C}$  labelling. The measurement of metabolic fluxes with  $^{13}\text{C}$  has been widely used for biological uses 273. The goal in this work was not to track oxalate along the body, but to specifically calculate the oxalate absorption in patients.

The complex interaction of oxalate with other ions makes it interesting not to rely only on one parameter (oxalate concentration) for the estimation of stone formation risk. The relevance of different approaches to determine lithogenic risk have described in Section 1.1.7. One of the most used techniques for the calculation of stone formation risk is RSS.

This work uses this approach to compare oxalate absorption to a general risk index that considers also the interactions between different components and the existing equilibria.

#### **4.4.1. Experimental Section**

##### **4.4.1.1. Sample description**

Urine samples were collected from 28 stone patients, who were given controlled diet and fluids. The isotopic labeling was achieved by administrating a capsule containing 50mg of sodium oxalate (double



labeled with  $^{13}\text{C}$ , abbreviated as  $^{13}\text{C}_2\text{-Ox}$ ), which corresponds to 33.82mg of  $^{13}\text{C}_2\text{-Ox}$  (Sodium oxalate- $^{13}\text{C}_2$  99.9%, Sigma Aldrich, Steinheim, Germany). The example of a capsule is shown in Figure 4.10.



Figure 4.10 The capsule administrated to the patients contained 50 mg of sodium oxalate containing only  $^{13}\text{C}_2\text{-Ox}$ .

24 hour urine samples were collected one day previous to the capsule ingestion. This value was used to calculate the RSS parameter. The following day, the patient was administrated the capsule and three urine samples were then collected. Sample 1 was collected from time 0 to 6 hours from the capsule intake; sample 2 from time 6 to 12 hours and sample 3 from 12 to 24 hours. The sum of these three fractions yielded the total amount of  $^{13}\text{C}_2\text{-Ox}$  excreted, so the percentage of absorbed oxalate could be calculated, taking the amount in the administrated capsule as reference.

#### 4.4.1.2. Sample preparation

Urine samples were collected from patients and immediately afterwards, 20  $\mu\text{l}$  HCl were added to 1 ml storing vials, for a proper conservation and prevention of oxalate precipitation. Vials were kept frozen at  $-30^\circ\text{C}$  until the analysis was performed. No sample treatment was required for the determinations other than 1:50 dilution of urine.

#### 4.4.1.3. Ion Chromatography – Mass Spectrometry analysis

The need to determine different carbon molecular weight for oxalate (87.9 for not labelled, or  $^{12}\text{C}_2\text{-Ox}$ , and 89.9 for labelled,  $^{13}\text{C}_2\text{-Ox}$ ) requires the use of a mass spectrometer for the determinations. The determination of  $^{13}\text{C}_2\text{-Ox}$  in urine has been reported in literature using Gas Chromatography – Mass Spectrometry 274 275. The methods reported in bibliography provide robust measurements. However, oxalate needs to undergo a derivatization process to make it volatile for the gas analysis. This reaction is often tedious and long, so the efficiency of the analysis is dramatically reduced. For this reason, the methodology selected in this work was Ion Chromatography coupled to Mass Spectrometry. Details on Mass Spectrometry applied to chromatography are provided in Section 4.1.1.1.

The ion chromatograph used was the same unit as described in Section 4.2.1.3. and it was directly coupled to a MSQ Plus Mass Spectrometer (Dionex, CA, USA). This MS was controlled from the

Chromeleon software, so the mass analyses were integrated with the chromatographic ones. The device could perform scans and also SIM measurements (Single Ion Monitoring). After identifying the most sensitive  $m/z$  ratios (88.9 and 90.9), the SIM mode was used, so only the target  $m/z$  ratios were measured. This increases the sensitivity and reduced the instrumental noise. Note that organic acids, as oxalate, tend to form  $[M-H]^+$  ions, instead of  $M^+$ , so the measured  $m/z$  values corresponded to 1 mass unit added to  $^{12}\text{C}_2\text{-Ox}$  or  $^{13}\text{C}_2\text{-Ox}$  276. An example of the measured masses is shown in Figure 4.11.

The conditions of the IC have been listed in Section 4.2.1.3. the MS was operated according to the following parameters: Electrospray Ionization (ESI) source, nitrogen as nebulizer gas, Probe temperature 450°C. Each mass included a window of  $\pm 0.25$  amu, so both isotopes were not overlap. Oxalate concentration in samples was only quantified using MS, since the conductivity detector signal included both isotopes (they have the same retention time).

In IC-MS analyses, naturally occurring oxalate was considered to correspond only to the 88.9 signal, and 90.9 represented fully isotopic labeled oxalate. Strictly, this is not true, since  $^{13}\text{C}$  has a natural abundance of 1%, so this percentage of natural oxalate should weight 88.9 (oxalate containing only one  $^{13}\text{C}$  atom) and 0.01% of natural oxalate should correspond to  $^{13}\text{C}_2\text{-Ox}$ . These amounts could be qualitatively seen during test mass scans. Nonetheless, the percentage they represent is so low that the error was not significant in the determinations.

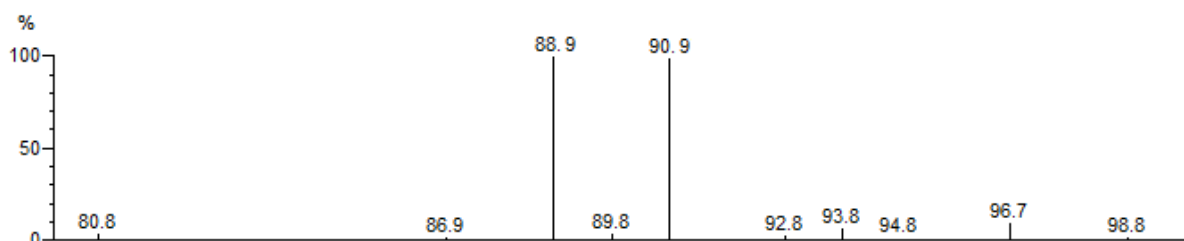


Figure 4.11 Mass scan ( $m/z$  80-100) of the interest region. y-axis represents relative intensity. The mass of  $[^{12}\text{C}_2\text{-Ox-H}]^+$  and  $[^{13}\text{C}_2\text{-Ox-H}]^+$  ions are clearly identified in this test sample that includes both isotopes.

#### 4.4.1.4. Relative Supersaturation calculations

The calculation of the RSS parameter was done with the EQUIL Software 56, as indicated in Section 1.1.7.1. This calculation included a list of urinary parameters that include all major components in urine: calcium, magnesium, potassium, sodium, ammonium, sulfate, phosphate, chloride, oxalate, citrate, uric acid and pH.

An aliquot of the samples was sent to the general laboratory in the facilities (Universitätsklinikum Zentrallabor). All the urinary parameters, but the  $^{13}\text{C}_2\text{-Ox}$  concentration, were determined there.

The list of analytes included in the RSS calculations does not include minor components in urine, which could have a relevant role in the crystallization process. However, the list of parameters indicated covers

all the major substances in urine and, more importantly, is the standard list of analytes that any clinical laboratory offers as urine analysis. Thus, the results obtained here could be easily extrapolated.

#### 4.4.2. Results and discussion

##### 4.4.2.1. Analysis methodology

The chromatographic separation of urinary anions was successfully achieved as described in Section 4.2.2.1. As stated,  $^{12}\text{C}_2\text{-Ox}$  and  $^{13}\text{C}_2\text{-Ox}$  were not separated in the chromatographic column, since they have the same chemical behavior. The quantification was done using MS.

The quality checks for the calibration curve and sample analysis were correctly achieved. Table 4.12 shows the results for the IC-MS determinations. These results offer robustness and perfect differentiation between both isotopes. The absence of cross-noise between both signals was checked (i.e. absence of signal at  $m/z$  88.9 when only  $^{13}\text{C}_2\text{-Ox}$  was in the solution).

Table 4.12 Calibration results for  $^{12}\text{C}_2\text{-Ox}$  and  $^{13}\text{C}_2\text{-Ox}$  determinations.

Parameter	$^{12}\text{C}_2\text{-Ox}$	$^{13}\text{C}_2\text{-Ox}$
Calibration range ( $\mu\text{M}$ )	0.5-10	0.075-1.5
Calibration curve	$y = 0.00045 \pm 1.00028 \cdot [\text{conc. ox}]$	$y = 0.0174 \pm 1.675 \cdot [\text{conc. ox}]$
$r^2$	0.9994	0.9998
LOD ( $\mu\text{M}$ )	0.039	0.033
LOQ ( $\mu\text{M}$ )	0.13	0.088

##### 4.4.2.2. Sample analysis

###### 4.4.2.2.1. Oxalate absorption

Patients were administrated the  $^{13}\text{C}_2\text{-Ox}$  containing capsule at day 2 (8.00 am). This was the starting time for the oxalate to run through the digestive tract and be absorbed (or not) during this itinerary. Since urine was collected from patients 6, 12 and 24 hours after this initial time, the oxalate absorption rate could be followed. Most of the oxalate was excreted within the first 6 hours.

In some cases, the amount of oxalate in the third urine sample was found below the LOD of the methodology (see Table 4.12). In most patients, the third value was clearly smaller than the two initial ones. Thus, the absorption of oxalate could be located during the first 12 hours.

The oxalate absorption results, based on  $^{13}\text{C}_2\text{-Ox}$  determination on the three fractions collected, report most of the results within the normal absorption range. The average absorption value is  $6 \pm 4 \%$ , and the range runs from 1.04 to 15.9 %.

These results fit with bibliography sources that report urinary oxalate levels similar for stone formers and healthy controls. Thus, normal oxalate absorption percentages should not have a dramatic effect in RSS values. This contrasts with calcium urine concentrations, since stone formers usually present hypercalciuria 252.

#### 4.4.2.2.2. Study of RSS and oxalate absorption

The complexity of urine and the multiple interactions between many of its components (major and minor) can be conveniently addressed using RSS. This Section introduces the RSS values for calcium oxalate in the analyzed samples.

Due to the large amount of data generated, specific results on concentration of the specific analytes and RSS parameters have been included as Supplemental Material (8.2. ), Table 8.4 and Table 8.5.

RSS parameters have been outlined in Table 4.13. The activity product (AP) is the same for COM and COD, since they share the same ions in their structures. RSS values are slightly higher for COM than COD, according to the smaller Ks for COM.

Most of the AP values lye in the  $10^{-8}$  region. Curiously, the two samples with a highest AP value ( $10^{-7}$ ) do not have particularly low urine volume (1.56 and 3.24 l), which could be thought to be the critical parameter that makes urine more concentrated. The two samples with a lower value ( $10^{-9}$ ) show normal or low urine volume: 1.89 and 0.71 l. According to the high/low AP values, the RSS for COM and COD are the highest and lowest within the data set.

Table 4.13 RSS results.

	AP CaOx	RSS COM	RSS COD
Mean	$6.54 \cdot 10^{-8}$	14.6	12.4
Range	$7.40 \cdot 10^{-8}$ - $1.05 \cdot 10^{-7}$	1.6 - 23.4	1.4 - 19.9
Standard deviation	$2.69 \cdot 10^{-8}$	6.00	5.11

The Ks values used by EQUIL software are: COM:  $2.24 \cdot 10^{-9}$  and COD:  $5.27 \cdot 10^{-9}$ .

In order to find relation between variables, especially with oxalate absorption, the correlation between all the variables was calculated. This date has been listed as Supplemental Material (8.2. ), Table 8.6.

A careful correlation analysis between the oxalate absorption and the AP and RSS values does not show a clear relation between them. Despite the oxalate load received by the patients, other sources might also affect the excretion and the total amount of oxalate found in urine. This hint indicates once more the relevance of the inhibitory capacity of urine. Even by a high oxalate intake a convenient amount of inhibitors is able to compensate the general lithogenic risk.

Table 4.14 General statistic parameters for all the variables measured in urine. Units: Volume (l), Density ( $\text{g}\cdot\text{cm}^3$ ), concentrations (mol/l).

	Volume	pH	Density	Na	K	Ca	Mg	$\text{NH}_4^+$
Mean	2.15	6.4	1.007	0.058	0.022	$2.6\cdot 10^{-03}$	$2.2\cdot 10^{-03}$	0.014
Maximum	3.24	7.1	1.010	0.099	0.068	$4.3\cdot 10^{-03}$	$5.0\cdot 10^{-03}$	0.025
Minimum	0.71	5.4	1.003	0.037	0.008	$3.0\cdot 10^{-04}$	$7.4\cdot 10^{-04}$	0.008
Range	2.53	1.7	0.007	0.062	0.060	$4.0\cdot 10^{-03}$	$4.2\cdot 10^{-03}$	0.017
Standard deviation	0.60	0.4	0.002	0.014	0.010	$9.5\cdot 10^{-04}$	$8.9\cdot 10^{-04}$	0.004
	$\text{Cl}^-$	$\text{PO}_4^{3-}$	$\text{SO}_4^{2-}$	Creat.	Uric Ac.	Oxalate	Citrate	
Mean	0.063	0.011	0.008	$6.8\cdot 10^{-03}$	$1.4\cdot 10^{-03}$	$1.7\cdot 10^{-04}$	$1.1\cdot 10^{-03}$	
Maximum	0.102	0.018	0.031	$1.8\cdot 10^{-02}$	$3.2\cdot 10^{-03}$	$8.0\cdot 10^{-04}$	$2.6\cdot 10^{-03}$	
Minimum	0.040	0.005	0.002	$2.4\cdot 10^{-03}$	$7.4\cdot 10^{-04}$	$9.5\cdot 10^{-05}$	$5.1\cdot 10^{-05}$	
Range	0.062	0.013	0.029	$1.5\cdot 10^{-02}$	$2.4\cdot 10^{-03}$	$7.1\cdot 10^{-04}$	$2.6\cdot 10^{-03}$	
Standard deviation	0.018	0.003	0.005	$2.9\cdot 10^{-03}$	$5.0\cdot 10^{-04}$	$1.3\cdot 10^{-04}$	$7.1\cdot 10^{-04}$	

The correlation analysis yielded an expected correlation (although only weak,  $r^2=0.42$ ) between calcium concentration and APCaOx, RSS COM and RSS COD. Due to the relevance of calcium in the crystallization process, its influence on the RSS was expected to be higher, together with oxalate concentration. The correlation of oxalate with RSS for COM and COD was very low. This, indeed, supports the literature that assigns more relevance to calcium than to oxalate in lithogenic risk 252.

Curiously, RSS values for the analyzed urines did moderately correlate with volume, but positively. This specific correlation was expected to be negative, since reduced urine volume has been clearly pointed out as decisive risk factor. This suggests that RSS should include a more extensive list of lithiasis inhibitors, in order to assess stone formation risk more precisely.

Citrate showed generally low correlation to other parameters. Interestingly, one of the highest values for citrate was seen for the correlation with magnesium. These two components are well known crystallization inhibitors (discussed in Section 1.1.6.2. ). Apparently, the inhibitory capacity of the analyzed urines presented similar trends for those two components. This situation did not have a remarkable influence in RSS values, since these were not significantly lower for patients who had high citrate/magnesium concentration values.

#### 4.4.3. Final remarks

The experiments presented in this Section have addressed the relevance of oxalate absorption in the digestive tract. As previously described, the results measured fit with the general range for this value.

The expected correlations between oxalate absorption and RSS values have not been clearly found. Despite the importance of oxalate as lithiasis promoter, its influence on the RSS as risk estimator is not

straight-forward. The numerous interactions between different urine components mask the direct influence of oxalate absorption on lithiasic risk.

Even for those patients who show higher oxalate absorption, the RSS parameter is not necessarily higher than for other groups. The importance of crystallization inhibitors is, once more, proven, based on RSS and variable correlation calculations.



**KNOWLEDGE  
TRANSFER: TURNING  
SCIENCE INTO  
EXPECTATIONS**





## 5.1. Knowledge Transfer as horizon

### 5.1.1. Basic concepts on Knowledge Transfer

It is a logical and well-known fact that scientists working at Universities and other research centers are devoted to the newest scientific knowledge. For a bunch of decades, researchers have poured their energies and resources in cutting-edge scientific advances. Not seldom, this gigantic effort has been conducted to basic science, with little interest by the University to go any further than publishing that research in a well rated scientific journal.

However, times are changing and so is the organization and playing rules of the society. Nowadays, the University is not considered as an isolated structure any more. On the contrary, it has been located at the very center of the regional development policies, since governments consider research centers as the main producers of basic and applied knowledge 277. While the USA was already aware of this metamorphosis, and offered impulse to their scientists to take their ideas to the market, the EU took a few more years to get on board. The arrival of the 21<sup>st</sup> century brought along also a repositioning of the public policies in regard to University budget and priorities for giving funding. The University does not turn its back to the private sector; they both work together, since it is the better way to enhance regional development, local economy and competitiveness 278.

Knowledge Transfer (KT) stands then as the transmission of the information generated in a research center to the industry or to a commercial agent. However, KT is not *simple* information; it also embraces a wide expertise, usually based on a long research career. It also involves the knowledge of procedures and related information that serve as a solid scaffold for any project. In other words, KT means the transfer of a whole *know-how* from the research center to a business unit or factory 279. The transfer of this know-how requires a close interaction between the researchers and the private sector agents.

To a certain extent, the collaboration between the two agents requires an adaptation period for the scientist. Usually researchers have little knowledge on how to commercialize an idea or which are the priorities in the private sector, and even the language to express the benefits or novelty of a scientific work can represent a challenge. In this sense, Universities have created the so-called “Scientific Parks”, aimed to lend a hand to their scientific community in these issues. A structure such as a Scientific Park usually includes a knowledge transfer office, which offers legal and specialized advice to laboratory researchers. These offices, which hang from the University structure, offer the scientist the possibility to find investors, continue their projects towards the market and even create university-based companies (spin-offs), in which the University gives actually venture capital 278,280. A structure such a Scientific Park also plays the role of offering business formation to the researchers working in the same institution, as a basic tool that encourages the entrepreneurship right from the laboratory.

In the Universitat Autònoma de Barcelona, the institution where this Doctoral Thesis has been mainly developed, the roles just described are overtaken by the *Parc de Recerca de la Universitat Autònoma de Barcelona* (PRUAB) or UAB Research Park 281.

The frame where the KT is naturally developed in is not simple. It has correctly been defined, taking DNA structure as a template, as a triple helix, formed by University, Government and Industry 282. University is not only an institution where teaching is magically combined with research; it is reconverting itself into an organization that on top of its former functions, signs contracts with private companies and provide the market with scientists trained at a high level. Industry is, of course, the player that focuses the production and commercial branches, whilst the government provides a stable environment for normal relationships to take place. In the society we are building step by step, with a solid focus in knowledge as the starting point to any advance, the University is raised to a closer position as industry and government used to have. This role is symbolically pictured in Figure 1.4Figure 5.1. KT stands, thus, as an interactive procedure and an exchange of experiences between the three parts of the system.

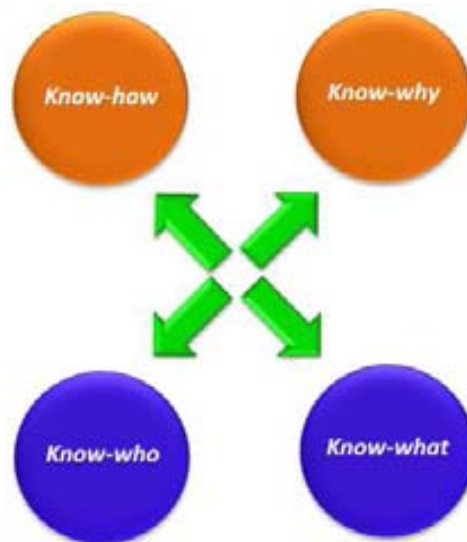


Figure 5.1 Picture intended to show a complex relation. University (orange) provides the *know-how*, and *know-why*, that is, the technical knowledge and procedures needed for the development and the basic, theoretical knowledge the expertise is based on. The private sector (blue) know *what* is needed in the market and, more importantly, *who* to contact for the commercialization of ideas. The government (green) provides a stable frame for these actions to take place and set the regulations to follow for the normal development of KT.

### 5.1.2. The University in the Knowledge Transfer context

Universities have generally started the promotion of such activities through the creation of Scientific Parks, so the question now is: what do researchers need to consider KT as the desired goal, to set it at the horizon of their research, instead of as a rare possibility to implement? As a matter of fact, the scientific community has already started working following these ideas; however, a definitive change in the general way of working is still expected 283.

Some studies have been focused precisely on the most valuable inputs for researchers to take part in knowledge transfer activities 283. Of course, the personal profile and professional formation condition in a major extent the engagement on KT. Transferring knowledge to the private sector requires support from the University to overcome technical and legal barriers; it has been seen that scientists who have a better backing from their institutions participate in KT activities much more actively. Also, recognition has been pointed out as an important, appreciated factor for researchers. This recognition is seen as economic reward (through royalties) and social recognition for the University.

Not all the institutions have the same success in stimulating KT enrolment. Their activity in the field can be measured, mainly, by two important and clear yardsticks: patents and spin-offs creation. These two points will be briefly described.

The implementation of the Bayh-Dole Act in the USA, back in 1980, whereby American Universities were allowed to actually own inventions developed in their facilities and also to own patents funded by federal grants, was strongly criticized already at that very moment 278. While that law represented a step forward in terms of encouraging researchers (through their institutions) generate *commercially exploitable* knowledge, some researchers saw those regulations as the government clipping the wings of those scientists devoted to basic, not applied science. For better or worse, the Bayh-Dole Act has made the USA one of the leading countries worldwide in regard to the knowledge transfer from Universities. That regulation served to create a KT culture among the University community. Other currents point out that this regulation did not encourage that much researchers; instead, their position in the university did 284. In the USA researchers are employees in the University, while in Europe they are usually civil servants, so the search of a solid funding is a major priority for the American scientific community in a major extent than for the European.

In regard to the creation of spin-offs, when KT is compared in the USA and the UK (as an example of European models), numbers are clear 278. American universities create an average of 2.8 spin-offs per year and institution, while the UK creates 1.3 companies. Besides, the mean number of patent licenses granted to US universities was 23.2 per year, while this number was reduced to 3.8 for British Universities. In essence, these values mean \$6.6 million revenues per US university per year (2.8% of the whole research budget), while for UK institutions they represented \$365,000 (1.1%). Those are data from 2004 and the landscape in Europe has changed dramatically, although USA is still a step forward in this sense.

Despite the consideration of spin-offs production for an institution as a marker for their KT activity, it should be considered that licensing patents can be somehow more economically profitable than the creation of a company 278. The patent field is also remarkably different in the US and EU.

Patents Offices still register a higher quote of University owned patents in the US than in the EU, although the underlying differences make the interpretation of this fact complex 285. The European model includes private firms in earlier stages of the patent development, so quite often they play the role of patent owner. At least, this has been done until recent years, when Universities have overtaken the ownership of patents. However, when it comes to patents in which the University is the *inventor* of

the patent, the quote between USA and the EU equilibrates. Therefore, the changes implemented in the recent years in Europe shall homogenize the patent field with the American case.

Despite the differences due to governmental, labor or cultural differences, the University stands noticeably as a fundamental pillar in the creation of knowledge. The so-called “capitalization of knowledge” implies, in fact, that public Universities have changed from dedicating funding to perform basic science into using this funding to produce not only self-sustainability for the research centers, but also to lift the economic level of their local regions. Through close links with the private sector, Universities have arose as a key point in local economies: they stimulate the professional hiring of highly trained scientists in private companies and encourage local, small companies to enroll in R&D projects.

### 5.1.3. Local and national environment (Spain)

The situation in the national context in which this thesis has been developed (Spain) follows the general characteristics described for the European countries. Therefore, this Section will be centered on the discussion of more specific details.

Spanish Universities bear an important part of the R&D developments registered in the country 286. Indeed, 26.7% of the total domestic R&D investments in Spain are attributed to these institutions. Conversely, 60.8% of the total professionals dedicated to R&D in Spain are researchers. This imbalanced numbers are the result of a complex situation on Spanish researchers: the entrepreneurship culture has been low for many decades and the incompatibilities of their duties at universities are usually an important hindrance for the development of KT activities.

New University policies are being set, so the KT in Spanish research centers becomes more efficient. Not only should the steps for a more effective KT be more accessible and clear for researchers (task that has already been done by KT Offices), but also scientists’ priorities should change, to pull KT at the top of those priorities list. As a matter of fact, Spanish scientists have become more concerned on the production of patents in recent years, as seen in Table 5.1. The data shown was gathered in a survey extended to public and private Spanish universities 287. Although extended to a short time, it can be seen how the interest of Spanish Universities in protecting the technology they developed, so it is possible to take it closer to its commercial exploitation, has generally increased during the last years. Not only the Universities are patenting more, but also they try to extend their patents to other countries, so a better coverage of the produced knowledge is achieved.

Table 5.1 Evolution of the patent activity in Spanish universities. Columns 2-4. Number of patents granted, according to the Office to which they were applied (Spanish, European or American). Column 5: Number of patents licensed. OEPM: Oficina Española de Patentes y Marcas, EPO: European Patent Office, USPTO: United States Patent and Trademark Office. Adapted from CRUE 287,288.

Year	OEPM (ES)	EPO (EU)	USPTO (US)	Patents licensed
2011	385	21	19	131
2009	295	23	11	112
2007	229	16	9	94

Naturally, the interest of the University is to protect knowledge via patents, KT requires *also* the intervention of the private sector in this game. So, Spanish researchers are actually taking into account very much this last point, since, as observed in Table 5.1, the slope of the licensing trend is remarkably positive.

The last point that will be analyzed in this brief introduction is the creation of spin-offs. According to a national study 287, Spanish universities are actively creating such type of research-related companies. As seen in Figure 5.2, the creation of spin-offs has clearly increased for the last years. Indeed, most of those companies are still in operation. However, only a very scarce number have achieved to execute a capital increase.

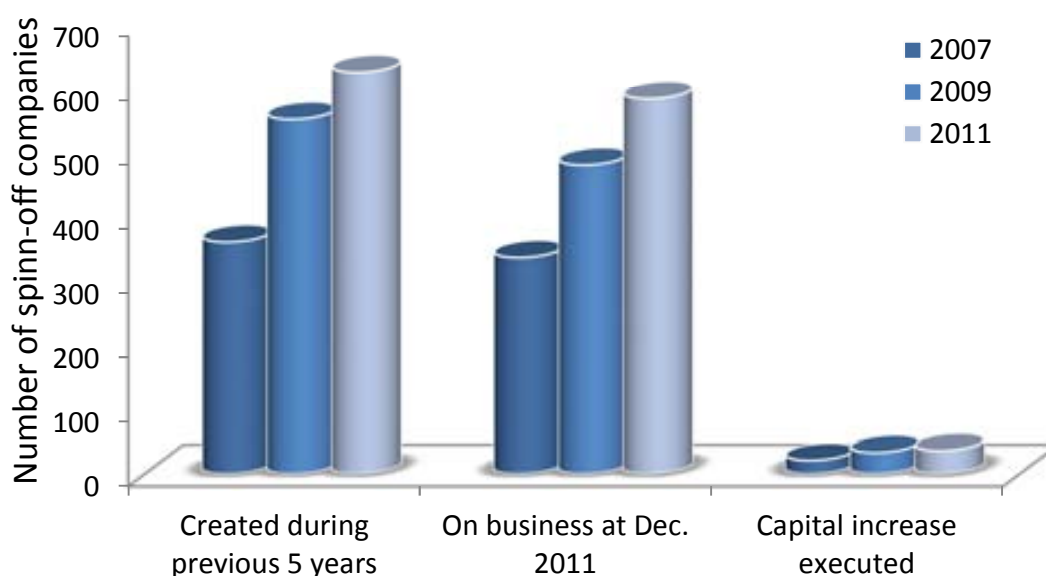


Figure 5.2 Plot of the number of spin-off companies created by Spanish universities. The plot accounts for the companies created during the previous 5 years to the date indicated, the number of those companies still in operation at the end of the indicated year and those which had executed a capital increase 287.

According to the information expressed in this Section, it can be seen that the three general markers of KT production: Protection of knowledge, Licensing of protected knowledge and Creation of spin-offs, show an increase in the Spanish research centers. This change in the way of doing science, or at least, the horizon at the back of the scientific work performed, is also reflected in PhD works.

This Section has introduced the relevance that KT has achieved in any scientific field. According to these principles, this Doctoral Thesis has been conducted keeping as a top priority the application of KT basis to the scientific developments established during its progress. Thus, some of the scientific work presented in the previous Sections has been protected, basically when it presented a clear patentability potential.

Due to the affiliation of the authors, the Patent Office at the University has allowed the correct management of the KT, starting by a patentability study and ending on the licensing of patents, if possible. Support of UAB Scientific Park, PRUAB, has also been continuous.

## 5.2. Patent: Method for the Characterization and Classification of Kidney Stones

This patent represents the first approach of KT from a scientific work performed in this thesis. It protects the methodology developed for the classification of urinary stones using NIR-Hyperspectral Imaging. The information on identification and priority date for this patent is shown in Table 5.2.

Table 5.2 Patent information. Method for the Characterization and Classification of Kidney Stones

Priority	PCT Application	Publication
Prior. Date: 06 Apr. 2011 No. P201130548 (ES)	Filing Date: 10 Apr. 2012 No. PCT/ES2012/070239	Pub. Date: 11 Oct. 2012 Pub. No. WO/2012/136874

The main goal of the developed methodology is to overcome some of the limitations of the most widespread techniques for the analysis of urinary stones.

As detailed in Section 1.3. , there are a number of described methodologies for the analysis of urinary stones, most of them based on spectroscopic measurements. However, their relevance in clinical laboratories is remarkably dissimilar, basically due to the availability of the required instruments, complexity of the techniques and related costs.

Clinical laboratories have centered their attention on the use of IR Spectroscopy, IRS, as the reference technique for the analysis of urinary stones. Its main advantages are the low cost of the analysis, their simplicity and the usefulness of the obtained results. However, there is an important drawback: the technique requires a trained analyst for the interpretation of the recorded spectra, and any spatial resolution is lost during the sample pre-treatment, since it includes grinding.

In this context, the protected methodology seems of high interest for its potential application as a new technique to use in clinical laboratories. Its advantages, from a scientific point of view, include the acquisition of a large number of spectra, so the classification power is increased up to the pixel resolution. Commercially available equipment is able to perform, within 5-10 seconds, several hundreds of spectra that can be used for the classification of the sample. In other words, the benefits of counting with that amount of information for each pixel independently from the neighbors are already a reality, using commercial instruments.

Once the usefulness of the technology has been made clear, it is also noteworthy to highlight that the use of such technique would require the purchase of more affordable equipment, so some adaptations to the methodology and instruments should be made. Nevertheless, the basic points and procedures needed have already been defined.

The robustness of the developed methodology has been proved in this Doctoral Thesis. In a first work, urinary stones were analyzed taking ROIs on the surface of the samples, so they were classified into groups 135. The stone analysis was performed by means of Artificial Neural Networks, so sorting the stone classes becomes independent of the analyst. This work yielded results comparable to those obtained by stereoscopic microscopy. Stone samples were classified according to the distribution in the stone of major and minor components, so the etiological factors were also related to the stone composition. This classification has been widely described in bibliography, and corresponds to stereoscopic microscopy 44 74. Precise details on the procedures and results of the study have been discussed in Section 1.3.3.

Despite the usefulness of this classification, a second study was conducted; in order to test the goodness of the developed methodology when compared with the most widely used technique, IRS. The challenge, in this case, was to achieve the same classification of the stones including quantification of components. From a commercial point of view, this step confirms the utility of the technique by confronting it to the conventional IRS, which readily offers a composition of the urinary stone as percentage of each component. As described in Section 2.3. , the newly developed methodology offers quantification results comparable to IRS, with the additional information corresponding to the spatial location of the components. Furthermore, the independence of the measurement and analysis of each pixel achieved by the HSI technique leads to the identification and location of minor components. This feature is especially interesting for the precise description of the stone history and the assignment of the best treatment for each patient.

The advantages discussed in this point represent the potential of this methodology for its implementation as routine methodology, once some technical issues are correctly adapted to the commercialization of a specific device. This potential has attracted the interest of private companies. Indeed, the associated patent has been licensed by a private company that focuses its business on offering home-care solutions for urinary stone patients.

The document of registration of this patent can be consulted as Supplemental Materials (**Error! Reference source not found.**).

### 5.3. myStone

“myStone” is a medical device specifically developed for the analysis and classification of urinary stones. It is the result of collaboration between two research groups: Computer Vision Centre (CVC) and Centre GTS. The former had developed a wide experience on image analysis and classification techniques based on image recognition. The latter had a solid knowledge on urinary lithiasis, including stone analysis and lithogenesis.

myStone is an optical device, able to recognize and classify urinary stones by image recognition. A classifier was trained for the recognition of different stone types and implemented in the hardware for an automatic analysis. This device was designed to overcome some of the handicaps detected in traditional stone analysis techniques. The main characteristics of those are listed in Table 1.12. In brief, the most popular approaches are IR Spectroscopy (IRS) and Microscopic Analysis (MA). IRS allows the quantification of components but offers no information on the location of each phase. MA allows the precise description of the components and their position to describe lithogenesis, yet it is time consuming and expensive. myStone should be considered an alternative to these possibilities, ready to its use in urological practice and clinical laboratories. It does not require especially trained users and can be installed on a desk, due to its small size.

### 5.3.1. Experimental Section

#### 5.3.1.1. Samples

The device was test with a set of 346 urinary stone samples, chosen from a library of more than 1500 items, collected from the Urology Service at the Hospital Universitari de Bellvitge, Barcelona (Spain). The samples included stones from all naturally occurring species. The selection criterion was to include as much variability within each class as possible, in order to create a robust and reliable database. The samples were either naturally expelled or collected through ESWL. They were rinsed with ethanol and water and conveniently dried until analysis. Each sample was collected from a single patient and episode, to assure they were independent. When a stone was collected as a whole unit it was cut using a surgical knife to expose the core.

The formation of a suitable database, that includes a wide variability within each stone class, is of major importance for the robustness of the classification. This is one of the basic pillars of the efficiency of the device.

The set of samples used for the training of the software included all naturally occurring components in urinary calculi. The stone types listed here were defined according to their chemical composition, so they are comparable to the main analysis techniques. The list of types of stones includes: calcium oxalate monohydrate (COM), calcium oxalate dihydrate (COD), calcium oxalate dihydrate transformed into monohydrate (TRA), brushite (BRU), carbonate apatite (CAP), struvite (STR), uric acid anhydrous (AUA), uric acid dihydrate (AUD), cystine (CYS), mixed stones of calcium oxalate and carbonate apatite (MXD) and mixed stones of calcium oxalate and uric acid (CO-UA).



### 5.3.1.2. Device set-up

The device was produced from low-cost, off-the-shelf components, which define a simple and robust piece of equipment. Since it has been especially developed for the analysis of urinary stones, the dimensions, components and their organization have been adapted to yield a high performance for this precise function. The basic components are camera, lenses, controller board and illumination board. Figure 5.3 shows a schematic view of the pieces distribution in the equipment. Samples are classified by taking pictures of them and using image recognition software.

The images of the samples, used for the description of the features of the stone necessary for the classification (texture, shape and color), are taken using a conventional camera, equipped with a Si sensor. The illumination energies used are found in the Vis-NIR range (400-1000 nm) within the sensitivity range of this sensor. In addition, an IR sensor located in this board provided a signal of the reflected light to the computer and complemented the information from the visible range. The operational parameters of the different illumination types were controlled by software. The lighting board was especially designed to allow the lenses observe the urinary stone, and LEDs were properly placed in the designed places so as to avoid shadows on the sample.

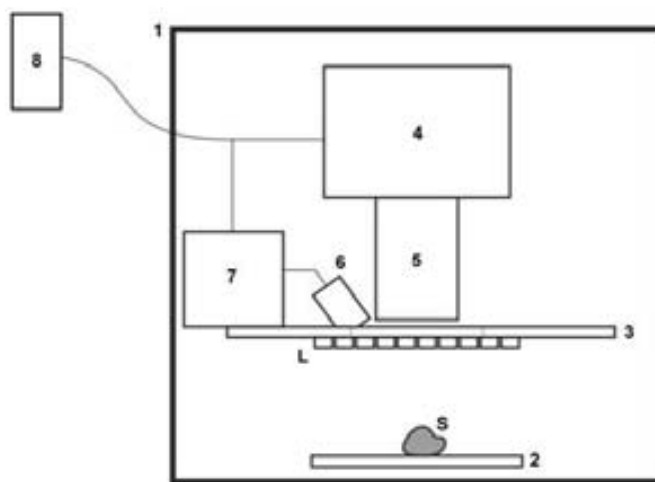


Figure 5.3 Scheme of the analysis device. The components are listed as follows: 1) Holding scaffold, 2) Sample tray, 3) Illumination board, 4) Camera, 5) Lenses, 6) IR sensor, 7) Controller board, 8) External computer, L) Illumination LEDs and S) Sample.

A mobile sample tray with a homogeneous background was designed. The sample was placed in the field of view of the camera and was optically distinguished from the background (segmentation). The correct focus of the image was achieved with a specific adjuster of the lenses. The sample was located beneath the camera and the illumination LEDs. All the components were embedded in a cover, specifically designed for this use. The camera and controller board connections to the computer were done through the cover. Figure 5.4 shows some detailed views on the device.

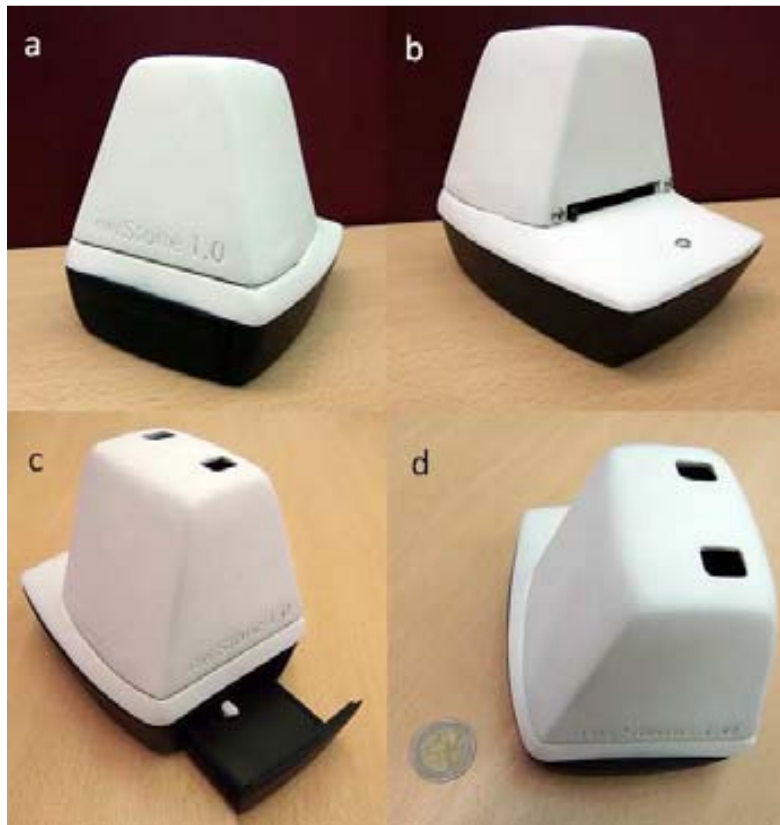


Figure 5.4 Views on the device. a, b. Front and rear views (the focus ring can be appreciated in Figure b). c. Stone sample located in the sample tray, ready for analysis. d. Top view. The coin serves as a measure of the device size. The two holes on the top are used for plugging the camera and controller board connections to computer.

### 5.3.1.3. Classification procedure

For the correct description of the process, some terms will be defined. Figure 5.5 describes each of the terms used here.

**Sample:** Urinary stone or group of fragments collected from a single patient in a single episode.

**Fragment:** Part of a urinary stone obtained from a patient (after ESWL) or after cutting a naturally expelled stone, to expose the inner part.

**View:** Point of view when observing the fragment with the camera: surface or cut, that is, outer or inner part of a fragment or sample.

**Image:** Picture recorded for each view, each one under particular illumination and exposure time conditions.

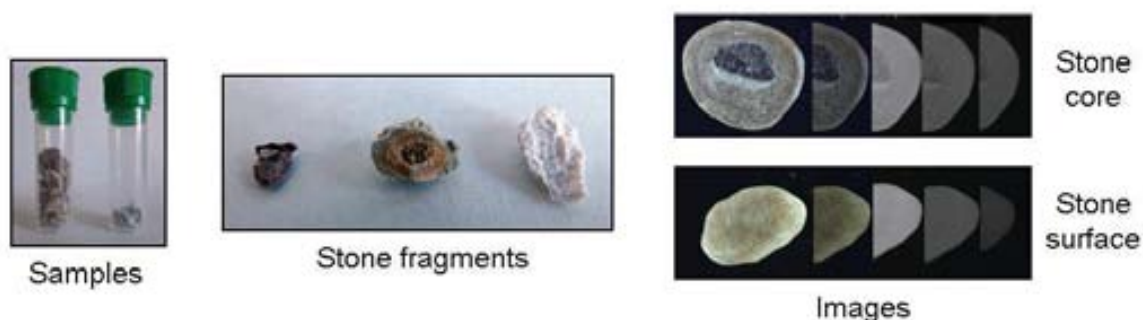


Figure 5.5 Examples of the terminology used in this work.

The classification results are based on the morphological description and chemical composition of the samples described in bibliography 44 74. Urinary calculi classes have been re-built to adapt them to the specific performance of the device and according to the specific treatment measures taken to avoid further stone episodes.

The image acquisition procedure requires the selection of a stone fragment and location in the sample tray. The device records 6 images by varying the illumination type and exposure time. Three illumination types (Visible and two IR sensors: 880 and 1000 nm) and 2 exposure times for each (0.5 and 1 seconds) were chosen. The different images are automatically captured by the device. The process can be repeated for inner/outer sides of the sample and also include different fragments of the same sample. The classification is done using image recognition tools, using parameters as color, texture, shape and size. Infrared LEDs allow supporting the classification with punctual chemical information measured at this energy range.

Once the images have been acquired, the software runs the analysis automatically, following a self-developed hierarchical classifier. The classification of samples was divided into three sequential and partial outputs. The versatility of the algorithm allowed the consideration of any of those classification results as final.

Urine pH values were given to the software as complementary information, so the classification vector created also included this characteristic number. The classifier was trained using some limit pH values, as seen in Table 5.3, which are based in bibliography. Beyond those limits, the probability for a class to be assigned decreased rapidly, so the values chosen were not extreme for each class, in order not to exclude samples precipitating close to the limit value.

First level (view classification): Using the set of 6 images from a single view a class probability was decided for that view. A vector of probabilities for each view was computed. This vector was based on the visual features of size, shape, color and texture of the image, combining the information from all the images. The classification output was an estimation of the probability (belief) that a fragment view (external or internal) belonged to each of the given classes. Although the measurement of chemical characteristics was not used by the device for the classification (with exception of the two IR sensors), the output classes were comparable to those obtained by chemical analysis (COD, COM, STR...).

Table 5.3 Limit pH values used for the classification. The ranges listed are the most probable for each type of urinary stone to occur (based on the sources listed in Section 1.2. ).

Type of stone	pH	Type of stone	pH
COM	>6	BRU	<6
COD	>6	CYS	<5.5
MXD	>6	UAA	<5.5
CAP	>6.5	UAD	<5.5
STR	>6.5	UA-CO	<6

The output of the first classification level was one of the following classes: BRU, CAP, COD, COM, CYS, MXD, STR, TRA, UAA or UAD. At this level, the results for each view (internal/external) were independent.

**Second level (fragment classification):** The classification of fragments was done once both views (inner and outer parts) had been assigned a class. The combination of the two individual view classifications in the first level produces a single fragment class. Therefore, the classification for each fragment was not only limited to the chemical components present in the stone, but also included their location and distribution. e.g. The class assigned to a fragment was different if compound A was inside the stone and B on the surface, or if the situation was the opposite. This second level of classification allowed the location of components in the stone, which leads to a better description of the lithogenesis.

The possible combinations of outer and inner views results are listed in Table 5.4. The diagonal shows the results for pure stones, while other cells indicate combinations sensitive to the location of components. The definition of the combined stone types was done attending to differences in the treatment the patient should receive after the stone episode. Hence, some combinations of diverging internal/external components have been merged as a single “treatment” group. It is interesting to remark that the classifier was trained with these constraints. They were not fixed rules; the software learnt the relation between inner-outer views and class.

Table 5.4 includes some stone types more complex than pure components. COMD defines a COM stone with only COD deposits on the surface, while COMCA represent CAP deposits. CCT includes calcium oxalate stones formed of COM, COD and/or TRA in variable amounts. CO-UA refers to mixed calcium oxalate and uric acid stones. CODCA describes a COD stone with CAP depositions. TRACA group is composed of TRA stones with CAP only in the outer part of the structure, so they cannot be considered MXD. CA-CO explains a stone type with similarities to MXD but with a much lower amount of calcium oxalate.

As any other data analysis or analytical technique, the possibility of the classifier making mistakes exists. In this case, it could erroneously assign a class to a fragment. Interestingly, not all the errors share the same importance, in terms of the treatment selected. The assignment of a class has a related “cost” or potential risk that a false classification would represent. The device has been trained to take this particularity into consideration, so the classifier would only assign certain classes if the degree of

certainty was high. Stone classes with a high cost value were only assigned with high probability when the classification error was low. These costs were defined for each class being confused with a different stone type and organized as a costs matrix (Table 5.5).

Table 5.4 Second level classification. The dependence of a fragment class on the classification obtained from inner and outer views follows the correspondence shown in this Table. The diagonal in this Table (in bold), indicates homogeneous stones. Cells filled with (-) denote unlikely combinations.

		Inner part/core									
		COM	COD	TRA	MXD	CAP	STR	BRU	UAA	UAD	CYS
Outer part/surface	COM	<b>COM</b>	TRA	TRA	MXD	CA-CO	STR	-	CO-UA	CO-UA	-
	COD	COMD	<b>COD</b>	TRA	MXD	CA-CO	STR	-	-	-	-
	TRA	CCT	TRA	<b>TRA</b>	MXD	CA-CO	STR	-	-	-	-
	MXD	COMCA	CODCA	TRACA	<b>MXD</b>	CA-CO	STR	-	-	-	-
	CAP	COMCA	CODCA	TRACA	MXD	<b>CAP</b>	STR	BRU	-	-	-
	STR	-	-	-	-	STR	<b>STR</b>	-	-	-	-
	BRU	-	-	-	-	BRU	STR	<b>BRU</b>	-	-	-
	UAA	CO-UA	-	-	-	-	-	-	<b>UAA</b>	UAD	-
	UAD	CO-UA	-	-	-	-	-	-	UAA	<b>UAD</b>	-
	CYS	-	-	-	-	-	-	-	-	-	<b>CYS</b>

The costs matrix also allows the simplification of the classification system, by merging stone classes with a low cost of confusion. That is, if two stone classes require similar treatments, the related cost value will be low, so they can be unified as a single, bigger stone type. This would lead to a lower specificity of the stone structure, but also would improve classification results.

Third level (sample classification): As described, more than one stone fragment for each sample was often analyzed, either by collecting pieces resulting from ESWL or by cutting stones. Diverging classes could be assigned to different fragments, even considering the same stone view (internal or external). These unequal results could be attributed either to inherent error in the device performance or to the heterogeneous nature of some samples, that made various fragments present different appearance and composition. This variability was taken into account using a third level of classification, based on the results obtained in the second level.

The possible combinations and the resulting class are shown in Table 5.6. Due to the Table size, only an example for the combination of classes is shown. As in the second classification level combinations, the criterion for the selection of a class was also based on the most suitable treatment after the stone episode.

Table 5.5 Costs matrix. To each class, a “cost” value is given, describing the cost of confusing it with any of the other classes. The criterion for assigning the value has been based on how suitable would be a treatment for preventing the further stone episodes for each pair of confused stone classes. Cost values have been graded in a 0-10 scale, being 10 the maximum cost (problematic confusion) and 0 the minimum (same treatment). The diagonal of the matrix (in bold) is 0, because it compares to identical classes.

		Recognized class																
		COM	COM-CA	COM-D	CCT	COD	COD-CA	TRA	TRA-CA	MXD	CAP	CA-CO	STR	BRU	UAA	UAD	CO-UA	CYS
Real Class	COM	<b>0</b>	2	2	2	5	5	2	3	6	8	8	9	8	7	7	5	10
	COMCA	2	<b>0</b>	2	1	5	5	5	5	6	8	8	9	8	7	7	6	10
	COMD	2	2	<b>0</b>	1	4	4	3	4	6	8	8	9	8	7	7	6	10
	CCT	3	2	2	<b>0</b>	4	4	3	3	5	8	7	9	8	7	7	6	10
	COD	2	3	3	4	<b>0</b>	1	0	3	6	8	8	9	8	8	8	7	10
	CODCA	2	3	3	3	2	<b>0</b>	2	0	3	7	4	9	8	8	8	7	10
	TRA	2	3	1	2	0	2	<b>0</b>	0	2	8	6	9	8	8	8	7	10
	TRACA	2	3	2	1	2	0	1	<b>0</b>	2	6	4	9	8	8	8	7	10
	MXD	6	6	6	6	6	4	6	4	<b>0</b>	3	1	7	8	9	9	7	10
	CAP	8	6	7	6	7	5	7	5	2	<b>0</b>	1	5	3	9	9	8	10
	CA-CO	8	6	7	6	5	3	5	3	1	1	<b>0</b>	5	3	9	9	8	10
	STR	10	10	10	10	10	10	10	10	7	5	5	<b>0</b>	7	10	10	10	10
	BRU	8	7	8	7	8	7	8	7	4	2	2	5	<b>0</b>	9	9	9	10
	UAA	5	6	5	5	5	6	5	6	8	9	9	10	9	<b>0</b>	0	2	10
	UAD	5	6	5	5	5	6	5	6	8	9	9	10	9	0	<b>0</b>	2	10
	CO-UA	2	3	2	3	5	6	5	6	8	9	9	10	8	2	2	<b>0</b>	10
	CYS	10	10	10	10	10	10	10	10	10	10	10	10	10	10	10	10	<b>0</b>

Table 5.6 Resulting classes for the third level of classification. In case that the stone types assigned to two different fragments in a single sample do not agree, each combination of individual fragments is re-assigned a single class. Cells marked with (-) denote unlikely combinations.

Fragment 1	Fragment 2	Resultant class	Fragment 1	Fragment 2	Resultant class	Fragment 1	Fragment 2	Resultant class
COM	COMD	COMD	COMD	CCT	CCT	CCT	CO-UA	CO-UA
COM	CCT	CCT	COMD	COMCA	TRACA	CCT	TRA	TRA
COM	COMCA	COMCA	COMD	CO-UA	CO-UA	CCT	TRACA	TRACA
COM	CO-UA	CO-UA	COMD	TRA	TRA	CCT	MXD	MXD
COM	TRA	TRA	COMD	TRACA	TRACA	CCT	CA-CO	CA-CO
COM	COD	TRA	COMD	MXD	MXD	CCT	CAP	CA-CO
COM	CODCA	CODCA	COMD	CA-CO	CA-CO	CCT	STR	STR
COM	TRA	TRA	COMD	CAP	CA-CO	CCT	BRU	-
COM	TRACA	TRACA	COMD	STR	STR	CCT	UAA	CO-UA
COM	MXD	MXD	COMD	BRU	-	CCT	UAD	CO-UA
COM	CA-CO	CA-CO	COMD	UAA	CO-UA	CCT	CYS	-
COM	CAP	CA-CO	COMD	UAD	CO-UA	CODCA	TRA	TRACA
COM	STR	STR	COMD	CYS	-	CODCA	TRACA	TRACA
COM	BRU	-	TRA	TRACA	TRACA	CODCA	MXD	MXD
COM	UAA	CO-UA	TRA	MXD	MXD	CODCA	CA-CO	MXD
COM	UAD	CO-UA	TRA	CAP	CA-CO	CODCA	CAP	CA-CO
COM	CYS	-	TRA	CA-CO	CA-CO	CODCA	STR	STR
COD	TRA	TRA	TRA	STR	STR	CODCA	BRU	BRU
COD	CODCA	CODCA	TRA	BRU	-	CODCA	UAA	CO-UA
COD	MXD	MXD	TRA	UAA	CO-UA	CODCA	UAD	CO-UA
COD	CA-CO	CA-CO	TRA	UAD	CO-UA	CODCA	CO-UA	CO-UA
COD	CAP	MXD	TRA	CO-UA	CO-UA	CODCA	CYS	-
COD	STR	STR	TRA	CYS	-	CA-CO	CAP	CA-CO
COD	BRU	-	MXD	CA-CO	MXD	CA-CO	STR	STR
COD	UAA	CO-UA	MXD	CAP	CA-CO	CA-CO	BRU	BRU
COD	UAD	CO-UA	MXD	STR	STR	CA-CO	UAA	-
COD	CO-UA	CO-UA	MXD	BRU	BRU	CA-CO	UAD	-
COD	CYS	-	MXD	UAA	-	CA-CO	CO-UA	-
TRACA	MXD	MXD	MXD	UAD	-	CA-CO	CYS	-
TRACA	CA-CO	CA-CO	MXD	CO-UA	-	UAA	UAD	UAD
TRACA	CAP	CA-CO	MXD	CYS	-	UAA	CO-UA	CO-UA
TRACA	STR	STR	STR	BRU	STR	UAA	CYS	-
TRACA	BRU	-	STR	UAA	-	UAD	CO-UA	CO-UA
TRACA	UAA	CO-UA	STR	UAD	-	UAD	CYS	-
TRACA	UAD	CO-UA	STR	CO-UA	-	CO-UA	CYS	-
TRACA	CO-UA	CO-UA	STR	CYS	-			
TRACA	CYS	-	BRU	UAA	-			
CAP	STR	STR	BRU	UAD	-			
CAP	BRU	BRU	BRU	CO-UA	-			
CAP	UAA	-	BRU	CYS	-			
CAP	UAD	-						
CAP	CO-UA	-						
CAP	CYS	-						

The device was configured with all three levels of classification, but it was able to operate giving results at any level. Due to this modular classification structure, the device can be adapted to each user.

### 5.3.2. Results and discussion

#### 5.3.2.1. Classification results

The device was tested with the described stone groups, taking as reference the classification of the samples using conventional stereoscopic microscopy. The results shown here correspond to 346 stones, from which 606 fragments were selected. According to the described procedure, 1212 different views (surface and core) were captured using different illumination conditions, leading to 7272 images. Some of the different stone types were recognizable using Visible radiation, as seen in Figure 5.6.

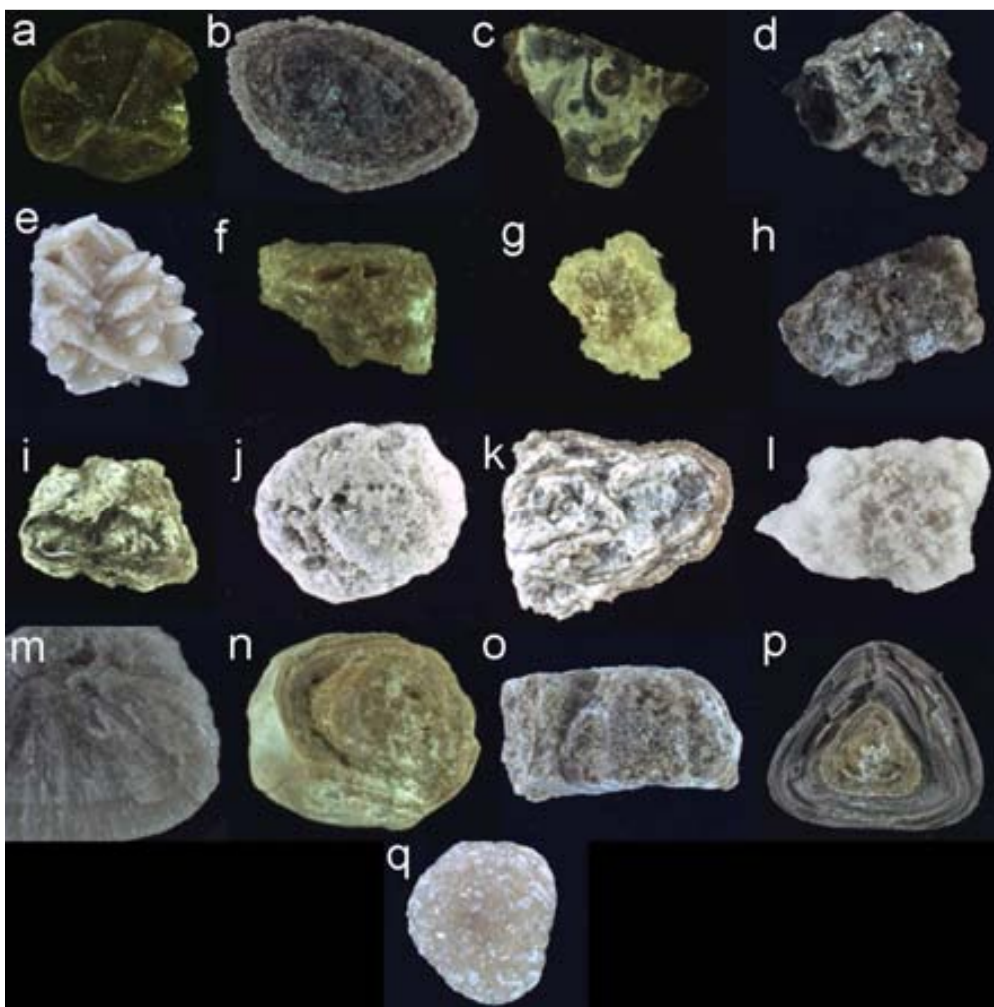


Figure 5.6 Visible images captured for different types of urinary stones. Either surface or cut sections of stones are shown for the best description of each type characteristics. a. COM, b. COMD, c. COMCA, d. CCT, e. COD, f. TRA, g. CODCA, h. TRACA, i. MXD, j. CAP, k. CA-CO, l. STR, m. BRU, n. UAA, o. UAD, p. CO-UA, q. CYS.



The classification results indicate different behavior of the device depending on the stone type. Some classes have similar appearance, so the rate of confusion was higher in those cases. The analysis is based on visual features, so similar samples would pose some problems for the differentiation of classes.

The performance of the device yields an overall correct classification rate of 74.1%. This value can be carefully analyzed using the data in Table 5.7, which shows results for each stone group. Some stone groups, which often had few samples for the model training, gave a low correct classification rate. The results are discussed in detail for those stone types. More details on stone structure and related treatment are available in Sections 1.2. and 1.4.2. The correct results only include the most probable class. If the second class, in terms of probability, was also considered as correct, the accuracy would reach 92.3%. This would make sense for those cases in which the second most probable class had a low associated cost (according to Table 5.5). The discussed values consider only the strictest case (the most probable class).

The class COMD, which is formed of COM with COD deposits on the surface, is not well classified. However, if the results assigned are observed, TRA arises as the most probable class, followed by COM itself. The cost of confusing COMD with TRA is low because the treatment for both stones does not differ dramatically, so this error would not lead to a very differing metaphylaxis. TRACA behaves in a similar way, since it is basically confused with MXD. In essence, both stone types include calcium oxalate and CAP within their structure in variable amounts, so the treatment for preventing further stone episodes is, again, very similar. In this case, the main difference between both stone types refers to structural features, not to etiological factors.

The device misclassifies CAP as STR. Although the etiological factors are different (STR is only produced in case of urinary tract infection), they are both phosphates and have a similar visual appearance and porous structure, as seen in Figure 5.6. Since they precipitate at high urine pH (usually >6.5), their treatment is not radically different, so their confusion does not have a severe effect on the possible metaphylaxis. However, it would be interesting to correctly distinguish both classes and properly assess the possible infection in the urinary tract.

Among the results for each class, the classification of CYS stones becomes the main drawback of the device. Probably due to the low number of stones analyzed (their incidence represents 1% of the total amount of cases) the classifier did not correctly learn to identify this stone type (see Table 5.7). This limitation would cause an erroneous diagnostic for CYS patients, who show specific etiological factors for the formation of stones (genetic disorders).

BRU is also affected by a low number of test samples. This class is often confused with uric acid stones, which have remarkably different etiological factors. The classifier does not yield satisfactory results for this stone type.

Interestingly, UAA and UAD are often confused with each other, as seen in Table 5.7. Nonetheless, this is a minor issue, since uric acid stones require the basification of urine regardless their crystal structure. Both groups can be merged into a single type (uric acid stones). This increases the percentage of correct classification above 95%.

Table 5.7 Classification results obtained in the device training. Known classes are plotted against the recognized class and results are given as % of correct classification for each stone type. The numbers correspond to a total of 606 stone fragments; the amount for each type is also indicated. Percentage values are weighted, considering the number of samples in each stone group.

		Recognized Class														No. of fragments	Rate correct answer (%)
		COM	COMD	COD	TRA	TRACA	MXD	CAP	CA-CO	STR	BRU	UAA	UAD	CO-UA	CYS		
Real Class	COM	<b>84</b>	0	1	6	0	3	0	0	0	0	0	0	3	0	97	<b>87</b>
	COMD	3	<b>0</b>	0	7	0	1	0	0	0	0	0	0	0	0	11	<b>0</b>
	COD	0	0	<b>10</b>	1	0	0	0	0	0	0	0	0	0	0	11	<b>91</b>
	TRA	10	0	1	<b>56</b>	0	11	0	0	0	0	0	0	1	1	80	<b>70</b>
	TRACA	0	0	0	0	<b>0</b>	7	0	0	0	0	0	0	0	0	7	<b>0</b>
	MXD	5	0	0	15	1	<b>99</b>	0	0	1	0	0	0	0	0	121	<b>82</b>
	CAP	0	0	0	0	0	0	<b>0</b>	1	20	0	0	0	0	0	21	<b>0</b>
	CA-CO	0	0	0	0	0	1	0	<b>15</b>	4	0	0	0	0	0	20	<b>75</b>
	STR	0	1	0	0	2	1	0	5	<b>58</b>	0	0	0	0	0	67	<b>87</b>
	BRU	0	0	0	0	0	0	0	0	0	<b>0</b>	7	2	0	3	12	<b>0</b>
	UAA	0	0	0	0	0	0	0	0	0	3	<b>44</b>	24	1	1	73	<b>60</b>
	UAD	0	0	0	0	0	0	0	0	0	1	20	<b>40</b>	0	0	61	<b>66</b>
	CO-UA	3	0	0	5	0	0	0	0	0	0	2	2	<b>7</b>	1	20	<b>35</b>
	CYS	0	0	0	0	0	0	0	0	0	4	0	0	0	<b>0</b>	4	<b>0</b>

### 5.3.2.2. Report

The report was automatically generated by the device and included relevant pictures of the sample in the visible energy range, so the device was also used as a microscope (See Figure 5.6).

The resulting class was indicated as a compilation of the probability for each relevant stone type. That is, the classifier was trained to assign a class to the sample as described in Section 5.3.1.3. , but also calculated the likelihood that a sample belonged to a given class. The probability values were calculated for stone views, so the second and third levels of classification were assigned later.

This output was displayed as pictured in Figure 5.7, so the distribution of probabilities was clearly seen.

In addition to the classification, and based on the third level of classification (sample class), some recommendations were attached to the report. This important output was specific to each stone type, so it was fully adapted to each particular patient. The recommendations were based on bibliography, and included some guidelines on diet and lifestyle for the patient along with some parameters to monitor the evolution of the stone episode, to guide the physician through the follow-up.

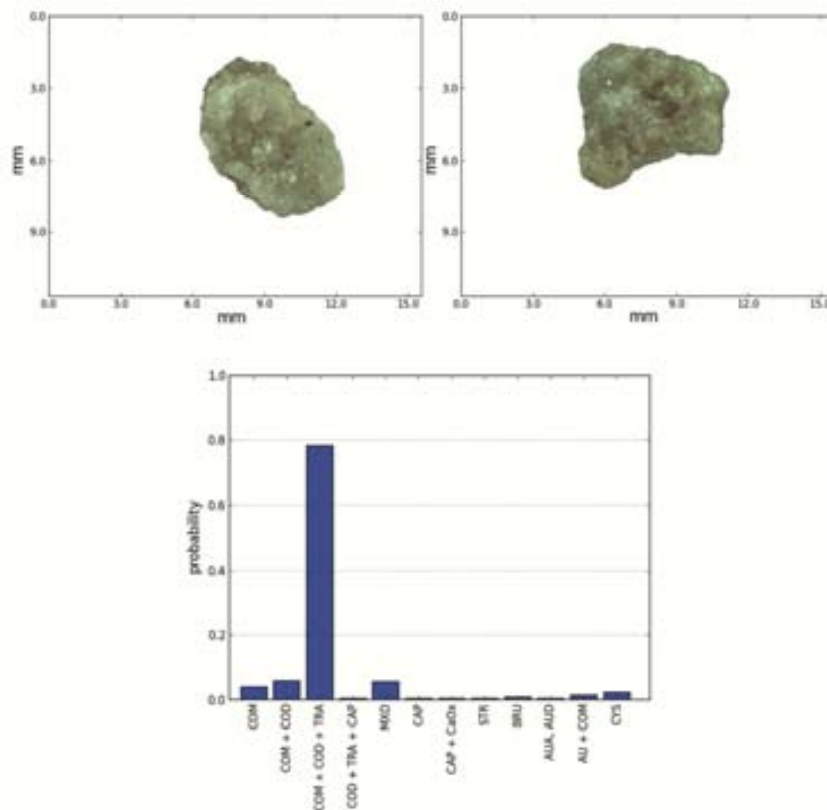


Figure 5.7 Results display, including pictures of the sample and the corresponding distribution of probabilities for classes.

### 5.3.3. Final remarks

This work represents a clear advance in the analysis of urinary calculi. The device presented here has been designed according to physicians' needs and the classification algorithm has been based on the comparison with two of the most relevant stone classification techniques: Infrared Spectroscopy and Stereoscopic Microscopy. This medical device offers similar results to the mentioned methodologies, while offering the possibility of an on-site analysis that is performed in few minutes. The analytical results include the composition of stones and the location of components within the structure, so the lithogenesis process can be described in detail for each patient. This advantage has a great impact on the treatment suggestions, since they are adapted to every specific case. On top of its analytical advantages, this desktop medical device is easy to use and requires no trained technician to perform the analysis.

The device is able to perform the stone analysis and also assign specific recommendations for each stone type, based on the composition and distribution of components in each stone. This leads to a personalized analysis that allows the precise description of the lithogenesis process. The correct metaphylaxis of the stone requires a precise description of the causes of formation, in order to control specific parameters. Only such treatment can help decrease the high recurrence rate associated to this disease.

When compared to the most spread stone analysis techniques, this device yields comparable information to stereoscopic microscopy. The analysis is done in shorter time as many of the techniques and the cost is low, for the analysis and the equipment. These differences can be clearly appreciated if the main features of myStone are compared to the rest of stone analysis methodologies (see Table 5.8).

Table 5.8 Comparison of the main characteristics of myStone with the principal stone analysis methodologies.

Feature	Chemical Analysis	IR Spectroscopy	Microscopic Analysis	X-Ray Diffraction	myStone
Component identification	✓	✓	✓	✓	✓
Chemical form identification	✗	✓	✓	✓	✓
Component quantification	✗	✓	Semiquant.	✓	Semiquant.
Location of components in the stone	✗	✗	✓	✗	✓
Classification according to formation causes	✗	✓	✓✓	✓	✓
Description of the history of the stone (description of the disorder)	✗	✗	✓	✗	✓
Trained technician needed	✗	✓	✓	✓	✗
Cost	€	€	€€€	€€	€
Analysis time	⌚	⌚⌚	⌚⌚⌚	⌚⌚	⌚

✓✓ Stands for an enhanced description of the disease, available only with this technique.

<sup>i</sup>Chemical analysis refers here to commercially available kits that do not require full knowledge in lithiasis.

<sup>ii</sup>IR Spectroscopy considers the analysis (by pellets or ATR) and spectral interpretation, not including data analysis software.

The listed features suggest this device as a robust and interesting commercial alternative to the traditional stone analysis methodologies, since its use could be easily implemented in physicians' offices and clinical laboratories.

#### 5.3.4. Patent

Due to the commercial interest of this research, this invention was protected under a patent application. The patent application was done a few months before the composition of this Dissertation. Thus, it had only been registered at the Spanish Patent Office (OEPM), with priority date 18<sup>th</sup> June 2014 and reference number P201430927. The registration document can be consulted as Supplemental Materials (**Error! Reference source not found.**).

Because of the high interest of this invention for commercialization purposes, public funding was received for the specific development of this device. In addition, the scientific and technical work was complemented by a market research. These issues are addressed in the next Sections.

## 5.4. Valorization Project: VALTEC

As described in the previous Section, the device myStone does show an interesting potential towards its commercialization. It exhibits remarkable advantages compared to the commercially available solutions that make this device a robust platform for the development of a product. This product should continue the path to enter the market. Naturally, this is a complex process, and a considerable investment needs to be done in economic and organizational terms.

In this sense, both research groups participating in the creation of myStone (CVC and GTS) applied to a VALTEC project to the Catalan government. VALTEC is the abbreviation from "Valorització Tecnològica" the Catalan for "Technological Valorization". These projects have the main goal of promoting the commercialization of ideas born in research laboratories. In other words, the Government helps economically those researchers who have developed any technology or product that needs some impulse to get closer to the market. Since myStone had been developed with the interest of producing a consumer-focused device, it stood within the scope of VALTEC program. The starting idea could be further developed until the final device was achieved, as seen in Figure 5.8.

The VALTEC project considered thus the development of an already started research. The whole picture of the environment and value chain of myStone is represented in Figure 5.9.

The basic research had previously been developed by both collaborating research groups. The wide experience on image analysis and image recognition tools (CVC) and the solid knowledge of GTS on urinary lithiasis and urinary stone analysis were a robust platform for supporting the idea of this new

medical device. Although particularly far from the market, basic research is needed for complementing any product with the know-how required for the development. It also supports the improvement of the device during its way into the market. During their basic research, GTS could establish a network of urologists and urinary stones experts, who helped on the development of the device.

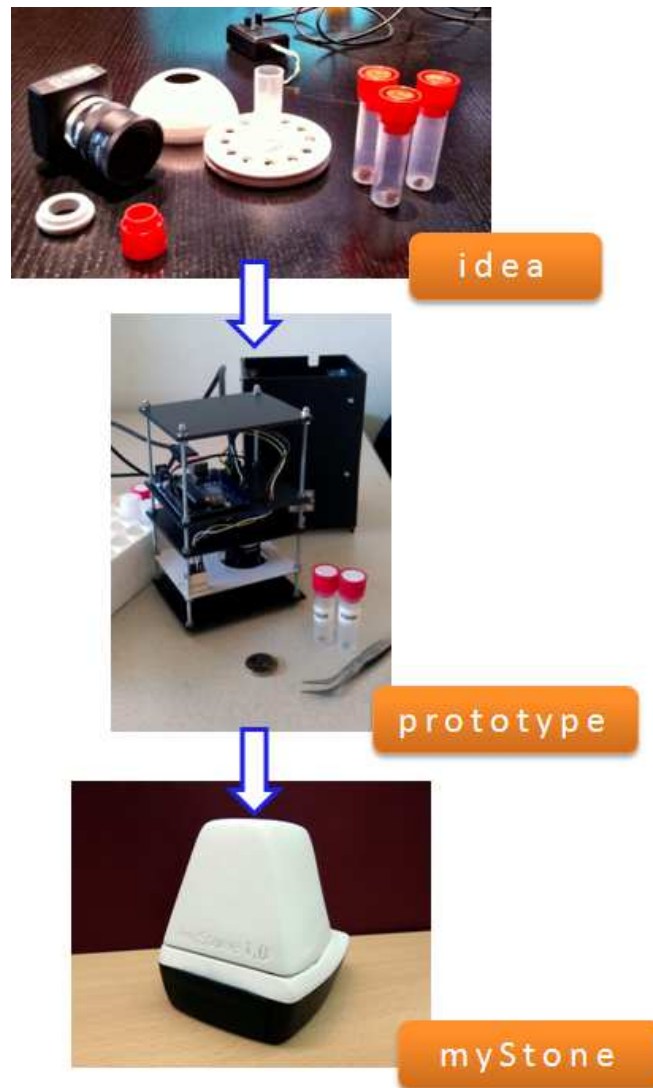


Figure 5.8 VALTEC project helped on the evolution of an initial idea, based on the experience of two complementary research groups into a functional prototype. This first prototype could be improved to optimize costs and enhance classification results.

Once the basic concerns in regard to objectives and organization were defined, the applied research phase started. A prototype was created and tested, as described in Section 5.3. This first device was already functional and served as the proof of concept that the project was feasible. The classification criteria were defined in this phase and also the organization of the classifier. Urologists were included in this phase of the development, so the output of the device was useful for the final users. It was during this phase when the VALTEC project was awarded.

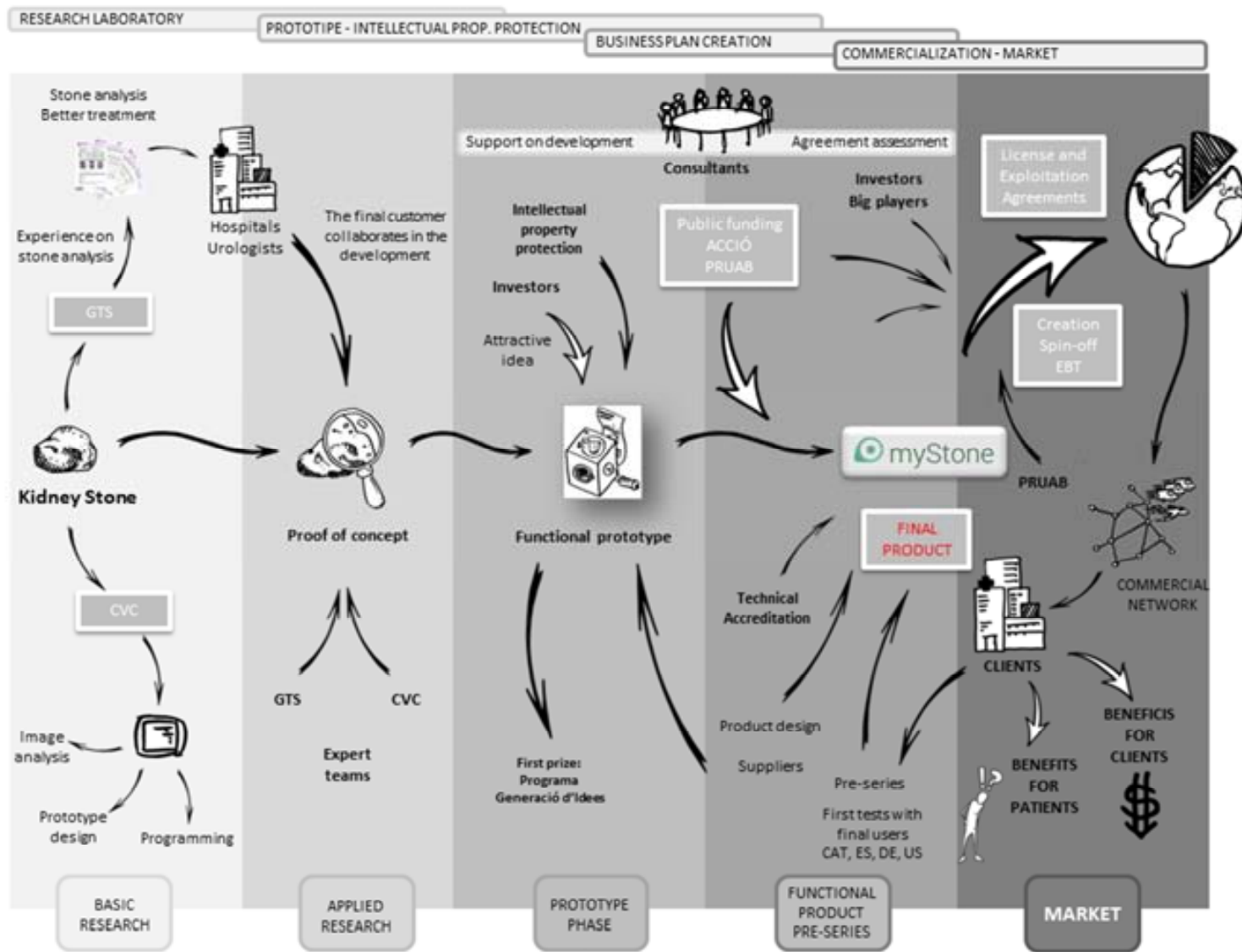


Figure 5.9 Value Chain for myStone project. The main players, their connections and the phases in the project where they play a role are depicted.

After this step, the patent for the protection of the device was applied, so the idea could be freely communicated and the process to take myStone closer to market could continue. This “Prototype” phase requires the production of a reduced number of identical “pre-series” devices, so they can be tested on-site by urologists, who are the final users and also the best judges of the good behavior of myStone. Also during this phase the presentation of the device in public, technological and medical forums was done. The identification of the best commercial and development partners is needed for the proper accomplishment of further steps in the “Laboratory to Market” process.

When this step is finalized, the technical accreditation of the device, along with the formalization of some commercialization/licensing/distribution agreements should be executed. In this final phase, the market will be reached, so the final customers will be able to test the device and operate with it. When this phase is started, building a solid network is a basic point for the proper commercialization of the device.

These tasks will be done by myStone team (GTS and CVC) for a period of two years, as described in the project application (2014-15). The research groups participating are very grateful to ACCIÓ (Generalitat de Catalunya) for the economic support and assessment given.

### 5.5. Business Plan

As stated in previous Section, the commercialization of this medical device required the careful assessment of the market characteristics and potential interest in the invention. Accordingly, some actions were taken, that allowed to value such items and the generation of a clearer way to get the invention closer to the market.

This part of the research was done by GTS and CVC in part, as a result of the participation of the team in the “Ideas Generation Program”, held by Parc de Recerca UAB. The outcome of that contribution was an initial Business Plan (BP) and the award with the first price among 20 participants. This primitive BP was further developed in collaboration with EADA Business School in Barcelona. A group of students<sup>3</sup> performed an extensive market research following myStone inventors’ indications. This Section will summarize the basic concepts addressed in that work, which will be used for the definition of a business idea based on the device 289.

---

<sup>3</sup> The group of students was formed by: Ida Grad, Martin Raygoza, Lucas Roos, Nikolaos Sarafidis and Larissa Schade. They were supervised by Alexis Mavrommatis.



### 5.5.1. Analysis of the idea

This step was done according to the 5 C's market analysis 290. This approach analyzes the business opportunity by defining five basic points in any BP: Company, Context, Channel, Consumer and Competitor.

#### 5.5.1.1. Company

Since there is not a registered company yet, it should be addressed whether there is interest (potential financial benefits) on funding it. This Section will address some issues on the creation of a hypothetical company.

The development team is formed by three researchers from GTS and two participants from CVC. They possess the expertise in urolithiasis and image recognition needed for the development of myStone. The device is fully operative and protected by patent, as described in Section 5.3. The importance of this point is remarkable, since a possible start-up company would already have an operative device and funding (through VALTEC Project, see Section 5.4. for testing it and implementing upgrades.

The company has a clear mission, namely the commercialization of highly technological devices for the improvement of the stone patients' quality of life through better and faster diagnostics, comprehensive information and practical advice.

This company offers a medical device based on a camera and related software that pictures, recognizes and classifies urinary stones. The ease of use of the device allows any employee in a clinic to use it; it requires only cutting the stone and pressing a button. The analysis time has been reduced to few minutes, so sending the samples to an external laboratory is not needed any longer. The stone analysis is complemented with recommendations on diet and lifestyle for the patient, as well as recommendations for the physician.

These clear advantages respect to other competitors allow the company to enter the market by offering a premium product, located at the top of the value chain. The added value offered, together with the production low cost, would allow this company to center their strategy on selling a high performance product, yet at a competitive price level.

Thus, the advantages of the company are focused on the product differentiation, lower costs and permanent innovation on the device, due to the R&D experience of the development team.

#### 5.5.1.2. Context

The analysis of the context in which the company would enter is of high importance for correctly define the market opportunity and focus the business strategy.

The importance of the disease, the medical and social concerns and its consequences for public healthcare institutions has been made clear in Section 1.5.

The last years have seen the economic landscape change all over the world and the Spanish market has not been an exception. The economic restrictions experienced in this country have also brought some important changes in the health market. This sector is regulated to a large extent and big healthcare companies control the general market. Population is aging, so the needs are changing, and emerging markets pose new, low-cost business approaches. In this context, the interest on medical devices is very high.

The attractiveness of the healthcare market, related to microeconomic aspects, can be analyzed using Porter's 5 Forces, a framework that defines an industry based on five external forces: buyers, suppliers, new entrants, rivalry and threat of substitutes 291. For a precise analysis, the information is related to the Spanish market, which will be the starting geographical area for the activity of the company. The source on which the statements in this Section are based is the "Health Care Equipment & Supplies in Spain - 2013" report 292.

1. **Buyers:** The Spanish market is formed by a limited number of buyers, who have an important bargain power on the producer. Buyers are used to purchase electronic devices, so they have a clear insight on the performance and competitors in this sector. In addition, buyer's requirements are high. This will increase competition and will make buyers look for quality, economy and a clear product differentiation. The supplier can charge a higher price if quality and high performance are offered. The buyers' power is moderate-high.
2. **Suppliers:** Generally, it is not desired to choose a single supplier. In this sector, the differentiation of raw products is low, so the power of suppliers can be given by contracts that cause switching costs to be high. The suppliers' power is moderate.
3. **New entrants:** The medical device sector is dominated by a few big players. Any newcomer needs to adapt to a market that regulates each aspect (from quality restrictions to technical requirements). As a new participant, the company will have to pass a bidding process (for public hospitals) and gain the urologists' approval with no brand identity yet. The new entrant's power is moderate.
4. **Rivalry:** As stated, the health sector is controlled by big companies that operate worldwide and base their business on economies of scale. They can negotiate prices with clinics. The key to get market share is to offer a high performance product, so the company will become a highly specialized firm in the urolithiasis field based on R&D. The rivalry risk is rather moderate.
5. **Threat of substitutes:** The absence of substitutes in the Spanish market suggests no risk from this side. This situation might change during the evolution of the business.

Besides the Porter's 5 forces, the macroeconomic approach can be done through a PESTLE analysis 293. This includes external, environmental factors that greatly influence the position of the company in the market, as: political, economic, social, technological, legal and environmental issues.

**Political Drivers:** The Spanish government has accomplished some regulations that should turn the economy into a more competitive and dynamic scenario. This fact could help this company as a start-up

company, since hospitals will have more freedom to access technological solutions that could sink their operations costs in a close future. Indeed, according to the health policies, the government relies on prevention as a key factor for the new organization of the health system 294.

**Economic Factors:** Due to the hard economic crisis affecting Spain since a few years ago, the degree of investment has dramatically decreased in all public organizations. This fact represents an important market entry barrier for myStone, since its benefits (not only medical but also economical) will have to be demonstrated before it reaches an adequate market share. In essence, myStone is an investment for any hospital.

**Socio-Cultural Drivers:** The public Social Health system in Spain is highly valued and protected through laws in this country. As a basic point for the inhabitants, hospitals are committed to offering the best health care possible to their patients. In this sense, the advantages of myStone against other methodologies, described in Section 5.3. , represent a plus for its implementation in hospitals.

**Technological Drivers:** Spain is traditionally weak when adopting technological innovations. Again, this point is against the implementation of myStone, which should demonstrate that the medical advantages it poses are linked to economic benefits or costs cuts for the hospital.

**Legal drivers:** Despite the existence of big companies in the health sector, the Spanish law encourages competitiveness and trustful advertisement, so the firm can profit from this regulations as an allied to enter the market.

**Environmental Drivers:** This point is not especially relevant for this company. The production does not include potentially harmful products and its use poses no environmental risks.

In regard to the market size, Spain has around 790 clinics and hospitals. The number of active urologists is 2033 (data from 2003) 295. This market size poses an interesting starting point for the company, which could enter this sector by own sales force.

The European healthcare market represents total sales of 72.6 € Billion and includes 11.000 companies. Spain has a market size of 8.3 € Billion, and together with Germany, France, UK and Italy, covers 75% of the European market 292. These numbers should be taken into account when selecting any further markets for the new firm to operate in.

#### 5.5.1.3. Channel

The health sector in Spain, as well as in other countries, is a complex network, with many actors and highly regulated.

Selling a medical device in Spain often requires the partnership of a distributor who is already in direct contact with the final customer. In addition, any good with a price above 18.000 € has to be purchased through a public tender 292. This is especially important, taking into account that each hospital or clinic is economically independent and take their own decisions on purchasing new devices.

Doctors, who are the final users of the medical device, are a key factor in the purchasing process. Distributors visit them often in order to build a long-term relationship. This point is basic when trying to commercialize the equipment, so Key Opinion Leaders will play an important role when selling the device.

### 5.5.1.4. Competitors

A basic point in the market analysis includes the competitors' identification. It is needed to clearly differentiate myStone from other competitors that already own a given market share.

In Spain, the typical companies operating in this sector are big enterprises that offer their products in different areas, so they reduce their dependence on a single one. The specialization is the best option for the new company. In the precise field of urinary stone analysis, many laboratories offer IR Spectroscopy, although only 3 centers in the whole country offer Microscopic Analysis and its enhanced description of the sample (see Section 1.3.3. ). Therefore, according to the information described in Section 5.3. , the advantages of myStone against potential direct competitors are clear.

Other companies, specialized in the treatment of urolithiasis, could also be considered indirect competitors. They operate in the same market sector and might have overlapping objectives. However, such companies could also be considered as partners for reaching foreign markets.

### 5.5.1.5. Customers

The customers' behavior should be carefully considered for the definition of a strategy. There is a general theory that divides the purchasing process into 5 consecutive stages 296.

1. Need recognition: The first step is the most important in the entire process. If the customer does not have a real need and the company does not fulfil it satisfactorily, no business can be done. In our case, hospitals are continuously treating urinary stones and the recurrence rate is high. Further stone episodes can be avoided, provided the stones are correctly analyzed. This is the point where myStone can offer a solution.
2. Information search: Once the need has been identified, the customer will try to gather information from known sources and searching for new inputs. The firm should educate the customers about the multiple benefits of purchasing this medical device and working with it.
3. Alternative evaluation: This step considers the assessment of the information obtained previously. All the possibilities will be studied. In this case, only three laboratories in Spain can offer such results, so the company should take into account the strengths and weaknesses of the competitors.
4. Purchase decision: The final decision will be made on the selected criteria, including from whom to buy, where to buy and when to buy. The efficiency of the firm in the previous step will have a remarkable influence in this one.

5. Post-purchase decision: The previous stages have created expectations on the customer. In this sense, the continuous improvement of the device is a key factor for the survival of myStone (e.g. better accuracy, easier use, new applications, etc.).

#### 5.5.1.6. Interviews to experts

In addition to the research performed to assess the market possibilities of myStone, some experts were interviewed, in order to get information from users, distributors and other people who might show interest on participating in the device commercialization. These have a strong influence on the purchasing decisions, so their feedback is especially useful for the implementation of changes in the device configuration.

The interviews conducted with urologists had the goal of defining three specific issues, namely:

- a. Is there a need for a stone analysis device that offers the possibility of on-site analysis?
- b. Which are the main requirements for the urologist to consider the purchase of the device?
- c. Does myStone, with its described advantages, fulfil those necessities?

The interviews were done to Spanish and other European doctors (from Germany and The Netherlands); a total of 15 specialists were included. The interviewed doctors answered to this question by assigning a value (1 to 5) to each specific feature. Figure 5.10 shows the results of the interviews.

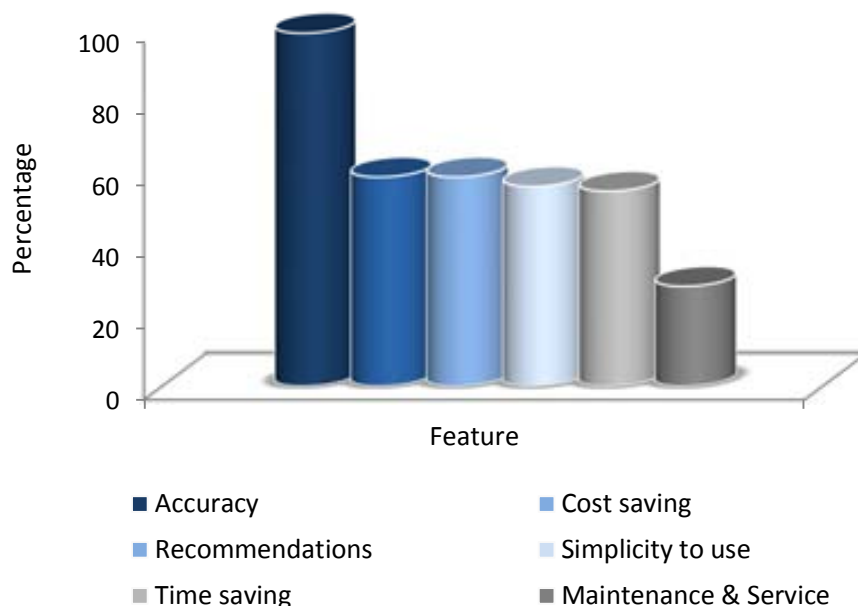


Figure 5.10 Results of the interviews on the importance for purchasing decision of each feature in myStone. Values express the percentage of doctors that assigned 5 (the maximum importance) to each item.

The feedback to question *a* revealed a clear possibility to implement the use of this device in clinics. While the availability of this on-site equipment is not a basic requirement for physicians, the generation of quick results (within a few minutes) was well received.

Question *b*, focused on the main requirements doctors would ask for a stone analysis, showed that the accuracy in the classification was an important point. The recommendations on diet and suggestions on metaphylaxis were also identified as a crucial feature. Maintenance and service was not seen as a basic aspect for the purchase decision.

The answers to the third question gathered, which was directed to the utility of myStone in the medical practice, showed the importance of the improvement of the device accuracy for its commercialization. As described in Section 5.3.2.1. , the accuracy of the device is 74.1%, but it should reach 90%, which is the value generally described as acceptable. The VALTEC funding, as described in Section 5.4. , will provide resources to enhance the performance of the device.

It could also be concluded that the strongest value proposition of this device are the recommendations on diet and treatment. Indeed, this is one of the main advantages myStone offers to the urologist and is highly valued by those: automatic analysis of the stone and personalized recommendations with no intervention of any specialist.

#### 5.5.1.7. SWOT Analysis

Once the analysis of the market and the environment of the hypothetical company has been made, a SWOT Analysis (Strengths – Weaknesses – Opportunities – Threats) can help summarize some of the company characteristics (Table 5.9).

Table 5.9 SWOT Analysis of the company.

Strengths	Weaknesses
<ul style="list-style-type: none"> <li>- Innovative device</li> <li>- Highly adaptable to customer/market</li> <li>- Funding for improvement available (VALTEC)</li> <li>- Company directly linked to university laboratories</li> <li>- R&amp;D based team</li> <li>- Device adaptable for new applications</li> <li>- Invention protected by patent</li> <li>- High added value</li> </ul>	<ul style="list-style-type: none"> <li>- Lack of brand awareness</li> <li>- Low market experience of the team</li> <li>- No solid customer network</li> <li>- Device does not quantify components (as IRS does)</li> <li>- Lack of technical approval</li> </ul>
Opportunities	Threats
<ul style="list-style-type: none"> <li>- Health systems evolving towards prevention</li> <li>- Administration: Self-management of each center</li> <li>- New values for health in society</li> <li>- Social impact of higher quality of life</li> </ul>	<ul style="list-style-type: none"> <li>- Adaptation to technology changes</li> <li>- “Big players” with an existing commercial network</li> <li>- Decline in public health budget (Spain)</li> <li>→ Lower market share</li> <li>- Developing countries can offer lower prices</li> </ul>

### 5.5.2. Business Strategy

Based on the market research and the opportunities seen through the information described in this Section, a business strategy will be presented. The information described here is referred to the creation of a start-up company, which should operate initially on the device developed. The actions to carry out take into account the mission of the company, namely offering high technological devices for the best treatment of the stone disease and becoming a reference in the urolithiasis sector.

An initial analysis of the potential stakeholders for the company was done and is represented in Figure 5.11. This Figure also identifies primary and secondary stakeholders. The former are potentially willing to economically take part in the company and keep a close relation. The latter are mostly external; they do not engage in economic transactions of the company, but can be affected by its actions.



Figure 5.11 Stakeholder analysis. Blue dots represent primary stakeholders, while grey dots identify secondary ones.

When the funding is achieved, the company should start the main actions, that is, the development of the device and its sell through the selected channel. The key actions, priorities and relations in the company are summarized following the idea of the Canvas Business Model 297. It provides a basic template for the key operations in the company. This information is represented in Figure 5.12.

This Figure does not introduce new concepts into the business idea, but organizes the information for a better description of the operations, goals and key actors in the company.

It is interesting to stress the importance of international distribution partners for the commercialization of the device. It has been previously stated that the company would start its operations in Spain. Nonetheless, a company must be born international, so the expansion of the ideas and business can be complete. Due to the particularities of the health market in each country, the agreement with different local partners for each of the markets myStone should enter to.

In regard to the revenues stream, there are different options for offering the myStone device. Naturally, directly selling the device would be the basic option, so special emphasis should be made on the savings myStone can provide to the buyer. In addition, leasing a piece of equipment could be an interesting alternative. This would provide the company with a continuous revenues stream and would offer the customer the possibility to keep the device after the leasing or exchange it for a new one.

### **5.6. Final remarks**

Due to the scientific scope of this Dissertation, the analysis on the economics and financial part of a possible company has not been included in this document. The commercial potential of the research done has been made clear, so the contribution of this work to knowledge transfer is evident.

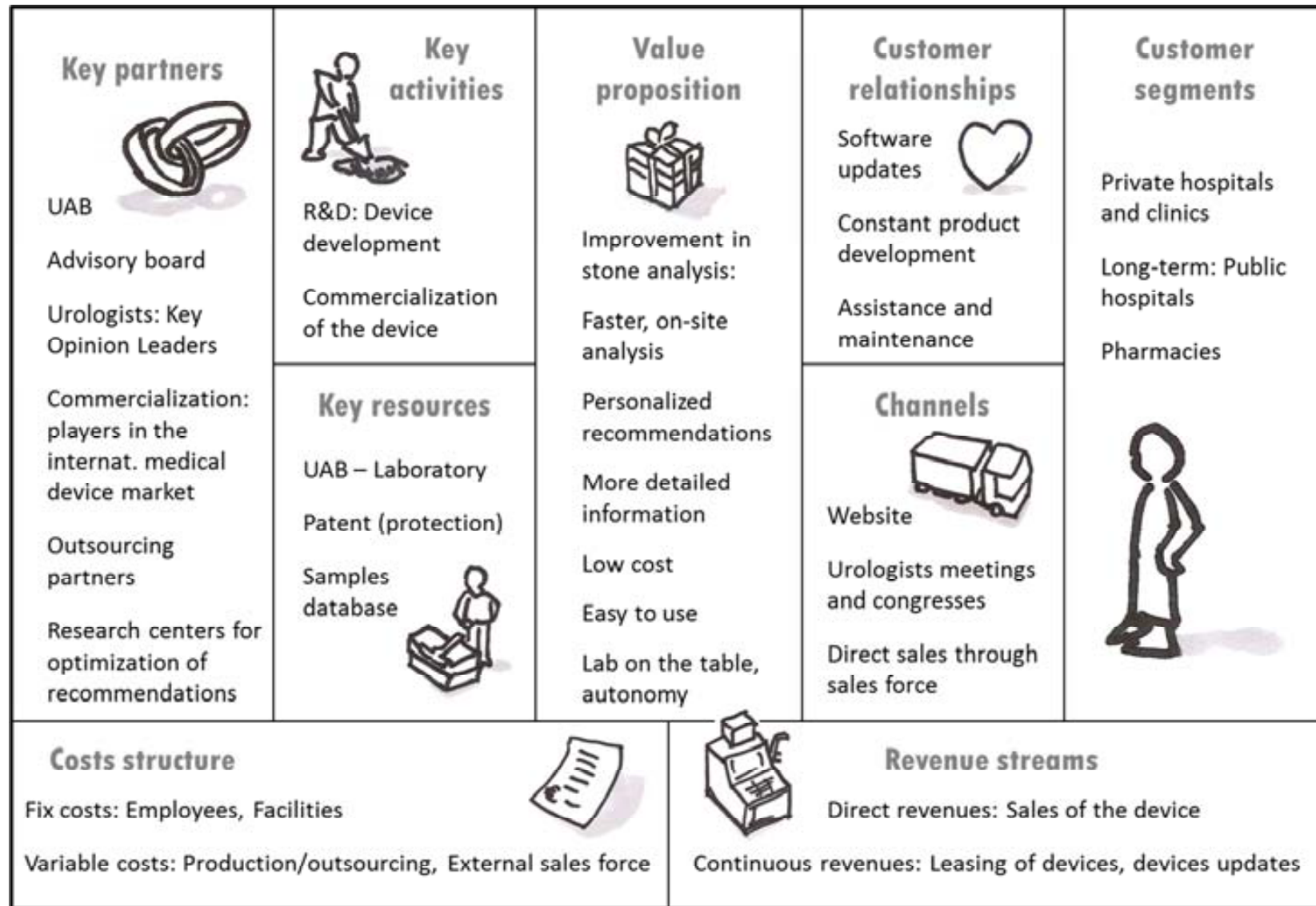
This final Section represents the culmination of the applied research developed during this Thesis. The knowledge in urinary lithiasis field acquired along the read has been expressed in some alternatives that show real commercial interest.

Patent management has a close link with research, and it is getting closer year after year. The publication of the results produced during this Thesis has always waited for the respective intellectual protection to be assured. The work developed here, especially myStone project, is the result of an intense collaboration work, not only with other researchers, but also with business experts and University and Government representatives.


In brief, this Section has shown the contribution of this Thesis to the modern side of University research, the side that places researchers in the core of knowledge and economic advances.



Figure 5.12 Adaptation of Canvas Business Model to the suggested company 297.







**CONCLUSIONS:  
CONDENSING THE  
CONCEPTS**



## 6.1. Conclusions

The exposed work is embedded in the urinary lithiasis field, and includes the use of several techniques, that offer a multiple approach to the challenges posed by this disease. Mainly image analysis and separation techniques have been used for the study of urinary stones, urine, or products that might affect their composition.

This work presents some results that widen the existent knowledge in urinary lithiasis and suggest some alternative solutions for its best management. The basic effort has been conducted to the prevention of urinary stones. Only by fully understanding the causes of formation and the precise evolution of the disease, a proper prevention can be achieved. This Dissertation provides additional tools to physicians, according to the main achievements.

This Section will gather detailed conclusions, which apply to the work presented along the manuscript. Attending to the structure of this Dissertation, this Section will list the conclusions following a similar structure.

### 6.1.1. Image analysis

The performance of the devices improves constantly, so the analytical challenges they can give an answer to, increase in number and complexity. Section 2. has focused those advantages on the analysis of urinary stones, using the large amount of information kept in calculi, witnesses of the disease evolution in each patient.

- i. The classification of urinary stones in groups (comparing to MA) has been possible using NIR-HSI. The system has been described in detail thanks to the use of PCA. The optimization of the classification conditions has allowed the achievement of satisfactory results.
- ii. The implementation of a new classification model, based on pixel-to-pixel analysis, has yielded very good results, comparable to those obtained by the reference technique (IR Spectroscopy). Indeed NIR-HSI possesses a considerable advantage against IRS, since it is able to precisely locate the components of the stone in the structure.
- iii. Only CAP and STR stone types escape from this comparison, since they are not completely resolved. Their physical structure and NIR spectrum are similar and do not have enough unique characteristics to differentiate them.
- iv. Despite its little drawbacks, NIR-HSI stands as a suitable alternative for routine laboratories for this type of analyses. It overcomes some limitations of the common techniques: it does not require trained analysts; it is faster than IRS or MA, is more cost effective than MA and has spatial resolution, which IRS lacks.

- v. High resolution IR microspectroscopy has proven to be a useful technique for the analysis of stone structure. It reveals structural information hidden to other alternatives, so describes in a further dimension the lithogenesis.
- vi. IR microspectroscopy should not be considered as an alternative for routine analysis to IRS or MA, due to the long time required for the analysis. Instead, it can provide very precise information, which should build the bases for a wider knowledge in stone formation.

### 6.1.2. Nanoparticles in urine

Section 3 has been focused on the analysis of NPs in urine. Although some studies had already addressed the relevance of particle size in the initial processes of urinary stone formation, most of the bibliography had attacked this characterization using microscopy. This approach requires a long time for each analysis, so this work tried to develop a methodology for NPs analysis which could be applied to routine laboratories.

- i. The FI-FFF methodology could be adapted to the characterization of urine NPs. Particles did not respond to a pattern of several individual populations, but to a continuous particle size distribution.
- ii. Opposite to the expected results, no significant differences in particle size and particle size distribution were observed between stone patients and healthy controls.
- iii. The suggestion of FI-FFF as an option for the early diagnosis of urinary lithiasis through NPs size determination cannot be derived from the results obtained here.

### 6.1.3. Crystallization promoters

Since diet is one of the most important sources of crystallization promoters, among them oxalate, two important cases have been studied. In this work, two specific cases (plant extracts and chocolate) have been analyzed, for the determination of their lithogenic risk. This Section intends to answer the question whether patients should or should not avoid their intake.

- i. The oxalate content of the plant extracts is remarkably diverging. In some cases, their daily dose accounts for as much as 8% of the total oxalate intake in a normal diet. The consumption of some of them should be seriously considered by CaOx stone patients.
- ii. The wide variety of chocolates studied also presents an important variability in the determined magnitudes. Oxalate has been identified as the most important component for the identification of different groups within the sample collection.
- iii. The correlation between oxalate and cocoa content is only weak, so the cocoa amount should not be directly taken as a direct risk for stone patients. Calcium and oxalate concentrations do show relation, apart from a few samples in the data set.
- iv. The intake of dark and caramel chocolates should be considered by stone patients, due to the large amount of oxalate (especially bioavailable oxalate) they contain. Conversely, milk chocolates and other sorts combined with nuts do not represent a clear risk for stone patients.

#### 6.1.4. Knowledge transfer

The scientific knowledge produced during the development of this Thesis has been protected or shifted towards the market when it was considered suitable. The most significant milestones are cited here.

- i. The NIR-HSI methodology for the automatic analysis and classification of urinary stones was protected by a European patent. This patent was licensed by a private firm in the urolithiasis field for its commercial exploitation.
- ii. A totally new medical device for the analysis of urinary stones was developed. This device uses image analysis and image recognition tools for the automatic, in-situ classification of urinary stones. The device is full operative and tested considering potential user's feedback.
- iii. Public funding for the specific development of the project was granted. Entrepreneurship prizes were won by presenting the business idea of this medical device. This confirms the interest of this project.
- iv. A market research centered on the creation of a company that commercializes the device was conducted. A general strategy and value proposition were described: analysis in-situ, more information available for the physician and better treatment options are the basic credentials.

## 6.2. Insights into the future

The work presented in this Dissertation has addressed some open issues in the study of urolithiasis. Among the most important conclusions, some future ideas should also be pointed out, in order to assure a proper continuation of this work.

- i. In regard to spectroscopic imaging, using NIR-HSI, it would be interesting to enlarge the scanned region. Some modern spectrometers allow the measurement of lower energy wavelengths (up to 2500 nm), so the scanned range could cover 1000-2500nm. Absorption bands could for some components might lie in this region, so the classification power of the technique might be improved. The classification problems of CAP/STR could be partially solved so.
- ii. Section 2.4 has shown a really precise methodology for the determination of the causes of stone formation. The analysis time, however, is far too long for its implementation in clinical laboratories, not to mention the impossibility to use synchrotron radiation regularly. Analysis time could be dramatically decreased if the point scan is substituted by a FPA (Focal Plane Array), which would measure up to 128x128 pixels at the same time (using already commercially available devices).
- iii. These imaging techniques would result much more attractive for clinical laboratories also if other applications were developed. The classification of other tissues or samples would allow its general use for many medical specialties, so the purchase and use of such equipment would become affordable. The high versatility of HSI techniques is an interesting feature that would allow such diversification.

- iv. Nanoparticles analysis in urine represents an exciting way of determining lithogenic risk in general population. This would offer a clear way to control the risk in clinical laboratories, using highly automated analysis. In addition to the particle size analysis, the chemical speciation of those particles is of special relevance. Due to the easy coupling FFF-ICP-MS, it would be interesting to assess whether the composition of the eluted particles changes for different sizes and/or for patients and controls.
- v. The newly developed medical device, myStone, is able to correctly classify most stone types. Nonetheless, some stone groups still lack classification efficiency. This could be improved by widening the library for the model training. The location of minor components, as well as the quantification of general amounts of substances, has not been achieved yet. An alternative would include the incorporation of a IR sensor to the equipment, since this would allow the recognition of other, more specific spectral features. As seen with the developed NIR-HSI methodology, the possibility to use the device with little variations to analyze other tissues or samples is very attractive for its use in clinics.





# **BIBLIOGRAPHY**

1. Finco, D. R. Kidney Function. In *Clinical Biochemistry of Domestic Animals*, 5th ed.; Kaneko, J. J., Harvey, J. W., Bruss, M. L., Eds.; Elsevier: Amsterdam, 1997; pp 441-484.
2. Chappel, C. Overview on the lower urinary tract. In *Urinary Tract*; Andersson, K. E., Michel, M. C., Eds.; Springer: Berlin, 2011; pp 1-14.
3. Bonsib, S. M. Renal anatomy and histology. In *Heptinstall's Pathology of the kidney*; Jennette, J. C., Olson, J. L., Schwartz, M. M., Silva, F. G., Eds.; Lippincott Williams & Wilkins: Philadelphia, 2006; pp 1-70.
4. Martini, F. *Anatomy and Physiology*; Pearson Education: Singapore, 2005.
5. Komers, R.; Meyer, T. W.; Anderson, S. Pathophysiology and nephron adaptation in chronic kidney disease. In *Diseases of the kidney and urinary tract*, 3rd ed.; Schrier, R. W., Ed.; Lippincott Williams & Wilkins: Philadelphia, 2007.
6. Kardasz, S. The function of the nephron and the formation of urine. *Anaesthesia and Intensive Care Medicine* **2012**, *13* (7), 309-314.
7. White, K. E. Research into the structure of the kidney glomerulus - making it count. *Micron* **2012**, *43*, 1001-1009.
8. Dehoorne, J.; Van't Hoff, W. Renal tubular disorders. *Current Paediatrics* **2003**, *13*, 487-495.
9. Tanner, G. A. Kidney function. In *Medical Physiology: Principles for Clinical Medicine*, 3rd ed.; Rhoades, R. A., Bell, D. R., Eds.; Philadelphia, 2009; pp 391-418.
10. Brikowski, T. H.; Lotan, Y.; Pearle, M. S. Climate-related increase in the prevalence of urolithiasis in the United States. *Proceedings of the National Academy of Sciences of the United States of America* **2008**, *105*, 9841-9846.
11. Moe, O. W. Kidney stones: pathophysiology and medical management. *Lancet* **2006**, *367*, 333-344.
12. Mongha, R.; Kumar, A. Current management of urolithiasis. *Apollo Medicine* **2009**, *6* (2), 156-160.
13. Robertson, W. G.; Hughes, H. Epidemiology of urinary stone disease in Saudi Arabia. In *Urolithiasis 2*; Ryall, R. L., Ed.; Pelum Press: New York, 1994; pp 453-455.
14. Alaya, A.; Nouri, A.; Belgith, M.; Saad, H.; Hell, I.; Hellara, W.; Jouini, R.; Najjar, M. F. Changes in kidney stones type according to sex and age in Tunisian patients. *Actas Urológicas Españolas* **2012**, *36* (3), 171-177.
15. Romero, V.; Akpınar, H.; Assimos, D. G. Kidney stones: A global picture of prevalence, incidence, and associated risk factors. *Reviews in Urology* **2010**, *12* (2), 86-96.
16. Lieske, J. C.; Peña de la Vega, L. S.; Slezak, J. M.; Bergstralh, E. J.; Leibson, C. L.; Ho, K. L.; Gettman, M. T. Renal stone epidemiology in Rochester, Minnesota: An update. *Kidney International* **2006**, *69*, 760-764.
17. Hughes, P. Kidney stones epidemiology. *Nephrology* **2007**, *12*, 26-30.
18. Baker, P. W.; Coyle, P.; Bais, R.; Rofe, A. M. Influence of season, age, and sex on renal stone formation in South Australia. *The Medical Journal of Australia* **1993**, *159* (6), 390-392.
19. Fink, H. A.; Arkonor, J. W.; Garimella, P. S.; MacDonald, R.; Cutting, A.; Rutks, I. R.; Monga, M.; Wilt, T. Diet, fluid or supplements for secondary prevention of nephrolithiasis: A systematic review and meta-analysis of randomized trials. *European Urology* **2009**, *56*, 72-80.
20. Tiselius, H. G. Who forms stones and why? *European Urology Supplements* **2011**, *10*, 408-414.
21. Parks, J. H.; Coe, F. L. Evidence for durable kidney stone prevention over several decades. *BJU International* **2009**, *103*, 1238-1246.
22. Kok, D. J. Metaphylaxis, diet and lifestyle in stone disease. *Arab Journal of Urology* **2012**, *10*, 240-249.

23. Cervellin, G.; Comelli, I.; Comelli, D.; Meschi, T.; Lippi, G.; Borghi, L. Mean temperature and humidity variations, along with patient ages, predict the number of visits for renal colic in a large urban Emergency Department: Results of a 9-year survey. *Journal of Epidemiology and Global Health* **2012**, *2*, 31-38.
24. Robertson, W. G. Stone formation in the Middle Eastern Gulf States: A review. *Arab Journal of Urology* **2012**, *10*, 265-272.
25. Curham, G. Nephrolithiasis. In *Primer on kidney diseases*, 4th ed.; Greenberg, A., Ed.; Elsevier: Philadelphia, 2005.
26. Kallidonis, P.; Liourdi, D.; Liatsikos, E. Medical treatment for renal colic and stone expulsion. *European Urology Supplements* **2011**, *10*, 415-422.
27. Cupisti, A.; Pasquali, E.; Lusso, S.; Carlino, F.; Orsitto, E.; Melandri, R. Renal colic in Pisa emergency department: epidemiology, diagnostics and treatment patterns. *Internal and Emergency Medicine* **2008**, *3*, 241-244.
28. Sebastian, A.; Tait, P. Renal imaging. *Medicine* **2011**, *39* (6), 333-338.
29. Sandhu, C.; Anson, K. M.; Patel, U. Urinary tract stones - Part I: Role of radiological imaging in diagnosis and treatment planning. *Clinical Radiology* **2003**, *58*, 415-421.
30. Ahangar, S.; Durrani, A. M.; Qadri, S. J.; Patloo, A. M.; Ganaie, R. G.; Khan, M. Laparoscopic trans-peritoneal pyelolithotomy in a pelvic kidney. *Saudi Journal of Kidney Diseases and Transplantation* **2012**, *23* (6), 1254-1257.
31. Daudon, M.; Traxer, O.; Jungers, P. *Lithiase urinaire*, 2nd ed.; Lavoisier: Paris, 2012.
32. Grases, F.; Costa-Bauzá, A.; Söhnle, O. *Cristalización en disolución. Conceptos básicos*; Reverté: Barcelona, 2000.
33. Muñoz Martínez, J. A. *Litiasis renal oxalocálcica. Avances en la comprensión de su etiología y mejoras en la metodología analítica para su estudio*; Doctoral Thesis; Universitat Autònoma de Barcelona: Bellaterra, 2004.
34. Arvaniti, E. C.; Lioliou, M. G.; Paraskeva, C. A.; Payatakes, A. C.; Ostvold, T.; Koutsoukos, P. G. Calcium oxalate crystallization on concrete heterogeneities. *Chemical Engineering Research and Design* **2010**, *88*, 1455-1460.
35. Babic-Ivancic, V.; Füredi-Milhofer, H.; Brown, W. E.; Gregory, T. M. Precipitation diagrams and solubility of uric acid dihydrate. *Journal of Crystal Growth* **1987**, *83*, 581-587.
36. Abbona, F.; Lundager Madsen, H. E.; Boistelle, R. Crystallization of two magnesium phosphates, struvite and newberyite: effect of pH and concentration. *Journal of Crystal Growth* **1982**, *57*, 6-14.
37. Kassemi, M.; Brock, R.; Nemeth, N. A combined transport-kinetics model for the growth of renal calculi. *Journal of Crystal Growth* **2011**, *332*, 48-57.
38. Khan, S. R. Calcium phosphate/calcium oxalate crystal association in urinary stones: Implications for heterogeneous nucleation of calcium oxalate. *The Journal of Urology* **1997**, *157*, 376-383.
39. Matlaga, B. R.; Coe, F. L.; Evan, A. P.; Lingeman, J. E. The role of Randall's Plaques in the pathogenesis of calcium stones. *The Journal of Urology* **2007**, *177* (1), 31-38.
40. Abdel-Aal, E. A.; Daosukho, S.; El-Shall, H. Effect of supersaturation ratio and Khella extract on nucleation and morphology of kidney stones. *Journal of Crystal Growth* **2009**, *311*, 2673-2681.
41. Boyce, W. H.; Finlayson, B.; Hench, L. L.; Smith, L. H. *Urolithiasis: Physical aspects*; National Academy of Sciences: Washington, 1972.

42. He, J. Y.; Ouyang, J. M.; Yang, R. E. Agglomeration of urinary nanocrystallites: Key factor to formation of urinary stones. *Materials Science and Engineering C* **2010**, *30*, 878-885.
43. Grases, F.; Costa-Bauzá, A.; García-Ferragut, L. Biopathological crystallization: a general view about the mechanisms of renal stone formation. *Advances in Colloid and Interface Science* **1998**, *74*, 169-194.
44. Grases, F.; Costa-Bauzá, A.; Ramis, M.; Montesinos, V.; Conte, A. Simple classification of renal calculi closely related to their micromorphology and etiology. *Clinica Chimica Acta* **2002**, *322* (1-2), 29-36.
45. Basavaraj, D. R.; Biyani, C. S.; Browning, A. J.; Cartledge, J. J. The role of urinary kidney stone inhibitors and promoters in the pathogenesis of calcium containing renal stones. *EAU-EBU Update Series* **2007**, *5*, 126-136.
46. Hamm, L. L.; Hering-Smith, K. S. Pathophysiology of hypocitraturic nephrolithiasis. *Endocrinology Metabolism Clinics of North America* **2002**, *31*, 885-893.
47. Christmas, K. G.; Gower, L. B.; Khan, S. R.; El-Shall, H. Aggregation and dispersion characteristics of calcium oxalate monohydrate: Effect on urinary species. *Journal of Colloid and Interface Science* **2002**, *256*, 168-174.
48. Rude, R. K. Magnesium deficiency: a cause of heterogeneous disease in humans. *Journal of Bone and Mineral Research* **1998**, *13*, 749-758.
49. Liebman, M.; Costa, G. Effects of calcium and magnesium on urinary oxalate excretion after oxalate loads. *The Journal of Urology* **2000**, *163*, 1565-1569.
50. Sharma, S.; Vaidyanathan, S.; Thind, S. K.; Nath, R. Urinary excretion of inorganic pyrophosphate by normal subjects and patients with renal calculi. *Urology International* **1992**, *48*, 404-408.
51. McLean, R. J.; Downey, J.; Clapham, L.; Wilson, J. W.; Nickel, J. C. Pyrophosphate inhibition of *Proteus mirabilis*-induced struvite crystallization in vitro. *Clinica Chimica Acta* **1991**, *200*, 107-118.
52. Grases, F.; Sanchis, P.; Costa-Bauza, A.; Bonnin, O.; Isern, B.; Perello, J.; Prieto, R. M. Phytate inhibits bovine pericardium calcification in vitro. *Cardiovascular Pathology* **2008**, *17* (3), 139-145.
53. March, J. G.; Simonet, B. M.; Grases, F. Determination of phytic acid by gas chromatography-mass spectroscopy: application to biological samples. *Journal of Chromatography B: Biomedical Sciences and Applications* **2001**, *757* (2), 247-255.
54. Muñoz, J. A.; López-Mesas, M.; Valiente, M. Minimum handling method for the analysis of phosphorous inhibitors of urolithiasis (pyrophosphate and phytic acid) in urine by SPE-ICP techniques. *Analytica Chimica Acta* **2010**, *658* (2), 204-208.
55. Grases, F.; March, P. A study about some phosphate derivatives as inhibitors of calcium oxalate crystal growth. *Journal of Crystal Growth* **1989**, *96*, 993-995.
56. Robertson, W. G. Methods for diagnosing the risk factors of stone formation. *Arab Journal of Urology* **2012**, *10*, 250-257.
57. Robertson, W. G.; Jones, J. S.; Heaton, M. A.; Stevenson, A. E.; Markwell, P. J. Predicting the crystallization potential of urine from cats and dogs with respect to calcium oxalate and magnesium ammonium phosphate (struvite). *Journal of Nutrition Supplements* **2008**, 1637S-1641S.
58. Laube, N.; Hergarten, S.; Hesse, A. Testing the predictability of the relative urinary supersaturation from the Bonn-Risk-Index for calcium oxalate stone formation. *Clinical Chemistry and Laboratory Medicine* **2001**, *39* (10), 966-969.
59. Pak, C. C.; Maalouf, N. M.; Rodgers, K.; Poindexter, J. R. Comparison of semi-empirical and computer derived methods for estimating urinary saturation of calcium oxalate. *The Journal of Urology* **2009**, *182* (6), 2951-2956.
60. Stevenson, A. E.; Robertson, W. G.; Markwell, P. J. Risk factor analysis and relative supersaturation as tools for identifying calcium oxalate stone-forming dogs. *Journal of Small Animal Practice* **2003**, *44*, 491-495.

61. Coe, F. L.; Wise, H.; Parks, J. H.; Asplin, J. R. Proportional reduction of urine supersaturation during nephrolithiasis treatment. *The Journal of Urology* **2001**, *166*, 1247-1251.
62. Robertson, W. G.; Stevenson, A. E. Methods for measuring the crystallization potential of urine - RSS vs APR. *Veterinary Focus* **2007**, *17* (1), 37-40.
63. Ferreira, M. C.; Paragon, B. M.; Gunn-Moore, D. A.; Sparkes, A.; Gerber, B. *Proceedings of the Nestle PURINA expert panel roundtable on feline urinary health*; Conference; Nestle Purina, 2011.
64. Pak, C. Y. Physicochemical basis for formation of renal stones of calcium phosphate origin: Calculation of the degree of saturation of urine with respect to brushite. *The Journal of Clinical Investigation* **1969**, *48*, 1914-1922.
65. Pak, C. Y.; Eanes, E. D.; Ruskin, B. Spontaneous precipitation of brushite in urine: Evidence that brushite is the nidus of renal stones originating as calcium phosphate. *Proceedings of the National Academy of Sciences* **1971**, *68* (7), 1456-1460.
66. Nicar, M. J.; Hill, K.; Pak, C. Y. A simple technique for assessing the propensity for crystallization of calcium oxalate and brushite in urine from the increment in oxalate or calcium necessary to elicit precipitation. *Metabolism* **1983**, *32* (9), 906-910.
67. Pak, C. Y.; Rodgers, K.; Poindexter, J. R.; Sakhaee, K. New methods of assessing crystal growth and saturation of brushite in whole urine: Effect of pH, calcium and citrate. *The Journal of Urology* **2008**, *180*, 1532-1537.
68. Laube, N.; Schneider, A.; Hesse, A. A new approach to calculate the risk of calcium oxalate crystallization from unprepared native urine. *Urological Research* **2000**, *28*, 274-280.
69. Laube, N.; Hergarten, S.; Hoppe, B.; Schmidt, M.; Hesse, A. Determination of the calcium oxalate crystallization risk from urine samples: The Bonn Risk Index in comparison to other risk formulas. *The Journal of Urology* **2004**, *172*, 355-359.
70. Kavanagh, J. P.; Laube, N. Why does the Bonn Risk Index discriminate between calcium oxalate stone formers and healthy controls? *The Journal of Urology* **2005**, *175*, 766-770.
71. Laube, N.; Hergarten, S. Can the Bonn Risk Index be replaced by a simple measurement of the urinary concentration of free calcium ions? *The Journal of Urology* **2005**, *173*, 2175-2177.
72. Porowski, T.; Mrozek, P.; Sidun, J.; Zoch-Zwierz, W.; Konstantynowicz, J.; Kirejczyk, J. K.; Motkowski, R.; Laube, N. Bonn Risk Index based micromethod for assessing risk of urinary calcium oxalate stone formation. *The Journal of Urology* **2010**, *183*, 1157-1162.
73. Lorenzo, V.; Torres, A.; Hernández, D.; Ayus, J. C. *Manual de Nefrología*, 2nd ed.; Elsevier España: Madrid, 2002.
74. Daudon, M.; Bader, C. A.; Jungers, P. Urinary calculi: review of classification methods and correlations with etiology. *Scanning Microscopy* **1993**, *73* (3), 1081-1104.
75. Leusmann, D. B. A classification of urinary calculi with respect to their composition and micromorphology. *Scandinavian Journal of Urology* **1991**, *25*, 141-150.
76. Worcester, E. M.; Coe, F. L. Calcium kidney stones. *New England Journal of Medicine* **2010**, *363* (10).
77. Ouyang, J. M.; Zheng, H.; Deng, S. P. Simultaneous formation of calcium oxalate (mono-, di-, and trihydrate) induced by potassium tartrate in gelatinous system. *Journal of Crystal Growth* **2006**, *293*, 118-123.
78. Hesse, A.; Jahnen, A.; Klocke, K.; Nolde, A.; Scharrel, O. *Nachsorge bei Harnsteinpatienten. Ein Leitfaden für die ärztliche Praxis.*; Gustav Fischer Verlag: Stuttgart, 1994.
79. Sandersius, S.; Rez, P. Morphology of crystals in calcium oxalate monohydrate kidney stones. *Urological Research* **2007**, *35*, 287-293.

80. Kuritz, J. W.; Carvalho, M.; Nakagawa, Y. Nephrocalcin isoforms coat crystal surfaces and differentially affect calcium oxalate monohydrate crystal morphology, growth, and aggregation. *Journal of Crystal Growth* **2003**, *255*, 392-402.
81. Iwata, H.; Iio, S.; Nishio, S.; Takeuchi, M. Architecture of mixed calcium oxalate dihydrate and monohydrate stones. *Scanning Microscopy* **1992**, *321*, 231-237.
82. Evan, A. P.; Lingeman, J. E.; Coe, F. L. Randall's plaque of patients with nephrolithiasis begins in basement membranes of thin loops of Henle. *The Journal of Clinical Investigation* **2003**, *111*, 607-616.
83. Randall, A. Etiology of primary renal calculus. *Int. Abs. Surg.* **1940**, *71*, 209.
84. Evan, A.; Lingeman, J.; Coe, F. L.; Worcester, E. Randall's plaque: Pathogenesis and role in calcium oxalate nephrolithiasis. *Kidney International* **2006**, *69*, 1313-1318.
85. Grases, F.; Costa-Bauzá, A.; Gomila, I.; Conte, A. Origin and types of calcium oxalate monohydrate papillary renal calculi. *Urology* **2010**, *76*, 1339-1345.
86. Pieras, E.; Grases, F.; Costa-Bauzá, A.; Ramis, M.; Piza, P.; Ozonas, M. Litiasis de oxalato cálcico monohidrato papilar y de cavidad: Estudio comparativo de factores etiológicos. *Archivos Españoles de Urología* **2006**, *59* (6), 147-154.
87. Brečević, L.; Škrčić, D.; Garside, J. Transformation of calcium oxalate hydrates. *Journal of Crystal Growth* **1986**, *74*, 399-408.
88. Conti, C.; Casati, M.; Colombo, C.; Realini, M.; Brambilla, L.; Zerbi, G. Phase transformation of calcium oxalate dihydrate-monohydrate: Effects of relative humidity and new spectroscopic data. *Spectrochimica Acta Part A* **2014**, *128*, 413-419.
89. Muñoz, J. A.; López-Mesas, M.; Valiente, M. Inhibitors of oxalocalcic lithiasis: Effects of their interactions on calcium oxalate crystallization. *Urology* **2012**, *80*, 1163.13-1163.18.
90. Grillenwater, J. Y.; Grayhack, J. T.; Howards, S. S.; Mitchell, M. E. *Adult and pediatric urology*, 4th ed.; Lippincott Williams & Walkins: Philadelphia, 2002.
91. Robertson, W. G.; Peacock, M. Pathogenesis of Urolithiasis. In *Urolithiasis: Etiology - Diagnosis*, 1st ed.; Schneider, H. J., Ed.; Springer Verlag: Berlin, 1989.
92. Pak, C. Y.; Adams-Huet, B.; Poindexter, J. R.; Pearle, M. S.; Peterson, R. D.; Moe, O. W. Relative effect of urinary calcium and oxalate on saturation of calcium oxalate. *Kidney International* **2004**, *66*, 2032-2037.
93. Grases, F.; March, P. Determination of phytic acid based on inhibition of crystalline growth of calcium oxalate monohydrate. *Analytica Chimica Acta* **1989**, No. 219, 89-95.
94. Brown, P.; Ackermann, D.; Finlayson, B. Calcium oxalate dihydrate (whedellite) precipitation. *Journal of Crystal Growth* **1989**, *98*, 285-292.
95. Khan, S. R.; Glenton, P. A. Experimental induction of calcium oxalate nephrolithiasis in mice. *The Journal of Urology* **2010**, *184*, 1189-1196.
96. Robertson, W. G.; Hughes, H. Importance of mild hyperoxaluria in the pathogenesis of urolithiasis. New evidence from studies in the Arabian peninsula. *Scanning Microscopy* **1993**, *7* (1), 391-401.
97. Coe, F. L.; Parks, J. H.; Evan, A.; Worcester, E. Pathogenesis and treatment of nephrolithiasis. In *Seldin and Giebisch's The Kidney: Physiology & Pathophysiology*, 5th ed.; Alpern, R. J., Caplan, M. J., Moe, O. W., Eds.; Academic Press: New York, 2012.
98. Bichler, K. H.; Eipper, E.; Naber, K.; Braun, V.; Zimmermann, R.; Lahme, S. Urinary infection stones. *International Journal of Antimicrobial Agents* **2002**, *19*, 488-498.
99. Dorozhkin, S. V. Amorphous calcium (ortho)phosphates. *Acta Biomaterialia* **2010**, *6*, 4457-4475.

100. Wopenka, B.; Pasteris, J. D. A mineralogical perspective on the apatite in bone. *Materials Science and Engineering C* **2005**, *25*, 131-143.
101. Schneider, H. J. Morphology of urinary tract concretions. In *Urolithiasis: Etiology - Diagnosis*, 1st ed.; Schneider, H. J., Ed.; Springer Verlag: Berlin, 1989.
102. Reid, D. G.; Jackson, G. J.; Duer, M. J.; Rodgers, A. L. Apatite in kidney stones is a molecular composite with glycosaminoglycans and proteins: Evidence from nuclear magnetic resonance spectroscopy, and relevance to Randall's plaque pathogenesis and prophylaxis. *The Journal of Urology* **2011**, *185*, 725-730.
103. Leusmann, D. B. Erste zusammenfassende Ergebnisse de kombinierten Phasen- und Gefügeanalyse von harnsteinen mittels Röntgenbeugung und Rasterelektronenmikroskopie. In *Pathogenese und Klinik der Harnsteine VIII*; Vahlensieck, W., Gasser, G., Eds.; Steinkopf: Darmstadt, 1982.
104. Gebhardt, M. Unterschiedliche Voerstellungen zur Phophat- und Oxalat- Steinbildung nach Röntgen- und REM- Untersuchungen. In *Pathogenese und Klinik der Harnsteine III*; Vahlensieck, W., Gasser, G., Eds.; Steinkopff: Darmstadt, 1982.
105. Parks, J. H.; Worcester, E. M.; Coe, F. L.; Evan, A. P.; Lingeman, J. E. Clinical implications of abundant calcium phosphate in routinely analyzed kidney stones. *Kidney International* **2004**, *66*, 777-785.
106. Moreira, D. M.; Freidlander, J. I.; Hartman, C.; Elsamra, S. E.; Smith, A. D.; Okeke, Z. Differences in 24-hour urine composition between apatite and brushite stone formers. *Urology* **2013**, *82*, 768-772.
107. Krambeck, A. E.; Handa, S. E.; Evan, A. P.; Lingeman, J. E. Profile of the brushite stone former. *Ther Journal of Urology* **2010**, *1367-1371*, 184.
108. Schwatz, B. F.; Stoller, M. L. Non-surgical management of infection-related renal calculi. *Urologic Clinics of North America* **1999**, *26* (1), 765-778.
109. Rieu, P. Lithiases d'infection. *Annales d'urologie* **2005**, *39*, 16-29.
110. Bichler, K. H.; Strohmaier, W. L.; Wechsel, H. Harnwegsinfektionen. Diagnostik und Therapie. *Schriftenreihe der Bezirksärztekammer Südwürttemberg* **1990**, *13*, 20-29.
111. Hess, B. Metabolic syndrome, obesity and kidney stones. *Arab Journal of Urology* **2012**, *10*, 258-264.
112. Grases, F.; Villacampa, A. I.; Costa-Bauzá, A.; Söhnel, O. Uric acid calculi: types, etiology and mechanisms of formation. *Clinica Chimica Acta* **2000**, *302*, 89-104.
113. Finlayson, B.; Smith, A. Stability of first dissociable proton of uric acid. *Journal of Chemical and Engineering Data* **1974**, *19* (1), 94-97.
114. Nakagawa, Y.; Asplin, J. R.; Goldfarb, D. S.; Parks, J. H.; Coe, F. L. Clinical use of cystine supersaturation measurements. *The Journal of Urology* **2000**, *164*, 1481-1485.
115. Hesse, A.; Berg, W.; Bothor, C. Scanning electron microscopic investigations on the morphology and phase conversions of uroliths. *Internal Urology and Nephrology* **1979**, *11*, 11-20.
116. Dosch, W. Genese und Wachstum von Harnsteinen. In *Pathogenese und Klinik der Harnsteine III*; Vahlensieck, W., Gasser, G., Eds.; Steinkopff: Darmstadt, 1979; pp 67-83.
117. Chow, G. K.; Strem, S. B. Contemporary urological intervention for cystinuric patients: immediate and long-term impact and implications. *The Journal of Urology* **1998**, *160*, 341-345.
118. Pak, C. Y.; Fuller, C. J. Assessment of cystine solubility in urine and of heterogeneous nucleation. *The Journal of Urology* **1983**, *129*, 1066.
119. Chou, Y. H.; Huang, C. N.; Li, W. M.; Huang, S. P.; Wu, W. J.; Tsai, C. C.; Chang, A. W.; Chen, S. M.; Lin, Y. L.; Lin, Y. P. Clinical study of ammonium acid urate urolithiasis. *Kaohsiung Journal of Medical Sciences* **2012**, *28*, 259-264.

120. Hughes, P. Kidney stones epidemiology. *Nephrology* **2007**, *26-30*, 12.
121. Servais, A.; Daudon, M.; Knebelman, B. Lithiases médicamenteuses. *Annales d'Urologie* **2006**, *40* (2), 57-68.
122. Marcet, A. *Versuch einer chemischen Geschichte und ärztlichen Behandlung der Steinkrankheiten*; J G Heyse: Bremen, 1818.
123. Stoller, M. L.; Meng, M. V. *Urinary Stone Disease*; Humana Press: New Jersey, 2007.
124. Heller, J. F. *Die Harnconcretionen, ihre Entstehung, Erkennung und Analyse*; Verlag von Tendler & Comp.: Vienna, 1860.
125. Hodgkinson, A. A combined qualitative and quantitative procedure for the chemical analysis of urinary calculi. *Journal of Clinical Pathology* **1971**, *24*, 147-151.
126. Schubert, G. Stone analysis. *Urological Research* **2006**, *34*, 146-150.
127. Beischer, D. E. Analysis of renal calculi by infrared spectroscopy. *The Journal of Urology* **1955**, 653-657.
128. Hesse, A.; Sanders, G. *Atlas of infrared spectra for the analysis of urinary concrements*; Georg Thieme Verlag: Stuttgart, 1988.
129. Selvaraju, R.; Thirupathi, G.; Raja, A. FT-IR spectral studies on certain human urinary stones in the patients of rural area. *Spectrochimica Acta Part A* **2012**, *93*, 260-265.
130. Chen, Z.; Wang, C.; Zhou, H.; Sang, L.; Li, X. Modulation of calcium oxalate crystallization by commonly consumed green tea. *CrystEngComm* **2012**, *12*, 845-852.
131. Gulley-Stahl, H. J.; Haas, J. A.; Schmidt, K. A.; Evan, A. P.; Sommer, A. J. Attenuated total internal reflection Fourier transform infrared spectroscopy: A quantitative approach for kidney stone analysis. *Applied Spectroscopy* **2009**, *63* (7), 759-766.
132. García Álvarez, J. L.; Torrejón Martínez, M. J.; Arroyo Fernández, M. Development of a method for the quantitative analysis of urinary stones, formed by a mixture of two components, using infrared spectroscopy. *Clinical Biochemistry* **2012**, *45*, 582-587.
133. Pucetaite, M.; Hendrixson, V.; Zelvy, A.; Jankevicius, F.; Tyla, R.; Ceponkus, J.; Sablinskas, V. Application of infrared spectroscopic imaging in specular reflection mode for determination of distribution of chemical components in urinary stones. *Journal of Molecular Structure* **2013**, *1031*, 38-42.
134. Kamoun, A.; Daudon, M.; Abdelmoula, J.; Hamzaoui, M.; Chaouachi, B.; Houissa, T.; Zghal, A.; Ammar, S. B.; Belkahia, C.; Lakhoua, R. Urolithiasis in Tunisian children: a study of 120 cases based on stone composition. *Pediatric Nephrology* **1999**, *13*, 920-925.
135. Blanco, F.; López-Mesas, M.; Serranti, S.; Bonifazi, G.; Havel, J.; Valiente, M. Hyperspectral imaging based method for fast characterization of kidney stone types. *Journal of Biomedical Optics* **2012**, *17* (7).
136. Uvarov, V.; Popov, I.; Shapur, N.; Abdin, T.; Gofrit, O. N.; Pode, D.; Duvdevani, M. X-Ray diffraction and SEM study of kidney stones in Israel: quantitative analysis, crystallite size determination, and statistical characterization. *Environmental Geochemistry and Health* **2011**, *33*, 613-622.
137. West, A. R. *Solid state chemistry and its applications*, 2nd ed.; Wiley: UK, 2014.
138. Bhatt, P. A.; Paul, P. Analysis of urinary stone constituents using powder X-ray diffraction and FT-IR. *Journal of Chemical Sciences* **2008**, *120* (2), 267-273.
139. Selvaraju, R.; Raja, A.; Thirupathi, G. FT-Raman spectral analysis of human urinary stones. *Spectrochimica Acta Part A: Molecular and Biomolecular Spectroscopy* **2012**, *99*, 205-210.
140. Fleming, D. E.; Van Riessen, A.; Chauvet, M. C.; Grover, P. K.; Hunter, B.; Van Bronswijk, W.; Ryall, R. L. Intracrystalline proteins and urolithiasis: A synchrotron X-Ray Diffraction study of calcium oxalate monohydrate. *Journal of Bone and Mineral Research* **2003**, *18* (7), 1282-1291.



141. Carpentier, X.; Bazin, D.; Combes, C.; Mazouyes, A.; Rouzière, S.; Albouy, P. A.; Foy, E.; Daudon, M. High Zn content of Randall's plaque: A u-X-ray fluorescence investigation. *Journal of Trace Elements in Medicine and Biology* **2011**, *25*, 160-165.
142. Stoller, M. L.; Meng, M. V. *Kidney Stones: The practical guide to medical and surgical management*; Humana Press: Totowa, NJ (USA), 2007.
143. Chaussy, C.; Brendel, W.; Schmiedt, E. Extracorporeal induced destruction of kidney stones by shock waves. *Lancet* **1980**, *2*, 1265.
144. Chaussy, C.; Schmiedt, E.; Jocham, D.; Brendel, W.; Forssmann, B.; Walther, V. First clinical experience with extracorporeally induced destruction of kidney stones by shock waves. *The Journal of Urology* **2002**, *167*, 844-847.
145. Schrier, R. W. *Manual of Nephrology*, 7th ed.; Lippincott Williams & Wilkins: Philadelphia, 2008.
146. Chaussy, C.; Fuchs, G. Extracorporeal shock wave lithotripsy. The evolution of a revolution. *Urologe A* **1989**, *28*, 126-129.
147. Pearle, M. S.; Calhoun, E. A.; Curhan, G. C. Urologic diseases in America project: urolithiasis. *The Journal of Urology* **2005**, *173*, 848-857.
148. Dornier, M. T. Dornier MedTech Global. <http://www.dornier.com/> (accessed Feb 23, 2014).
149. Rassweiler, J. J.; Knoll, T.; Köhrmann, K. U.; McAteer, J. A.; Lingeman, J. E.; Cleveland, R. O.; Bailey, M. R.; Chaussy, C. Shock Wave Technology and Application: An Update. *European Urology* **2011**, *59*, 784-796.
150. Eisenmenger, W. The mechanisms of stone fragmentation is ESWL. *Ultrasound in Medicine & Biology* **2001**, *27* (5), 683-693.
151. Seitz, C.; Liatsikos, E.; Porpiglia, P.; Tiselius, H.; Zwergel, U. Medical therapy to facilitate the passage of stones: What is the evidence? *European Urology* **2009**, *56*, 455-471.
152. Preminger, G. M.; Tiselius, H. G.; Assimos, D. G. Guideline for the management of ureteral calculi. *The Journal of Urology* **2007**, *178*, 2418-2434.
153. Assimos, D. G. Predictive factors and management of Steinstrasse after Shock Wave Lithotripsy in pediatric urolithiasis - A multivariate analysis study. *The Journal of Urology* **2013**, *189* (6), 2307-2308.
154. Gravina, G. L.; Costa, A. M.; Ronchi, P.; Galatioto, G. P.; Angelucci, A.; Castellani, D.; Narcisi, F.; Vicentini, C. Tamsulosin treatment increases clinical success rate of single Extracorporeal Shock Wave Lithotripsy of renal stones. *Urology* **2005**, *66*, 24-28.
155. Preminger, G. M.; Assimos, D. G.; Lingeman, J. E.; Nakada, S. Y.; Pearle, M. S.; Wolf, J. S. AUA Guideline on management of staghorn calculi: diagnosis and treatment recommendations. *The Journal of Urology* **2005**, *173*, 1991-2000.
156. Galvin, D. J.; Pearle, M. S. The contemporary management of renal and ureteric calculi. *BJU International* **2006**, *98*, 1283-1288.
157. Knoll, T.; Buchholz, N.; Wendt-Hordahl, G. Extracorporeal shockwave lithotripsy vs. percutaneous nephrolithotomy vs. flexible ureterorenoscopy for lower-pole stones. *Arab Journal of Urology* **2012**, *10*, 336-341.
158. Sooriakumaran, P.; Kaba, R.; Andrews, H. O.; Buchholz, N. P. Evaluation of the mechanism of damage of flexible ureteroscopes and suggestions for ureteroscope preservation. *Asian Journal of Andrology* **2005**, *7*, 433-438.
159. Skolarikos, A. A.; Papatsoris, A. G.; Mitsogiannis, I. C.; Chatzidarellis, C.; Liakouras, C.; Deliveliotis, C. Current status of ureteroscopic treatment for urolithiasis. *International Journal of Urology* **2009**, *16*, 713-717.
160. Sandhu, C.; Anson, K. M.; Patel, U. Urinary tract stones - Part II: Current status of treatment. *Clinical Radiology* **2003**, *58*, 422-433.

161. Straub, M.; Strohmaier, W. L.; Berg, W.; Beck, B.; Hoppe, B.; Laube, N. Diagnosis and metaphylaxis of stone disease. *World Journal of Urology* **2005**, *23*, 309-323.
162. Coe, F. L.; Parks, J. H.; Evan, A.; Worcester, E. Pathogenesis and treatment of nephrolithiasis. In *The Kidney*; Seldin, Giebisch, Eds.; Elsevier: Amsterdam, 2008; pp 1945-1977.
163. Lemann, J. Relationship between urinary calcium and net acid excretion as determined by dietary protein and potassium: A review. *Nephron* **1999**, *81* (1), 18-25.
164. Kok, D. J.; Poindexter, J.; Pak, C. Y. Calculation of titratable acidity from urinary stone risk factors. *Kidney International* **1993**, *44*, 120-126.
165. Pizzato, A. C.; Barros, E. J. Dietary calcium intake among patients with urinary calculi. *Nutrition research* **2003**, *23*, 1651-1660.
166. Jaeger, P.; Robertson, W. G. Role of dietary intake and intestinal absorption of oxalate in calcium stone formation. *Nephron Physiology* **2004**, *98*, 64-71.
167. Lewandowski, S.; Rodgers, A. L. Idiopathic calcium oxalate urolithiasis: risk factors and conservative treatment. *Clinica Chimica Acta* **2004**, *345*, 17-34.
168. Raju, S. B. Primary hyperoxaluria. *Clinical Queries: Nephrology* **2013**, *2*, 179-183.
169. Siener, R.; Pretzold, J.; Bitterlich, N.; Altheld, B.; Metzner, C. Determinants of urolithiasis in patients with intestinal fat malabsorption. *Urology* **2013**, *81*, 17-24.
170. Chutipongtanate, S.; Chaiyarit, S.; Thongboonkerd, V. Citrate, not phosphate, can dissolve calcium oxalate monohydrate crystals and detach these crystals from renal tubular cells. *European Journal of Pharmacology* **2012**, *689*, 219-225.
171. Fritsche, H. M.; Dötzer, K. Improving the compliance of the recurrent stone-former. *Arab Journal of Urology* **2012**, *10*, 342-346.
172. Erasmus, M. Niersteen. <http://www.niersteen.com/> (accessed Feb 26, 2014).
173. Strohmaier, W. L. Economics of stone disease/treatment. *Arab Journal of Urology* **2012**, *10*, 273-278.
174. Saigal, C. S.; Joyce, G.; Timilsina, A. R. Direct and indirect costs of nephrolithiasis in an employed population: opportunity for disease management? *Kidney International* **2005**, *173*, 1808-1814.
175. Lotan, Y.; Buendia Jimenez, I.; Lenoir-Wijnkoop, I.; Daudon, M.; Molinier, L.; Tack, I.; Nuhiten, M. J. Primary prevention of nephrolithiasis is cost-effective for a national healthcare system. *BJU International* **2012**, E1060-E1067.
176. Grabe, M. The estimated cost of treatment of urinary tract stones in a Swedish municipal hospital. In *Renal Stones*; Akademityrck AB: Edsbruk, 1996; pp 17-20.
177. Chandhoke, P. S. When is medical prophylaxis cost-effective for recurrent calcium stones? *The Journal of Urology* **2002**, *39*, 166-170.
178. Strohmaier, W. L. Economic aspects of evidence-based metaphylaxis. *Urologe A* **2006**, *45*, 1406-1409.
179. Ghani, K. R.; Roghmann, F.; Sammon, J. D.; Tredeau, V.; Sukuman, S.; Rahbar, H.; Kuman, R.; Karakiewicz, P. I.; Peabody, J. O.; Menon, M.; Sun, M.; Trinh, Q. Emergency Department visits in the United States for upper urinary tract stones: Trends in hospitalization and charges. *The Journal of Urology* **2014**, *191* (1), 90-96.
180. Lotan, Y.; Pearle, M. S. Economics of stone management. *EAU Update Series* **2005**, *3*, 51-60.
181. Bruckenberger, E. Beispiel Nierenlithotripter Ursachen des Kostenbooms. *Deutsches Arzenblatt* **1988**, 383-394.
182. Parks, J. H.; Coe, F. L. The financial effects of kidney stone prevention. *Kidney International* **1996**, *50*, 1706-1712.

183. Robertson, W. G. The economic case for the biochemical screening of stone patients. In *Urolithiasis 2000*; Preminger: Capetown, 2000; pp 150-153.
184. Hesse, A.; Klocke, K.; Nolde, A.; Vahlensieck, W. Advances in medical treatment of renal stones. *Urological Research* **1992**, *20*, 90-93.
185. Nolde, A.; Hesse, A.; Scharrel, O.; Vahlensieck, W. Modellprogramm zur Nachsorge bei rezidivierenden Harnsteinpatienten. *Urologe B* **1993**, *33*, 148-154.
186. Resnick, M. I.; Persky, L. Summary of the National Institutes of Arthritis, Diabetes, Digestive and Kidney Diseases conference of urolithiasis: state of the art and future research needs. *The Journal of Urology* **1995**, *153*, 4-9.
187. Van der Meer, F. D.; Van der Werff, H. A.; Van Ruitenbeek, F. A.; Hecker, C. A.; Bakker, W. H.; Noomen, M. F.; Van der Meijde, M.; Carranza, E. M.; De Smeth, J. B.; Woldai, T. Multi- and hyperspectral geologic remote sensing: A review. *International Journal of Applied Earth Observation and Geoinformation* **2012**, *14*, 112-128.
188. Prats-Montalban, J. M.; de Juan, A.; Ferrer, A. Multivariate image analysis: A review with applications. *Chemometrics and Intelligent Laboratory Systems* **2011**, *107*, 1-23.
189. Xiong, Z.; Sun, D. W.; Zeng, X. A.; Xie, A. Recent developments on hyperspectral imaging systems and their applications in detecting quality attributes of red meats: A review. *Journal of Food Engineering* **2014**, *132*, 1-23.
190. Amigo, J.; Cruz, J.; Bautista, M.; MasPOCH, S.; Coello, J.; Blanco, M. Study of pharmaceutical samples by NIR chemical-image and multivariate analysis. *Trends in Analytical Chemistry* **2008**, *27*, 696-713.
191. Serranti, S.; Gargiulo, A.; Bonifazi, G. Characterization of post-consumer polyolefin wastes by hyperspectral imaging for quality control in recycling processes. *Waste Management* **2011**, *31*, 2217-2227.
192. Sacre, P. Y.; De Bleye, C.; Chavez, P. F.; Netchacovitch, L.; Hubert, P.; Ziemons, E. Data processing of vibrational chemical imaging for pharmaceutical applications. *Journal of Pharmaceutical and Biomedical Analysis* **2014**, Article in Press, DOI: 10.1016/j.jpba.2014.04.012.
193. Gendrin, C.; Roggo, Y.; Spiegel, C.; Collet, C. Monitoring galenical process development by near infrared chemical imaging: One case study. *European Journal of Pharmaceutics and Biopharmaceutics* **2008**, *68*, 828-837.
194. Reeves, J. B. Near- versus mid-infrared diffuse reflectance spectroscopy for soil analysis emphasizing carbon and laboratory versus on-site analysis: Where are we and what needs to be done? *Geoderma* **2010**, *158*, 3-14.
195. Wu, D.; Sun, D. W. Advanced applications of hyperspectral imaging technology for food quality and safety analysis and assessment: A review - Part I: Fundamentals. *Innovative Food Science and Emerging Technologies* **2013**, *19*, 1-14.
196. Peuchant, E.; Heches, X.; Sess, D.; Clerc, M. Discriminant analysis of urinary calculi by near-infrared reflectance spectroscopy. *Clinica Chimica Acta* **1992**, *205* (1), 19-30.
197. Dumas, P.; Sockalingum, G. D.; Sulé-Suso, J. Adding synchrotron radiation to infrared microspectroscopy: what's new in biomedical applications? *Trends in Biotechnology* **2007**, *25* (1), 40-44.
198. Hirschmugl, C. J.; Gough, K. M. Fourier Transform Infrared spectrochemical imaging: Review of desing and applications with a Focal Plane Array and multiple beam synchrotron radiation source. *Applied Spectroscopy* **2012**, *66* (5), 475-491.
199. Miller, L. M.; Smith, R. J. Synchrotrons versus globars, point-detectors versus focal plane arrays. Selecting the best source and detector for specific infrared microspectroscopy and imaging applications. *Vibrational Spectroscopy* **2005**, *38*, 237-240.

200. Miller, L. M.; Dumas, P. Chemical imaging of biological tissue with synchrotron infrared light. *Biochimica et Biophysica Acta - Reviews on Biomembranes* **2006**, *1758* (7), 846-857.
201. Yoon, S.; Park, S.; Lawrence, K.; Windham, W. Line-scan hyperspectral imaging system for real-time inspection of poultry carcasses with fecal material and ingesta. *Computer and Electronics in Agriculture* **2011**, *79*, 159-168.
202. Kessler, C. J.; Porter, T. H.; Firth, D.; Sager, T. W.; Hemphill, M. W. Factor Analysis of trends in Texas acidic deposition. *Atmospheric Environment* **1992**, *26* (6), 1137-1146.
203. Velicer, W. F.; Jackson, D. N. Component Analysis versus Common Factor Analysis: Some issues in selecting an appropriate procedure. *Multivariate Behavioral Research* **1990**, *25* (1), 1-28.
204. Zhao, J.; Shi, L. Automated learning of factor analysis with complete and incomplete data. *Computational Statistics and Data Analysis* **2014**, *72*, 205-218.
205. Patil, V. H.; Singh, S. N.; Mishra, S.; Donovan, D. T. Efficient theory development and factor retention criteria: Abandon the "eigenvalue greater than one" criterion. *Journal of Business Research* **2008**, *61*, 162-170.
206. Brereton, R. G. *Applied Chemometrics for Scientists*; Wiley: West Sussex, UK, 2007.
207. Brereton, R. G. *Chemometrics. Data analysis for the laboratory and chemical plant*; Wiley: West Sussex, UK, 2003.
208. Gaskin, C. J.; Happell, B. On exploratory factor analysis: A review of recent evidence, an assessment of current practice, and recommendations for future use. *International Journal of Nursing Studies* **2014**, *51*, 511-521.
209. Hanrahan, G. Computational neural networks driving complex analytical problem solving. *Analytical Chemistry* **2010**, *82* (11), 4307-4313.
210. Brougham, D. F.; Ivanova, G.; Gottschalk, M.; Collins, D. M.; Eustace, A. J.; O'Connor, R.; Havel, J. Artificial Neural Networks for classification in metabolomics studies of whole cells using <sup>1</sup>H Nuclear Magnetic Resonance. *Journal of Biomedicine and Biotechnology* **2011**, DOI: 10.1155/2011/158094.
211. Havel, J.; Lubal, P.; Farkova, E. Evaluation of chemical equilibria with the use of artificial neural networks. *Polyhedron* **2002**, *21*, 1375-1348.
212. Gorry, P. A. General least-squares smoothing and differentiation by the convolution (Savitzky-Golay) method. *Analytical Chemistry* **1990**, *62* (2), 570-573.
213. Subramanian, J.; Simon, R. Overfitting in prediction models - Is it a problem only in high dimensions? *Contemporary Clinical Trials* **2013**, *36* (2), 636-641.
214. MathWorks. MATLAB and Simulink for Technical Computing. <http://www.mathworks.com/index.html> (accessed July 2014).
215. Kuncheva, L. I. *Combining Pattern Classifiers. Methods and Algorithms*; Wiley: New Jersey, 2004.
216. Hastie, T.; Tibshirani, R.; Friedman, J. *The elements of statistical learning: Data mining, inference and prediction*, 2nd ed.; Springer: New York, 2009.
217. SciPy. Scipy org. <http://www.scipy.org> (accessed March 2014).
218. Scikit-Learn. Machine Learning in Python. <http://scikit-learn.org> (accessed March 2014).
219. Asplin, J. R.; Lingeman, J.; Kahnoski, R.; Mardis, H.; Parks, J. H.; Coe, F. L. Metabolic urinary correlates of calcium oxalate dihydrate in renal stones. *The Journal of Urology* **1998**, *159*, 664-668.
220. Lasch, P.; Naumann, D. Spatial resolution in infrared microspectroscopic imaging of tissues. *Biochimica et Biophysica Acta* **2006**, *1758*, 814-829.
221. Lasch, P. Spectral pre-processing for biomedical vibrational spectroscopy and microspectroscopic imaging. *Chemometrics and Intelligent Laboratory Systems* **2012**, *117*, 100-114.

222. Nilsson, L. Separation and characterization of food macromolecules using field-flow fractionation: A review. *Food Hydrocolloids* **2013**, *30*, 1-11.
223. Limbach, L. K.; Li, Y.; Grass, R. N.; Brunner, T. J.; Hintermann, M. A.; Muller, M.; Gunther, D.; Starck, W. J. Oxide nanoparticle uptake in human lung fibroblasts: Effects of particle size, agglomeration and diffusion at low concentrations. *Environmental Science and Technology* **2005**, *39* (23), 9370-9376.
224. Christian, P.; Von der Kammer, F.; Baalousha, M.; Hofmann, T. Nanoparticles: structure, properties, preparation and behaviour in environmental media. *Ecotoxicology* **2008**, *17* (5), 326-343.
225. Lead, J. R.; Wilkinson, K. J. *Environmental Colloids: Behaviour, structure and characterization.*; John Wiley and Sons: New York, 2007.
226. Lespes, G.; Gigault, J. Hyphenated analytical techniques for multidimensional characterization of submicron particles: A review. *Analytica Chimica Acta* **2011**, *692*, 26-41.
227. Kim, K. H.; Moon, M. H. High speed two-dimensional protein separation without gel by isoelectric focusing-asymmetrical Flow Field Flow Fractionation: Application to urinary proteome. *Journal of proteome research* **2009**, *8*, 4272-4278.
228. Laube, N.; Mohr, B.; Hesse, A. Laser-probe-based investigation of the evolution of particle size distribution of calcium oxalate particles formed in artificial urines. *Journal of Crystal Growth* **2001**, *233*, 367-374.
229. Robertson, W. G.; Peacock, M.; Marshall, R. W.; Marshall, D. H.; Nordin, B. E. Saturation-inhibition index as a measure of the risk of calcium oxalate stone formation in the urinary tract. *New England Journal of Medicine* **1976**, *294*, 249-252.
230. Duan, C. Y.; Xia, Z. Y.; Zhang, G. N.; Gui, B. S.; Xue, J. F.; Ouyang, J. M. Changes in urinary nanocrystallites in calcium oxalate stone formers before and after potassium citrate intake. *International Journal of Nanomedicine* **2013**, *8*, 909-918.
231. Daudon, M.; Jungers, P. Clinical value of crystalluria and quantitative morphoconstitutional analysis of urinary calculi. *Nephron Physiology* **2004**, *98*, 31-36.
232. Ouyang, J. M.; Xia, Z. Y.; Zhang, G. N.; Chen, H. Q. Nanocrystallites in urine and their relationship with the formation of kidney stones. *Reviews Inorganic Chemistry* **2012**, *32* (2-4), 101-110.
233. Zhang, G. N.; Ouyang, J. M.; Xue, J. F.; Shang, Y. F. Property changes of urinary nanocrystallites and urine of uric acid stone formers after taking potassium citrate. *Materials Science and Engineering C* **2013**, *33*, 4039-4045.
234. Wahlund, K. G. Flow field-flow fractionation: Critical overview. *Journal of Chromatography A* **2013**, *1287*, 97-112.
235. Wahlund, K. G.; Giddings, J. C. Properties of an Asymmetrical Flow Field-Flow Fractionation channel having one permeable wall. *Analytical Chemistry* **1987**, *59*, 1332-1339.
236. Ratanathanawongs, S. K.; Giddings, J. C. Rapid size characterization of chromatographic silicas by Flow Field-Flow Fractionation. *Chromatographia* **1994**, *38* (9-10), 545-555.
237. Giddings, J. C. *Unified Separation Science*; Wiley-Interscience: New York, 1991.
238. Yadav, S.; Scherer, T. M.; Shire, S. J.; Kalonia, D. S. Use of dynamic light scattering to determine second virial coefficient in a semidilute concentration regime. *Analytical Biochemistry* **2011**, *411* (2), 292-296.
239. Förster, S.; Schmidt, M. Polyelectrolytes in solution. *Physical Properties of Polymers* **1995**, *120*, 51-133.
240. Zimm, B. H. The scattering of light and the radial distribution function of high polymer solutions. *Journal of Chemical Physics* **1948**, *16*, 1093.
241. Brar, S. K.; Verma, M. Measurement of nanoparticles by light-scattering techniques. *Trends in Analytical Chemistry* **2011**, *30* (1), 4-17.

242. Turkey, J. W. *Exploratory data analysis*; Addison Wesley: Massachusetts, 1976.
243. Dubascoux, S.; Von der Kammer, F.; Le Hécho, I.; Gautier, P.; Lespes, G. Optimisation of asymmetrical flow field flow fractionation for environmental nanoparticles separation. *Journal of Chromatography A* **2008**, *1206*, 160-165.
244. Bednar, A. J.; Poda, A. R.; Mitrano, D. M.; Kennedy, A. J.; Gray, E. P.; Ranville, J. F.; Hayes, C. A.; Crocker, F. H.; Steevens, J. A. Comparison of on-line detectors for field flow fractionation analysis of nanomaterials. *Talanta* **2013**, *104*, 140-148.
245. Assemi, S.; Newcombe, G.; Hepplewhite, C.; Beckett, R. Characterization of natural organic matter fractions separated by ultrafiltration using flow field-flow fractionation. *Water Research* **2004**, *38* (6), 1467-1476.
246. Litzen, A.; Wahlund, K. G. Zone broadening and dilution in rectangular and trapezoidal asymmetrical Flow Field-Flow Fractionation channels. *Analytical Chemistry* **1991**, *63*, 1001-1007.
247. Curhan, G. C.; Willett, W. C.; Knight, E. L.; Stampfer, M. J. Dietary factors and the risk of incident kidney stones in younger women. *Archives of Internal Medicine* **2004**, *164* (8), 885-891.
248. Meschi, T.; Nouvenne, A.; Borghi, L. Lifestyle recommendations to reduce the risk of kidney stones. *Urology Clinics of North America* **2011**, *38*, 313-320.
249. Siener, R. Impact of dietary habits on stone incidence. *Urological Research* **2006**, *34*, 131-133.
250. Frassetto, L.; Kohlstadt, I. Treatment and prevention of kidney stones: An update. *American Family Physician* **2011**, *84* (11), 1234-1242.
251. Robertson, W. G. Mild hyperoxaluria: a critical review and future outlook. In *Kidney Stones - 8th European Symposium on Urolithiasis*; Borghi, L., Meschi, T., Briganti, A., Schianchi, T., Novarini, A., Eds.; Editoriale Bios: Cosenza, 1999; pp 33-42.
252. Holmes, R. P.; Goodman, H. O.; Assimos, D. G. Contribution of dietary oxalate to urinary oxalate excretion. *Kidney International* **2001**, *59*, 270-276.
253. Siener, R.; Bangen, U.; Sidhu, H.; Hönow, R.; Von Unruh, G.; Hesse, A. The role of *Oxalobacter formigenes* colonization in calcium oxalate stone disease. *Kidney International* **2013**, *83*, 1144-1149.
254. Hesse, A.; Schneeberger, W.; Engfeld, S. Intestinal hyperabsorption of oxalate in calcium oxalate stone formers: application of a new test using [<sup>13</sup>C] oxalate. *Journal of the American Society of Nephrology* **1999**, *10*, 329-333.
255. Massey, L. K.; Roman-Smith, H.; Sutton, R. L. Effect of dietary oxalate and calcium on urinary oxalate and risk of formation of calcium oxalate kidney stones. *Journal of the American Dietetic Association* **1993**, *93*, 901-906.
256. Skoog, D. A.; Holler, F. J.; Nieman, T. A. *Principios de análisis instrumental*; McGraw Hill: Madrid, Spain, 1992.
257. Thomas, R. *Practical Guide to ICP-MS*; Marcel Dekker, 2004.
258. Nakata, P. A. Advances in our understanding of calcium oxalate crystal formation and function in plants. *Plant Science* **2003**, *164*, 901-909.
259. Siener, R.; Hönow, R.; Seidler, A.; Voss, S.; Hesse, A. Oxalate contents of species of the Polygonaceae, Amaranthaceae and Chemopodiaceae families. *Food Chemistry* **2006**, *98*, 220-224.
260. Hönow, R.; Gu, K. R.; Hesse, A.; Siener, R. Oxalate content of green tea of different origin, quality, preparation and time of harvest. *Urological Research* **2010**, *38*, 377-381.
261. Kawazu, Y.; Okimura, M.; Ishii, T.; Yui, S. Varietal and seasonal differences in oxalate content of spinach. *Scientia Horticulturae* **2003**, *97*, 203-210.
262. Okombo, J.; Liebman, M. Oxalate content of selected breads and crackers. *Journal of Food Composition and Analysis* **2010**, *23*, 118-121.

263. Liebman, M.; Okombo, J. Oxalate content of selected pasta products. *Journal of Food Composition and Analysis* **2009**, *22*, 254-256.
264. Webb, G. P. *Dietary supplements & functional foods*; Blackwell Publishing: Oxford, 2006.
265. Kawamura, K.; Barrie, L. A.; Toom-Sauntry, D. Intercomparison of the measurements of oxalic acid in aerosols by gas chromatography and ion chromatography. *Atmospheric Environment* **2010**, *44*, 5316-5319.
266. Del Nozal, M. J.; Bernal, J. L.; Diego, J. C.; Gómez, L. A.; Ruiz, J. M.; Higes, M. Determination of oxalate, sulfate and nitrate in honey and honeydew by ion-chromatography. *Journal of Chromatography A* **2000**, *881*, 629-638.
267. Morita, A.; Tuji, M. Nitrate and oxalate contents of tea plants (*Camellia sinensis* L.) with special reference to types of green tea and effect of shading. *Soil Science & Plant Nutrition* **2002**, *48* (4), 547-533.
268. Singh, N. P.; Prakash, A. Herbal drugs and acute renal injury. *Medicine Update* **2008**, *18*.
269. Di Mattia, C.; Martuscelli, M.; Sacchetti, G.; Beheydt, B.; Mastrocola, D.; Pittia, P. Effect of different conching processes on procyanidin content and antioxidant properties of chocolate. *Food Research International* **2014**, *63*, 367-372.
270. Torres-Moreno, M.; Torrescasana, E.; Salas-Salvadó, J.; Blanch, C. Nutritional composition and fatty acids profile in cocoa beans and chocolates with different geographical origin and processing conditions. *Food Chemistry* **2015**, *166*, 125-132.
271. Schroder, T.; Vanhanen, L.; Savage, G. P. Oxalate content in commercially produced cocoa and dark chocolate. *Journal of Food Composition and Analysis* **2011**, *24*, 916-922.
272. Borchers, A. T.; Keen, C. L.; Hannum, S. M.; Gershwin, M. E. Cocoa and chocolate: Composition, bioavailability, and health implications. *Journal of Medicinal Food* **2000**, *3* (2), 77-105.
273. Antoniewicz, M. R. <sup>13</sup>C metabolic flux analysis: optimal design of isotopic labeling experiments. *Current Opinion in Biotechnology* **2013**, *24*, 1116-1121.
274. von Unruh, G. E.; Langer, M. A.; Paar, D. W.; Hesse, A. Mass spectrometric - selected ion monitoring assay for an oxalate absorption test applying [<sup>13</sup>C<sub>2</sub>] oxalate. *Journal of Chromatography B* **1998**, *716*, 343-349.
275. Prenen, J. A.; Boer, P.; van Leersum, L.; Oldenburg, S. J.; Endeman, H. J. Urinary oxalate excretion, as determined by isotope dilution and indirect colorimetry. *Clinica Chimica Acta* **1983**, *2* (24), 251-261.
276. Wang, L.; Henday, S. M.; Schnute, W. C. *Determination of 32 low molecular mass organic acids in beverages using IC/MS*; Application note; Dionex Corporation: Sunnyvale, CA, USA, 2008.
277. Cooke, P. Regional innovation systems - an evolutionary approach. In *Regional innovation systems: The role of governance in a globalized world*; Cooke, P., Heidenreich, M., Braczyk, H., Eds.; Routledge: London, 2004.
278. Huggins, R.; Johnston, A.; Steffenson, R. Universities, knowledge networks and regional policy. *Cambridge Journal of Regions, Economy and Society* **2008**, *1*, 321-340.
279. Ponomariov, B.; Boardman, C. Organizational behavior and human resources management for public to private knowledge transfer: An analytic review of the literature. *OECD Science, Technology and Industry Working Papers* **2012**, *01*.
280. Markman, G.; Phan, P.; Balkin, D.; Gianiodis, P. Entrepreneurship and university-based technology transfer. *Journal of Business Venturing* **2005**, *20*, 241-263.
281. UAB. Parc de Recerca UAB. <http://parc.uab.es> (accessed March 09, 2014).

282. Etzkowitz, H. Innovation in innovation: The triple helix of university-industry-government relations. *Social Science Information* **2003**, 42 (3), 293-337.
283. Padilla-Meléndez, A.; Garrido-Moreno, A. What motivates researchers to engage in knowledge transfer exchanges? *International Journal of Entrepreneurial Behaviour & Research* **2012**, 18 (4), 417-439.
284. Erdős, K.; Varga, A. The academic entrepreneur: myth or reality for increased regional growth in Europe? In *Creative Knowledge Cities*; Van Geenhuizen, M., Nijkamp, P., Eds.; Edward Elgar: Glos (UK), 2012.
285. Crespi, G. A.; Geuna, A.; Nomaler, Ö.; Verspagen, B. University IPRs and knowledge transfer: is university ownership more efficient? *Economics of Innovation and New Technology* **2010**, 19 (7), 627-648.
286. Berbegal-Mirabent, J.; Lafuente, E.; Solé, F. The pursuit of knowledge transfer activities: An efficiency analysis of Spanish universities. *Journal of Business Research* **2013**, 66, 2051-2059.
287. Grupo Trabajo Indicadores. *Informe de la Encuesta de Investigación y Transferencia de Conocimiento de las Universidades Españolas*; CRUE: Madrid, 2012.
288. Castro, E.; Conesa, F.; Cristobal, P.; Cueto, L. F.; de Pablo, B.; Grau, A.; Guede, R.; Lucena, F.; Marquet, G.; Pérez, C.; Pérez, C.; Sánchez, F.; Valero, P.; Vinaixa, L. *Informe de la encuesta de investigación y transferencia de conocimiento 2010 de las universidades españolas*; CRUE - Red OTRI de Universidades: Madrid, 2010.
289. Grad, I.; Raygoza, M.; Roos, L.; Sarafidis, N.; Schade, L.; Mavrommatis, A. *Business Plan myStone*; Master in Management Dissertation; EADA Business School: Barcelona, 2014.
290. Wilson, R. M.; Gilligan, C. *Strategic marketing management*, 3rd ed.; Elsevier: Oxford, 2005.
291. Rice, J. F. *Adaptation of Porter's five forces model to risk management*; Defense Acquisition University: Fort Belvoi VA, USA, 2010.
292. ICEX. *Healthcare equipment & supplies in Spain*; Spanish Institute for Foreign Trade: Madrid, Spain, 2013.
293. Singh, G. Environmental factors affecting success of a new business. *ZENITH International Journal of Business Economics & Management Research* **2013**, 3 (4), 69-79.
294. Departament de Salut. *Pla de Salut 2011-2015*; Generalitat de Catalunya: Barcelona, Spain, 2010.
295. Actas Urológicas Españolas. *SciELO*; Asociación Española de Urología, 2003.
296. Monczka, R. M.; Handfield, R. B.; Giunipero, L. C.; Patterson, J. L. *Purchasing & Supply chain Management*, 4th ed.; South-Western CENGAGE Learning: Mason, USA, 2009.
297. Osterwalder, A.; Pigneur, Y. *Business Model Generation*; John Wiley & Sons: Hoboken, NJ, USA, 2010.
- 298.
299. Argi, G. Argi Group. <http://www.argigrup.com> (accessed May 2014).





**SUPPLEMENTAL  
MATERIAL**



**8.1. Determination of urinary lithiasis promoters and inhibitors in chocolate – Data tables (Section 4.3.**

Table 8.1. Results of the chocolate samples analysis. These values correspond to the total amount (sample homogenized using HCl). Units: mg/100g chocolate (dry weight).

Type of chocolate	Commercial brand	Oxalate		Na		Mg		K		P		Ca	
		Total	SD	Total	SD	Total	SD	Total	SD	Total	SD	Total	SD
Nougat	Ritter Sport	32.9	2.5	12.3	0.3	16.6	0.1	99.7	1.2	118.4	2.7	38.4	1.2
Joghurt		28.1	3.5	22.5	0.4	11.6	0.1	97.6	1.7	105.7	2.4	50.4	1.5
White		2.9	2.3	16.0	0.1	4.5	0.1	63.1	0.0	88.1	0.2	40.0	0.2
Milk and cereal		31.8	3.3	17.1	0.2	11.7	0.4	83.0	1.3	96.2	1.4	52.8	2.7
Hazelnut		59.1	10.9	10.4	0.1	14.5	0.3	85.3	0.7	100.8	2.8	34.1	0.7
Cookies		35.8	5.8	25.5	0.6	10.5	0.2	71.2	1.2	78.5	1.4	29.5	0.2
Milk chocolate		43.4	1.2	13.1	0.7	13.0	1.3	84.5	10.7	101.3	1.6	45.2	3.6
Cereals		35.3	1.2	25.0	1.0	11.7	0.4	73.6	2.6	89.8	1.6	29.5	2.7
Marzipan		125.2	0.3	0.6	0.7	30.6	0.3	96.3	3.2	114.4	5.6	25.0	2.1
Coconut		4.6	4.8	27.6	0.4	7.2	0.2	73.0	1.1	83.7	1.8	35.8	1.1
Himbeer-Cranberry Joghurt		26.9	2.2	18.9	0.2	11.5	0.0	85.1	0.1	94.8	2.2	55.9	1.6
Cookies and nuts		52.8	1.4	18.8	0.1	16.2	0.2	94.9	0.5	119.9	0.4	40.3	0.4
Alps milk chocolate		62.2	3.6	15.6	0.3	11.4	0.2	79.4	1.4	98.4	1.7	39.7	2.0
Erdbeer Joghurt		24.9	0.0	18.8	0.6	10.8	0.2	83.5	2.3	82.1	4.0	37.9	1.9
Dark Mousse		Merci	20.9	1.9	23.6	0.2	10.6	0.1	105.8	1.4	121.1	2.3	54.4
Cafe-Crème	27.8		1.9	22.5	0.8	11.6	0.4	96.7	3.0	122.7	5.9	48.9	2.0
Milk Praline	38.4		8.5	15.2	0.4	13.9	0.3	100.1	2.2	115.0	0.3	49.9	1.2
Hazelnut	80.3		3.9	15.9	0.1	27.2	0.2	137.2	2.1	140.1	5.6	80.3	0.7
Dark Cream	107.4		2.3	2.8	0.5	31.2	0.1	96.1	2.4	115.8	0.6	29.6	2.0
Marzipan	48.0		0.5	17.2	0.5	21.4	0.0	123.7	2.4	148.5	7.3	71.6	0.5
Almonds	37.0		2.8	14.9	0.9	14.3	1.5	95.0	7.3	105.2	4.2	40.3	3.9
Dark chocolate	Moser Roth	246.0	3.3	38.7	1.1	57.3	1.9	188.2	4.8	132.3	7.2	14.4	0.1
Dark chocolate		220.1	1.1	0.8	0.2	47.3	1.7	163.8	5.2	104.1	3.6	12.4	1.4
Milk chocolate		29.4	0.9	19.2	0.6	11.7	0.2	88.7	3.5	109.7	2.5	55.5	2.1
Bitter		33.7	0.6	23.8	0.4	10.9	0.0	81.9	0.8	80.6	0.9	32.7	0.4

Table 8.1 Continuation from previous page.

Type of chocolate	Commercial brand	Oxalate		Na		Mg		K		P		Ca	
		Total	SD	Total	SD	Total	SD	Total	SD	Total	SD	Total	SD
Dark chocolate	Moser Roth	281.1	4.2	37.9	0.9	53.0	1.4	192.2	4.5	106.1	1.5	14.7	1.9
Dark bitter	Herren Schokolade	205.1	1.5	4.4	0.3	42.1	1.5	146.0	6.0	107.8	1.4	17.1	2.3
Milk chocolate with almonds	Choceur	191.5	1.0	14.0	0.7	26.9	0.2	116.8	2.0	149.1	3.3	55.2	2.8
White		2.6	0.5	28.1	0.7	6.6	0.2	89.2	2.0	119.7	3.3	67.6	2.8
Bitter		91.2	1.4	11.7	0.0	21.8	0.0	106.9	0.3	109.4	4.8	34.1	0.6
Milk chocolate		36.2	1.7	18.1	1.0	12.7	0.6	101.4	5.6	125.7	6.6	45.7	4.9
Delicate bitter		249.7	6.9	29.6	0.6	55.2	1.3	243.1	5.3	107.4	3.2	15.6	1.3
Marzipan		8.7	0.0	25.9	1.3	5.4	0.4	80.7	6.6	84.1	5.8	41.5	3.8
Creamy milk chocolate		137.0	5.2	5.6	0.7	27.6	0.2	123.7	3.2	52.3	4.4	12.6	1.7
Milk and nuts		129.5	0.4	6.7	0.4	26.8	0.1	86.8	1.9	93.6	0.2	19.6	1.4
Milk chocolate		51.3	4.4	16.6	0.5	17.1	0.5	101.9	2.7	82.2	2.4	35.7	3.0
Alps milk chocolate		52.4	2.3	22.3	1.9	18.4	0.2	134.7	2.2	125.6	7.7	59.9	1.9
Hazelnuts		51.6	5.0	24.4	0.3	17.0	0.0	128.8	0.8	106.4	2.1	53.8	1.1
Grapes nuts		48.4	9.2	19.1	1.0	18.8	0.6	139.6	4.4	116.1	1.8	70.5	3.3
Coconut		29.9	2.6	16.6	0.6	12.1	0.6	105.6	4.1	68.9	3.0	22.4	2.3
Marzipan		Mirabell Mozartkugeln	103.3	1.2	4.8	0.3	19.8	0.9	71.8	3.3	80.6	5.6	18.3
Kakaobohnen	-	378.4	1.5	1.7	0.1	20.0	0.2	102.3	0.7	30.1	1.1	2.0	0.6
Milk Choc. w/ Honey and almond nougat	Toblerone	42.5	2.3	11.1	0.0	12.1	0.1	71.1	1.1	81.9	1.1	37.3	0.5
Milk chocolate	Schogetten	28.8	0.5	20.8	0.6	11.3	0.1	93.9	2.1	109.1	0.7	51.8	1.7
Bitter		39.6	0.5	16.9	0.9	12.4	0.6	82.6	3.4	75.7	2.7	29.4	3.1
White		19.9	0.5	27.8	1.0	9.9	0.3	99.7	2.9	117.3	4.8	52.0	3.4
Milk chocolate	Milka	34.3	1.1	23.6	1.2	13.7	0.2	111.6	4.5	121.5	3.8	49.0	2.9
Delicate bitter		102.0	2.4	16.2	1.6	26.0	1.6	135.9	9.3	104.8	9.5	42.4	8.5

Table 8.1 Continuation from previous page.

Type of chocolate	Commercial brand	Oxalate		Na		Mg		K		P		Ca		
		Total	SD	Total	SD	Total	SD	Total	SD	Total	SD	Total	SD	
White	Milka	32.9	1.6	25.4	1.2	12.5	0.2	117.2	2.2	108.5	2.8	44.9	1.7	
Milk chocolate	Gut & Günstig	48.6	1.4	20.5	0.3	15.2	0.4	110.4	2.2	90.4	2.8	55.9	0.2	
Milk and hazelnuts	Gut & Günstig	62.7	7.5	19.6	0.2	19.6	0.0	126.4	1.0	107.7	2.2	76.9	1.6	
Milk chocolate w/ walnuts	Nussknacker	46.8	4.0	18.9	0.6	17.1	0.2	115.0	2.3	115.7	4.3	58.9	0.6	
Caramel dark	Confiserie Premium Trüffel	25.9	0.0	13.1	0.4	9.3	0.3	72.4	3.5	76.9	0.9	30.9	3.5	
Cherry dark		31.2	0.1	13.7	0.4	10.6	0.7	76.4	3.7	72.0	1.1	36.5	0.6	
Orange dark		93.3	4.2	7.2	0.0	23.2	0.8	57.7	2.3	107.0	2.5	24.3	0.9	
Cream hazelnut		24.3	0.6	15.6	0.1	9.3	0.1	78.7	0.2	80.4	4.2	37.7	0.8	
Pistachio dark		101.4	0.3	5.9	0.3	27.4	0.2	121.0	0.8	74.5	2.2	23.1	0.4	
Lemon dark		4.1	0.0	17.3	0.2	4.2	0.1	61.5	4.3	69.1	2.0	40.2	0.7	
Latte Macchiato		3.6	0.0	16.9	0.3	4.4	0.3	65.4	0.2	64.7	0.7	32.8	0.7	
Vanille dark		4.4	0.0	14.9	0.4	3.3	0.0	52.7	2.0	52.4	1.1	28.4	1.0	
Cocoa powder		Bensdorp	619.3	14.4	13.8	0.1	56.8	0.0	384.1	0.1	144.2	1.7	13.6	0.3
Nougat Cream		Noccionlino	39.1	1.2	13.8	2.0	14.1	0.3	105.9	3.7	56.7	3.5	30.1	0.9
Shortbread Cookies (Hawaii)	Candies Big Island	21.9	0.3	0.0	0.4	0.0	1.2	2.2	3.2	1.6	2.9	0.5	1.7	
Caramel	Storck	43.4	4.8	71.3	0.0	25.1	0.5	136.8	0.5	117.5	3.9	56.7	0.5	
Original Schokolade	Dr. Oetker	115.3	0.3	68.5	0.1	29.3	0.8	174.9	4.4	40.9	1.0	12.8	1.9	
Bitter	Dr. Oetker	181.7	2.9	0.5	2.1	35.9	0.3	122.9	3.8	48.7	2.5	7.0	2.8	
Caramel	Crispy bits	17.7	1.0	45.7	1.4	8.7	0.4	93.1	5.2	76.5	1.3	31.2	3.8	
Milk chocolate	Lindt Excellence	28.3	0.6	26.4	0.1	11.9	0.3	103.7	0.8	86.5	0.8	47.8	1.3	
Milk chocolate	Ja	46.9	1.8	22.2	0.9	16.4	0.6	132.2	3.4	91.1	2.0	49.0	2.0	
Caramel	Mars	19.5	0.0	44.1	0.9	8.4	0.4	72.2	2.6	69.3	7.6	25.0	1.8	
Caramel	Bounty	18.0	0.2	27.7	0.8	9.9	0.2	87.7	3.0	55.9	6.7	19.8	2.3	
Milk caramel	Bounty	13.4	0.3	24.7	0.6	12.1	0.3	93.1	2.4	66.1	4.8	28.2	1.1	

Table 8.1. Continuation from previous page.

Type of chocolate	Commercial brand	Oxalate		Na		Mg		K		P		Ca	
		Total	SD	Total	SD	Total	SD	Total	SD	Total	SD	Total	SD
Caramel	Milky Way	14.0	0.4	51.4	0.2	6.5	1.1	71.0	4.9	73.5	2.3	27.6	1.9
Milk	Dove	19.7	0.2	22.4	0.2	11.1	0.1	107.9	0.6	98.2	1.5	52.9	0.0
Milk caramel	Dove caramel	12.4	0.5	41.8	1.5	9.5	0.3	99.4	5.6	103.9	5.4	44.4	2.6
Milk	Malteser	21.5	0.3	26.2	1.1	11.9	0.5	123.6	5.1	129.4	8.9	55.9	2.8
Schoka-Kola	Schoka-Kola	174.8	1.6	2.5	0.2	43.5	1.4	177.5	7.6	82.8	8.3	24.6	2.3
Caramel	Snickers	23.1	0.1	53.9	0.3	14.0	0.8	79.3	4.8	89.0	5.1	35.3	1.1
Caramel cookie	Twix	15.0	1.3	43.3	1.5	5.7	0.2	52.6	2.1	51.8	6.1	26.3	2.5
Hazelnut cream	Ferrero	90.6	4.6	7.8	0.0	17.9	0.4	115.0	1.9	91.1	1.4	31.1	0.9
Coconut		231.4	46.7	15.2	1.0	23.1	0.6	120.7	4.9	68.6	11.3	33.2	5.1
Hazelnut		87.8	0.9	21.6	0.4	21.3	0.1	109.5	1.4	115.3	6.4	54.2	1.6
Nuts		92.4	5.6	30.0	1.0	17.4	0.6	127.2	4.9	104.0	11.3	47.7	5.1
White		101.7	6.8	9.4	0.2	20.1	0.3	95.3	2.6	67.3	1.7	22.0	1.6
Joghurt		22.6	0.2	14.3	1.5	9.1	0.7	75.6	6.6	74.0	4.4	39.4	5.7
Hanuta		86.3	1.8	38.4	0.6	22.1	0.6	139.2	1.6	77.6	3.4	26.9	0.8
Milk chocolate		Ferrero Kinder	10.8	2.5	25.1	0.8	9.3	0.3	117.4	3.8	150.0	4.1	68.3
Milk chocolate		48.1	1.8	13.4	1.3	13.6	0.4	92.3	3.6	67.7	5.1	29.6	2.0
Mint chocolate	After Eight	49.7	1.2	3.7	0.6	11.8	0.0	47.4	1.8	24.5	1.1	19.9	1.0
Erdnuss	M&M	57.4	4.1	12.3	2.2	23.2	0.9	107.9	6.7	69.5	0.4	29.1	1.8
Peanuts	Mr. Tom	54.1	2.8	25.8	0.0	31.2	0.2	109.9	0.4	116.0	4.4	22.8	0.9

Table 8.2 Results of the chocolate samples analysis. Values correspond to the soluble amount (sample homogenized using H<sub>2</sub>O). Units: mg/100g chocolate (dry weight).

Type of chocolate	Commercial brand	Oxalate		Na		Mg		K		P		Ca	
		Total	SD	Total	SD	Total	SD	Total	SD	Total	SD	Total	SD
Nougat	Ritter Sport	13.0	7.8	3.1	0.0	1.5	0.1	21.9	0.1	18.7	3.5	1.9	0.3
Joghurt		3.7	1.8	20.7	0.9	6.4	0.2	81.9	3.2	72.0	5.0	20.7	2.3
White		1.1	0.0	13.0	0.3	2.5	0.0	52.4	0.7	45.4	0.7	10.5	0.1
Milk and cereal		6.4	0.7	16.1	0.2	4.9	0.2	71.3	1.6	57.4	1.5	26.1	2.2
Hazelnut		7.8	8.7	10.4	0.3	14.2	0.4	83.2	1.8	93.6	3.7	34.9	0.6
Cookies		6.5	2.3	21.3	0.8	4.0	0.1	57.5	2.1	42.1	0.8	10.3	1.5
Milk chocolate		5.7	0.1	14.0	0.2	7.0	0.1	81.8	0.3	66.2	0.8	32.0	0.3
Cereals		8.4	0.2	18.7	0.8	4.4	0.1	53.9	1.7	44.6	1.6	5.2	0.2
Marzipan		60.2	0.1	0.3	0.3	14.0	0.4	65.7	1.0	59.1	1.4	10.2	1.2
Coconut		1.1	3.2	22.9	0.4	4.1	0.1	67.6	1.3	50.4	1.3	4.9	0.2
Himbeer-Cranberry Joghurt		5.3	5.2	16.1	0.2	5.4	0.0	68.3	0.8	65.9	4.2	36.3	0.6
Cookies and nuts		6.2	0.2	13.3	0.4	4.6	0.1	62.3	1.6	46.0	1.2	3.6	0.3
Alps milk chocolate		5.0	1.0	16.1	0.3	5.7	0.0	76.1	1.1	61.5	2.2	19.2	0.1
Erdbeer Joghurt		4.7	0.5	17.0	1.1	6.3	0.3	70.3	2.9	66.8	3.0	17.7	1.6
Dark Mousse		Merci	33.0	0.4	5.9	0.4	15.5	0.2	93.0	1.9	74.0	0.7	8.4
Cafe-Crème	5.4		0.0	24.5	0.1	6.1	0.6	104.2	1.4	82.7	0.7	24.8	1.4
Milk Praline	5.8		0.4	19.4	0.1	4.9	0.0	79.6	0.6	63.2	3.1	16.9	0.8
Hazelnut	4.2		0.5	13.2	0.2	4.3	0.1	73.0	1.1	59.9	1.6	29.4	0.9
Dark Cream	8.5		2.0	15.1	0.1	18.8	0.7	129.3	2.2	104.1	3.0	32.6	1.1
Marzipan	44.5		0.4	2.3	0.4	11.9	0.1	63.4	2.4	44.2	2.0	7.8	1.9
Almonds	5.5		0.5	14.2	1.5	5.0	0.1	86.3	7.2	64.6	2.2	16.8	2.8
Milk chocolate	2.7		0.4	14.9	0.9	12.3	1.3	92.9	0.9	94.3	7.9	38.9	0.1
Dark chocolate	Moser Roth	147.1	0.3	26.0	0.7	23.3	0.6	114.0	3.2	70.7	0.0	7.5	0.9
Dark chocolate		129.7	1.8	0.6	0.0	21.3	0.1	97.5	0.7	60.8	1.0	2.2	0.2
Edel Vollmilch		3.5	0.5	17.0	1.0	4.7	0.2	74.7	4.0	61.8	3.7	17.2	1.1
Bitter		4.7	0.3	25.2	1.0	4.8	0.6	88.9	3.4	48.4	1.3	13.3	2.6



Table 8.2 Continuation from previous page.

Type of chocolate	Commercial brand	Oxalate		Na		Mg		K		P		Ca	
		Total	SD	Total	SD	Total	SD	Total	SD	Total	SD	Total	SD
Milk chocolate	Moser Roth	158.1	17.1	31.7	2.1	32.2	1.9	144.1	9.3	129.9	11.1	0.0	1.5
Dark bitter	Herren Schokolade	99.1	6.3	3.1	0.1	23.5	0.6	110.4	1.8	63.6	0.9	7.8	0.6
Milk chocolate with almonds	Choceur	109.5	0.0	10.5	1.0	5.3	0.1	70.7	2.4	50.7	2.0	11.9	0.1
White		1.2	0.2	24.1	1.0	3.2	0.1	74.0	2.4	58.2	2.0	16.0	0.1
Bitter		7.7	0.1	10.5	0.0	10.2	0.0	86.5	0.4	63.5	0.9	11.9	0.3
Milk chocolate		4.7	0.1	15.8	0.6	4.8	0.1	81.1	2.8	63.6	0.9	13.1	1.4
Milk chocolate		5.8	0.6	13.7	0.4	5.3	0.2	69.5	1.6	45.4	1.1	3.3	1.4
Delicate bitter		123.9	3.9	21.9	0.2	22.5	0.2	156.3	1.2	74.3	3.8	3.7	0.4
Marzipan		2.1	0.0	23.5	0.9	3.5	0.5	70.6	4.3	47.9	7.4	13.4	2.8
Creamy milk chocolate		90.6	11.3	5.0	0.3	22.5	0.4	97.0	2.5	95.1	6.8	0.6	1.6
Milk and nuts		56.8	3.5	5.8	1.0	11.5	0.5	61.0	4.6	44.4	5.1	4.6	2.2
Alps milk chocolate		4.8	0.4	17.7	1.8	5.8	0.1	94.0	2.3	67.7	3.0	17.7	1.9
Hazelnuts		6.5	0.6	20.5	0.4	5.9	0.0	96.9	1.6	62.5	0.9	12.8	1.7
Grapes nuts		5.6	0.7	13.2	0.2	7.6	0.1	110.7	0.7	79.0	0.9	24.6	0.3
Coconut		7.5	0.6	17.2	0.4	6.5	0.2	102.8	1.6	58.6	1.4	17.3	1.4
Marzipan	Mirabell Mozartkugeln	26.3	2.6	4.0	0.5	8.4	0.2	58.2	1.9	39.3	3.3	0.0	1.4
Cocoa beans	-	225.4	3.0	0.0	0.0	6.9	0.1	40.1	0.1	16.5	2.3	0.0	0.0
Milk Choc. w/ Honey and almond nougat	Toblerone	5.1	3.6	8.7	0.0	3.8	0.0	53.3	0.2	40.3	0.3	4.8	0.3
Milk chocolate	Schogetten	5.3	0.1	17.6	0.6	4.7	0.2	71.2	2.6	56.9	2.5	15.5	2.6
Bitter		6.6	0.8	14.0	0.7	4.8	0.2	58.7	2.9	43.9	1.2	6.5	1.6
White		5.1	0.0	23.2	0.5	5.3	0.1	83.4	2.0	69.1	6.5	13.5	0.9
Milk chocolate	Milka	5.1	0.1	20.4	0.4	5.8	0.0	88.3	1.7	65.5	4.3	13.9	1.8
Delicate bitter		8.8	0.7	12.7	0.4	8.8	0.2	96.1	2.5	60.2	4.1	12.3	1.3

Table 8.2 Continuation from previous page.

Type of chocolate	Commercial brand	Oxalate		Na		Mg		K		P		Ca		
		Total	SD	Total	SD	Total	SD	Total	SD	Total	SD	Total	SD	
White	Milka	7.0	0.3	22.7	1.2	5.9	0.2	103.2	2.1	70.8	0.9	15.9	1.8	
Milk chocolate	Gut & Günstig	6.1	0.9	14.6	0.1	4.8	0.1	73.5	0.2	49.0	0.4	7.0	1.4	
Milk and hazelnuts		5.3	0.5	16.9	0.2	6.7	0.0	96.0	1.0	66.2	2.2	15.7	1.6	
Milk chocolate w/ walnuts	Nussknacker	6.8	1.6	14.5	0.4	4.6	0.0	78.0	1.1	55.9	2.0	10.4	1.4	
Caramel dark	Confiserie Premium Trüffel	4.2	0.3	10.0	0.2	3.4	0.1	52.6	0.4	38.2	3.6	8.6	0.1	
Cherry dark		5.3	0.2	12.4	0.5	4.3	0.2	63.9	2.7	46.3	1.0	11.6	0.9	
Orange dark		28.2	7.5	4.5	0.0	9.9	0.1	46.9	1.4	75.0	1.5	9.6	0.4	
Cream hazelnut		4.3	0.2	14.9	0.1	4.4	0.0	70.1	0.2	48.6	5.9	12.8	0.3	
Pistachio dark		20.8	0.2	4.6	0.5	9.6	0.1	50.3	2.2	81.7	0.7	2.0	1.7	
Lemon dark		2.3	0.0	16.3	0.5	2.6	0.0	57.1	0.1	46.8	0.5	16.0	0.2	
Latte Macchiato		2.6	0.1	14.3	0.4	2.6	1.5	56.4	10.3	41.3	7.0	10.8	1.8	
Vanille dark		2.0	0.0	14.2	0.4	2.1	0.2	50.8	3.3	37.8	1.5	12.7	1.1	
Cocoa powder		Bensdorp	571.3	33.7	7.3	0.1	12.1	0.0	208.0	0.1	42.5	1.7	0.0	0.3
Nougat Cream		Noccionlino	8.7	1.5	8.3	0.1	3.1	0.0	66.8	0.1	31.5	0.1	4.7	0.6
Shortbread Cookies (Hawaii)	Candies Big Island	5.6	0.0	0.0	3.0	0.0	1.1	2.0	5.4	2.5	4.3	0.0	2.9	
Caramel	Storck	6.2	0.2	59.5	0.1	7.8	0.5	102.5	2.2	60.1	0.4	13.5	0.7	
Chocolate powder	Dr. Oetker	60.7	0.8	45.9	0.2	6.2	0.3	107.1	2.3	17.5	0.9	7.7	1.5	
Bitter		124.5	1.7	0.1	2.0	17.8	0.2	82.1	4.1	46.4	2.3	0.0	1.2	
Caramel	Crispy bits	4.9	0.3	43.9	1.1	5.2	0.2	90.4	3.0	59.4	2.0	15.6	1.1	
Milk chocolate	Lindt Excellence	4.6	0.4	22.9	0.1	4.8	0.0	86.0	1.8	59.0	0.1	16.0	0.0	
Milk chocolate	Ja	6.7	0.2	18.9	0.4	6.3	0.1	107.7	2.1	58.7	2.1	9.8	1.8	
Caramel	Mars	4.9	0.1	41.1	0.4	4.0	0.1	63.4	1.2	41.2	2.0	21.2	0.5	
Caramel	Bounty	5.1	0.5	22.9	1.3	4.3	0.2	70.8	3.6	36.5	6.8	18.1	2.3	
Milk caramel		4.2	0.1	21.3	0.1	5.0	0.1	72.7	0.2	38.0	2.8	8.8	0.8	

Table 8.2 Continuation from previous page.

Type of chocolate	Commercial brand	Oxalate		Na		Mg		K		P		Ca	
		Total	SD	Total	SD	Total	SD	Total	SD	Total	SD	Total	SD
Caramel	Milky Way	4.0	0.1	47.1	0.3	3.4	0.7	59.6	4.0	43.7	6.5	14.9	1.5
Milk	Dove	4.9	0.2	19.3	1.1	4.8	1.3	89.0	5.2	59.9	4.8	24.9	3.0
Milk caramel	Dove caramel	4.8	0.0	32.2	0.5	4.2	1.4	77.5	4.7	56.4	6.0	14.3	2.8
Milk	Malteser	6.0	0.2	21.0	0.8	5.4	0.2	96.3	4.2	70.3	3.1	19.8	2.4
Schoka-Kola	Schoka-Kola	90.6	0.9	1.7	0.1	23.9	0.9	125.5	4.0	91.7	3.8	1.7	1.3
Caramel	Snickers	6.1	0.5	49.6	1.1	4.6	0.1	80.9	1.3	55.1	0.0	31.0	1.8
Caramel cookie	Twix	5.5	0.1	33.9	0.7	2.6	0.1	46.9	1.2	28.9	4.5	5.8	1.0
Nutella	Ferrero	15.6	0.9	5.6	0.2	4.1	0.1	78.6	1.0	37.5	1.2	3.6	0.3
Coconut		4.9	1.2	11.0	0.9	4.7	0.3	79.1	6.2	42.9	6.1	7.7	1.3
Hazelnut		8.8	0.4	20.0	0.7	4.5	0.2	73.9	5.7	56.3	2.4	17.8	2.2
Nuts		16.3	2.0	27.6	0.2	7.1	0.4	113.2	1.2	72.6	0.7	23.5	1.2
White		19.3	1.6	8.7	0.5	6.1	0.0	75.1	3.2	47.2	1.7	7.9	1.7
Joghurt		5.4	0.9	12.6	0.3	8.6	0.1	73.4	1.2	69.7	3.1	38.9	0.0
Hanuta		30.5	2.2	31.5	0.7	8.1	0.1	108.5	1.8	51.4	1.5	6.7	2.1
Milk chocolate	Ferrero Kinder	3.4	0.0	18.5	0.9	5.1	0.2	87.7	3.8	70.5	5.0	21.6	2.2
Milk chocolate		9.7	0.4	11.0	0.4	4.5	0.1	72.3	1.0	44.6	0.5	11.4	0.0
Mint chocolate	After Eight	28.8	2.6	2.8	0.9	5.7	0.1	34.6	2.3	21.7	5.5	7.8	0.4
Erdnuss	M&M	10.5	0.1	9.8	1.1	5.3	0.1	70.9	2.7	42.3	0.5	12.1	1.0
Peanuts	Mr. Tom	13.9	1.4	18.4	0.1	4.4	0.2	66.8	2.4	36.2	0.2	6.5	0.9
Chocolate powder	Dr. Oetker	60.7	0.8	45.9	0.2	6.2	0.3	107.1	2.3	17.5	0.9	7.7	1.5

Table 8.3 Results of HCA classification. Each number corresponds to a different cluster, and samples are sorted into them according to distance criteria. Note that the number of clusters is decided arbitrarily (here the results show a classification based on 10 clusters).

Type of chocolate	Commercial brand	Cluster
Nougat	Ritter Sport	2
Joghurt	Ritter Sport	1
White	Ritter Sport	1
Milk and cereal	Ritter Sport	1
Hazelnut	Ritter Sport	1
Cookies	Ritter Sport	1
Milk chocolate	Ritter Sport	1
Cereals	Ritter Sport	1
Marzipan	Ritter Sport	3
Coconut	Ritter Sport	1
Himbeer-Cranberry Joghurt	Ritter Sport	1
Cookies and nuts	Ritter Sport	1
Alps milk chocolate	Ritter Sport	1
Erdbeer Joghurt	Ritter Sport	1
Dark Mousse	Merci	2
Cafe-Crème	Merci	1
Milk Praline	Merci	1
Hazelnut	Merci	1
Dark Cream	Merci	1
Marzipan	Merci	2
Almonds	Merci	1
Milk chocolate	Merci	1
Dark chocolate (85% cocoa)	Moser Roth	3
Dark chocolate (70% cocoa)	Moser Roth	3
Edel Vollmilch	Moser Roth	1
Bitter	Moser Roth	3
Milk chocolate	Moser Roth	1
Dark bitter	Herren Schokolade	3
Bitter	Dr. Oetker	3

Type of chocolate	Commercial brand	Cluster
Milk chocolate with almonds	Choceur	1
White	Choceur	1
Bitter	Choceur	3
Milk chocolate	Choceur	1
Delicate bitter	Choceur	3
Marzipan	Choceur	3
Creamy milk chocolate	Choceur	1
Milk and nuts	Choceur	1
Hazelnuts	Choceur	1
Milk chocolate	Choceur	1
Alps milk chocolate	Choceur	1
Coconut	Choceur	5
Grapes nuts	Choceur	1
Marzipan	Mirabell Mozartkugeln	2
Cocoa beans	-	4
Milk Choc. w/ Honey and almond nougat	Toblerone	1
Milk chocolate	Kinder Ferrero	1
Milk chocolate	Schogetten	1
Bitter	Schogetten	3
White	Schogetten	1
Milk chocolate	Milka	1
White	Milka	1
Delicate bitter	Milka	1
Milk chocolate	Gut & Günstig	1
Milk and hazelnuts	Gut & Günstig	1
Cocoa powder	Bensdorp	4
Nougat Cream	Noccionlino	5
Shortbread Cookies (Hawaii)	Candies Big Island	7

Table 8.3 Continuation from previous page.

Type of chocolate	Commercial brand	Cluster
Caramel	Storck	6
Milk chocolate w/ wallnuts	Nussknacker	1
Caramel dark	Confiserie Premium Trüffel	8
Cherry dark	Confiserie Premium Trüffel	8
Orange dark	Confiserie Premium Trüffel	9
Cream hazelnut	Confiserie Premium Trüffel	8
Pistachio dark	Confiserie Premium Trüffel	9
Lemon dark	Confiserie Premium Trüffel	8
Latte Macchiato	Confiserie Premium Trüffel	8
Vanille dark	Confiserie Premium Trüffel	8
Caramel	Crispy bits	1
Milk chocolate	Lindt Excellence	1
Milk chocolate	Ja	5
Caramel	Mars	6
Milk caramel	Bounty	5
Caramel	Bounty	5
Caramel	Milky Way	6
Milk	Dove	1

Type of chocolate	Commercial brand	Cluster
Milk caramel	Dove caramel	1
Milk	Malteser	1
Schoka-Kola	Schoka-Kola	3
Caramel	Snickers	6
Caramel cookie	Twix	6
Hazelnut cream	Ferrero	5
Coconut	Ferrero	5
Hazelnut	Ferrero	1
Nuts	Ferrero	1
White	Ferrero	5
Joghurt	Ferrero	1
Hanuta	Ferrero	5
Mint chocolate	After Eight	7
Milk chocolate	Ferrero Kinder	5
Erdnuss	M&M	5
Peanuts	Mr. Tom	5
Chocolate powder	Dr. Oetker	0

## **8.2. Determination of Oxalate absorption using isotopic labeling - Data tables (Section 4.4.**

Table 8.4 Concentration values used for the RSS calculations. Units: Volume (L), Density ( $\text{g}\cdot\text{cm}^{-3}$ ), Concentrations (mmol/l).

Sample	Volume	pH	Density	Na	K	Ca	Mg	$\text{NH}_4^+$	$\text{Cl}^-$	$\text{PO}_4^{3-}$	$\text{SO}_4^{2-}$	Creat.	Uric acid	Oxalate	Citrate
1	2.75	6.89	1.004	10.91	5.09	0.45	0.47	3.78	12.00	2.11	2.18	1.40	0.32	0.03	0.01
2	1.7	5.4	1.004	26.47	8.24	0.74	0.44	9.41	27.06	6.06	3.71	2.97	0.44	0.17	0.03
3	1.89	6.58	1.004	22.75	10.05	1.58	1.44	6.03	25.40	4.81	2.54	2.83	0.55	0.06	1.39
4	2.1	6.67	1.008	26.67	11.43	1.65	1.51	6.00	28.10	6.00	3.33	3.49	0.62	0.07	0.79
5	0.71	6.75	0	115.5	95.77	5.14	7.00	12.39	143.7	21.97	44.08	24.92	4.44	0.28	3.38
6	2.4	6.71	1.006	26.25	5.83	0.94	0.54	4.21	25.42	3.83	2.38	1.98	0.40	0.05	0.21
7	0.99	7.07	1.01	100.0	29.29	3.31	2.81	10.00	94.95	17.68	10.51	8.71	1.54	0.12	1.48
8	2.25	6.29	1.01	31.56	11.56	1.44	0.93	5.16	33.78	5.87	3.96	3.32	0.53	0.05	0.36
9	2.42	6.63	1.007	27.69	10.74	1.27	0.60	6.49	30.58	4.30	3.26	2.52	0.67	0.05	0.47
10	1.95	6.17	1.009	31.79	9.74	0.98	0.61	12.62	38.97	5.95	3.03	3.59	0.84	0.08	0.36
11	2.85	6.82	1.008	17.89	7.72	1.08	0.86	5.82	18.60	3.86	2.25	2.50	0.39	0.04	0.20
12	1.09	6.53	1.005	37.61	8.26	1.21	2.09	8.35	37.61	4.50	2.20	2.50	0.70	0.12	0.05
13	2.65	6.4	1.006	15.47	7.55	0.51	0.48	4.26	15.09	2.87	2.42	2.18	0.48	0.05	0.42
14	2.5	6.64	1.007	26.00	8.80	1.25	0.76	4.36	26.40	4.12	2.40	2.17	0.54	0.05	0.44
15	2.77	6.49	1.007	15.52	7.94	0.81	1.01	4.62	17.33	3.21	2.45	2.21	0.45	0.05	0.33
16	1.56	6.37	1.009	35.90	10.90	2.53	1.56	6.79	30.77	7.50	6.92	6.35	1.31	0.10	0.73
17	2.75	6.62	1.006	20.73	6.18	1.00	0.75	5.45	26.55	3.82	2.18	1.93	0.59	0.04	0.05
18	3.24	6.24	1.005	15.43	4.63	0.57	0.61	3.06	14.20	2.90	1.05	1.25	0.25	0.25	0.32
19	2.65	6.51	1.008	19.62	6.79	0.89	0.84	5.62	19.62	3.66	2.04	2.60	0.48	0.05	0.63
20	2.25	6.35	1.007	28.89	12.00	1.63	1.86	6.04	35.11	4.62	3.42	2.09	0.57	0.06	0.57
21	2.05	6.76	1.008	32.68	11.22	0.94	1.32	6.00	30.24	5.46	3.66	2.45	0.55	0.06	0.79
22	2.68	6.25	1.007	20.90	7.46	1.03	0.66	5.63	22.01	3.40	2.24	1.99	0.45	0.04	0.79
23	0.88	5.96	1.01	78.41	19.32	4.90	2.67	24.43	98.86	17.50	11.70	8.07	1.58	0.12	0.59
24	2.9	6.68	1.007	24.83	7.24	1.08	0.85	5.14	30.69	4.52	2.93	2.06	0.48	0.03	0.34
25	1.8	6.18	1.009	36.67	15.00	1.33	1.04	8.61	45.56	9.39	5.94	5.82	1.13	0.09	0.82
26	2.4	6.66	1.007	22.92	8.75	1.09	0.79	3.83	27.08	4.21	3.54	3.21	0.55	0.07	0.18
27	1.71	5.51	1.005	28.65	12.87	0.18	0.96	7.49	30.41	6.55	6.08	3.22	0.64	0.12	0.29
28	2.5	6.79	1.009	22.40	10.80	1.21	0.84	4.08	23.20	4.32	2.88	2.97	0.66	0.05	0.83

Table 8.5 Results from RSS calculations.

Sample	AP (CaOx)	RSS (COM)	RSS (COD)
1	$1.81 \cdot 10^{-08}$	4.0	3.4
2	$7.36 \cdot 10^{-09}$	1.6	1.4
3	$7.96 \cdot 10^{-08}$	17.7	15.1
4	$8.99 \cdot 10^{-09}$	2.0	1.7
5	$7.52 \cdot 10^{-08}$	16.8	14.3
6	$4.73 \cdot 10^{-08}$	10.5	9.0
7	$8.69 \cdot 10^{-08}$	19.4	16.5
8	$8.11 \cdot 10^{-08}$	18.1	15.4
9	$6.75 \cdot 10^{-08}$	15.1	12.8
10	$8.17 \cdot 10^{-08}$	18.2	15.5
11	$6.27 \cdot 10^{-08}$	14.0	11.9
12	$4.95 \cdot 10^{-08}$	11.0	9.4
13	$8.37 \cdot 10^{-08}$	18.7	15.9
14	$7.06 \cdot 10^{-08}$	15.8	13.4
15	$1.05 \cdot 10^{-07}$	23.4	19.9
16	$8.50 \cdot 10^{-08}$	18.9	16.1
17	$1.03 \cdot 10^{-07}$	22.9	19.5
18	$6.68 \cdot 10^{-08}$	14.9	12.7
19	$8.34 \cdot 10^{-08}$	18.6	15.8
20	$4.45 \cdot 10^{-08}$	9.9	8.4
21	$7.52 \cdot 10^{-08}$	16.8	14.3
22	$7.16 \cdot 10^{-08}$	16.0	13.6
23	$6.24 \cdot 10^{-08}$	13.9	11.8
24	$8.23 \cdot 10^{-08}$	18.4	15.6
25	$1.37 \cdot 10^{-08}$	3.1	2.6
26	$3.37 \cdot 10^{-08}$	7.5	6.4
27	$8.66 \cdot 10^{-08}$	19.3	16.4
26	$7.49 \cdot 10^{-08}$	16.7	14.2
27	$8.88 \cdot 10^{-08}$	19.8	16.9
28	$3.73 \cdot 10^{-08}$	10.4	9.3



Table 8.6 Correlation values for all the variables analyzed.

	Volume	pH	Density	Na	K	Ca	Mg	NH <sub>4</sub> <sup>+</sup>	Cl <sup>-</sup>	PO <sub>4</sub> <sup>3-</sup>	SO <sub>4</sub> <sup>2-</sup>	Creat.	Uric acid	Oxalate	Citrate	Ox. Absorp
Volume	1.000	0.060	-0.051	-0.341	-0.401	-0.083	-0.305	0.232	-0.264	-0.407	-0.531	-0.521	-0.412	0.219	-0.073	0.141
pH	0.060	1.000	0.326	0.461	0.309	0.576	0.462	-0.355	0.318	0.140	0.165	0.163	0.251	-0.282	0.374	-0.403
Density	-0.051	0.326	1.000	0.637	0.168	0.576	0.178	-0.017	0.500	0.579	0.122	0.372	0.230	-0.326	-0.065	-0.432
Na	-0.341	0.461	0.637	1.000	0.599	0.623	0.435	-0.234	0.869	0.765	0.559	0.550	0.470	-0.201	0.156	-0.488
K	-0.401	0.309	0.168	0.599	1.000	0.461	0.708	-0.183	0.684	0.561	0.929	0.781	0.769	-0.111	0.462	-0.399
Ca	-0.083	0.576	0.576	0.623	0.461	1.000	0.588	-0.264	0.556	0.533	0.386	0.539	0.491	-0.268	0.274	-0.380
Mg	-0.305	0.462	0.178	0.435	0.708	0.588	1.000	-0.353	0.481	0.317	0.622	0.494	0.449	-0.130	0.435	-0.529
NH <sub>4</sub> <sup>+</sup>	0.232	-0.355	-0.017	-0.234	-0.183	-0.264	-0.353	1.000	0.061	-0.045	-0.277	-0.206	0.055	-0.092	-0.074	0.382
Cl <sup>-</sup>	-0.264	0.318	0.500	0.869	0.684	0.556	0.481	0.061	1.000	0.712	0.608	0.564	0.590	-0.253	0.114	-0.477
PO <sub>4</sub> <sup>3-</sup>	-0.407	0.140	0.579	0.765	0.561	0.533	0.317	-0.045	0.712	1.000	0.572	0.752	0.621	-0.096	0.124	-0.241
SO <sub>4</sub> <sup>2-</sup>	-0.531	0.165	0.122	0.559	0.929	0.386	0.622	-0.277	0.608	0.572	1.000	0.863	0.782	-0.103	0.317	-0.406
Creat.	-0.521	0.163	0.372	0.550	0.781	0.539	0.494	-0.206	0.564	0.752	0.863	1.000	0.827	-0.127	0.211	-0.341
Uric ac.	-0.412	0.251	0.230	0.470	0.769	0.491	0.449	0.055	0.590	0.621	0.782	0.827	1.000	-0.172	0.357	-0.184
Oxalate	0.219	-0.282	-0.326	-0.201	-0.111	-0.268	-0.130	-0.092	-0.253	-0.096	-0.103	-0.127	-0.172	1.000	-0.057	0.337
Citrate	-0.073	0.374	-0.065	0.156	0.462	0.274	0.435	-0.074	0.114	0.124	0.317	0.211	0.357	-0.057	1.000	-0.127
Oxalate absorpt	0.141	-0.403	-0.432	-0.488	-0.399	-0.380	-0.529	0.382	-0.477	-0.241	-0.406	-0.341	-0.184	0.337	-0.127	1.000

### **8.3. Published Article: Journal of Biomedical Optics (Section 2.2.)**

# Journal of Biomedical Optics

SPIEDigitalLibrary.org/jbo

## **Hyperspectral imaging based method for fast characterization of kidney stone types**

Francisco Blanco  
Montserrat López-Mesas  
Silvia Serranti  
Giuseppe Bonifazi  
Josef Havel  
Manuel Valiente



# Hyperspectral imaging based method for fast characterization of kidney stone types

Francisco Blanco,<sup>a</sup> Montserrat López-Mesas,<sup>a</sup> Silvia Serranti,<sup>b</sup> Giuseppe Bonifazi,<sup>b</sup> Josef Havel,<sup>c,d,e</sup> and Manuel Valiente<sup>a</sup>

<sup>a</sup>Universitat Autònoma de Barcelona, Centre Grup de Tècniques de Separació en Química (GTS), Unitat de Química Analítica, Departament de Química, 08193 Bellaterra, Spain

<sup>b</sup>Sapienza–Università di Roma, Dipartimento di Ingegneria Chimica Materiali Ambiente, 00184 Roma, Italy

<sup>c</sup>Masaryk University, Department of Chemistry, Faculty of Science, Kamenice 5/A14, 625 00 Brno, Czech Republic

<sup>d</sup>Masaryk University, Department of Physical Electronics, Faculty of Science, Kotlářská 2, 611 37 Brno, Czech Republic

<sup>e</sup>Masaryk University, R&D center for low-cost plasma and nanotechnology surface modifications, Kotlářská 2, 611 37 Brno, Czech Republic

**Abstract.** The formation of kidney stones is a common and highly studied disease, which causes intense pain and presents a high recidivism. In order to find the causes of this problem, the characterization of the main compounds is of great importance. In this sense, the analysis of the composition and structure of the stone can give key information about the urine parameters during the crystal growth. But the usual methods employed are slow, analyst dependent and the information obtained is poor. In the present work, the near infrared (NIR)-hyperspectral imaging technique was used for the analysis of 215 samples of kidney stones, including the main types usually found and their mixtures. The NIR reflectance spectra of the analyzed stones showed significant differences that were used for their classification. To do so, a method was created by the use of artificial neural networks, which showed a probability higher than 90% for right classification of the stones. The promising results, robust methodology, and the fast analytical process, without the need of an expert assistance, lead to an easy implementation at the clinical laboratories, offering the urologist a rapid diagnosis that shall contribute to minimize urolithiasis recidivism. © 2012 Society of Photo-Optical Instrumentation Engineers (SPIE). [DOI: 10.1117/1.JBO.17.7.076027]

Keywords: kidney stone; hyperspectral imaging; artificial neural networks; renal calculi characterization.

Paper 11631 received Oct. 28, 2011; revised manuscript received May 30, 2012; accepted for publication Jun. 26, 2012; published online Jul. 25, 2012.

## 1 Introduction

Urolithiasis, the formation of calculi within the urinary tract, is a rather common disease, which affects approximately 10% to 12% of the population in developed countries.<sup>1</sup> In this field, much effort has been done,<sup>2</sup> basically addressing the reduction of the recidivism rates and the increasing of the quality of life of patients, while cutting the medical costs for related treatments and surgery.

A careful study of the structure of the expelled kidney stone can give key information on the stone formation process and the urine conditions during the crystal growth.<sup>3</sup> Thus, by specifically analyzing the core and outer shells of the sample, it is possible to determine the material that was serving as the precipitation nucleus and the substances that were precipitating afterwards. This information will provide a robust diagnosis that could lead to the appropriate treatment for every patient.

So far, several methodologies have been developed for the classification of kidney stones. The most extended ones are the examination of kidney stones by stereoscopic microscopy<sup>3,4</sup> and infrared (IR) analysis.<sup>5,6</sup> The former has an advantage in which it allows the identification of different substances on the whole area of the sample; so it is possible to fully determine the morphological characteristics of the stone. However, this methodology is laborious and, more significantly, it is strongly dependent on the operator. Concerning IR methodologies, they

require grinding the sample losing so the possibility of any spatial analysis.

In addition, the use of other techniques, namely near infrared (NIR),<sup>7</sup> scanning electron microscopy-energy-dispersive X-ray spectroscopy (SEM-EDS),<sup>8</sup> and even X-ray diffraction,<sup>9</sup> has also been assessed. NIR spectroscopy showed a good performance for the determination of the composition of renal calculi and quantification for mixtures. Nevertheless those works still require some sample pretreatment which makes the analysis impractical to be applied in hospital facilities.

### 1.1 Hyperspectral Imaging Technique

Hyperspectral imaging (HSI) or chemical imaging technique is based on the utilization of an integrated hardware and software architecture able to measure a spectrum for each pixel of the acquired image, being then possible to characterize the whole surface of the sample,<sup>10,11</sup> characteristics really useful for the objectives of the present work. It is desirable to analyze samples with flat surface because it always yields a better spectrum as the signal-to-noise (S/N) ratio increases due to better recording of the reflected radiation from the sample to the detector.

The acquired information is contained in a three-dimensional (3-D) dataset, characterized by two spatial dimensions and one spectral dimension, the so-called “hypercube”. According to the different wavelength and the spectral sensitivity of the device, several physical-chemical characteristics of a sample can be investigated and analyzed. For these reasons, HSI techniques

Address all correspondence to: Manuel Valiente, Universitat Autònoma de Barcelona, Centre Grup de Tècniques de Separació en Química (GTS), Unitat de Química Analítica, Departament de Química, 08193 Bellaterra, Spain. Tel: 34 93 581 2903; Fax: 34 93 581 1985; E-mail: Manuel.Valiente@uab.cat

represent an attractive solution for characterization, classification, and quality control of different products in many different fields, such as pharmaceuticals,<sup>12,13</sup> medicine,<sup>14,15</sup> food inspection,<sup>16,17</sup> artworks,<sup>18</sup> and materials recycling.<sup>19–22</sup>

There are two conventional ways to construct the hypercube; the first one known as the “staring imager” configuration and the second known as “pushbroom” acquisition.

The “staring imager” configuration keeps the image field of view fixed, obtaining images one wavelength after another.<sup>23</sup> Hypercubes obtained using this configuration thus consist of a three-dimensional stack of images (one image for each wavelength examined), stored in band sequential (BSQ) format. Wavelength in the “staring imager” configuration is typically moderated using a tuneable filter being the acousto-optic tuneable filters (AOTFs) or the liquid crystal tuneable filters (LCTFs), the most predominantly employed. AOTFs have been used in the construction of commercially available NIR-CI systems. The main advantages of AOTFs are the good transmission efficiency, fast scan times, and large spectral range. On the other hand, LCTFs show greater promise in filtering of Raman images due to the superior spectral bandpass and image quality.

The “pushbroom” configuration is based on the acquisition of simultaneous spectral measurements from a series of adjacent spatial positions, which require relative movement between the object and the detector.<sup>24</sup> Some devices produce hyperspectral images based on a point step and acquire mode: spectra are obtained at single points on a sample, then the sample is moved and another spectrum taken. Hypercubes obtained using this configuration are stored in the band interleaved by pixel (BIP) format. Advances in detector technology have reduced the time required to acquire hypercubes. Line mapping instruments record the spectrum of each pixel in a line of sample which is simultaneously recorded by an array detector; the resultant hypercube is stored in the band interleaved by line (BIL) format.

In this study, a “pushbroom” configuration was adopted, based on the utilization of a device of the ImSpector™ series spectrometers, developed by SpecIm™ (Finland). The spectrographs are constituted by optics based on volume type holographic transmission grating.<sup>10</sup> The grating is used in patented prism-grating-prism construction (PGP element), characterized by a high diffraction efficiency, good spectral linearity, and nearly free geometrical aberrations due to the on-axis operation principle.

For handling of the huge amount of data available from HSI, chemometric techniques are required. Principal component analysis (PCA) is usually used for screening the raw data before the application of a classification technique such as artificial neural network (ANN). ANNs show an ever-increasing number of applications in many fields, since they can satisfactorily solve complex analytical problems.<sup>25–27</sup> Although simple in structure, the vast number of interconnections inside the ANN structure show an interesting potential for calculations.

The aim of the present study is to evaluate the application of HSI in the NIR field (1000 to 1700 nm) for the characterization and classification of renal calculi with the help of ANN, as this would be helpful for medical diagnosis, improving the conventional characterization done so far. In fact, HSI seems to be an interesting possibility to implement in hospital analyses where kidney stone samples have to be analyzed. This technique has already been used for testing a resolution method by analyzing two examples of kidney stones<sup>28</sup> and it has also been proved to

be useful for other medical applications such as surgery monitoring.<sup>29,30</sup> However, HSI has not been deeply used for the study of kidney stones, once removed from the human body, or for the classification of the different types of kidney stones. On the other hand, ANNs have already been used in medicine with good results, even in urology,<sup>31</sup> where the main applications have been related to cancer diagnostics and other illnesses, although they have never been used for the classification of kidney stones.

## 2 Materials and Methods

### 2.1 Sample Preparation

Two hundred and fifteen samples were selected from a library of more than 1400 renal calculi. Samples were collected at the urology service of the Hospital, Universitari de Bellvitge, Barcelona (Spain). All kidney stones were obtained either by surgical removal or by natural expulsion. After collection, the stones were thoroughly rinsed with water and ethanol. Once cleaned, the stones were stored in individual clean vials showing no decomposition or damage in the structure during periods longer than a year.

Eleven types of different kidney stone components, including their mixtures, were considered. Firstly, seven main types of kidney stones were considered as formed by the pure compounds: uric acid anhydrous (AUA), brushite (BRU), calcium oxalate dihydrate (COD), calcium oxalate monohydrate (COM), cystine (CYS), hydroxyapatite (HAP), and struvite (STR). Secondly, mixtures of the former ones, namely: uric acid dihydrate (AUD), mixed calcium oxalate and hydroxyapatite (MXL), mixed calcium oxalate and hydroxyapatite (MXD), and COD transformed into COM (TRA) were analyzed. The selection criterion was based on variability appearance, for each type of stone.

For HSI technique, it is desirable to get a flat surface for the analysis, so all the samples were cut with a surgical knife, although it was also possible to measure and correctly classify round parts of stones. The inner part of the whole sample was used for the analysis, since the equipment allows the measurement of the entire stone. Besides, the use of the complete stone helped on the characterization of all its parts, contributing to the correct classification of each sample. Many samples showed a heterogeneous surface. In those cases, both the external part of the stone and the core were analyzed.

### 2.2 Conventional Methodologies

Samples were firstly analyzed by means of stereoscopic microscopy. The analyses were carried out as described in the reported bibliography.<sup>3,4</sup> For those samples that were not well characterized by this method, an SEM-EDS analysis was performed.<sup>8</sup> For this purpose, two different SEM equipments were used: JEOL JSM-6300 Scanning Electron Microscope (Japan), coupled to an Oxford Instruments Link ISIS-200 (UK) X-Ray Dispersive Energy Spectrometer (Univ. Autònoma de Barcelona); and a HITACHI S2500 (Japan) Scanning Electron Microscope, coupled to a KeveX 8000 (USA) X-Ray Dispersive Energy Spectrometer (Univ. “La Sapienza” of Rome). The structure of the samples was analyzed, and the EDS analysis was performed on some parts of the stone to confirm the elemental composition of the sample. Some representative results are shown in Figs. 1 and 2.

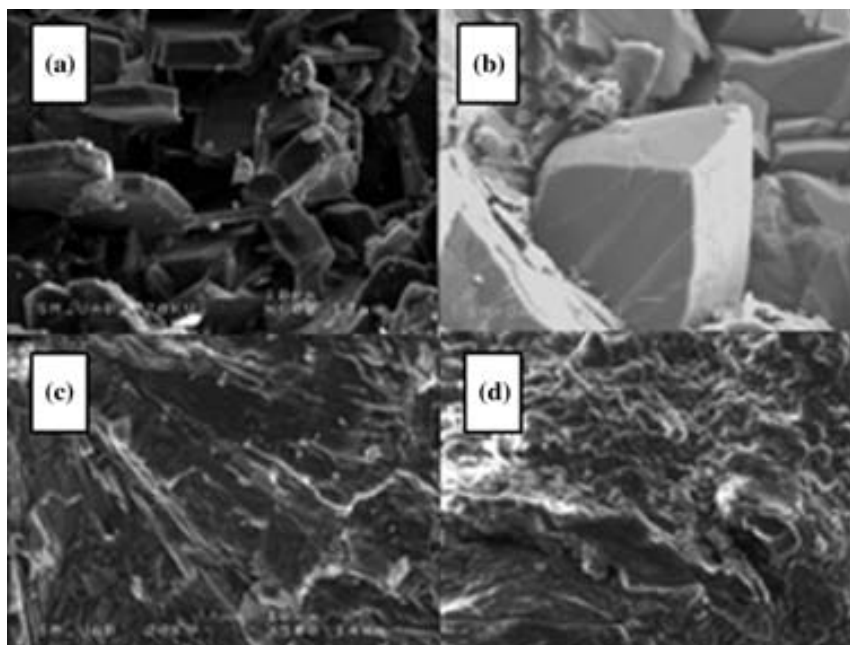


**Fig. 1** SEM images of the internal part of some kidney stones. (a) AUD, (b) COD, (c) COM, and (d) HAP.

The results coming out from these conventional methodologies were used as references for the results obtained from HSI data.

### 2.3 Hyperspectral Imaging Device and Architecture Set-Up

The HSI system used (Univ. “La Sapienza” of Rome) was constituted by the following components: optics, spectrograph, camera, translation unit, energizing source, and control unit (Fig. 3). The core of the system was a spectral camera NIR (Specim, Finland) embedding an ImSpector™ N17E imaging spectrograph working in the wavelength region 1000 to 1700 nm and a Te-cooled InGaAs photodiode array camera (spatial resolution: rms spot radius <math><15\ \mu\text{m}</math>; spectral resolution: 7 nm; 121 wavelengths measured).

The spectrometer was coupled to a 50 mm lens. The resolution of the image width was 320 pixels, while the number of frames, that is, the resolution of the image in the  $Y$  axes varied

from 200 to 350 pixels, depending on the number of samples measured at a time.

The energizing source was constituted by a diffused light cylinder with aluminium internal coating, embedding five halogen lamps that produce an intense and continuous spectrum signal, which was optimized for the NIR region.

The spectral camera was hosted in a laboratory platform equipped with an adjustable speed (from 0 to 50 mm/s) conveyor belt (width = 26 cm and length = 160 cm). Spectra acquisition can be carried out continuously or at specific time intervals. The device was fully controlled by a PC unit equipped with the Spectral Scanner™ v.2.3 acquisition/preprocessing software (DV srl, Italy).

The spectra of the samples were measured fixing them to a plastic holder with the inner side upwards, so the core was visible to the detector.

The stones previously classified as pure compounds, by means of conventional methodologies, were used for creating a library of compounds, which could be later applied for the classification of unknown samples.

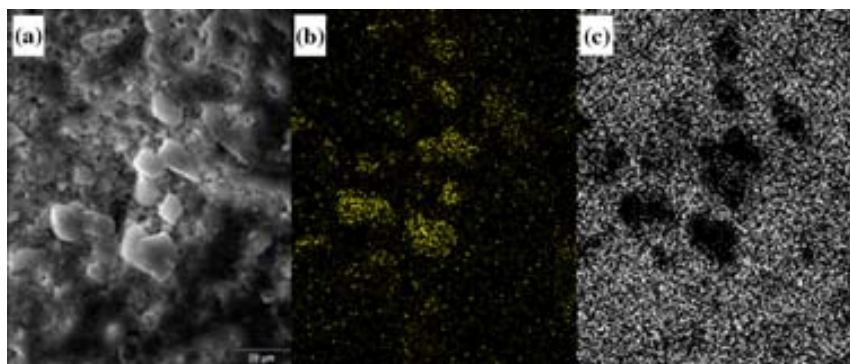


**Fig. 2** Mapping experiments on the surface of a kidney stone. (a) SEM image of some a struvite kidney stone; (b) mapping for Mg; and (c) mapping for Ca.



**Fig. 3** HSI based architecture employed for the acquisition of the kidney stones spectra.

## 2.4 Spectra Handling

The acquisition of the spectral signatures was carried out after a preliminary calibration performed in two steps: i) black image acquisition and ii) measurements of “white reference image” using a standard white ceramic tile. After the calibration phase, the spectral image was acquired and the reflectance ( $R$ ) was computed according to the following equation:

$$R = \frac{r_s - r_b}{r_w - r_b},$$

where  $r_s$  is the reflectance measured for the sample,  $r_b$  is the reflectance measured for the black (background noise), and  $r_w$  is the reflectance of the standard white (100% reflectance).

The analysis of the stones was performed on five randomly selected region of interests (ROIs) on the surface of the sample in order to avoid the selection of any part of the stone that might contain organic matter. Then, all the regions in a sample were considered as a single sample for data treatment. Although the ROIs analysis loses the information for every single pixel, it has two main advantages. First, it is a way of smoothing the data, since the surface of the sample might not be homogeneous considering adjacent pixels due to organic matter which could have been trapped into the structure of the stone during the crystallization process. Second, the amount of information that is going to be handled is much smaller than in the analysis of the full pixel matrix.

Additionally, an image analysis for each individual pixel was performed using a PCA treatment to show the capabilities of this technique for handling entire images on the classification process.

## 2.5 Data Treatment

For the analysis of the data, three different methods were used: factor analysis (FA), PCA, and ANN.

Although FA and PCA share the same main goal, that is, the reduction of the number of variables of the system by finding latent connections between real variables, they have a basic difference that allows obtaining different information.<sup>32</sup>

FA is based on correlation between variables, and the number of factors considered descriptors of the system is selected according to the associated eigenvalue.<sup>33,34</sup> Several criteria have been suggested in order to decide this number of factors. Kaiser’s rule, which states that only those factors with an associated eigenvalue greater than 1 are representative for the system,<sup>32</sup> has been applied in this study. All other factors stand for linear combinations of real variables, describing only noise.

On the other hand, PCA is based on the variance of the data.<sup>35</sup> Therefore, the main principal component (PC) for the system follows the direction in which the data have a bigger variance.

Due to these properties, FA was used to check how many different components can be distinguished in all the samples, while PCA was useful for the variable selection.

With regard to ANNs, they are considered a sophisticated and powerful computational tool which solves difficult analytical problems by learning from real cases. An ANN is a computational model formed from a certain number of single units, artificial neurones or nodes, connected with coefficients (weights),  $w_{ij}$ , which constitute the neural structure. Despite many different structures that ANNs can take, already described in the literature,<sup>25,36</sup> the structure used in this study was constituted by three layers: inputs, one hidden layer, and outputs. The input layer receives the information about the system (the nodes of this layer are simple distributive nodes, which do not alter the input value at all). The hidden layer processes the information initiated at the input, while the output layer is the observable response or behavior. The algorithm chosen for the learning process was the backpropagation. The optimization of the ANN was carried out by minimizing the root mean square (RMS) error,<sup>37</sup> when modifying the number of nodes in the hidden layer.

## 2.6 Software

HSI data has been treated using the following software: STATISTICA (Tulsa, OK);<sup>38</sup> The Unscrambler v 9.1 (Camo Process, Oslo, Norway);<sup>39</sup> MATLAB v 7.0 (MA, USA),<sup>40</sup> PLS toolbox by Eigen-vector Research, Inc. and TRAJAN v 3.0 (Horncastle, UK).<sup>41</sup>

## 3 Results

### 3.1 Factor Analysis

The software STATISTICA was used to perform FA on the data. The data used for this analysis was the spectra corresponding to the seven types of different components, since they represent the whole variety of substances studied.

Figure 4 shows how the weight of the Eigenvalue associated to each factor decreases for less important factors, being the seventh factor the last one having a value greater than 1. According to Kaiser’s rule, it can be seen that FA distinguishes the main species forming renal calculi.

Taking into account these results, a PCA analysis was carried out in order to create a model that is able to classify the different types of kidney stones analyzed.

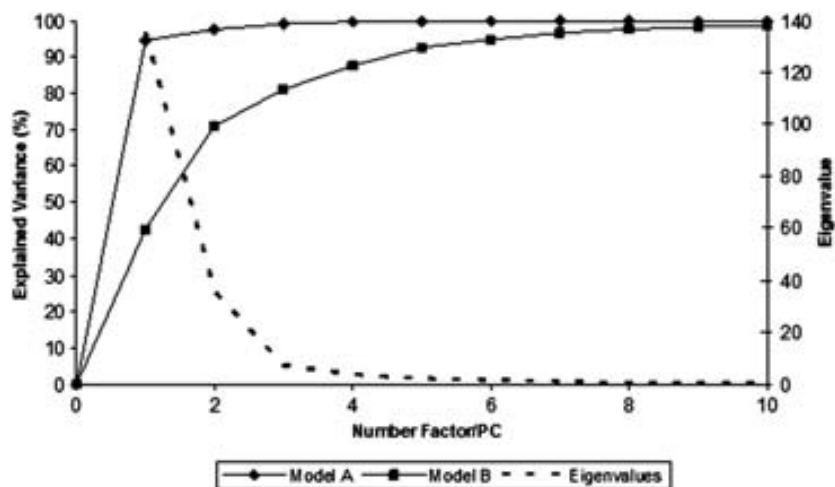


**Fig. 4** Eigenvalues for the seven main groups of renal calculi and explained variance for the PCA model. Model A: reflectance data, Model B: first derivative.

### 3.2 Principal Components Analysis

PCA was used for screening the spectral data. It was useful for selecting variables before performing the classification, which was made using ANNs.

#### 3.2.1 PCA on each type of renal calculi: identification of outliers

To determine the existence of outliers within the raw data, a PCA analysis was performed on the seven types of kidney stones, including each type of different samples of the same chemical composition. The data was cleaned in order to have a more reliable database.

The elimination of any point from the original samples is a crucial step, since it decreases the variability of the system. Moreover, there is no way to be completely positive whether a sample is correctly considered as an outlier. Hence, the criterion for the determination of outliers was based on the variability of the spectra. Due to the biological nature of the samples, the structure of the crystals that form the kidney stone might contain organic matter. Moreover, the surface measured may not be completely regular (even after cutting with a surgical knife), thus having a reflectance value differing from the average of the group.

The software ‘The Unscrambler’ was used to perform PCA analysis on 5 ROIs for every type of each group of samples considering each ROI as a different sample in terms of the software application. In this very first step, the whole range of variables was taken into account for the calculations, that is, 97 variables. By organizing the data, it was possible to check if any of the regions or even a whole sample was really different from the rest.

A point was considered an outlier if it was located outside the Hotelling  $T^2$  ellipse of the scores plot. Nonetheless, a sample was not considered if many regions of it were in such a position. In this way, the over-fitting of the data was avoided.

#### 3.2.2 PCA on the seven main groups of renal calculi

After cleaning the data, a PCA was performed on the seven main groups of renal calculi in order to create a model able to correctly classify the kidney stones studied. This model was

done taking all variables into calculation. The efficiency was checked by means of cross-validation and all data was mean centered.

Firstly, the model was directly calculated from the acquired reflectance spectra. Figure 4 Model A shows that, in this case, the two first PCs stand for the 95% of the variance of the model, having the rest of PCs a really low value.

In order to get a wider distribution of the variance of the data, the first derivative of the raw spectra was calculated. This step requires a previous smoothing of the data, which was done by means of the Savitzky-Golay algorithm, using a 5-point window. In this case, a much distributed explanation of the variance is seen; namely, up to 7 PCs are needed to explain the 96% of the variance for the model (Fig. 4 Model B).

Consequently, it can be concluded that first derivative magnifies the slight differences existing between the seven groups of renal calculi. For this reason, the first derivative of the spectra was used for further treatment of the data.

#### 3.2.3 Variable selection

Multivariate methods can certainly give a higher amount of information than univariate ones, though many variables from the measured range might not give valuable data, but noise. In this sense, we can take advantage profit from the fact that one of the basic statements of PCA is the reduction of number of variables, by taking only the information contained in the independent variables. Actually, not all the regions of the NIR spectrum give relevant information to the model. Then, by choosing those wavelengths with the greatest classification capabilities, the noise of the system is reduced thereby increasing its precision and simplifying the calculations.

To achieve this goal, the selection of variables is based on their loading value. In a PCA analysis, the loadings stand for the weight that every real variable has on each of the principal components. The wavelengths to be taken into further calculations are those that have a highest value for the loading for each PC. The representation of the loadings of every wavelength for each PC (Fig. 5) is a clear way to see the most important wavelengths, since it can be seen which regions of the spectrum are mostly influencing for a given PC. On the other hand, the regions of the spectrum that have a bigger weight on a given



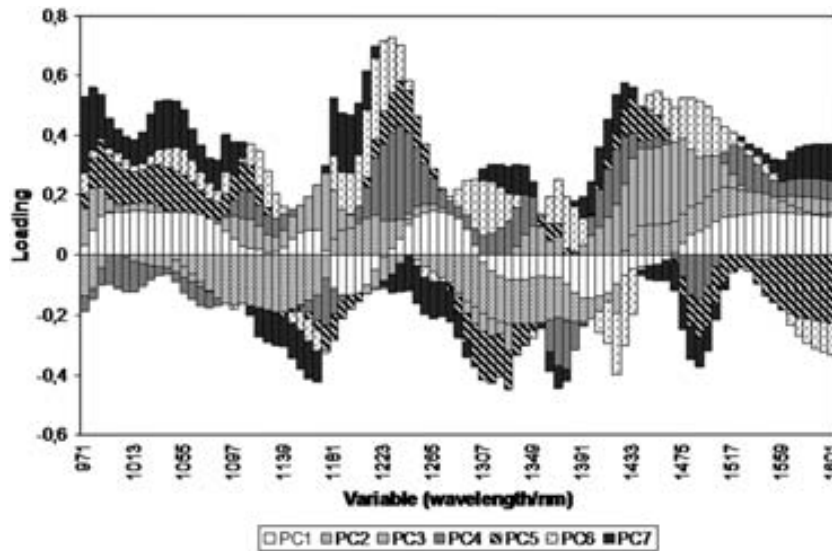


Fig. 5 Loadings of each variable for the seven first PCs.

PC should correspond to the vibration wavelength of the compound classified by this PC.

Following the above mentioned path, it was possible to define the variables defining every compound from the information in Fig. 5 and the representation of the scores values, see results in Table 1.

### 3.3 ANN: Optimization of the Neural Network

The software 'TRAJAN' was used for creating the ANN model, using the first derivative of the reflectance spectra measured.

The raw data of the spectra contain all the measured wavelengths, so in order to decrease the number of variables in the system 50 wavelengths were selected according to the values of the loadings for each wavelength, as shown in Fig. 5. In this way, a matrix of 140 samples (seven main types of kidney stones) and 50 variables was used for the analysis.

The ANN to be optimized was defined as: (inputs, number of nodes in the hidden layer, outputs), where inputs stand for the number of samples used to create the model, and outputs, the number of types of kidney stones, that is (140, n, 7). The value for the outputs was a single variable, which could take up to seven different nominal values.

The algorithm used for the optimization of the structure was the backpropagation. After the optimization of the ANN, it was seen that the optimum number of nodes in the hidden layer was four, and the value after which a non decrease in the RMS error<sup>24</sup> was observed. To avoid an overfitting of the model, no more nodes were used.

## 4 Discussion

### 4.1 PCA and Variable Selection

It has been seen that PCA allows for the determination of the main variables that define the system. For instance, the scores and loadings for PC2 can be also analyzed (see Fig. 6). In this case, AUA and CYS have opposite scores sign, meaning that PC2 is clearly differentiating between these two components. PC2 is well defined with positive loading values for wavelengths from the ranges 1188 TO 1230 nm and 1440 to 1542 nm. All these vibrations are associated to C–H bond vibrations. This association perfectly fits with the structure of cystine, since this is the only component of the studied set which has C–H bonds. On the other hand, wavelengths 971 to 978 nm and 1083 to 1167 nm have negative loading values for PC2. In

Table 1 Characteristic NIR vibrations for each type of renal calculi.

Type of kidney stone	Characteristic PC	$\Delta$ with highest loading (nm)	Associated NIR vibrations
CYS	PC1 < 0 ... PC2 > 0	1188–1230, 1440–1542	CH, CH <sub>2</sub> , CH <sub>3</sub>
AUA	PC1 < 0 ... PC2 < 0	971–978, 1083–1167	Ar-OH
COD COM	PC3 > 0 ... PC2 > 0 PC3 < 0 ... PC4 > 0	1426–1475	H <sub>2</sub> O
BRU	PC3 < 0 ... PC4 < 0	1223–1244	CH
HAP STR		Not well defined	

this case, the associated bond vibrations are the Ar-OH, which can be related only to AUA.

Additionally to this case, some other data defining the rest of compounds can be observed in Table 1. Clearly, the vibration differentiating COM and COD is the band for water.

It can be appreciated that the NIR bands that define BRU appear in the range of C-H vibrations. This fact might be explained due to especially high amount of organic matter contained in BRU calculi, since no C-H bonds are found in brushite structure.

The main drawback the PCA has shown was the difficulty to distinguish HAP and STR results which can be clearly seen in Fig. 6, where these two compounds appear as two overlapped clusters. These results can be understood because of their very similar composition. Struvite calculi are basically hydroxyapatite stones with a variable amount of struvite crystals spread within the whole stone. It means that most of the sample is similar to a pure HAP kidney stone.

Though the only exception of HAP and STR renal calculi, the PCA analysis has shown to be useful for the classification of the components of kidney stones.

#### 4.2 Image Analysis

A different PCA analysis was also performed on the seven groups of kidney stones, taking directly the hyperspectral cube and using the software MATLAB.

One sample from each type of kidney stone was analyzed, getting a classification pixel-by-pixel. As in the previous PCA, the data used was the first derivative of the spectra and the data were again mean centered.

Some samples considered pure compounds (as characterized by means of stereoscopic and SEM-EDS microscopies) were used to create a model for later classification of unknown samples.

The identification of the different compounds was done by interpretation of the colors obtained when creating reconstructed RGB images from the hyperspectral cube. When using this kind

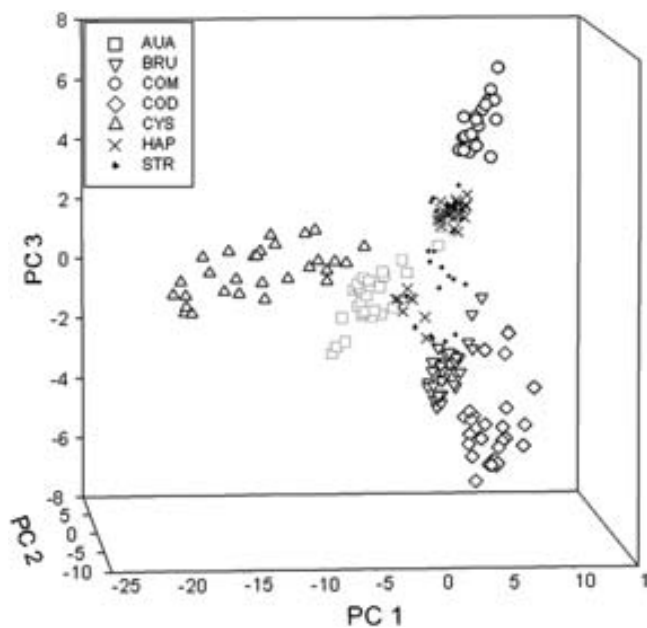


Fig. 6 3D representation of scores for PC1, PC2, and PC3.

of representation, the scores values for each of the 3 PCs used for the plot will determine the color of the pixel.

Figure 7 shows different colors for each kind of kidney stones, providing a simple way to distinguish a type among the others, except for STR and HAP. Indeed, the results obtained analyzing the hyperspectral cube completely matched with those obtained by taking ROIs from the samples.

Moreover, the software allows the selection of a group of pixels from the scores representation. Therefore, it is possible to identify which area of a sample or group of samples contain a given compound, when the scores values of each one are known.

An example is shown in Fig. 8. Three different areas are highlighted: COD, COM, and the interface, namely TRA.

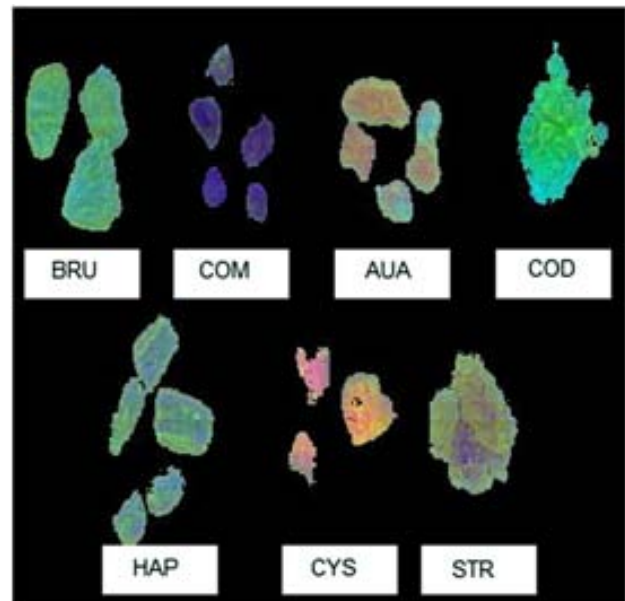


Fig. 7 RGB image for the seven main groups of renal calculi.

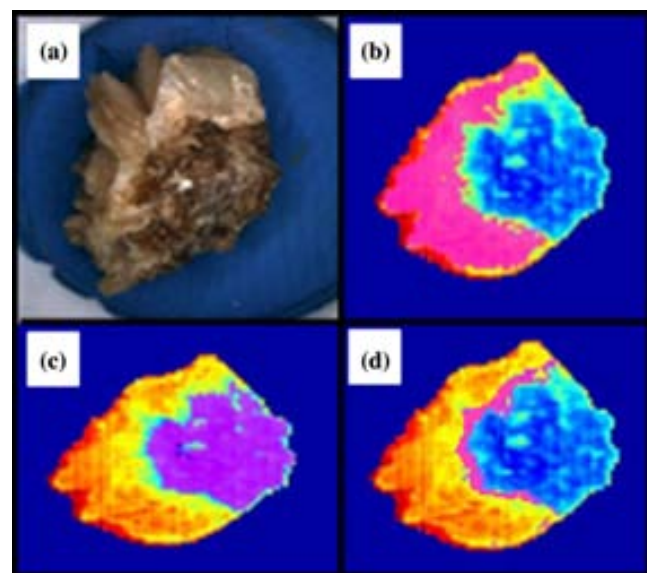


Fig. 8 (a) Image of the real stone; highlighted: (b) COD, (c) COM, and (d) TRA.

This last compound is the result of the slow change that the COD (kinetic derivative) undergoes into COM (more stable).

### 4.3 ANN Performance

The model was applied to the seven groups of main compounds forming kidney stones, using the previous conditions. The results, checked with cross-validation leave-one-out, show up to 100% of accuracy for the classification.

The next step was to further reduce the number of variables in the system, so that the foretold advantages of the variable reduction become clearer. With only 30 wavelengths selected, the accuracy for the classification remained at 100%.

When even less variables are taken for the calculations, the percentage for right classification dropped down to 95% at most. Consequently, the final choice was the model including 30 wavelengths.

However, due to the importance of a precise classification regarding the diagnostic for the patient, the really interesting objective is the classification of 11 groups of different types of kidney stones, that is, the seven main compounds and their mixtures.

Thus, an optimization of a new ANN model, capable for the classification of this much more complex data was required. For this purpose, 50 wavelengths were introduced as variables, being the structure of the optimized ANN (215, 13, 11). In this case, the rate of well-classified samples reached 94.4%. The reader is referred to Table 2 for the accurate classification of the set of 215 samples of kidney stones used for this study showing the classification obtained by the conventional technique and that developed in the present work.

**Table 2** Comparison between the results obtained using conventional techniques (stereoscopic microscopy and SEM) and the new developed methodology (HSI-ANN). Note: For the classification of the samples by HSI, a library of substances was defined with some stones considered as pure compounds. The items highlighted are the erroneously classified.

Sample	Classification conventional tech.	Classification HSI
1	COM	COM
2	COM	COM
3	TRA	TRA
4	MXD	MXD
5	AUA	AUA
6	COM	COM
7	STR	STR
8	TRA	TRA
9	HAP	HAP
10	COM	COM
11	MXL	MXL

**Table 2** (Continued).

Sample	Classification conventional tech.	Classification HSI
12	COM	COM
13	COD	COD
14	AUA	AUA
15	AUA	AUA
16	STR	STR
17	COD	COD
18	STR	STR
19	HAP	HAP
20	MXD	MXD
21	COM	COM
22	COM	COM
23	COM	COM
24	MXD	MXD
25	AUA	AUA
26	AUA	AUA
27	COD	COD
28	AUA	AUA
29	COM	COM
30	HAP	HAP
31	MXD	MXD
32	MXL	MXL
33	TRA	COM
34	STR	STR
35	MXD	MXD
36	COM	COM
37	COM	COM
38	AUA	AUA
39	AUD	AUD
40	STR	STR
41	TRA	TRA
42	TRA	TRA
43	COM	COM
44	COM	COM
45	HAP	HAP

**Table 2** (Continued).

Sample	Classification conventional tech.	Classification HSI
46	COD	COM
47	MXD	MXD
48	MXL	MXL
49	TRA	TRA
50	TRA	TRA
51	COM	COM
52	AUA	AUA
53	AUA	AUA
54	COD	COD
55	COD	COD
56	COM	COM
57	AUA	AUA
58	HAP	HAP
59	BRU	BRU
60	HAP	HAP
61	TRA	TRA
62	COM	COM
63	AUA	AUA
64	COM	COM
65	COM	COM
66	STR	STR
67	COD	COD
68	COD	COD
69	MXL	MXL
70	HAP	HAP
71	COM	COM
72	TRA	COD
73	AUA	AUA
74	AUA	AUA
75	STR	STR
76	STR	STR
77	TRA	TRA
78	COM	COM
79	COM	COM

**Table 2** (Continued).

Sample	Classification conventional tech.	Classification HSI
80	MXD	MXD
81	AUA	AUA
82	COD	COD
83	HAP	HAP
84	COD	COD
85	COD	COD
86	COM	COM
87	AUD	AUD
88	MXL	MXL
89	TRA	TRA
90	TRA	COM
91	TRA	TRA
92	COM	COM
93	COD	COD
94	COM	COM
95	STR	STR
96	MXD	MXD
97	HAP	HAP
98	BRU	BRU
99	AUD	AUD
100	COD	COD
101	COD	COM
102	AUA	AUA
103	HAP	HAP
104	HAP	HAP
105	TRA	TRA
106	COM	COM
107	COM	COM
108	COM	COM
109	COD	COM
110	CYS	CYS
111	STR	STR
112	STR	STR
113	TRA	TRA

**Table 2** (Continued).

Sample	Classification conventional tech.	Classification HSI
114	HAP	HAP
115	BRU	BRU
116	MXL	MXD
117	TRA	TRA
118	TRA	TRA
119	COD	COD
120	COD	COD
121	HAP	HAP
122	COM	COM
123	MXD	MXD
124	AUD	AUD
125	BRU	BRU
126	AUA	AUA
127	AUA	AUA
128	TRA	TRA
129	CYS	CYS
130	MXL	MXL
131	AUA	AUA
132	TRA	TRA
133	COM	COM
134	STR	STR
135	AUD	AUD
136	COD	COD
137	AUA	AUA
138	MXL	MXL
139	COM	COM
140	AUD	AUD
141	AUA	AUA
142	BRU	BRU
143	TRA	COM
144	COD	COD
145	COD	COD
146	COD	COD
147	COM	COM

**Table 2** (Continued).

Sample	Classification conventional tech.	Classification HSI
148	COM	COM
149	HAP	HAP
150	CYS	CYS
151	AUD	AUD
152	AUA	AUA
153	TRA	TRA
154	TRA	TRA
155	AUD	AUD
156	MXL	MXL
157	BRU	BRU
158	COD	COD
159	MXD	MXD
160	MXD	MXD
161	COM	COM
162	STR	STR
163	COM	COD
164	TRA	TRA
165	COD	COD
166	HAP	HAP
167	CYS	CYS
168	CYS	CYS
169	AUD	AUD
170	STR	STR
171	AUD	AUD
172	TRA	TRA
173	COM	COM
174	COM	COM
175	AUA	AUA
176	AUD	AUD
177	MXL	MXL
178	BRU	BRU
179	CYS	CYS
180	AUD	AUD
181	COD	COD

**Table 2** (Continued).

Sample	Classification conventional tech.	Classification HSI
182	COD	COD
183	STR	STR
184	MXD	MXL
185	AUD	AUD
186	HAP	HAP
187	TRA	TRA
188	HAP	HAP
189	AUD	AUD
190	COM	TRA
191	AUD	AUD
192	STR	STR
193	STR	STR
194	COD	COD
195	CYS	CYS
196	BRU	BRU
197	BRU	BRU
198	TRA	TRA
199	TRA	TRA
200	TRA	TRA
201	COM	COM
202	CYS	CYS
203	AUD	AUD
204	COD	COD
205	AUA	AUA
206	AUA	AUA
207	MXD	MXL
208	CYS	CYS
209	CYS	CYS
210	BRU	BRU
211	STR	STR
212	STR	STR
213	HAP	HAP
214	AUD	AUD
215	AUA	AUA

As seen in this Table, the error for the last model, including all types of kidney stones, is only slightly higher than that for the simpler model. Nevertheless, the second model offers a great advantage, since it is able to deal with any of the kidney stone types usually found. The prediction differences between the newly developed methodology and the conventional techniques involve basically calcium oxalate kidney stones. Considering the similar nature of those types of stones and the fact that their composition often includes mixtures of lithogenic substances, observed differences appear to be logical. Information collected in Table 3 summarizes the results discussed here that represent an efficient classification of kidney stones from a very simple methodology.

In this work, the suitability of the NIR-HSI technique with the use of ANNs for the characterization of kidney stones has been demonstrated. The regions of the NIR reflectance spectra that have the strongest power for the classification of the different components have been identified. The use of ANNs for the hyperspectral data treatment has proved to produce similar results to those obtained from conventional techniques, including samples containing compound mixtures. However, it is important to remark that the conventional methodology requires trained operators, whereas ANNs perform the classification independently from the operator's knowledge.

The implementation of this developed methodology as a routine analysis in medical practice might be achievable for a clinical laboratory, and it would be simple to perform. The method requires little training for its use, and no special knowledge about chemistry is needed. Once the software has been installed in the computer, the fast measurements allow a quick and easy classification of the stones. This application would allow obtaining a faster and much robust diagnosis, increasing the quality of treatment to each specific patient.

**Table 3** Percentage of samples correctly classified by the developed HSI-ANN methodology.

Type of kidney stone	No. of samples	No. samples correctly classified	% of correct classification
COM	39	37	94.9
COD	27	24	88.9
TRA	27	23	85.2
HAP	18	18	100
STR	19	18	100
MXL	10	9	90
MXD	13	11	84.6
BRU	25	25	100
AUA	17	17	100
AUD	10	10	100
CYS	10	10	100
Total			94.4

## Acknowledgments

The Spanish Ministry for Science and Innovation (MICINN) is acknowledged for financial support to the present study (Project CTQ2009-07432 (subprogram PPQ)). The Spanish-Italian Program for Integrated Actions is acknowledged to allow joint experiments with respective scientists (Grant of Reference IT2009-0024). Prof. Josef Havel acknowledges the support of MICINN to his sabbatical stay at UAB (SAB2009-0005), the J. H. Support from Ministry of Education, Youth and Sports of the Czech Republic (Projects MSM, 0021622411, 0021627501, and CZ.1.05/2.1.00/03.0086), and the Czech Science Foundation (Projects No. 104/08/0229, 202/07/1669).

## References

- O. W. Moe, "Kidney stones: pathophysiology and medical management," *Lancet* **367**(9507), 333–344 (2006).
- C. Pak, "Kidney stones," *Lancet* **351**(9118), 1797–1801 (1998).
- F. Grases et al., "Simple classification of renal calculi closely related to their micromorphology and etiology," *Clin. Chim. Acta* **322**(1–2), 29–36 (2002).
- A. Nayir, "Determination of urinary calculi by binocular stereoscopic microscopy," *Pediatr. Nephrol.* **17**(6), 425–432 (2002).
- E. V. Wilson, M. J. Bushiri, and V. K. Vaidyan, "Characterization and FTIR spectral studies of human urinary stones from Southern India," *Spectrochim. Acta A* **77**(2), 442–445 (2010).
- C. A. Lehmann, G. L. McClure, and I. Smolens, "Identification of renal calculi by computerized infrared spectroscopy," *Clin. Chim. Acta* **173**(2), 107–116 (1988).
- E. Peuchant et al., "Discriminant analysis of urinary calculi by near-infrared reflectance spectroscopy," *Clin. Chim. Acta* **205**(1–2), 19–30 (1992).
- D. R. Basavaraj et al., "The Role of Urinary Kidney Stone Inhibitors and Promoters in the Pathogenesis of Calcium Containing Renal Stones," *EAU-EBU Update Ser.* **5**(3), 126–136 (2007).
- A. I. Ancharov et al., "Model experiment of in vivo synchrotron X-ray diffraction of human kidney stones," *Nucl. Instrum. Meth. A* **575**(1–2), 221–224 (2007).
- T. Hyvarinen, E. Herrala, and A. Dall'Ava, "Direct sight imaging spectrograph: a unique add-on component brings spectral imaging to industrial applications," *Proc. SPIE* **3302**, 165–356 (1998).
- P. Geladi, H. Grahn, and J. Burger, "Multivariate images, hyperspectral imaging: background and equipment," in *Techniques and Applications of Hyperspectral Image Analysis*, H. Grahn and P. Geladi, Eds., pp. 1–15, John Wiley & Sons, West Sussex, England (2007).
- J. M. Amigo et al., "Study of pharmaceutical samples by NIR chemical-image and multivariate analysis" *TRAC-Trend Anal. Chem.* **27**(8), 696–713 (2008).
- A. A. Gowen et al., "Recent applications of chemical Imaging to pharmaceutical process monitoring and quality control," *Eur. J. Pharm. Biopharm.* **69**(1), 10–22 (2008).
- R. Jolivot, P. Vabres, and F. Marzani, "Reconstruction of hyperspectral cutaneous data from an artificial neural network-based multispectral imaging system," *Comput. Med. Imaging Graph.* **35**(2), 85–88 (2011).
- Z. Liu et al., "Classification of hyperspectral medical tongue images for tongue diagnosis," *Comput. Med. Imaging Graph.* **31**(8), 672–678 (2007).
- A. A. Gowen et al., "Hyperspectral imaging—an emerging process analytical tool for food quality and safety control," *Trends Food Sci. Tech.* **18**(12), 590–598 (2007).
- A. Del Fiore et al., "Early detection of toxigenic Fungi on maize by hyperspectral imaging analysis," *Int. J. Food Microbiol.* **144**(1), 64–71 (2010).
- M. Kubik, "Hyperspectral imaging: a new technique for the non-invasive study of artworks," in *Physical Techniques in the Study of Art, Archaeology and Cultural Heritage 2*, D. Creagh and D. Bradley, Eds., pp. 199–259, Elsevier, Amsterdam (2007).
- G. Bonifazi and S. Serranti, "Imaging spectroscopy based strategies for ceramic glass contaminants removal in glass recycling," *Waste Manage.* **26**(6), 627–639 (2006).
- G. Bonifazi and S. Serranti, "Hyperspectral imaging based procedures applied to bottom ash characterization," *Proc. SPIE* **6755**, 67550B (2007).
- G. Bonifazi et al., "Innovative sensing technologies applied to post-consumer polyolefins recovery," *Metal Int.* **14**(2), 5–10 (2009).
- S. Serranti, A. Gargiulo, and G. Bonifazi, "Characterization of post-consumer polyolefin wastes by hyperspectral imaging for quality control in recycling processes," *Waste Manage.* **31**(11), 2217–2227 (2011).
- E. Lewis et al., "Near-infrared chemical imaging as a process analytical tool," in *Process Analytical Technology*, K. Bakeev, Ed., p. 187, Blackwell Publishing, Oxford (2005).
- K. C. Lawrence et al., "Calibration of a pushbroom hyperspectral imaging system for agricultural inspection," *T ASABE* **46**(2), 513–521 (2003).
- G. Hanrahan, "Computational neural networks driving complex analytical problem solving," *Anal. Chem.* **82**(11), 4307–4313 (2010).
- P. J. Lisboa, E. C. Ifeachor, and P. S. Szczepaniak, *Artificial Neural Networks in Biomedicine*, Springer, London (2000).
- S. Agatonovic-Kustrin and R. J. Beresford, "Basic concepts of artificial neural network (ANN) modeling and its application in pharmaceutical research," *Pharmaceut. Biomed.* **22**(5), 717–727 (2000).
- S. Piqueras et al., "Resolution and segmentation of hyperspectral biomedical images by multivariate curve resolution-alternating least squares," *Anal. Chim. Acta* **705**(1–2), 182–192 (2011).
- M. S. Holzer et al., "Assessment of renal oxygenation during partial nephrectomy using hyperspectral imaging," *J. Urology* **186**(2), 400–404 (2011).
- L. Jafari-Saraf and I. L. Gordon, "Hyperspectral imaging and ankle: brachial indices in peripheral arterial disease," *Ann. Vasc. Surg.* **24**(6), 741–746 (2010).
- J. T. Wei et al., "Understanding artificial neural networks and exploring their potential applications for the practicing urologist," *Urology* **52**(2), 161–172 (1998).
- J. E. Arruda et al., "A guide for applying principal-components analysis and confirmatory factor analysis to quantitative electroencephalogram data," *Int. J. Psychophysiol.* **23**(1–2), 63–81 (1996).
- C. J. Kessler et al., "Factor analysis of trends in Texas acidic deposition," *Atmos. Environ.* **26**(6), 1137–1146 (1992).
- W. F. Velicer and D. N. Jackson, "Component analysis versus common factor analysis: some issues in selecting an appropriate procedure," *Multivariate Behav. Res.* **25**(1), 1–28 (1990).
- R. G. Brereton, *Applied Chemometrics for Scientists*, Wiley, England (2007).
- D. F. Brougham et al., "Artificial neural networks for classification in metabolomic studies of whole cells using 1 h nuclear magnetic resonance," *J. Biomed. Biotechnol.* (2011).
- J. Havel, P. Lubal, and M. Farková, "Evaluation of chemical equilibria with the use of artificial neural networks," *Polyhedron* **21**(14–15), 1375–1384 (2002).
- Statsoft, "Big Data Analytics, Enterprise Analytics, Data Mining Software, Statistical Analysis, Predictive Analytics", 2012, <http://www.statsoft.com/> (July 2012).
- Camo, "Leading Multivariate Data Analysis & Design of Experiments Software", 2012, <http://www.camo.com/rt/Products/Unscrambler/unscrambler.html> (July 2012).
- MathWorks, "MATLAB and Simulink for Technical Computing", 2012, <http://www.mathworks.com/index.html> (July 2012).
- Trajan Software, "Trajan Software Ltd", 2012, <http://www.trajan-software.demon.co.uk/> (July 2012).

**8.4. Published Article: Journal of Biophotonics  
(Section 2.4.)**



## FULL ARTICLE

# High precision mapping of kidney stones using $\mu$ -IR spectroscopy to determine urinary lithogenesis

Francisco Blanco, Pilar Ortiz-Álias, Montserrat López-Mesas\*, and Manuel Valiente

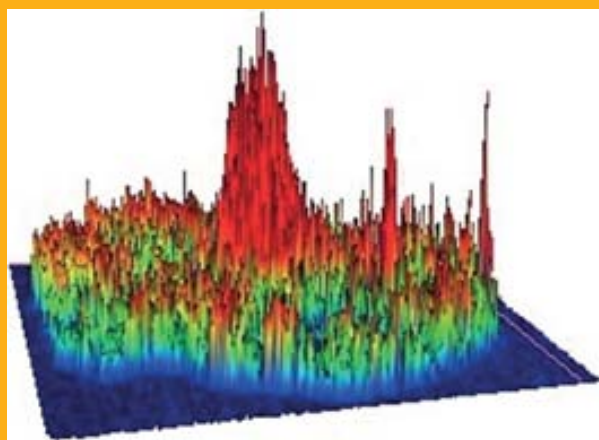
Centre Grup de Tècniques de Separació en Química (GTS), Unitat de Química Analítica, Departament de Química, Universitat Autònoma de Barcelona, 08193, Bellaterra, Spain

Received 19 December 2013, revised 13 March 2014, accepted 2 July 2014

Published online 2 August 2014

**Key words:** IR microspectroscopy, kidney stones analysis, mapping, chemical imaging

Evolution of urinary lithiasis is determined by the metabolism and life-style of the related patient. The appropriate classification of the stone is mandatory for the identification of the lithogenic process. In this study, cross-sections from a single stone of each of the most frequent urolithiasis types (calcium oxalate mono and dihydrate and carbonate apatite) have been selected and imaged using IR microspectroscopy. Moreover, the use of high definition sFTIR (synchrotron source) has revealed hidden information to the conventional FTIR. This work has demonstrated that minor components become key factors on the description of the stages of stone formation.



Intensity map for COM (1630  $\text{cm}^{-1}$  peak). The high spatial definition achieved is key for the precise description of the kidney stone history.

## Glossary

COM: Calcium Oxalate Monohydrate

COD: Calcium Oxalate Dihydrate

CAP: Carbonate Apatite

SEM-EDS: Scanning Electron Microscopy – Energy-Dispersive X-Ray Spectroscopy

sFTIR: Synchrotron FTIR

## 1. Introduction

Improvements in medicine are continuously undergoing more precise diagnosis, producing better results whilst represent minimal disturbances for the patient [1]. Recent developments have clearly pointed out that medical sciences are among the cutting-edge uses of bio and nanotechnologies [2–4]. Such scienti-

\* Corresponding author: e-mail: montserrat.lopez.mesas@uab.cat

fic development is usually linked to advances in the instruments and methodologies developed for these purposes (usually related to analysis speed and spatial resolution improvements) [5]. Working in the micro and nanoscales is only possible if such spatial resolution is achieved [6].

The study and classification of kidney stones has been the target of clinical scientists since the first chemical analysis were done on this type of samples [7]. Although chemical analysis of the ions contained in a stone can easily identify phosphate or calcium oxalate lithiasis, it cannot distinguish between different forms of calcium oxalate stones (mono and dihydrate, which stand for two thirds of the total amount of cases) [8]. This important drawback was once correctly solved by IR spectroscopy. The IR spectra of each form of calcium oxalate, as well as those for phosphates or uric acid, show unique characteristics. For a number of decades, IR spectroscopy has been considered the reference technique for the analysis of kidney stones [9, 10]. Grinding the sample for IR analysis is still the main inconvenience, because of the loss of spatial distribution of the different minority compounds present in the kidney stone.

The location of major and minor components in the stone is of major importance. The precise point of the stone where each component precipitates is generally linked to the urine conditions at the time of the corresponding solid formation. The metabolic changes that the patient suffers remain imprinted in the stone, defining a particular distribution of the components [11].

The currently expanding imaging techniques stand as an interesting approach to offer a higher amount of information about the sample. These techniques are not only able to quantify the amount of each component in the sample, as traditional IR does [12, 13], but also locate them in the structure of the stone. Several works have shown the usefulness of chemical imaging directly in the field of kidney stones, using IR spectroscopy. These previous studies have shown chemical maps of kidney stones with a spatial resolution of 100  $\mu\text{m}$  to 300  $\mu\text{m}$  using IR radiation [14], 50–100  $\mu\text{m}$  for a study using NIR spectroscopy [15] and 100  $\mu\text{m}$  in a work using IR radiation and also quantifying components [16].

The present work represents a step forward from the current clinical IR analysis that solves its main drawback, the lack of spatial definition, using IR microspectroscopy, including the results available when high-resolution equipment is used. The use of FT-IR spectroscopy from a Synchrotron Radiation light source (sFTIR) may reveal hidden information to conventional light sources. Among the variety of techniques which can be coupled to a synchrotron light source, IR stands as an especially useful one for the analysis of biological samples.

As many other biomaterials, kidney stones have already been analyzed by means of synchrotron radiation. However, most of the studies conducted so far have been performed using X-ray spectroscopy or diffraction [17–20]. These techniques are not considered nowadays in the routine clinical laboratory.

Other technical alternatives readily allow a higher spatial resolution than that achieved in this work. More sophisticated approaches, based on 50  $\mu\text{m}$  AsSe fibers with a 100–125 nm gold coating on the tip have reached 240 nm spatial resolution [21]. In addition, a spatial resolution of 200 nm had been achieved using a bench top laser IR source combined with ATR topography [22]. Indeed, a simpler bench top thermal source allows a routinely achievable resolution below 10  $\mu\text{m}$  [23].

Due to the particularly long time requirements for the analyses and the limited availability of the equipment, it may be challenging to include such techniques in the general clinical laboratories. The use of Focal Plane Array detectors (FPA) stands as a suitable option for decreasing the mapping time for large sample areas. The commercially available detectors reach arrays of 128  $\times$  128 pixels and have been already used for the analysis of biological samples [24, 25].

The aim of this application is to stress the usefulness of such approaches as reference techniques for the upcoming advances in clinical analysis. The information obtained from these experiments will contribute to a better understanding of the lithiasic process, which, in turn, may lead to better diagnostics, which end up in more appropriate treatments for the patient.

## 2. Experimental

### 2.1 Samples

Kidney stones were collected from the urology services at the Hospital Universitari de Bellvitge, Barcelona (Spain). Since calcium urolithiasis stands as the diagnostic result for approximately 85% of stone patients, with two thirds of the cases being calcium oxalate in any of its forms, a total of three samples were studied in order to reflect this distribution of frequencies. These included a sample of pure calcium oxalate monohydrate, a sample containing mono and dihydrate calcium oxalate and a carbonate apatite sample. These samples were previously classified by means of optical and electronic microscopies, as described in bibliography [11]. The IR measurements required flat and thin layers of the samples. Kidney stones were embedded in an epoxy resin and polished until they reached approximately 30  $\mu\text{m}$  thickness.

## 2.2 Methods

### 2.2.1 Stereoscopic microscopy

The first sample analysis was completed using a conventional, stereoscopic microscope by visual description of the sample. For this classification, morphological features of the stones, as well as their texture, color and structure were chosen as the criteria for the determination of the stone types [11].

### 2.2.2 SEM-EDS

Electronic microscopy allowed the observation of the fine structure of the stone and the determination of the presence of crystals or other structures in the sample. In addition to this technique, elemental analysis was performed, using Energy-Dispersive X-ray Spectroscopy (EDS). These measurements were used for the verification of the purity of the samples. The equipment used was a JEOL JSM-6300 Scanning Electron Microscope (Japan), coupled to an Oxford Instruments Lind ISIS-200 X-ray Dispersive Energy Spectrometer (UK), located at the Universitat Autònoma de Barcelona.

### 2.2.3 Spectroscopic measurements

Spectroscopic measurements were performed at the SOLEIL Synchrotron facilities in Paris, France. The equipment used was located in the SMIS beamline. The hypercube data was created by measuring reflectance IR spectra of a given area of the sample. For this purpose, two microscopes were used, which differed on the energy source, global or synchrotron.

#### 2.2.3.1 Global source IR mapping

Spectral maps from samples were measured by means of a Thermo Scientific Nicolet iN10 FT-IR Spectrometer. The spot size was set at  $80 \times 80 \mu\text{m}^2$ . The surface of the sample was divided into a grid, where a spectrum was measured each  $50 \mu\text{m}$  in both axes. The mapping spot size was larger than the step size, procedure known as oversampling [26, 27]. This process does not bring more spectral information, yet it results in images with better fidelity to the visible image. Oversampling also reduces the risk of an interesting feature of the surface (such as small particles) that is missed or measured at the edge of a pixel. This ensures a better description of layers in-

terfaces. Mapping experiments require finding a balance between number of points and spectral quality (measuring time per spectrum). While an oversampling ratio of 2 is often used, this parameter was adapted in our work, to take into account the mentioned constraints. The software processes the signal of overlapped points as an average of them. The measured range was from  $720 \text{ cm}^{-1}$  to  $4000 \text{ cm}^{-1}$ , with a resolution of  $8 \text{ cm}^{-1}$  and storing 16 interferograms for each point of measurement. A background using an Au layer was previously measured by storing 500 spectra, and was used to correct the mapping spectra of the samples. The measurement of the IR spectra for a whole sample required typically 8 to 10 hours, depending on the size of the analyzed surface. Due to timing reasons, the number of spectra stored for the sample was lower than that for the background.

#### 2.2.3.2 Synchrotron radiation IR mapping

For the measurements using synchrotron based IR microspectroscopy, a Thermo Nicolet Continuum FT-IR microscope was used. In this case, due to the higher brightness of the radiation source, a smaller spot size was used:  $10 \times 10 \mu\text{m}^2$ . The step size was  $6 \mu\text{m}$ , also considering oversampling. The spectral range was the same as that for the global source, yet with a higher resolution, reaching  $4 \text{ cm}^{-1}$ . For a better S/N ratio achievement, 100 spectra were collected for each point of measurement. Likewise, the background was collected measuring an Au layer and averaging 500 spectra.

### 2.2.4 Data analysis

The software package OMNIC 8.0 (Thermo Scientific) was used for data acquisition and processing. The ratio of all spectra to the background was calculated and afterwards Kramers-Kronig correction algorithm was applied. The resulting data was then processed for the production of chemical maps, plotted as RGB color images. In this work RGB images have been produced not only based on the intensity of a single peak, but also using the ratio of intensities of two peaks. When plotting the ratio of intensities for various peaks, the effects of a possible uneven area in the sample, which might cause a biased signal, were avoided. Indeed, the samples used in this work, due to the porous structure of the stones and little imperfections during the polishing process, showed remarkable differences in the intensities of selected peaks for neighboring pixels, which were attributed to surface effects. Certainly, an analysis based on peaks ratios was not quantitative, but

**Table 1** Frequencies for the characterization of components.

Component	Spectral band ( $\text{cm}^{-1}$ )	Associated vibration
COM	780	C–C/C–O single bond stretching
	1318	C–C/C–O single bond stretching
	1630	C–O double bond stretching
COD	1680	C–O double bond stretching
CAP	1060	P–O double bond stretching

the goal of this work was directed to a qualitative description of the samples; any quantitative result is only indicative.

### 2.2.5 Spectral bands

From the many peaks observed in the IR spectra of each of the three analyzed stones, only a few characteristic spectral bands were chosen (Table 1) which have already been described as useful for the study of COM, COD and CAP [12].

## 3. Results and discussion

### 3.1 Calcium oxalate monohydrate (COM)

The chosen sample had been previously classified as pure COM by stereoscopic microscopy. In this analysis, concentric circumferences were appreciated within the structure of the stone, yet their nature could not be analyzed, due to lack of resolution of the visual technique. Mapping spectra covering the whole area of the sample were done using the FT-IR microscope with a globar source.

The chemical map for the peak at  $1630\text{ cm}^{-1}$  shows the maximum intensity at the core area of the stone (see Figure 1a). However, this trend is inverted when the peak at  $1318\text{ cm}^{-1}$  is taken into consideration, as pictured in Figure 1b. The first peak is, as known, a feature of calcium oxalate spectrum, since it corresponds to the C=O bond stretching vibration. This spectral band is also seen in organic matter, while the strong intensity recorded at  $1318\text{ cm}^{-1}$ , C–O and C–C bonds stretching, is especially intense for COM. According to bibliography [11], COM kidney stones tend to grow from a core with a high content in organic matter, what corroborates the previous observation. The intensity ratio for the peak at  $1630\text{ cm}^{-1}$  to that at  $1318\text{ cm}^{-1}$  is plotted in Figure 1c, in order to discard any possible effect from the surface on the signal intensity. This ratio shows a much higher intensity at the core of the stone. The intensity quickly decreases when the distance to the core of the sample increases. There-

fore, only strictly the core of the stone shows this profile. Figure 1a evidences two other regions of the sample with a high value for the intensity of this peak.

In order to further describe those regions, the ratio of the intensity of the  $1630\text{ cm}^{-1}$  to the  $780\text{ cm}^{-1}$  was also calculated and displayed. The peak at  $780\text{ cm}^{-1}$  is a characteristic band for COM, while the other studied compounds hardly present it. According to Figure 1d, the core of the stone shows the highest intensity for this ratio, along with the same areas illustrated in Figure 1c. Since COM dominates the composition of the structure, the peak should be found overall on the analyzed surface. This peak has an intense signal, so the amide I band (C=O stretching) is overlapped and not clearly identified. As shown in the referred regions of the stone, the peak around  $1630\text{ cm}^{-1}$  has a high intensity, while that at  $780\text{ cm}^{-1}$  disappears. The spectra in the core region also show a band at  $1500\text{ cm}^{-1}$ , which can be attributed to amide II (N–H bond stretching) and is not observed in the surroundings of the core. These re-

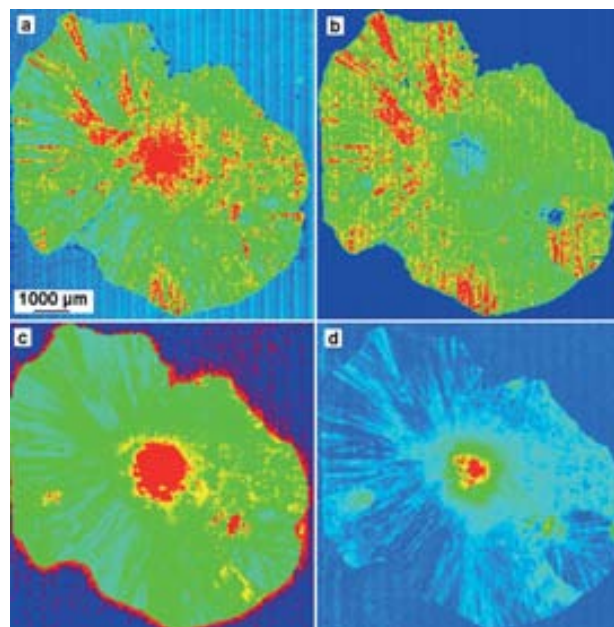


**Figure 1** Mapping plots of the complete sample. (a) Intensity of the peak at  $1630\text{ cm}^{-1}$ . (b) Intensity of the peak at  $1318\text{ cm}^{-1}$ . (c) Ratio of intensities  $1630\text{ cm}^{-1}$  to  $1318\text{ cm}^{-1}$ . (d) Ratio of intensities  $1630\text{ cm}^{-1}$  to  $780\text{ cm}^{-1}$ .

sults support the observation that a considerable region around the core of the stone has an important amount of organic matter. These observations fit with some bibliography sources, which point out the strong dependence of the COM crystal growth on organic matter [28], and its location in the core of the stone [11]. The observation of secondary spots with these spectral features suggests the existence of new nucleation points, that promoted the precipitation of new COM crystals and they were later integrated within the structure. The absence of a CAP peak ( $1060\text{ cm}^{-1}$ ) dismisses the influence of a Randall's plaque during the development of the stone, since these structures are based on calcium phosphates [29].

Concerning the circular structures observed surrounding the core of the stone; the spectra in this area reveal that this component is actually not COM (Figure 2a). The peak with a maximum located at  $1680\text{ cm}^{-1}$  suggests that the circular COM layers are separated by a thin COD layer. It is important to note that the intensity for the COD peak shows maximum intensity at the points where the interfaces are located. Likewise, the intensity of the peak at  $1630\text{ cm}^{-1}$ , corresponding to COM, is plotted in a wider area in Figure 2b. In this case, the circular interfaces are recognized as a minimum. The core shows a high intensity for both wavelengths due to the high signal at this point, that masks any difference appreciated in other areas. The intensity of the spectral band at  $1630\text{ cm}^{-1}$  is stronger than that for  $1318\text{ cm}^{-1}$  but the peak can still be distinguished from that for COD.

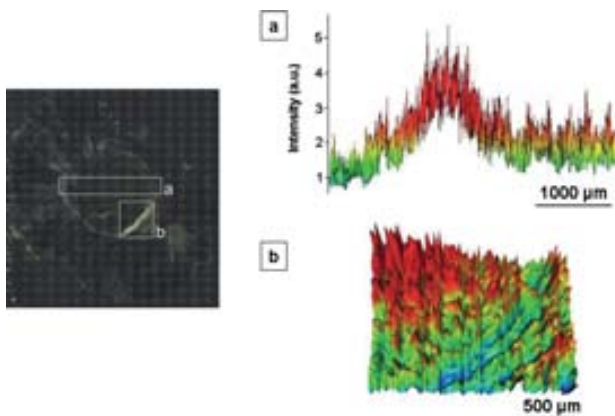


**Figure 2** (a) Map from the highlighted area, based on the intensity for the peak at  $1680\text{ cm}^{-1}$ . The maximum of the COD peak overlaps with the location of the concentric circumferences. (b) Chemical map from the selected sample area, the intensity for the peak at  $1630\text{ cm}^{-1}$  is plotted. The circumferences appear this time as minimum intensity pixels. Note the thickness of the COD surfaces does not exceed  $100\text{ }\mu\text{m}$ . Comparable results were obtained when the intensity for the peak at  $1318\text{ cm}^{-1}$  was plotted.

According to these findings, it can be concluded that the growing process of the columnar COM crystals that build up the structure of the stone was temporarily hindered due to the deposition of a thin COD layer. These changes were possibly due to punctual and regular changes in the composition of the urine, characterized by a high calcium concentration, condition that especially favors the formation of the kinetic derivative (COD). The patient has suffered these conditions regularly, fact that lead to the formation of these concentric circles, since a layer of COD covered the, at that precise time, whole kidney stone. When the conditions necessary for the formation of solid concretions of COM were achieved again, the thermodynamic derivative continued precipitating.

It was not possible to characterize the composition of these thin layers by using traditional optical microscopy. The  $\mu$ -IR technique has shown a great advantage for the description of such small areas of the stone. Although the analysis of a single sample is not enough for the description of a general behavior of the COM stones precipitation mechanisms, this finding is highly interesting, due to the frequency in which this type of structure is found.

### 3.2 Calcium oxalate dihydrate and monohydrate (COD and COM)

The analysis of this sample by stereoscopic microscopy revealed a COD stone. COD suffers normally a slow transformation into the most stable COM derivative due to a long-term contact with urine. Optical microscopy cannot help to define precise limits of the regions where COD or COM are most abundant, so the goal of the  $\mu$ -IR mapping measurements is to precisely locate those components.

Firstly, a global source FT-IR microscope was used for the analysis of a large surface of the sample. Due to the high area of the stone and time limitations, the half of the sample was mapped which included the core of the stone as well as a large surface area. This region can be considered representative of the whole kidney stone.

A map based on the intensity of the signal at  $1680\text{ cm}^{-1}$ , corresponding to COD, can be seen in Figure 3a. As expected, the strongest signal for COD is found in the outer part of the stone, since it is the one of latest formation.

Alternatively, the intensity for the band at  $1630\text{ cm}^{-1}$  (COM) is much higher on the core of the sample. The residual signal seen on the most external part of the stone is due to the high intensity of the C=O bond vibration. These results are plotted in Figure 3b.

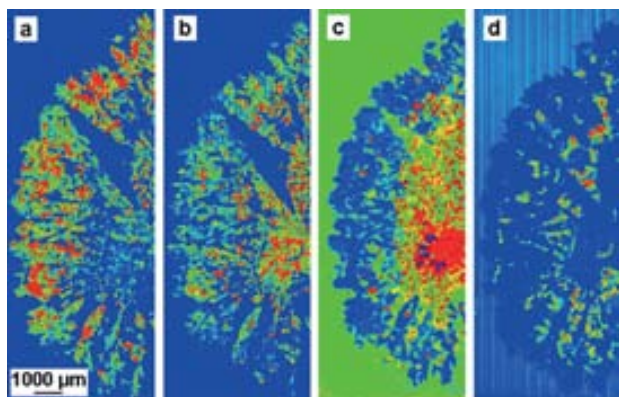


**Figure 3** Mapping plots, (a) intensity of the peak at  $1680\text{ cm}^{-1}$  (COD). (b) Intensity of the peak at  $1630\text{ cm}^{-1}$  (COM). (c) Ratio of intensities of the peak at  $1630\text{ cm}^{-1}$  to  $1680\text{ cm}^{-1}$ . (d) Intensity of the peak at  $1060\text{ cm}^{-1}$  (CAP).

The characteristic spectral bands for the carbonyl group in COM and COD are overlapped. Their vibration energy is close and their intensity is high. The chemical map may appear to be biased because of the proximity of the bands, but the features of both spectra allow their unique recognition. This band overlapping can actually be overcome when the ratio of intensities for such peaks is used for the graphical representations.

In order to correctly define the composition for each area of the stone, a map of the sample, based on the relative intensities between the bands  $1630\text{ cm}^{-1}$  and  $1680\text{ cm}^{-1}$ , is displayed (Figure 3c). The areas dominated by COM will appear in red and in blue when COD dominates showing the distribution of calcium oxalate. As it can be seen, in the core a full conversion is achieved, later discussed. From the core outwards, a first radial section of medium intensity is found. This suggests that this area, due to a continuous contact with the urine (because of the porous structure of the stone), continued their transformation to the most stable derivative. Finally, the surface of the stone comprises pure COD, in its characteristic sharp crystals. It can be concluded that the transformation have been produced progressively.

Figure 4a pictures the variation of the composition throughout the stone, from the nucleus to the surface. For this picture, the ratio of the peaks at  $1630\text{ cm}^{-1}$  to  $1680\text{ cm}^{-1}$ , that is COM/COD, was used. As previously, COM regions will appear as red areas. The IR spectra for the highlighted points are plotted in Figure 4b.

Point 1 corresponds to the core area. The curve resembles in a great extent the spectrum for pure COM and practically no shoulder for the COD band can be appreciated, so it can be assumed that the transformation has been virtually complete. Micro-

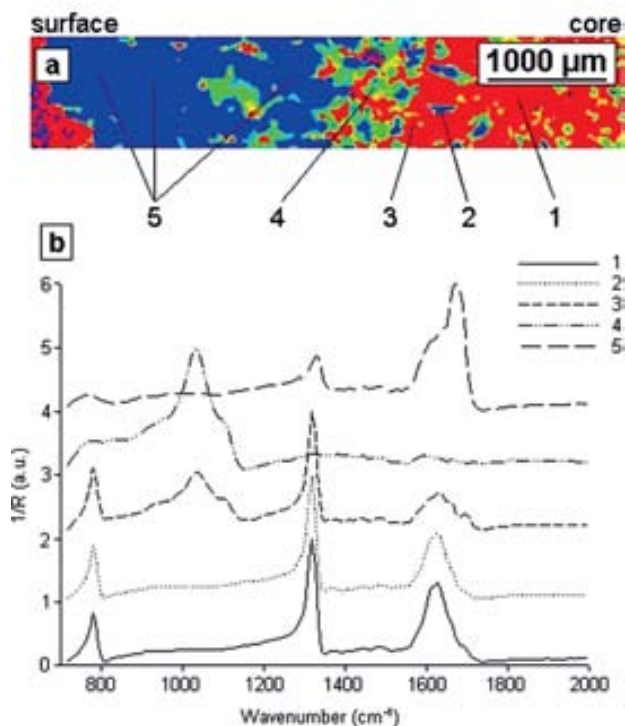


**Figure 4** (a) Map of the central area of the sample, from the core to the surface of the stone. Intensities according to the ratio  $1630\text{ cm}^{-1}$  (COM) to  $1680\text{ cm}^{-1}$  (COD). (b) IR spectra corresponding to the indicated points in the mapping image.

scopic analysis of the sample reveals a poorly compact structure, far from that seen in directly formed COM stones, fact that supports the initial precipitation of COD.

The space immediately adjacent to the core is represented by Point 2. Although COM is still the substance that dominates the region, a shoulder can already be seen at  $1680\text{ cm}^{-1}$ , so COD was not totally transformed.

The next radial sphere surrounding the core has a different fingerprint. A spectral band at  $1060\text{ cm}^{-1}$ , that perfectly fits the absorption region for CAP, can be seen in Point 3. Indeed, CAP is the only component in some fragments of the stone located in this middle area (see Point 4).

This information suggests that, after the core area was formed, the patient experienced rather different urine conditions, probably a dramatic increase in the pH value that led to the formation of large CAP deposits.

At last, the area closest to the surface is analyzed in Point 5. This can be regarded as the youngest area of the stone, so pure COD shall be expected to be found here. This curve entirely fits with this assumption.

In this sample, the location of the positions where CAP is found is of especial interest. As it can be

seen in Figure 3d, by following the spectral band at  $1060\text{ cm}^{-1}$ , CAP is mostly located in the middle parts of the stone. Therefore, it could be stated that the conditions for the formation of these solid concretions did not occur either at the first steps of the stone growing nor during the final stages.

A second reasonable interpretation of this figure could also be done. The careful inspection of the red areas in the picture defines cavities in the structure of the stone. This fact may point out to a change in the urine conditions at the later stages of the stone formation. The urine, probably at a rather basic pH, could run through the cavities of the stone and loose its dynamic flow in these internal paths, were CAP could have been stored as solid depositions at a later stage in the stone formation.

A further analysis of these results could locate the precipitation of CAP during the formation of the stone, due to changes in the urine composition. After the precipitation of calcium oxalate, pH and the concentration of some precipitation promoters could change, favouring the formation of CAP solid concretions.

For this sample, also a single measurement using sFTIR, which allows a higher resolution, was also performed. A single, straight line of 30 points, covering a distance of  $180\text{ }\mu\text{m}$  from the core towards the surface of the sample, was analyzed (as indicated in Figure 5a). Figure 5b shows new, more precise information, which was not available when using a globar source IR spectrometer. It appears clear that the band for COM is the one dominating the core

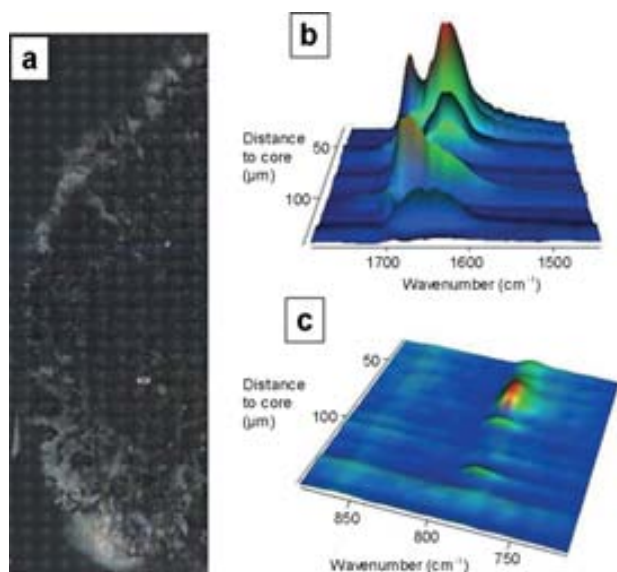


**Figure 5** sFTIR measurements (a) localization of the measured line map in the sample surface. (b) Representation of the carbonyl group absorption band. (c) Representation of the absorption band at  $780\text{ cm}^{-1}$ , characteristic for COM.

of the stone. However, a smaller band for COD ( $1680\text{ cm}^{-1}$ ) is also seen in the core region. Thus, it can be understood that the transformation of COD into COM did not take place in a full extent, as it seemed in the previous experiments. The spectra for the outer part of the stone evidence the only existence of COD, as already seen by lower resolution IR spectroscopy and stereoscopic microscopy.

Likewise, Figure 5c supports these results, since the spectral band at  $780\text{ cm}^{-1}$ , a specific signal for COM, decreases as the position of the spectrum gets closer to the surface of the sample.

The greater resolution allowed by the coupling of a synchrotron light source to  $\mu$ -IR spectroscopy has led to the best description of the sample. The preliminary results showed by the sFTIR measurements have shown the usefulness of advanced techniques for difficult cases, where they can contribute to precisely depict the lithogenesis process.

### 3.3 Carbonate apatite (CAP)

When analysing CAP kidney stones, the co-precipitation of other substances is often seen. For instance, struvite ( $\text{MgNH}_4\text{PO}_4$ ), a mineral likely to precipitate in bacteriological infection conditions, can be found mixed with CAP stones in variable amounts. Furthermore, due to relatively similar precipitation circumstances, calcium oxalate is also highly expected to be found within the structure of CAP samples.

Before performing this work, the CAP stone used was analyzed using stereoscopic and SEM microscopies. When SEM-EDS analyses were performed on the stone, no magnesium peak was found at any point of the structure, so the existence of struvite was discarded. The existence of calcium oxalate deposits can be more difficult to identify; if the agglomerations are small enough, the signal for phosphorous (CAP) may still appear, and the crystal structure differences between both components might be hard to appreciate.

The sample was analyzed using a globar energy source. CAP stones are much softer than other stone types. As a consequence, some of the sample material could have been lost during the preparative polish procedures. This area is seen as a big blue zone in Figure 6.

Figure 6 shows that most of the measured surface is CAP, since the intensity for the characteristic spectral band is maximal. Although the big blue region has a similar spectrum to the holding resin, the spectra of the small areas of low intensity for the  $1060\text{ cm}^{-1}$  band show different patterns.

Once the presence of struvite was dismissed using SEM-EDS as previously described, the existence of calcium oxalate within the structure was checked.

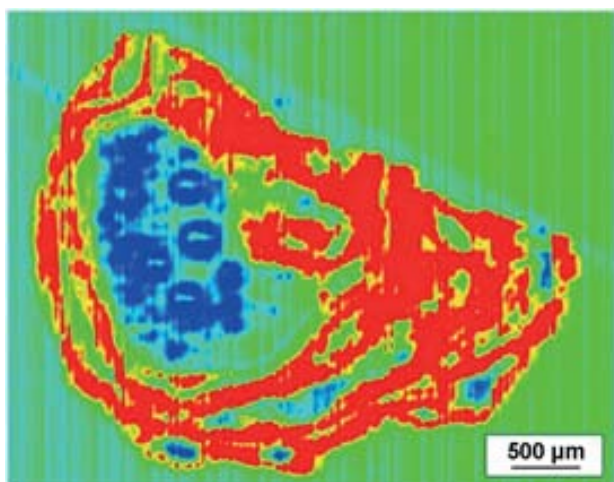


**Figure 6** Map of the stone, intensity of the peak at  $1060\text{ cm}^{-1}$ .

With this concern, the intensity of the calcium oxalate spectral band at  $1680\text{ cm}^{-1}$  is plotted in Figure 7a. It can be appreciated that some regions show an especially intense signal for calcium oxalate. These areas depict lines crossing the whole stone.

Point 1 in Figure 7a describes an outer area of the stone with a focalized region of calcium oxalate precipitation. If the spectrum from this spot is taken (Figure 7b), the peak position reveals the predominance of COD. In fact, the CAP spectral band is not appreciated, so no phosphates were precipitating together with calcium oxalate. In a latter step, CAP continued depositing on the surface of the stone, covering the COD deposits.

Likewise, Point 2 is representative for a long layer of calcium oxalate deposits in the stone, which suggests that the conditions in the urine at that point lead to the precipitation of calcium oxalate rather than CAP, for a given period of time. As seen in Figure 7b, the spectra from this region show a maximum absorption band at  $1630\text{ cm}^{-1}$ , so the main component can be thought to be COM. However, the existence of a shoulder at  $1680\text{ cm}^{-1}$  suggests the presence of COD. It could be thought that COD precipitated initially and then it got transformed into the thermodynamically more stable COM. According to the Figure 7b, there is a noticeable peak for CAP, so COD precipitated along with CAP.

It is worth to say that the thickness of each of these layers is lower than  $150\text{ }\mu\text{m}$ , a similar size as the porous in the structure of mixed stones. This makes particularly difficult to distinguish them via stereoscopic microscopy, and the precise structure of the crystals might not be completely resolved using SEM microscopy.

In the case of the present sample,  $\mu$ -IR spectroscopy has allowed the precise description of three stages within the stone formation process.

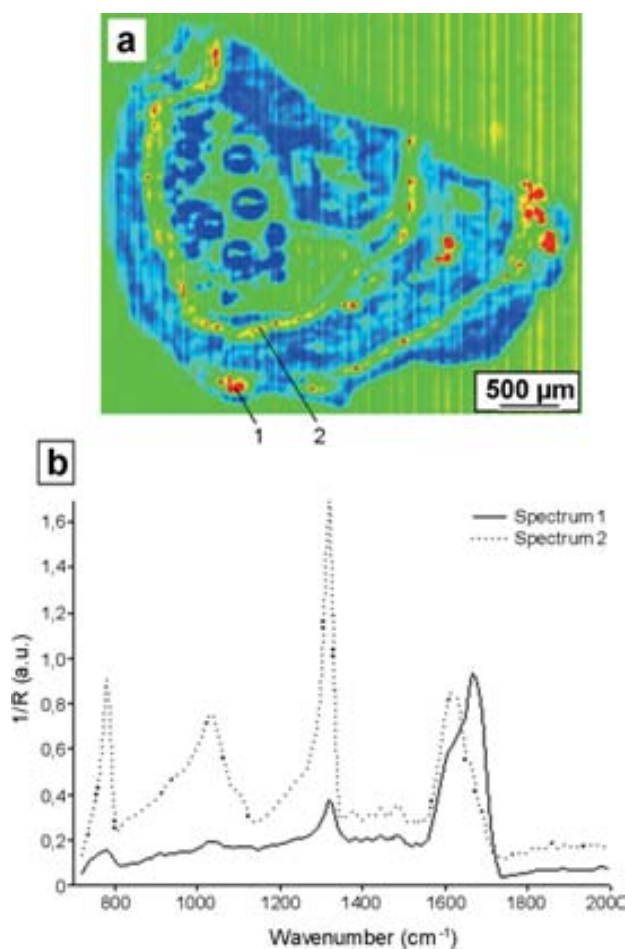


**Figure 7** (a) Map of the whole sample, based on the intensity of the spectral band at  $1680\text{ cm}^{-1}$ . (b) IR spectra measured for the points highlighted in Figure 7a.

## 4. Conclusion

This work has revealed once more the importance of a good resolution power for the best description of the kidney stones, getting information different to those obtained by the use of traditional techniques.

Indeed, minor components in some stones have been located, fact that helps in the definition of the stone history, that is, lithogenesis. This history is directly linked to the metabolic disturbances the patient has gone through, so their precise description leads to the definition of the best management of the disease and selected treatment.

The formulation of precise, statistically robust results is hampered by the limited number of samples that could be included in the study. However, this work points out IR microspectroscopy as an interesting approach for the study of renal calculi. It is clear that, due to the time needed for the measurements, the related costs and their availability, the experi-



ments described here, even including synchrotron radiation are not likely to become a routine analysis technique for clinical laboratories. However, the information provided by these techniques serves as validation of the already existing methodologies. It widens the knowledge on kidney stone formation mechanisms, as the description of precipitation patterns.

This work can be considered as the use of a more advanced approach than the available IR spectroscopy for the analysis of kidney stones. It is important to highlight that the results are comparable to those usually managed by physicians.

Some of the limitations seen in this work could be solved with existing technology. The use of FPA can provide a higher analysis speed to the methodology, a required improvement to become suitable for routine analysis. As described in the introduction, higher spatial resolution is readily available in commercial devices, so their use would emphasize the advantages of defining the stone structure with higher precision.

In order to be totally attractive to clinical laboratories, the analysis should become inexpensive and new applications (for new tissues) should be developed. This would help take profit of the most modern spectrometers, which are often used in research for the analysis of biological samples.

**Acknowledgements** The authors acknowledge SOLEIL Synchrotron Facilities for the founding through the ELISA program, project 20101061. The authors especially recognize the kind and valuable support offered by Dr. Paul Dumas and Dr. Christophe Sandt, Beamline Scientists at SMIS Beamline (SOLEIL). Likewise, the Spanish Ministries of Education and MINECO are also acknowledged for the financial support through Becas PFU, reference AP2009-3245 and the project CTM2012-30970, respectively.

**Author biographies** Please see Supporting Information online.

## References

- [1] J. L. Gibson, D. K. Martin, and P. A. Singer, *Health Serv. Res.* **2**(14), (2002).
- [2] G. Abuduxike and S. M. Aljunid, *Biotechnol. Adv.* **30**, 1589–1601 (2012).
- [3] P. Boisseau and B. Loubaton, *C.R. Phys.* **12**, 620–636 (2011).
- [4] T. F. Massoud and S. S. Gambhir, *Trends Mol. Med.* **13**(5), 183–191 (2007).
- [5] M. Erali, K. V. Voelkerding, and C. T. Wittwer, *Exp. Mol. Pathol.* **85**, 50–58 (2008).
- [6] G. Trinci, R. Massari, M. Scandellari, F. Scopinaro, and A. Soluri, *Nucl. Instrum. Meth. A* **626/627**, 120–127 (2011).
- [7] G. Richet, *Kidney Int.* **48**, 876–886 (1995).
- [8] A. Hodgkinson, *J. Clin. Pathol.* **24**, 147–151 (1971).
- [9] A. Hesse, R. Kruse, and W. J. Geilenkeuser, *Clin. Chem. Lab. Med.* **43**(3), 298–303 (2005).
- [10] G. Rebentich, W. Berg, W. Pirlich, and D. Omán, *Int. Urol. Nephrol.* **20**(1), 35–45 (1988).
- [11] F. Grases, A. Costa-Bauzá, M. Ramis, V. Montesinos, and A. Conte, *Clin. Chim. Acta* **322**, 29–36 (2002).
- [12] J. L. García, M. J. Torrejón, and M. Arroyo, *Clin. Biochem.* **45**, 582–587 (2012).
- [13] I. Singh, *Int. Urol. Nephrol.* **40**, 595–602 (2008).
- [14] M. Pucetaite, V. Hendrixson, and A. Zelvys, *J. Mol. Struct.* **1031**, 38–42 (2013).
- [15] F. Blanco, M. López-Mesas, S. Serranti, G. Bonifazi, J. Havel, and M. Valiente, *J. Biomed. Opt.* **17**(7) (2012).
- [16] H. J. Gulley-Stahl, J. A. Haas, K. A. Schmidt, A. P. Evan, and A. J. Sommer, *Appl. Spectrosc.* **63**(7), 759–766 (2009).
- [17] L. M. Miller and P. Dumas, *BBA-REVBiomembranes* **1758**(7), 846–857 (2006).
- [18] A. I. Ancharov, S. S. Potapov, T. N. Moiseenko, I. V. I. V. Feofilov, and A. I. Nizovskii, *Nucl. Instrum. Meth. A* **575**, 221–224 (2007).
- [19] D. Bazin, X. Carpentier, I. Brocheriou, P. Dorfmueller, S. Aubert, C. Chappard, D. Thiaudière, S. Reguer, G. Waychunas, P. Jungers, and M. Daudon, *Biochimie* **91**, 1294–1300 (2009).
- [20] X. Carpentier, D. Bazin, C. Combes, A. Mazouyes, S. Rouzière, P. A. Albouy, E. Foy, and M. Daudon, *J. Trace Elem. Med. Bio.* **25**, 160–165 (2011).
- [21] J. Generosi, G. Margaritondo, M. Kropf, H. Hirling, S. Catsicas, K. Johnsson, N. H. Tolk, D. W. Piston, and A. Cricenti, *J. Appl. Phys.* **104**, 106102 (2008).
- [22] G. A. Hill, J. H. Rice, S. R. Meech, D. Q. M. Craig, P. Kuo, K. Vodopyanov, and M. Reading, *Opt. Lett.* **34**(4) 431–433 (2009).
- [23] R. Mendelsohn, C. R. Flach, and D. J. Moore, *Biochim. Biophys. Acta.* **1758**, 923–933 (2006).
- [24] K. M. Dorling and M. J. Baker, *Trends Biotechnol.* **31**(8) 437–438 (2013).
- [25] L. M. Miller and R. J. Smith, *Vib. Spectrosc.* **38**, 237–240 (2005).
- [26] P. Lasch and D. Naumann, *Biochim. Biophys. Acta.* **1758**, 814–829 (2006).
- [27] P. Lasch, *Chemotetr. Intell. Lab* **117**, 100–114 (2012).
- [28] J. W. Kuritz, M. Carvalho, and Y. Nakagawa, *J. Cryst. Growth* **255**, 392–402 (2003).
- [29] B. R. Matlaga, F. L. Coe, A. P. Evan, and J. E. Lingeman, *J. Urology* **177**(1), 31–38 (2007).

**8.5. Patent: NIR-HSI stone classification methodology  
(Section 5.2.)**

(12) SOLICITUD INTERNACIONAL PUBLICADA EN VIRTUD DEL TRATADO DE COOPERACIÓN EN MATERIA DE PATENTES (PCT)

(19) Organización Mundial de la Propiedad Intelectual  
Oficina internacional



(10) Número de Publicación Internacional  
**WO 2012/136874 A1**

(43) Fecha de publicación internacional  
11 de octubre de 2012 (11.10.2012) **WIPO | PCT**

(51) Clasificación Internacional de Patentes:  
*G01N 21/00* (2006.01) *G06F 19/00* (2011.01)  
*G06T 1/40* (2006.01) *A61B 6/00* (2006.01)  
*G01J 3/40* (2006.01)

(21) Número de la solicitud internacional:  
PCT/ES2012/070239

(22) Fecha de presentación internacional:  
10 de abril de 2012 (10.04.2012)

(25) Idioma de presentación: español

(26) Idioma de publicación: español

(30) Datos relativos a la prioridad:  
P201130548 6 de abril de 2011 (06.04.2011) ES

(71) Solicitantes (para todos los Estados designados salvo US):  
**UNIVERSITAT AUTONOMA DE BARCELONA** [ES/ES]; Edifici A, Campus universitari s/n, E-08193 Bellaterra, Cerdanyola del Valles (ES). **MASARYK UNIVERSITY** [CZ/CZ]; Zerotinovo nám. 617/9, 601 77 Brno (CZ). **UNIVERSITÀ LA SAPIENZA** [IT/IT]; Piazzale Aldo Moro, 5, I-00185 Roma (IT).

(72) Inventores: e

(75) Inventores/Solicitantes (para US solamente): **BLANCO, Francisco** [ES/ES]; Edifici Eureka, Campus de la UAB s/n, E-08193 Cerdanyola del Vallès (ES). **BONIFAZI, Giuseppe** [IT/IT]; Transfer Technology Office, P.zzale Aldo Moro, 5, I-00185 Roma (IT). **GARGIULO, Aldo** [IT/IT]; Transfer Technology Office, P.zzale Aldo Moro, 5, I-00185 Roma (IT). **HAVEL, Josef** [CZ/CZ]; Vychodilova 14, 616 00 Brno (CZ). **LÓPEZ, Montserrat** [ES/ES]; Edifici Eureka, Campus de la UAB, E-08193 Cerdanyola del Vallès (ES). **SERRANTI, Silvia** [IT/IT]; Transfer Technology Office, P.zzale Aldo Moro, 5, I-00185 Roma

(IT) **VALIENTE, Manuel** [ES/ES]; Edifici C, Campus de la UAB s/n, E-08193 Cerdanyola del Vallès (ES).

(81) Estados designados (a menos que se indique otra cosa, para toda clase de protección nacional admisible): AE, AG, AL, AM, AO, AT, AU, AZ, BA, BB, BG, BH, BR, BW, BY, BZ, CA, CH, CL, CN, CO, CR, CU, CZ, DE, DK, DM, DO, DZ, EC, EE, EG, ES, FI, GB, GD, GE, GH, GM, GT, HN, HR, HU, ID, IL, IN, IS, JP, KE, KG, KM, KN, KP, KR, KZ, LA, LC, LK, LR, LS, LT, LU, LY, MA, MD, ME, MG, MK, MN, MW, MX, MY, MZ, NA, NG, NI, NO, NZ, OM, PE, PG, PH, PL, PT, QA, RO, RS, RU, RW, SC, SD, SE, SG, SK, SL, SM, ST, SV, SY, TH, TJ, TM, TN, TR, TT, TZ, UA, UG, US, UZ, VC, VN, ZA, ZM, ZW.

(84) Estados designados (a menos que se indique otra cosa, para toda clase de protección regional admisible): ARIPO (BW, GH, GM, KE, LR, LS, MW, MZ, NA, RW, SD, SL, SZ, TZ, UG, ZM, ZW), euroasiática (AM, AZ, BY, KG, KZ, MD, RU, TJ, TM), europea (AL, AT, BE, BG, CH, CY, CZ, DE, DK, EE, ES, FI, FR, GB, GR, HR, HU, IE, IS, IT, LT, LU, LV, MC, MK, MT, NL, NO, PL, PT, RO, RS, SE, SI, SK, SM, TR), OAPI (BF, BJ, CF, CG, CI, CM, GA, GN, GQ, GW, ML, MR, NE, SN, TD, TG).

Publicada:

- con informe de búsqueda internacional (Art. 21(3))
- antes de la expiración del plazo para modificar las reivindicaciones y para ser republicada si se reciben modificaciones (Regla 48.2(h))
- la fecha de presentación de la solicitud internacional está dentro del plazo de dos meses a partir de la fecha de expiración del periodo de prioridad (Regla 26bis.3)

(54) Title: METHOD FOR THE CHARACTERISATION AND CLASSIFICATION OF KIDNEY STONES

(54) Título : PROCEDIMIENTO DE CARACTERIZACIÓN Y CLASIFICACIÓN DE CÁLCULOS RENALES

(57) Abstract: The invention relates to a method for the characterisation and classification of kidney stones, comprising the following steps in which: (a) a plurality of samples of kidney stones are obtained and cut in order to observe the interior thereof, obtaining the flattest surface possible; (b) hyperspectral imaging (HSI) is used to obtain the spectra of the pre-cut kidney stones, with a plurality of regions of interest (ROI) being selected and the image being analysed using principal component analysis (PCA); (c) the main species are identified using factor analysis (FA); (d) atypical values are identified using principal component analysis (PCA); (e) the different types of kidney stones are analysed using principal component analysis (PCA); and (f) the artificial neural network (ANN) technique is applied to the data obtained from the principal component analysis (PCA) for the classification thereof.

(57) Resumen: Procedimiento de caracterización y clasificación de cálculos renales, que comprende las siguientes etapas: (a) se toman una pluralidad de muestras de cálculos renales y se cortan para observar su interior, obteniendo una superficie lo más plana posible, (b) se aplica la técnica de Formación de Imágenes Hiperespectrales (HSI) obteniendo los espectros de los cálculos renales anteriormente cortados, seleccionando una pluralidad de Regiones de Interés (ROI) y analizando la imagen a través de Análisis de Componentes Principales (PCA) (c) se identifican las especies principales mediante Análisis de Factores (FA) (d) se identifican valores atípicos a través de Análisis de Componentes Principales (PCA) (e) se analizan los diferentes tipos de cálculos renales a través de un Análisis de Componentes Principales (PCA) (f) a los datos obtenidos del Análisis de Componentes Principales (PCA) se aplica la técnica de Redes Neuronales Artificiales (ANN) para su clasificación.

WO 2012/136874 A1

**8.6. Patent application: Stone analysis device  
(Section 5.3.)**



MINISTERIO  
DE INDUSTRIA, TURISMO  
Y COMERCIO



Oficina Española  
de Patentes y Marcas

## Justificante de presentación electrónica de solicitud de patente

Este documento es un justificante de que se ha recibido una solicitud española de patente por vía electrónica, utilizando la conexión segura de la O.E.P.M. Asimismo, se le ha asignado de forma automática un número de solicitud y una fecha de recepción, conforme al artículo 14.3 del Reglamento para la ejecución de la Ley 11/1986, de 20 de marzo, de Patentes. La fecha de presentación de la solicitud de acuerdo con el art. 22 de la Ley de Patentes, le será comunicada posteriormente.

Número de solicitud:	P201430927	
Fecha de recepción:	18 junio 2014, 13:19 (CEST)	
Oficina receptora:	OEPM Madrid	
Su referencia:	14-7011 pat es	
Solicitante:	UNIVERSITAT AUTÒNOMA DE BARCELONA	
Número de solicitantes:	2	
País:	ES	
Título:	Método y sistema para la clasificación automática de cálculos renales, programa de ordenador y producto de programa de ordenador	
Documentos enviados:	Descripcion.pdf (20 p.) Reivindicaciones.pdf (5 p.) Resumen.pdf (1 p.) Dibujos.pdf (1 p.) OLF-ARCHIVE.zip	package-data.xml es-request.xml application-body.xml es-fee-sheet.xml feesheet.pdf request.pdf
Enviados por:	CN=ENTIDAD TORNER JUNCOSA I ASSOCIATS SL - CIF B63182802 - NOMBRE JUNCOSA MIRO JAIME - NIF 39833361Y,OU=703011251,OU=fnmt clase 2 ca,O=FNMT,C=es	
Fecha y hora de recepción:	18 junio 2014, 13:20 (CEST)	
Codificación del envío:	B2:98:3C:66:5E:48:D6:A6:FE:23:30:D0:95:1F:3E:44:F5:2D:A3:58	

/Madrid, Oficina Receptora/

